UNIVERSITÀ DEGLI STUDI FIRENZE

DOTTORATO DI RICERCA IN FISICA E ASTRONOMIA

INDIRIZZO FISICA - XXXIII CICLO

Settore disciplinare - FIS02

Holographic description for beyond Standard Model scenarios

Dottorando:
Alessio Caddeo

Tutori:
Dr. Francesco Bigazzi

Prof. Aldo L. Cotrone

Coordinatore:
Prof. Raffaello D'Alessandro

Contents

Acknowledgements

Introduction

The Standard Model of particle physics describes three of the four Nature's fundamental interactions in an impressively accurate way. It is a gauge theory with gauge algebra $su(3) \times su(2) \times u(1)$, the first factor being associated to QCD and the other two factors to the electroweak sector. Consistently with gauge-anomaly cancellation, the model features six quark flavors and six leptons whose interactions are determined by gauge symmetry and renormalizability. These particles have vanishing bare mass in the ultraviolet due to the chirality of the model but acquire mass through their couplings with the Higgs field once the latter condenses. In this respect, the observation by ATLAS [1] and CMS [2] at LHC in 2012 of the last building block of the Standard Model, namely the Higgs boson, constitutes its triumph.

Nevertheless, there are reasons to believe that the Standard Model cannot be the ultimate theory of fundamental physics. First of all, it does not take into account the gravitational interaction. Besides that, several issues have been raised.

One of these goes under the name of *strong CP problem*, and consists in the experimental evidence that the Standard Model's strong sector is CP-symmetric to a very good approximation, although CP-breaking effects in the strong sector are not forbidden by the gauge structure of the Standard Model. The breaking of the CP symmetry in QCD would result, for instance, in a non-vanishing value of the neutron's electric dipole moment. However, so far, no such effects have been observed by experiments, which have then put a strict bound on QCD CP-breaking [3, 4]. The strong CP problem would not arise if one of the quarks were massless (after Higgs field condensation). However, there is evidence [5] that all the quarks are massive. Thus, the Standard Model does not provide an explanation of the absence of CP-breaking effects in the strong sector.

The most compelling solution to the strong CP problem is the so-called *Peccei-Quinn mechanism* [6], which consists in extending the Standard Model in such a way that an extra $U(1)$ (anomalous) global symmetry acting by chiral rotations on quarks arises. In order to solve the strong CP problem, the extra symmetry has to be spontaneously broken; hence a pseudo-Nambu-Goldstone boson has to appear [7, 8]. The latter is a very light pseudoscalar particle called *axion* that has so far eluded experimental detection.

Besides its simplicity in solving the strong CP problem, the Peccei-Quinn mechanism is deemed as compelling because the axion also provides a good dark

matter candidate [9]. Whether the axion can completely solve the dark matter problem is currently under debate. Nevertheless, if it exists, it surely contributes to the dark matter abundance. Being able to address two separate problems at the same time, the axion is the most sought-after particle beyond the Standard Model.

It is clearly a crucial goal to study and classify how the axion might interact with ordinary matter. In order to solve the strong CP problem, the axion must necessarily be coupled to the QCD topological density so that it enters the QCD Lagrangian with a non-renormalizable operator. An ultraviolet completion is then needed. In the last decades, several models have been put forth (see [10] for an updated review). Two important classes of models are the DFSZ [11,12] and the KSVZ [13,14] scenarios. In the first case, the Standard Model's matter fields are charged under the Peccei-Quinn $U(1)_{PQ}$ symmetry, whereas in the second case, they are not.

Although our focus will be on the QCD axion, it is worth mentioning that scenarios where axion-like particles appear regardless of their role in solving the strong CP problem have been considered as well [15]. From a more theoretical perspective, axions deserve attention for they are also common in string theory compactifications [16].

As we have tacitly stated above, another reason to believe that the Standard Model needs to be extended is its inability to account for the dark matter. The dark matter gives about the 26% of the Universe's energy [17]. Its presence is inferred only from gravitational observations because it still eludes detection via other interactions. The lack of dark matter evidence at laboratory experiments also leads to the possibility that dark matter might be given by a sector that is coupled only gravitationally with the Standard Model. Thus, it is important to consider experimental alternatives to colliders. Gravitational waves, recently detected for the first time by the LIGO and VIRGO collaboration [18], offer such an alternative. Besides LIGO and VIRGO, several gravitational wave experiments are projected for the future, promising to explore a wide range of gravitational wave frequencies.

Gravitational waves open a new window on high-energy fundamental physics for the following reason. A stochastic background of gravitational waves is produced in cosmological first-order phase transitions [19–22]. The Standard Model does not predict any first-order phase transition in the early Universe since the electroweak and the QCD transitions (at small baryon density) are actually crossovers [23,24]. However, several extensions of the Standard Model conceived to address the dark matter problem do predict first-order phase transitions. As a result, through the detection of stochastic gravitational waves we can get information on high-energy physics.

A system that admits a first-order phase transition is characterized by a potential that displays two minima, which are degenerate at the critical temperature. If we consider a cosmological setting where the temperature is higher than the critical one, the system will start its evolution in the global minimum

configuration. During the cosmological evolution, the temperature decreases. As soon as it goes below the critical value, the system will find itself in a so-called *false vacuum*. At this point, a first-order phase transition can be triggered by the production of bubbles of true vacuum [25–27]. In this process, gravitational waves are produced essentially in three ways: collisions among bubbles, production of plasma sound waves, and turbulence.

In the literature, there are formulae that allow one to compute the gravitational wave spectrum in terms of few parameters such as the bubble nucleation rate, the energy released in the transition, and the velocity of the bubble (see, e.g., [19–22] for reviews). These parameters have to be computed from a microscopic model. A clear aim is then to study microscopic models that feature first-order phase transitions and extract the parameters needed to find the gravitational wave spectrum, especially if they address the dark matter problem.

According to the formalism developed in [25–27], in order to find the parameters that characterize a first-order phase transition, one has to find a so-called *bounce solution*, which describes the aforementioned vacuum bubbles. The latter is a solution of the system's Euclidean equations of motion found imposing boundary conditions that enforce the interpolation between the false and the true vacua. In realistic models, to solve such a problem is usually challenging, and one has to conceive effective approaches that capture the main features of the transition, allowing for estimates of its parameters. Moreover, such a task is often complicated by the strongly-coupled dynamics of the microscopic model. Indeed, many Standard Model extensions aimed to account for the dark matter involve strongly-coupled QCD-like hidden gauge sectors [28]. Dark matter is expected to be stable and effectively neutral with respect to the Standard Model, two properties that are easily met by introducing new confining gauge sectors whose stable excitations (pions, baryons, glueballs etc, depending on the model) provide dark matter candidates.

We see that several Standard Model extensions involve strongly-coupled gauge sectors. To study quantum field theories in their strongly-coupled regime is in general a difficult task because perturbation theory, the most powerful quantum field theory tool, ceases to provide reliable results and therefore alternative methods have to be employed.

A successful non-perturbative approach is provided by *lattice gauge theory*, which exploits numerical methods after discretizing spacetime. It allows one to get a lot of information on the strongly-coupled gauge theories. To make an example, the glueball spectrum of Yang-Mills theory can be computed with lattice methods [29]. Nevertheless, the lattice approach carries its own issues, especially when it comes to problems where operators that are imaginary in Euclidean signature are involved, as it happens for the QCD θ angle. Furthermore, lattice methods are not very suitable for studying the real-time dynamics of gauge theories.

An alternative way of studying strongly-coupled theories is to use *dualities*. We say that there is a duality whenever two apparently different theories describe

the very same physics. Dualities can be *exact* or *infrared*. In the first case, one has two equivalent theories that eventually look different. Examples of exact dualities are the Kramers-Wannier duality of the Ising model and the T-duality for a scalar field in two dimensions. In the second case, two different theories become the same one in the low-energy regime. A well-known example of infrared duality is *particle/vortex duality* in three dimensions, which relates the $O(2)$ model to the Abelian Higgs model [30,31].

Dualities are particularly powerful when they map the strongly-coupled regime of one theory to the weakly-coupled regime of another theory. In that case, studying the weakly-coupled theory using perturbative methods, one obtains information on the other theory's strongly-coupled dynamics.

A prominent example of weak/strong duality is the *gauge/gravity duality*. It relates quantum field theories in d dimensions to (string) gravitational theories in at least $d + 1$ dimensions [32–34].[1] Since the quantum field theory lives in one dimension less, the duality is often called *holographic correspondence*. It was discovered in 1997 by exploiting two different descriptions of the D-branes, extended dynamical objects of string theory. The best-understood case involves $\mathcal{N} = 4$ Super-Yang-Mills theory, a conformal and supersymmetric cousin of Yang-Mills theory, and Type IIB String Theory on an (asymptotically) $AdS_5 \times S^5$ background. These two theories are by now considered exactly equivalent. The large amount of supersymmetry allows one to have computational control and perform non-trivial checks of the duality [35].

At strong coupling and large gauge group's rank (large-λ and large-N), the string theory side is well approximated by classical ten-dimensional supergravity, and computations usually become easier. We then see the strength of the duality: by performing relatively simple classical computations, we get information on the highly-non-trivial strongly-coupled dynamics of the dual quantum field theory.

The holographic correspondence is now believed to hold also for theories that do not exhibit supersymmetry and conformal symmetry. As a result, it has found numerous applications, from high-energy to condensed matter physics.

The gauge theory of utmost interest is surely four-dimensional $SU(3)$ Yang-Mills theory, which displays confinement and mass gap, phenomena for which a thorough understanding is still lacking. A string theory dual that admits a reliable supergravity approximation is currently unknown and probably does not even exist. Nevertheless, we can conceive models that admit supergravity duals and that capture QCD physics in some regimes. With this line of thought, two different approaches have been developed. In the first one, one engineers string theory models that better resemble low-energy $SU(N)$ QCD in some regime (usually at strong coupling and large-N). These models are usually called *top-down*. In the second case, one studies gravitational models regardless of their string theory origin. This second approach is called *bottom-up*. Clearly, both approaches have their perks and pitfalls and have to be taken as complementary tools.

---

[1]The gravitational side often involves an additional compact space.

In this thesis, we will work within the top-down context. The top-down holographic model that better resembles QCD in the planar and strongly-coupled regime is the Witten-Sakai-Sugimoto (WSS) model [36, 37]. It exhibits all the low-energy features of QCD: confinement, mass-gap, and chiral symmetry breaking. The gauge sector is obtained as the low-energy limit of the theory living on the worldvolume of a stack of N $D4$-branes wrapped on a circle. At strong coupling and in the planar limit, the theory is described by the low-energy limit of a Type IIA supergravity solution. Fields in the fundamental representation, *i.e.* quarks, are obtained by introducing N_f pairs of $D8/\overline{D8}$ branes, which, in the $N_f \ll N$ regime, can be treated as probes in the geometry produced by the $D4$-branes and therefore studied using the Dirac-Born-Infeld action. The gravitational dual theory furnishes analytical control on confinement, mass gap, and chiral symmetry breaking.

The model allows one to easily introduce the θ angle [38], and therefore it has been employed to study the associated physics, such as the θ dependence of the Yang-Mills vacuum energy, of the glueball masses, of the baryon spectrum, and to compute the neutron's electric dipole moment [39–42]. Furthermore, the model exhibits an interesting phase diagram with two first-order phase transitions, one associated to confinement, the other associated to chiral symmetry breaking. Depending on the model's parameters, the two transitions may occur at different temperatures [43].

In this thesis, we apply the WSS model to address the two problems discussed above, namely the strong CP problem and the computation of the spectrum of gravitational waves produced in cosmological first-order phase transitions. In the first case, the WSS model is meant to describe QCD. In the second case, it is used to model dark sectors.

Concerning the strong CP problem, we present an ultraviolet complete model, built on the WSS one, where the axion appears as the pseudo-Nambu-Goldstone boson coming from the condensation of a massless extra quark. Thus, the $U(1)_{PQ}$ global symmetry is provided by the extra flavor's chiral symmetry. In this respect, the model falls in the KSVZ class. As we have mentioned above, a massless quark automatically solves the strong CP problem. Since the Standard Model quarks are massive, we need an extra quark. Phenomenology is not spoiled as long as the quark condenses at a scale much larger than the QCD dynamical scale. As a result, a mechanism that results in a separation between the two scales is required. In our model, such a separation is provided by a strongly-coupled and non-local version of the Nambu-Jona-Lasinio (NJL) mechanism [44].

From the holographic perspective, the introduction of the axion in the WSS model is achieved by adding an extra $D8/\overline{D8}$ brane pair, which implements the non-local NJL mechanism if one chooses suitable boundary conditions. The model reproduces the axion-dressed QCD chiral Lagrangian known in the literature [45], from which coupling between the axions and the nucleons can be computed. We study the behavior of the model in the deconfined phase and extract the axion mass from the topological susceptibility of the gauge theory. However,

the peculiar model's ultraviolet completion makes the axion properties differ from those expected from QCD, essentially because of the absence of asymptotic freedom.

Next, we study the two first-order phase transitions of the WSS model. This study is interesting *per se* and useful in view of the application to the computation of the gravitational wave spectra. The first phase transition of the model separates the confined phase from the deconfined one. From the holographic perspective, it is a Hawking-Page phase transition. In order to find the aforementioned bounce solution, one should solve ten-dimensional supergravity equations of motion with non-trivial boundary conditions. Since several fields are involved in the computations, the problem turns out to be daunting. Hence, we take an effective approach, developed in [46] within the Randall-Sundrum context, thanks to which the problem is formulated in terms of a single scalar field. Using holographic renormalization techniques, we derive an effective action for this scalar field and then solve its equation of motion to find the bounce solution. At this point, the bubble nucleation rate is easily computed.

The second phase transition, occurring when the gauge sector is deconfined, separates the chiral symmetric vacuum from the asymmetric one. Holographically, in the probe approximation, the transition involves the embedding of the $D8$-branes so that the bounce is a solution of the equations of motion derived from the Dirac-Born-Infeld action. Also in this case, the exact solution of the problem is not available due to the non-linearities of the equations of motion. We address the problem by using a variation approach. We first apply it to the study of the known configurations, finding an impressive fit. We then use it to extract the bounce solution, from which the bubble nucleation rate can be computed.

In the last part of the thesis, we adopt the WSS model to describe several scenarios put forth in the literature to account for the dark matter. The scenarios differ mainly for the dynamical scale's value and the matter content. We consider scenarios where a strongly-coupled gauge sector featuring a first-order phase transition is present. Exploiting the results obtained in the study of the WSS phase transitions, we compute the parameters needed to find the associated gravitational wave spectrum.

We firstly consider three scenarios where the confinement phase transition implies the (eventual) chiral one. In the first one, called *Dark HQCD 1*, the Standard Model is extended with a dark $SU(N)$ Yang-MIlls theory coupled to extra quarks: dark matter is given by dark mesons and baryons. The gauge theory confines at a scale that ranges from ~ 100 MeV to $\sim 10^9$ MeV depending on the scenario under consideration. These scales correspond to gravitational wave frequencies expected to be probed by space-based experiments such as LISA, BBO and DECIGO. The second scenario that we consider, named *Dark Glueball*, is given by the unflavored version of the Dark HQCD 1 scenario. Dark matter is thus provided by stable glueballs. Viable dark glueball models have dynamical scale ranging from some eV to tens of MeV, corresponding to gravitational wave frequencies within reach of experiments that exploit Pulsar-Timing-Arrays, such

as NANOGrav, EPTA, and PTTA. In this scenario, constraints coming from the Cosmic Microwave Background (CMB) measurements, and from measurements of the elements' abundance in Big Bang Nucleosynthesis (BBN) require the dark sector to be at a lower temperature than the Standard Model. The third scenario is called *Dark Axion* and deals with the axion model proposed in [13, 47], where the gravitational waves are produced during the Peccei-Quinn phase transition. Phenomenological bounds require that the phase transition's dynamical scale sits between 10^8 GeV and 10^{17} GeV (see e.g. [48]), corresponding to frequencies larger than those probed by ground-based experiments such as LIGO/VIRGO, ET, and CE.

Next, we consider two scenarios where a chiral symmetry phase transition separated from the confinement one occurs. The first scenario is identical to the Dark HQCD 1 scenario, except for the fact that the chiral symmetry breaking scale is separated from the confinement one. For this reason, we will refer to *Dark HQCD 2* for this scenario. The appealing feature of this case is that it predicts a gravitational wave spectrum with two peaks, one for each of the two phase transitions. The second scenario involves the holographic QCD axion model proposed in this thesis. This is the only scenario where the WSS model is used to describe QCD rather than a dark sector. As for the Dark Axion case, the Peccei-Quinn transition scale has to be very large to satisfy phenomenological constraints.

Comparing our results with the sensitivity curves of gravitational wave experiments, we find a large region of parameter space corresponding to gravitational wave signals that are expected to be detected by near-future experiments. In particular, the characteristic case where the gravitational wave spectrum exhibits two peaks turns out to be within the reach of the future experiments. Moreover, it is worth mentioning that our glueball scenario is compatible with the results recently reported by NANOGrav [49].

The thesis is organized as follows. The first two chapters provide a review of background material. The remaining chapters constitute the original part of the thesis.

In chapter 1, we introduce the $1/N$ expansion of QCD and the gauge/gravity duality. We study two complementary descriptions of the D-branes, and discuss how to argue from these the equivalence between $\mathcal{N} = 4$ SYM theory and Type IIB String Theory on $AdS_5 \times S^5$. We finally discuss the holographic dictionary that allows one to pass from one side of the duality to the other.

In chapter 2, we review the Witten-Sakai-Sugimoto model. We first describe the gauge sector and discuss how the holographic correspondence allows us to study confinement and mass gap. We then discuss how quarks are introduced in the model. We derive the low-energy theory that describes mesons and baryons and discuss how chiral anomaly is holographically realized in the model. Finally, we study the model at finite temperature.

In chapter 3, we discuss how to generalize the Witten-Sakai-Sugimoto model in order to solve the strong CP problem through the introduction of the QCD

axion. We derive the low-energy theory from which the axion couplings with the nucleons can be computed and then study the model's temperature dependence, extracting the axion mass from the topological susceptibility. As a byproduct of our computations, we will derive the topological susceptibility of $\mathcal{N} = 4$ SYM theory at strong coupling and finite temperature, a result that was missing in the literature.

In chapter 4, we study the two first-order phase transitions occurring in the WSS model using two effective approaches to infer the bounce solution and, from that, the bubble nucleation rate.

In chapter 5, we consider the WSS model as describing different hidden gauge sectors motivated by dark matter. Using the results of chapter 4, we compute the spectrum of stochastic gravitational waves produced in cosmological first-order phase transitions predicted by the considered scenarios and compare them with the sensitivity curves of gravitational wave experiments.

Chapter 1

The Holographic Correspondence

The holographic correspondence concerns a class of dualities between gravitational theories in $d+1$ dimensions and quantum field theories in d dimensions, discovered more than twenty years ago in [32–34]. The difference of the number of dimensions, firstly advocated by Susskind and 't Hooft in [50, 51], justifies the adjective *holographic*. The duality realizes in a non-trivial way the relation between gauge and string theories conjectured by 't Hooft in [52], where the large-N expansion of gauge theories was firstly proposed.

The holographic correspondence is a weak/strong duality: in the regime in which the theory on one side is weakly coupled, the other side's theory is strongly coupled. This is a welcome feature from the application point of view, for it allows us to investigate the strongly-coupled regime of gauge theories, which is usually not accessible with perturbative methods. On the other hand, if we consider the conjecture at the non-perturbative level, it yields a non-perturbative definition of quantum gravity. The focus of this thesis is on the former application.

In [32], the holographic correspondence was discovered or, more precisely, conjectured, within the string theory framework by exploiting two different, complementary descriptions of the D-branes. In the best-understood case, the duality involves on one side $4d$ $\mathcal{N} = 4$ Super-Yang-Mills (SYM) theory and on the other side Type IIB String Theory on a background with asymptotically $\text{AdS}_5 \times S^5$ metric and Ramond-Ramond flux on S^5. Numerous checks of the duality in this particular case have been successfully performed, thanks to the control ensured by supersymmetry.

The holographic correspondence has been subsequently generalized to more general case, even non-supersymmetric and non-conformal ones (see, e.g., [35] for the earlier developments, and [53] for a more recent review). In this thesis, we will mainly work with a non-supersymmetric and non-conformal holographic theory, the Witten-Sakai-Sugimoto model, reviewed in chapter 2.

The present chapter is organized as follows. In section 1.1, we present the large-N expansion of gauge theories. After explaining why it is useful to promote the gauge group's rank to an expansion variable, we show that the expansion organizes the Feynman diagrams according to their topology, similarly to what happens in

string perturbation theory. Section 1.2 deals with the holographic correspondence. We start with some heuristic comments on a possible relation between gauge and string theory. In subsections 1.2.1 and 1.2.2 we study D-branes, respectively, as supergravity solution and as microscopic dynamical objects. Starting from these descriptions, in subsection 1.2.3 we review the argument used in [32] to conjecture the holographic correspondence. Finally, in section 1.3, we discuss how gauge theory observables can be holographically computed and how to generalize the holographic prescriptions for the finite temperature cases.

1.1   Large-N QCD

In this section, we describe 't Hooft's idea [52] of studying QCD by promoting the gauge group's rank to a perturbative variable. We start explaining the motivations that underlie the large-N limit; then, we discuss the $1/N$ expansion. Good reviews on the topic are [54, 55].

Why large-N

Let us consider pure $SU(N)$ Yang-Mills theory in four dimensions,

$$S = -\frac{1}{2g_{YM}^2} \int d^4x \, \mathrm{Tr}\, F^{\mu\nu} F_{\mu\nu} \;, \tag{1.1.1}$$

where

$$F_{\mu\nu} = \partial_\mu A_\nu - \partial_\nu A_\mu - i[A_\mu, A_\nu] \tag{1.1.2}$$

is the usual non-Abelian field strength and the trace is taken over the gauge indices (which are understood). The theory is scale-invariant at the classical level because g_{YM} is dimensionless, and no other dimensionful parameters appear. However, at the quantum level, there is a non-trivial renormalization group flow. At one loop,

$$\frac{dg_{YM}}{d\log\mu} = -\frac{11N}{3} \frac{g_{YM}^3}{(4\pi)^2} \;. \tag{1.1.3}$$

After integration, we obtain

$$\frac{1}{g_{YM}^2(\mu_1)} - \frac{1}{g_{YM}^2(\mu_2)} = -\frac{22}{3} \frac{N}{(4\pi)^2} \log\left(\frac{\mu_2}{\mu_1}\right) \;. \tag{1.1.4}$$

By dimensional transmutation, the theory exhibits a dimensionful quantity Λ_{QCD} that is invariant under renormalization group transformations. It is defined as the energy scale for which the coupling function $g_{YM}(\mu)$ diverges at one loop,

$$\Lambda_{QCD} = \Lambda_{UV} \exp\left(-\frac{3}{22} \frac{16\pi^2}{g_{YM}^2 N}\right) \;. \tag{1.1.5}$$

Here, g_{YM}^2 is the coupling at an ultraviolet scale Λ_{UV}.

Four-dimensional $SU(N)$ Yang-Mills theory is believed to be gapped and confining. The scale Λ_{QCD} is therefore expected to give the mass-gap scale. Since g_{YM} is dimensionally transmuted into Λ_{QCD}, which we would like to keep fixed because it carries a physical meaning, it is evident that the theory does not suggest any weak-coupling limit.

't Hooft's idea [52] was to consider the rank of the gauge group as a variable and to take the limit of large N. If we do this while keeping g_{YM}^2 and Λ_{UV} constant, we have $\Lambda_{QCD} = \Lambda_{UV}$, which is an unsatisfactory result because we would like to separate the dynamical scale from the ultraviolet cut-off. Another possibility is to take the so-called *'t Hooft limit*

$$g_{YM} \to 0 , \qquad N \to \infty , \qquad \lambda = g_{YM}^2 N = \text{constant} . \qquad (1.1.6)$$

Even though the coupling goes to zero in the limit, the theory is still non-trivial since the number of degrees of freedom diverges.

The 't Hooft limit may be deemed as unrealistic since in the real world $N = 3$, which is not a small number. The main motivation for taking it as a serious approach is that it preserves several phenomena of hadronic physics observed in the $N = 3$ case and clearly not accessible with the usual QCD perturbation theory (see [55] for a detailed discussion on this point).

$1/N$ expansion

Let us consider how the $1/N$-expansion looks like by considering vacuum diagrams, namely diagrams without external legs, which contribute to the effective action. The Yang-Mills Lagrangian

$$\mathcal{L} = -\frac{N}{2\lambda} \text{Tr} \, F^{\mu\nu} F_{\mu\nu} \qquad (1.1.7)$$

is proportional to N, hence each interaction vertex introduces a factor of N/λ, each propagator a factor $(N/\lambda)^{-1}$, and each loop a factor of N. Thus, a generic diagram with V vertices, E propagators and F index contractions goes as

$$\text{diagram} \sim \left(\frac{\lambda}{N}\right)^E \left(\frac{N}{\lambda}\right)^V N^F . \qquad (1.1.8)$$

Let us write the gluon fields using fundamental indices,

$$(A_\mu)_j^i , \qquad i = 1, \ldots, N . \qquad (1.1.9)$$

The gluon propagator takes the form

$$\langle (A_\mu)_j^i(x)(A_\nu)_l^k(y) \rangle = \frac{\lambda}{N} D_{\mu\nu}(x-y) \left(\delta_l^i \delta_j^k - \frac{1}{N} \delta_j^i \delta_l^k \right) . \qquad (1.1.10)$$

The second term in (1.1.10) can be neglected at the leading order in $1/N$, and hence, perturbatively in this limit, we are not able to distinguish $U(N)$ from

$$i \xrightarrow{\hspace{3cm}} l \qquad = \quad \langle (A_\mu)^i_j(x)(A_\nu)^k_l(y)\rangle \sim \frac{\lambda}{N}$$
$$j \xleftarrow{\hspace{3cm}} k$$

Figure 1.1. *Gluon propagator using 't Hooft's double-line representation.*

$$\sim \quad \frac{N}{\lambda} \qquad\qquad\qquad \sim \quad \frac{N}{\lambda}$$

Figure 1.2. *Cubic (left) and quartic (right) vertices of Yang-Mills theory using 't Hooft's double-line representation.*

$SU(N)$. Since the gluon fields have two indices, it is useful to represent the gluon propagators with two lines, as depicted in Figure 1.1. Using this representation, the triple and quartic interactions look as in Figure 1.2.

   Let us now consider vacuum diagrams like the two presented in Figure 1.3. After some inspection, we see that each propagator introduces an edge in the diagram, whereas each loop gives a diagram face. The power of N in (1.1.8) turns out to be a topological invariant, known as *Euler characteristic*,

$$\chi = F + V - E = 2 - 2h \ . \tag{1.1.11}$$

On the right-hand side, h is the number of holes of the two-dimensional surface without boundaries on which we can draw the diagram. We have then

$$\text{diagram} \sim \lambda^{E-V} N^\chi \ . \tag{1.1.12}$$

Thus, the $1/N$ expansion organizes the Feynman diagrams according to their topology. The leading contribution involves diagrams with the topology of a sphere - graphs drawn on the surface of a two-dimensional sphere. Equivalently, they can be drawn in a two-dimensional plane and therefore are called *planar*. For this reason, the 't Hooft limit is often called planar as well.

   The string perturbation theory in the coupling constant g_s is an expansion in topology as well. The worldsheets' contribution is weighted by $g_s^{-\chi}$, and led 't Hooft to conjecture that, in the large-N limit, the gauge theory becomes a theory of strings with $g_s \sim 1/N$ [52].

   Concerning the dependence on λ, the combination $E - V$ is not a topological invariant. In the weak-coupling limit $\lambda \ll 1$, diagrams with few edges contribute more. In the strong-coupling regime $\lambda \gg 1$, the dominant diagrams are expected to be those with a large number of edges, which somehow fill the diagrams. In string theory, the worldsheets are smooth surfaces whose fluctuations are controlled by α'/L^2, where $\alpha' = l_s^2$ is the square of the string length and L^{-2} is
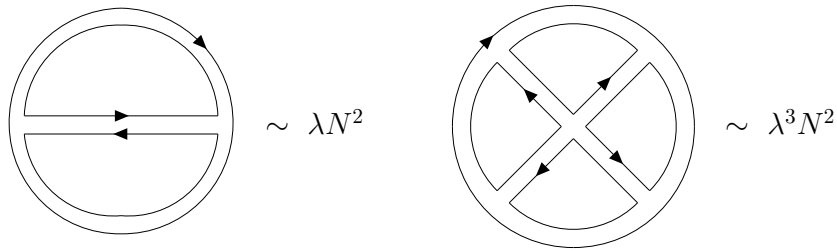
Figure 1.3. *Two examples of planar diagrams. We call E, V and F, respectively, the number of propagators, vertices and fundametal loops. Left: $E = 3$, $V = 2$, $F = 3$. Right: $E = 8$, $V = 5$, $F = 5$.*

the characteristic curvature of the background where the strings propagate. By comparison, we expect a correspondence between λ and some negative power of α'/L^2. As we will discuss in section 1.2, such a correspondence is realized in a non-trivial way. Its realization is understood better when we consider a supersymmetric and conformal version of QCD, which is $\mathcal{N} = 4$ Super-Yang-Mills theory.

So far, we have discussed vacuum diagrams. Let us consider correlation functions of gauge-invariant single-trace local operators $\mathcal{O}(x)$. The latter create glueball states from the vacuum. For instance, we could consider $\mathcal{O}_{\mu\nu\rho\sigma} = \mathrm{Tr}\, F_{\mu\nu} F_{\rho\sigma}$. The correlators of single-trace operators can be computed by the generating functional method, deforming the theory action to

$$S = -\frac{N}{2\lambda} \int d^4x \, \mathrm{Tr}\, F_{\mu\nu} F^{\mu\nu} + N \int d^4x J\mathcal{O} \ . \tag{1.1.13}$$

Notice that it is important that $\mathcal{O}$ is a single-trace operator so that the source term that we are adding behaves as a vertex, and therefore it does not spoil the N-counting of the diagrams. The connected n-point function is then given by

$$\langle \mathcal{O}_1 \ldots \mathcal{O}_n \rangle_c = \frac{1}{(iN)^n} \frac{\delta}{\delta J_1} \ldots \frac{\delta}{\delta J_n} \log Z[J] \ . \tag{1.1.14}$$

Since $\log Z[J] \sim N^2$, the n-point connected correlator goes as

$$\langle \mathcal{O}_1 \ldots \mathcal{O}_n \rangle_c \sim N^{2-n} \ . \tag{1.1.15}$$

A generic correlation function displays a disconnected component. Let us take the $n = 2$ case, for simplicity,

$$\langle \mathcal{O}\mathcal{O} \rangle \sim \langle \mathcal{O} \rangle \langle \mathcal{O} \rangle + \langle \mathcal{O}\mathcal{O} \rangle_c \ . \tag{1.1.16}$$

From (1.1.15), we see that the disconnected contribution goes as N^2, whereas the connected one as N^0. As a result, in the large-N limit, correlation functions of single-trace operators factorize, and $1/N^2$ powers suppress quantum fluctuations. The large-N limit suppresses the interactions of singlet degrees of freedom. It is
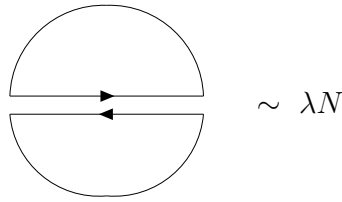
Figure 1.4. *Vacuum diagram with a fermion loop using 't Hooft representation. In this case, the number of propagators, vertices and fundamental loops are, respectively, $E = 3$, $V = 2$, $F = 2$.*

a classical limit in a peculiar sense: the dimensions of operators in a product add, even though they may considerably differ from the classical ones.

It can be shown that the theory at large-N exhibits an infinite spectrum of stable states with increasing masses [55].

Let us consider quarks, namely fermion fields in the fundamental representation of the gauge group. We normalize fermion fields so that the Lagrangian be proportional to N,

$$\mathcal{L} = \frac{N}{\lambda} \left[-\frac{1}{2} \operatorname{Tr} F^{\mu\nu} F_{\mu\nu} + i\bar{\psi}\slashed{D}\psi \right] \ . \tag{1.1.17}$$

Fermion fields carry a single fundamental gauge index and therefore have to be represented by single lines in the 't Hooft diagrams. An example is provided by Figure 1.4.

We see that fermions introduce boundaries in the diagrams. When we include fermions, the $1/N$ expansion is still an expansion over topologies. The diagrams still contribute as N^χ, where the Euler characteristic in the presence of b boundaries is generalized to

$$\chi = 2 - 2h - b \ . \tag{1.1.18}$$

If we consider N_f fermions and keep N_f constant in the 't Hooft limit, diagrams containing fermion loops get suppressed with N_f/N powers with respect to the planar diagrams without fermions. Since in real-world QCD $N_f > N$, the 't Hooft limit could be considered unsatisfactory. A valid alternative is then the *Veneziano limit* [56]

$$N_f, N \to \infty \ , \qquad \frac{N_f}{N} = \text{constant} \ , \qquad \lambda = \text{constant} \ . \tag{1.1.19}$$

Remarkably, baryons can be treated in the large-N limit as well [55]. However, we will not need to go into more detail on this.

So far, we have discussed the QCD case, which is the case of interest in this thesis. However, it should be clear that all the considerations we made only depend on the fact that we are dealing with a theory of matrices, meaning of fields Φ^i_j where the interactions are constrained by the fact that only matrix

multiplications can appear. As a result, all the discussion can be easily generalized to adjoint scalar and fermion fields, which appear, in particular, in the $\mathcal{N} = 4$ Super-Yang-Mills theory that plays a pivotal role in holography. Matrix models remain non-trivial in the large-N limit - they do not become solvable models. In contrast, vector theories become free in the the large-N limit (barring self-energy corrections). In this case, the gravitational dual description is highly non-trivial [57].

1.2   AdS/CFT correspondence

In section 1.1, we stated that matrix theories in the large-N limit become theories of closed strings, hence theories with gravity. This statement seems to clash with the Weinberg-Witten theorem, which asserts that a Poincaré-invariant theory with a conserved energy-momentum tensor cannot include particles with spin $j > 1$ that have a non-vanishing momentum. As a result, it seems not possible for a gauge theory to tacitly be a theory of gravity since the latter requires the presence of a massless spin-2 field propagating in the bulk (if the number of spacetime dimensions is greater than three).

In fact, the Weinberg-Witten theorem relies on the assumption that all the particles live in the same number of spacetime dimensions. Even though such an assumption sounds reasonable, we can argue that it has to be questioned when gravity enters the discussion. Indeed, we know that in a gravitational theory, the number of degrees of freedom, measured by the entropy, is subextensive, meaning that it is proportional to the area rather than to the volume of a given region under consideration [58]. Ordinary quantum field theory gives extensive entropies. As a result, if a dual gravitational description of a gauge theory exists, we expect that to be defined in a space with at least one dimension more [50,51].

It is then natural to try to understand the meaning of the extra dimension. It turns out that it must be interpreted as the gauge theory's energy scale. From the Wilsonian point of view, we know that each theory can be thought of in terms of a continuum of theories defined at different energies. The renormalization group theory equations are local, meaning that we do not need information from the deep IR or deep UV in order to see how the theory looks like at a given energy. It is then natural to ask which gravitational theory we should expect from scale-invariant quantum field theories. It is actually straightforward to find out which form the metric has to take in this case. If we consider five-dimensional metrics with Poincaré invariance in $3 + 1$ dimensions and invariance under scale transformation, the most general ansatz is

$$ds^2 = \left(\frac{L}{z}\right)^2 \left[dz^2 + \eta_{\mu\nu}dx^\mu dx^\nu\right] \ , \tag{1.2.1}$$

which is the metric of five-dimensional anti-de Sitter (AdS) spacetime in Poincaré coordinates, where scale transformations are defined by

$$(x^\mu, z) \rightarrow (\lambda x^\mu, \lambda z) \ . \tag{1.2.2}$$

AdS is a maximally symmetric solution of the Einstein equation of motion with a negative cosmological constant. It has a conformal boundary at spatial infinity, where Minkowski space appears. For this reason, with a slight abuse of language, we will often say that the gauge theory lives on the AdS boundary.[1] In the following, we will study the holographic correspondence in more detail. We will see how the metric (1.2.1) emerges from a string theory construction.

The comments above do not involve supersymmetry. Though the best-understood case exhibits supersymmetry, the holographic correspondence is believed to hold regardless of the presence of supersymmetry. Clearly, the latter allows us to have more control over the duality. However, most of the systems of phenomenological interest are not supersymmetric. In this thesis, we will be interested in non-supersymmetric cases. In chapter 2, we will discuss the top-down model that better resembles QCD, where supersymmetry is absent.

In the remaining of this section, we will illustrate the two different points of view on D-branes, from which we can argue the equivalence between $\mathcal{N} = 4$ SYM theory and Type IIB String Theory on $\mathrm{AdS}_5 \times S^5$ with a Ramond-Ramond F_5 flux on S^5.

1.2.1   Low-energy string theory

The AdS/CFT correspondence has been derived in a string theory context. In this thesis, we will always work with Type IIB and, mostly, Type IIA string theory. At the perturbative level, they are theories of closed strings. Let us recall their massless spectrum. The Neveu-Schwarz-Neveu-Schwarz sector is shared by both string theories and features the dilaton, the metric, and the Kalb-Ramond 2-form,

$$\phi \ , \qquad g_{\mu\nu} \ , \qquad B_{\mu\nu} \ . \tag{1.2.3}$$

In Type IIB string theory, the Ramond-Ramond sector displays a 0-form, a 2-form, and a 4-form whose field strength is self-dual,

$$C_0 \ , \qquad C_2 \ , \qquad C_4 \ , \qquad F_5 = *F_5 \ . \tag{1.2.4}$$

In the Type IIA theory, the Ramond-Ramond sector exhibits a 1-form and a 3-form,

$$C_1 \ , \qquad C_3 \ . \tag{1.2.5}$$

---

[1]This is an abuse of language because the gauge theory encodes the physics of the gravitational dual theory for any value of the radial coordinate, not just for the boundary. As we will see, the long-distance region of AdS describes the ultraviolet energy scales of the dual gauge theory [32, 59, 60]. Moreover, using such a language, we risk to confuse holography with what occurs when we put a theory on a manifold with a boundary and boundary degrees of freedom are required in order to cancel anomalies. The latter phenomenon, for instance, occurs when we consider $3d$ Chern-Simons theory for the fractional quantum Hall effect, where chiral boson on the boundary are required. As we will mention in footnote 3 of the present chapter, in the case of Type IIB string theory on $\mathrm{AdS}_5 \times S^5$, the boundary degrees of freedom do not give the full $\mathcal{N} = 4$ SYM theory.

The Neveu-Schwarz-Ramond sector gives the fermionic superpartners.

At the non-perturbative level, the theories admit p-dimensional dynamical entities, called *Dp-branes*, where open strings can end, so that also open strings are present in Type IIA and Type IIB string theories. D-branes source the Ramond-Ramond forms C_{p+1} [61], thus, from the comments above we see that Type IIB String Theory admits D(-1), $D1$ and $D3$-branes, whereas Type IIA string theory admits $D0$, $D2$ and $D4$-branes. D-branes play a pivotal role in understanding the holographic correspondence. We have two different descriptions of D-branes. In the remaining of this subsection, we illustrate how they appear as classical solutions of supergravity, the low-energy effective theory of string theory. In subsection 1.2.2, we will comment on their description as planes where open strings end.

By studying the propagation of a closed string in a background sourced by the massless fields of the string theory spectrum that we mentioned above, one finds that the consistency of string theory (in particular, the requirement of the vanishing of the gauge Weyl anomaly on the string's worldsheet) constrains the background fields to satisfy some equations of motion [62]. For example, the metric must satisfy the Einstein equations, corrected by higher derivative terms. The low-energy supergravity actions reproduce these equations of motion. Even though we will not need all the terms of the actions, let us write them for completeness. The action of Type IIB supergravity reads

$$S_{IIB} = S_{NS} + S_{RR}^{(B)} + S_{CS}^{(B)} \tag{1.2.6a}$$

where

$$S_{NS} = \frac{1}{2\kappa_{10}^2} \int d^{10}x \sqrt{-g} e^{-2\phi} \left(\mathcal{R} + 4\partial_M\phi\partial^M\phi - \frac{1}{2}|H_3|^2 \right) , \tag{1.2.6b}$$

$$S_{RR}^{(B)} = -\frac{1}{4\kappa_{10}^2} \int d^{10}x \sqrt{-g} \left(|F_1|^2 + |\tilde{F}_3|^2 + \frac{1}{2}|\tilde{F}_5|^2 \right) , \tag{1.2.6c}$$

$$S_{CS}^{(B)} = -\frac{1}{4\kappa_{10}^2} \int C_4 \wedge H_3 \wedge F_3 . \tag{1.2.6d}$$

Here,

$$2\kappa_{10} = (2\pi)^7 \alpha'^4 , \tag{1.2.7}$$

and

$$\tilde{F}_3 = F_3 - C_0 H_3 , \tag{1.2.8a}$$

$$\tilde{F}_5 = F_5 + \frac{1}{2}B_2 \wedge F_3 - \frac{1}{2}C_2 \wedge H_3 . \tag{1.2.8b}$$

It is worth mentioning that Type IIB action enjoys a classical $SL(2,\mathbf{R})$ symmetry that gets broken into $SL(2,\mathbf{Z})$ by non-perturbative effects [63]. This acts on the complex coupling

$$\tau = C_0 + ie^{-\phi} \tag{1.2.9}$$

as

$$\tau \to \frac{a\tau + b}{c\tau + d} \ , \qquad ad - bc = 1 \ , \tag{1.2.10}$$

and rotates the vector (B_2, C_2).

The Type IIA supergravity action can be derived reducing $11d$ supergravity on a circle. It reads

$$S_{IIA} = S_{NS} + S_{RR}^{(A)} + S_{CS}^{(A)} \tag{1.2.11}$$

where S_{NS} is given by (1.2.6b) and

$$S_{RR}^{(A)} = -\frac{1}{4\kappa_{10}^2} \int d^{10}x \sqrt{g} \left(|F_2|^2 + |\tilde{F}_4|^2 \right) \ , \tag{1.2.12a}$$

$$S_{CS}^{(A)} = -\frac{1}{4\kappa_{10}^2} \int B_2 \wedge F_4 \wedge F_4 \ . \tag{1.2.12b}$$

Here,

$$\tilde{F}_4 = \mathrm{d}C_3 - C_1 \wedge F_3 \ . \tag{1.2.13}$$

These actions admit p-brane solutions [64], namely solutions with Poincaré symmetry in $(p+1)$ dimensions and with non-vanishing Ramond-Ramond charge. They are expected to describe the backreaction of a collection of N coincident Dp-branes on the spacetime [65–67], where N is related to the Ramond-Ramond magnetic flux of the solution. The metric takes the form

$$ds^2 = \frac{1}{\sqrt{H(r)}} \eta_{\alpha\beta} dx^\alpha dx^\beta + \sqrt{H(r)} \delta_{ij} dx^i dx^j \ , \tag{1.2.14a}$$

where the indices α, β label the coordinates in the directions parallel to the brane worldvolume and the Latin indices the coordinates in the transverse space. Moreover, r is defined by $r^2 = \delta_{ij} x^i x^j$. The solution is characterized by

$$e^{\phi(r)} = g_s |H(r)|^{(3-p)/4} \ , \tag{1.2.14b}$$

$$H(r) = 1 + \left(\frac{R_p}{r} \right)^{7-p} \ , \tag{1.2.14c}$$

$$C_{01...p}(r) = g_s^{-1} \left(\frac{1}{H(r)} - 1 \right) \ , \tag{1.2.14d}$$

where R_p is a characteristic length scale of the spacetime, related to the string coupling constant g_s and the number of coincident branes N by

$$R_p^{7-p} = \frac{g_s N (2\pi\sqrt{\alpha'})^{7-p}}{(7-p)V(S^{8-p})} \ , \tag{1.2.14e}$$

where $V(S^n)$ is the volume of a n-sphere,

$$V(S^n) = \frac{2\pi^{(n+1)/2}}{\Gamma\left(\frac{n+1}{2}\right)} \ . \tag{1.2.15}$$

Supergravity is a good approximation of string theory in the regime in which α'-corrections can be neglected. This occurs when the curvature of the solution (1.2.14) is small in string units, namely $R_p^2/\alpha' \gg 1$. From (1.2.14e), we see that this occurs if

$$g_s N \gg 1 \ . \tag{1.2.16}$$

As we will discuss in subsection 1.2.3, the correspondence exploits the *near-horizon limit* $r \to 0$ with r/α' held fixed. The $p = 3$ solution is non-singular in this limit and reduces to the $\text{AdS}_5 \times S^5$ metric. Let us show this. Using spherical coordinates in the transverse space and calling

$$L^4 \equiv (R_3)^4 = 4\pi g_s N \alpha'^2 \ , \tag{1.2.17}$$

the metric reads

$$ds^2 = \left(1 + \frac{L^4}{r^4}\right)^{-1/2} \eta_{\alpha\beta} dx^\alpha dx^\beta + \left(1 + \frac{L^4}{r^4}\right)^{1/2} \left(dr^2 + r^2 d\Omega_5^2\right) \ . \tag{1.2.18}$$

In the near-horizon limit, $L \gg r$ and therefore $H \approx L^4/r^4$, so that

$$ds^2 = \frac{r^2}{L^2}\eta_{\alpha\beta} dx^\alpha dx^\beta + \frac{L^2}{r^2}\left(dr^2 + r^2 d\Omega_5^2\right) \ . \tag{1.2.19}$$

Changing coordinates according to $z = L^2 r^{-1}$, the metric (1.2.19) becomes

$$ds^2 = \frac{L^2}{z^2}\left(\eta_{\alpha\beta} dx^\alpha dx^\beta + dz^2\right) + L^2 d\Omega_5^2 \ , \tag{1.2.20}$$

Thus, the metric obtained with the near-horizon limit of the three-brane supergravity solution is the product of the five.dimensional AdS metric and of the five-dimensional sphere S^5. Both share the same scale L. The dilaton is constant,

$$e^\phi = g_s \ , \tag{1.2.21}$$

and the field strength of the C_4 Ramond-Ramond form, $F_5 = dC_4$, carries a flux on the five-sphere,

$$\int_{S^5} F_5 = (2\pi)^4 N \ . \tag{1.2.22}$$

The cases $p \neq 3$ exhibit a singularity and a diverging or vanishing dilaton for $r \to 0$. In these cases, the supergravity description is still valid far from the singularity. Near the singularity, one has to use full string theory or M-theory.

It is useful to consider also non-extremal black p-brane solutions, which exhibit an event horizon at $r = r_0$. The metric reads

$$ds^2 = \frac{1}{\sqrt{H(r)}}\left[-f(r)dt^2 + \delta_{ab}dx^a dx^b\right] + \sqrt{H(r)}\left[\frac{dr^2}{f(r)} + r^2\Omega_{n+1}\right] \ , \tag{1.2.23a}$$

where

$$f(r) = 1 - \left(\frac{r_0}{r}\right)^{7-p} \ , \qquad H(r) = 1 + \left(\frac{L_p}{r}\right)^{7-p} \tag{1.2.23b}$$

and

$$L_p^{7-p} = R_p^{7-p}\sqrt{1 + \frac{1}{4}\left(\frac{r_0}{R_p}\right)^{2(7-p)}} - \frac{r_0^{7-p}}{2} \ . \tag{1.2.23c}$$

The relation between N and the spacetime length scale is

$$L_p^{(7-p)/2}\sqrt{r_0^{7-p} + L_p^{7-p}} = \frac{g_s N (2\pi\sqrt{\alpha'})^{7-p}}{(7-p)V(S^{8-p})} \ . \tag{1.2.24}$$

The black-brane solution carries a non-vanishing temperature, given by

$$T = \frac{7-p}{4\pi r_0 \sqrt{H(r_0)}} \ . \tag{1.2.25}$$

In this thesis, a pivotal role is played by the solution (1.2.23) with $p = 4$. Indeed, after two Wick rotations, it provides the background dual to the Witten-Sakai-Sugimoto model. We will study this solution in chapter 2.

1.2.2 D-branes

In subsection 1.2.1, we presented the geometry expected to describe the backreaction of N D-branes. Such a description is valid in the regime $g_s N \gg 1$. The D-branes are fundamental objects of string theory, for which also a microscopic description is known. In string perturbation theory around flat spacetime, they appear as hyperplanes where open strings end. Since the open string's coupling is $g_s N$, perturbation theory works as long as

$$g_s N \ll 1 \ . \tag{1.2.26}$$

The Dp-branes break ten-dimensional Poincaré invariance $SO(1,9)$ into $SO(1,p)\times SO(9-p)$. The first factor represents Poincaré invariance along the branes' worldvolume, whereas $SO(9-p)$ constitutes a global symmetry for the branes.

In subsection 1.2.1, we mentioned that string theory gauge invariance imposes equations of motion for the background fields on which closed strings propagate and that the supergravity actions reproduce the equations. Following the same logic in the open string case, one analogously finds equations of motions for the massless fields of the open string spectrum. The bosonic sector features a $SO(1,p)$ vector and $9-p$ scalars rotated by $SO(9-p)$,

$$A_\alpha \ , \qquad \varphi^I \ , \tag{1.2.27}$$

where $\alpha = 0, \ldots, p$ and $I = p+1, \ldots, 9$. When we consider a stack of N branes, the fields also carry two Chan-Paton indices, one in the fundamental and the other one in the antifundamental of $U(N)$ (if we consider oriented strings),

$$(A_\alpha)^i_j \ , \qquad (\varphi^I)^i_j \ , \tag{1.2.28}$$

with i and j running from 1 to N. In the $N = 1$ case, the equations of motion imposed on these fields are reproduced by the Dirac-Born-Infeld (DBI) action

$$S_{DBI} = -\mu_p \int d^{p+1}x \, e^{-\phi} \sqrt{-\det\left(g_{\alpha\beta} + 2\pi\alpha' F_{\alpha\beta} + B_{\alpha\beta}\right)} \,, \qquad (1.2.29)$$

where $g_{\alpha\beta}$ and $B_{\alpha\beta}$ are the pullbacks on the brane of the metric and the Kalb-Ramond two-form, $F_{\alpha\beta} = \partial_\alpha A_\beta - \partial_\beta A_\alpha$, and

$$\mu_p = \frac{1}{(2\pi)^p \alpha'^{(p+1)/2}} \,. \qquad (1.2.30)$$

The branes have a tension. When the dilaton is constant, the tension is given by $T_p = \mu_p g_s^{-1}$. Otherwise, one defines an effective tension $T_{eff} = \mu_p e^{-\phi}$.

Let us consider a low-energy limit in which we keep the leading order-terms in the α' expansion. Calling $X^\mu = (X^\alpha, X^I)$ the string embedding functions, we can choose the static gauge

$$X^\alpha = x^\alpha \,, \qquad\qquad \alpha = 0, \ldots, p \,, \qquad (1.2.31a)$$
$$X^I = 2\pi\alpha' \varphi^I \,, \qquad\qquad I = p+1, \ldots, 9 \,, \qquad (1.2.31b)$$

so that

$$g_{\alpha\beta} = \eta_{\alpha\beta} + (2\pi\alpha')^2 \partial_\alpha \varphi^I \partial_\beta \varphi^I \,. \qquad (1.2.32)$$

Assuming vanishing $B_{\alpha\beta}$, if we expand the determinant appearing in (1.2.29), at leading order we find

$$-\det\left(g_{\alpha\beta} + 2\pi\alpha' F_{\alpha\beta}\right) = 1 + (2\pi\alpha')^2 \left[\frac{1}{2} F_{\alpha\beta} F^{\alpha\beta} + \partial_\alpha \varphi^I \partial^\alpha \varphi^I\right] \,. \qquad (1.2.33)$$

Neglecting the constant term coming from the 1 in (1.2.33), the DBI action reads

$$S_{DBI} = -(2\pi\alpha')^2 T_p \int d^{p+1}x \left[\frac{1}{4} F_{\alpha\beta} F^{\alpha\beta} + \frac{1}{2} \partial_\alpha \varphi^I \partial^\alpha \varphi^I\right] \,, \qquad (1.2.34)$$

that is the sum of the Maxwell action and the action of $(9 - p)$ free scalars. The electric coupling is given by $e^2 = 1/(2\pi\alpha')^2 T_p$.

A generalization of the DBI action (1.2.29) to the non-Abelian case is unknown. However, we can write the non-Abelian generalization of its low-energy approximation (1.2.34),

$$S_{DBI} = -(2\pi\alpha')^2 T_p \int d^{p+1}x \, \text{Tr} \left[\frac{1}{4} F_{\alpha\beta} F^{\alpha\beta} + \frac{1}{2} D_\alpha \varphi^I D^\alpha \varphi^I - \frac{1}{4} \sum_{i\neq j} [\phi^I, \phi^J]^2\right] \,. \qquad (1.2.35)$$

Here, $D_\alpha \phi^I = \partial_\alpha \phi^I + i[A_\alpha, \phi^I]$ is the covariant derivative and Tr the trace over the Chan-Paton indices.

The action (1.2.35) describes a $U(N)$ Yang-Mills theory coupled to adjoint scalars. In the $p = 3$ case, it gives the action of the bosonic part of four-dimensional $\mathcal{N} = 4$ Super-Yang-Mills theory with gauge group $U(N)$. The latter is a superconformal theory at the quantum level, so that no dimensional transmutation occurs, differently from what occurs in the non-supersymmetric Yang-Mills case discussed in section 1.1.

Comparing the action (1.2.35) with the Yang-Mills action

$$S_{YM} = -\frac{1}{4g_{p+1}^2} \int d^{p+1}x \operatorname{Tr} F_{\alpha\beta} F^{\alpha\beta} \ , \tag{1.2.36}$$

we find

$$g_{p+1}^2 = \frac{1}{(2\pi\alpha')^2 T_p} \ . \tag{1.2.37}$$

Recalling the expression (1.2.30) of the brane tension $T_p = \mu_p/g_s$, we finally find

$$g_{p+1}^2 = (2\pi)^{p-2} g_s l_s^{p-3} \ . \tag{1.2.38}$$

As we mentioned in subsection 1.2.1, the D-branes source the Ramond-Ramond fields. The D-brane action then includes also Chern-Simons couplings with the Ramond-Ramond fields C_p [63],

$$S_{CS} = \mu_p \sum_q \int_{Dp} C_{q+1} \wedge \operatorname{Tr} e^{2\pi\alpha' F + B_2} \ , \tag{1.2.39}$$

where the sum runs over the Ramond-Ramond fields that are present in the theory and the exponential represents a Taylor expansion with non-vanishing terms coming from the field strength's powers that, together with the Ramond-Ramond forms, give a $(p + 1)$-form integrand.

1.2.3 Arguing the correspondence

We have seen that D-branes can be described either by the classical solution (1.2.14) or by some non-Abelian generalization of the DBI action (1.2.29). The two descriptions are valid, respectively, when $g_s N \gg 1$ and $g_s N \ll 1$. We have seen that they lead to apparently quite different physics - a gravitational theory on the one hand and a gauge theory on the other hand. However, the computations of massless fields' absorption cross-sections performed using the two descriptions, remarkably, agree [68,69]. Let us then consider in more detail the relation between the two descriptions, following the reasoning that led Maldacena to conjecture the holographic correspondence [32].

Let us focus on $D3$-branes and start with the $g_s N \ll 1$ description. We have ten-dimensional Type IIB String Theory in flat spacetime $\mathbf{R}^{1,9}$ with N coincident $D3$-branes, and both closed and open string excitations. At low energies, we can integrate out the massive excitations and obtain an effective action, which, schematically, reads

$$S = S_{bulk} + S_{brane} + S_{int} \ . \tag{1.2.40}$$

The action S_{bulk} is the ten-dimensional Type IIB supergravity action (1.2.6) corrected by higher-derivative terms, S_{brane} is the action of four-dimensional $\mathcal{N} = 4$ SYM theory with gauge group $U(N)$, again corrected by higher derivative terms and finally S_{int} takes into account interactions between closed and open string excitations. In the $\alpha' \to 0$ limit, the system reduces to two decoupled theories:

- free supergravity;

- four-dimensional $\mathcal{N} = 4$ Super-Yang-Mills theory with gauge group $U(N)$.

Indeed, expanding the metric g around the Minkowski one η, $g \sim \eta + h$, we have schematically

$$S_{bulk} \sim -\frac{1}{2\kappa_{10}} \int \sqrt{g}R \sim \int d^{10}x \left[(\partial h)^2 + \kappa_{10}(\partial h)^2 h + \dots \right] . \qquad (1.2.41)$$

Recalling (1.2.7), we see that in the $\alpha' \to 0$ limit, gravity becomes free. Interactions are controlled by κ_{10} as well, thus open and string modes decouple. In contrast, $\mathcal{N} = 4$ SYM theory remains interacting.

Let us consider the low-energy limit of the solution (1.2.14) describing the $D3$-branes in the $g_s N \gg 1$ regime. The important point is to realize that the low-energy limit involves the energy measured by an observer placed at $r \to \infty$. The factor $H(r)^{-1/2}$ appearing in the supergravity solution (1.2.14) plays a crucial role. Let us call E_r the energy measured by an observer placed at a value r of the radial coordinate, and E the energy measured from an observer at infinity. Since $H(r)$ goes to 1 at infinity, the gravitational redshift gives

$$E = \frac{r}{L}E_r \sim \frac{r}{\sqrt{\alpha'}}E_r , \qquad (1.2.42)$$

where we used (1.2.17). The low-energy limit reads

$$\sqrt{\alpha'}E \sim rE_r \ll 1 . \qquad (1.2.43)$$

This condition is met by:

- low-energy massless states propagating in the bulk;

- arbitrarily excited states localized near the horizon.

In the low-energy limit, these two kinds of excitations decouple. The bulk excitations have long wavelengths and therefore cannot interact with the excitations near the throat, as confirmed by the fact that their absorption cross-section vanishes in the limit [68, 69].

Let us consider in more detail the limit that we take. We want to keep fixed both the energies measured by an observer at infinity and the energy of a string

extended from a brane placed at r and the N branes located at $r = 0$ since we would like to keep excitations with arbitrary energy E_r,

$$\sqrt{\alpha'} E_r = \text{fixed} . \qquad (1.2.44)$$

From (1.2.42), we see that the precise limit we want to consider is

$$r \to 0 , \qquad \alpha' \to 0 , \qquad \frac{r}{\alpha'} = \text{fixed} . \qquad (1.2.45)$$

Both descriptions feature two decoupled theories, one of which is free bulk supergravity. Besides that, we find two theories that look very different. On one side, we have four-dimensional $\mathcal{N} = 4$ SYM; on the other side, we have Type IIB String Theory compactified on $AdS_5 \times S^5$ with a Ramond-Ramond flux on S^5. The reasoning made so far does not represent a proof of the equivalence of these two theories. Indeed, the two pictures are valid in two incompatible regimes, $g_s N \ll 1$ and $g_s N \gg 1$. Nevertheless, we can conjecture that the low-energy limit we have taken commutes with the variation of g_s that leads from one description to the other, and therefore that the two theories are equivalent.

Since we miss a true derivation of the duality, it is not obvious how far one can conjecture. For instance, one could think that the duality holds only in the supergravity approximation or only in the extreme large-N limit. However, it is by now believed[2] that the duality holds in the following strong meaning:[3]

$U(N)$ $\mathcal{N} = 4$ Super-Yang-Mills theory is exactly dual to Type IIB String Theory compactified on $AdS_5 \times S^5$ with N units of F_5 flux on S^5.

In general, since the bulk is fluctuating, we clearly mean that the spacetime has to be asymptotically $AdS_5 \times S^5$. In the bulk, also the topology may differ from the $AdS_5 \times S^5$ one.

From the discussion above, it is clear that the duality is weak/strong, meaning that in the regime in which one theory is weakly-coupled, the other theory is strongly-coupled. For this reason, on the one hand, the duality is hard to check. On the other hand, it provides an extremely powerful tool since it allows us to perform computations at weak coupling utilizing a theory in order to investigate the strongly-coupled dynamics of the other. In particular, in the large-λ and large-N regime, the classical supergravity approximation is reliable so

---

[2]See, e.g., [70] for some comments on this point.

[3]In fact, which is the precise gauge group that the gravitational theory describes is a subtle point. Indeed, it is often stated that the gauge group is $SU(N)$. The usual argument goes as follows. On one side, the $U(1)$ factor of $\mathcal{N} = 4$ SYM theory is decoupled from $SU(N)$. On the other side, there is no decoupled bulk field; thus, the bulk describes only the $SU(N)$ part of the $U(N)$ gauge group of the $D3$-branes. However, AdS_5 has a boundary. Type IIB string theory features a so-called BF topological theory involving the Type IIB's B_2 and C_2 fields, as we can see from (1.2.6d). Topological theories defined on a manifold with boundaries require the presence of boundary degrees of freedom. In the BF theory in five dimensions, a $U(1)$ gauge field inhabits the manifold boundary. Once one takes care of this point, one retrieves the $U(1)$ factor of the gauge group [71–73].

that computations involving observables of the gauge theory at strong coupling are considerably simplified. Indeed, recalling (1.2.7) and defining the Planck length $l_{Pl}^8 \sim \kappa_{10}$, we have

$$\left(\frac{L}{l_{Pl}}\right)^8 \sim N^2 \ , \qquad \left(\frac{L}{l_s}\right)^8 \sim \lambda^2 \ , \qquad (1.2.46)$$

so at large-N and large λ we can neglect, respectively, quantum gravity and stringy corrections. Looking at the duality in the other direction, we can consider $\mathcal{N} = 4$ SYM theory as a non-perturbative definition of string theory on AdS.

In fact, some checks are easy to perform. First of all, if two theories are equivalent, they have to exhibit the same global symmetries. On the gravitational side, we have a $SO(2,4)$ symmetry coming from the isometries of AdS_5 and a $SO(6)$ symmetry from the those of S^5. Moreover, as we mentioned in section 1.2.1, Type IIB string theory has a $SL(2,\mathbf{Z})$ symmetry. On the gauge theory side, we have the same symmetries. The symmetry $SO(2,4)$ is the conformal symmetry in four dimensions, $SU(4) \simeq SO(6)$ is the R-symmetry and $SL(2,\mathbf{Z})$ is a symmetry that acts on

$$\tau = \frac{\theta}{2\pi} + i\frac{4\pi}{g_{YM}^2} \qquad (1.2.47)$$

as in (1.2.10). Furthermore, both theories have 32 supersymmetry charges.

It is possible to perform other checks of the duality by considering quantities that do not depend on the coupling, so that we can compare the supergravity large-λ result with the gauge theory large-λ ones. For instance, quantities related to anomalies, the spectrum of chiral operators, the moduli space, and renormalization group deformations [35].

We have argued the duality in this particular supersymmetric and conformal case. This is the best-understood example of holographic duality. Holographic dualities between theories with gravity and gauge theories are now believed to hold regardless of supersymmetry and conformal symmetry. For this reason, we generally speak of *gauge/gravity duality*.

Clearly, the gauge theory of major interest is QCD. In general, it is believed that a string holographic theory that is dual to QCD exists. However, it is expected that this holographic theory does not admit any regime for which the classical supergravity approximation might give a reliable description. Nonetheless, we can conceive models that capture aspects of QCD in some relevant regimes. In this direction, there are *bottom-up* models, which are not derived from any string theory construction, as that proposed in [74, 75], and *top-down* ones such as the Witten-Sakai-Sugimoto model [36, 37] reviewed in chapter 2. In this thesis, we focus on the latter model. We will apply it to problems where QCD or hidden QCD-like theories are involved, such as the strong CP problem and the gravitational waves emitted during cosmological first-order transitions predicted by strongly-coupled gauge sectors.

In this section, we have given arguments in favor of the duality. In the next section, we will describe how the physical quantities are mapped by the duality.

1.3 Holographic dictionary

Once the duality is stated, we have to understand how the correspondence works and how it can be exploited to perform computations. The prescriptions that allow us to pass from one side of the duality to the other were proposed in [33, 34] and go under the name of *holographic dictionary.*

The idea is that a field ϕ in the bulk is dual to a gauge-invariant local operator $\mathcal{O}$ of the quantum field theory carrying the same quantum numbers. Boundary conditions have to be imposed on the field, and the restriction ϕ_0 of the field to the boundary[4] acts as a source for the dual operator,

$$S_{QFT} \rightarrow S_{QFT} + \int_{bdry} d^d x \, \phi_0(x) \mathcal{O}(x) \ . \tag{1.3.1}$$

As suggested by (1.2.42), the long-distance region of AdS describes the gauge theory at ultraviolet scales [32, 59, 60]. For this reason, the boundary value of the bulk field is naturally interpreted as a deformation of the bare Lagrangian.

The bulk theory partition function will depend on this boundary condition. At the same time, the boundary field theory partition function depends on the source ϕ_0 - it is a generating functional $Z_{QFT}[\phi_0]$. The duality implies that the partition function of the two theories coincide,

$$Z_{QFT}[\phi_0] = \langle e^{i \int \phi_0 \mathcal{O}} \rangle_{QFT} = Z_{bulk}[\phi_0] \ . \tag{1.3.2}$$

Correlation functions of boundary operators $\mathcal{O}$ can be then computed by taking functional derivatives with respect to ϕ_0,

$$\langle \mathcal{O}(x_1) \dots \mathcal{O}(x_n) \rangle_{QFT} = \frac{1}{i^n} \frac{\delta}{\delta \phi_0(x_1)} \dots \frac{\delta}{\delta \phi_0(x_n)} \log Z_{bulk}[\phi_0] \ . \tag{1.3.3}$$

Clearly, $Z_{bulk}[\phi_0]$ is a very complicated object since it is a quantum gravity (string theory) partition function. However, in the large-N and large-λ limit, we can use the classical supergravity approximation so that

$$Z_{QFT}[\phi_0] = \langle e^{i \int \phi \mathcal{O}} \rangle_{QFT} \approx \exp \left(i S_{class}^{on\text{-}shell}[\phi_0] \right) \ . \tag{1.3.4}$$

On the right-hand side of (1.3.4), the action is the classical supergravity action computed on a solution of the scalar field equation of motion that obeys the chosen boundary condition. In fact, there might be several saddle points. In that case, the right-hand side becomes a sum over the saddle points. Moreover, the on-shell action is typically divergent due to infrared divergences of the bulk. Since the infrared scales of the bulk are mapped into the ultraviolet scales of the boundary theory, these turn out to be ultraviolet divergences of the gauge theory. One then has to introduce specific boundary counterterms in order to cancel the

---

[4]More precisely, ϕ_0 is the boundary restriction of the field ϕ once we extract a suitable power of the holographic coordinate. For example, in the AdS case, for $z \to 0$, $\phi \sim z^{d-\Delta} \phi_0$. If the field ϕ is massive, $d \neq \Delta$ and therefore, strictly speaking, ϕ_0 is not the boundary value of ϕ.

divergences. This procedure can be performed systematically and goes under the name of *holographic renormalization* [76, 77]. We will see in detail specific examples in section 2.6 and chapter 4.

The right-hand side of (1.3.4) is often an easy object to work with. We then see the power of holography: by taking derivative of an on-shell classical action, we compute correlators of the strongly-coupled dual gauge theory.

In order to proceed with the prescription described so far, we should understand which bulk fields are dual to which boundary operators. In general, this is not an easy task. However, there are simple entries of the dictionary: conserved currents. The metric field and gauge fields in the bulk are dual, respectively, to the energy-momentum tensor and conserved vector currents of the dual gauge theory,

$$g_{\mu\nu} \quad \leftrightarrow \quad T_{\mu\nu} \ , \tag{1.3.5a}$$

$$A_\mu \quad \leftrightarrow \quad J_\mu \ . \tag{1.3.5b}$$

Like the metric, the field A has to be integrated in the bulk path integral. Thus, *global symmetries of the boundary theory are dual to gauge symmetries of the bulk theory.*

String theory constructions help in understanding the map between operators. For instance, in the $\mathcal{N} = 4$ SYM case, it is clear from the discussion in subsection 1.2.2 that the dilaton is dual to the Yang-Mills Lagrangian,

$$\phi \leftrightarrow \mathrm{Tr}\, F \wedge *F \ . \tag{1.3.6}$$

and that

$$C_0 \leftrightarrow \mathrm{Tr}\, F \wedge F \ , \tag{1.3.7}$$

Indeed, we implicitly stated these maps when identified the complex coupling τ in (1.2.10) and (1.2.47). By analyzing the near-boundary behavior of fields, one finds that *the mass m of a bulk field ϕ is dual to the scaling dimension Δ of the dual boundary operator,*

$$\mathrm{mass}^2 \leftrightarrow \Delta \ . \tag{1.3.8}$$

For instance, in AdS_{d+1}, the map for a scalar field reads

$$\Delta = \frac{d}{2} + \sqrt{\left(\frac{d}{2}\right)^2 + m^2 L^2} \ , \tag{1.3.9}$$

where L is the AdS radius. As a consequence,

- if $m^2 > 0$, then $\Delta > d$ and $\mathcal{O}$ is irrelevant

- if $m^2 = 0$, then $\Delta = d$ and $\mathcal{O}$ is marginal

- if $m^2 < 0$, then $\Delta < d$ and $\mathcal{O}$ is relevant

A peculiar property of AdS spacetime is that scalar fields with negative mass squared do not lead to instabilities as long as they obey the Breitenlohner-Freedman bound [78, 79]

$$m^2 L^2 \geq -\left(\frac{d}{2}\right)^2 . \tag{1.3.10}$$

By using (1.3.4), we can compute correlation functions of local operators of the boundary theory. Gauge theories are characterized by non-local observables as well. An important example is the Wilson loop,

$$W[C] = \text{Tr} \exp\left(i \int_C A\right) , \tag{1.3.11}$$

where C is a closed curve on the boundary, and the trace is taken in the fundamental representation of the gauge group. Its importance relies on the fact that it constitutes an order parameter for deconfinement [80]. Let us take C to be the rectangle with sides of length τ and l lying on the Euclidean (t, x_1) subspace. The correlator $\langle W[C] \rangle$ gives the amplitude of an infinitely massive quark/antiquark pair separated by a distance l that propagates for a time τ. In the large-τ limit, such correlator yields the quark/antiquark potential $V(l)$,

$$\langle W[C] \rangle \sim \exp\left(-\tau V(l)\right) . \tag{1.3.12}$$

If the potential $V(l)$ is linear in l, the argument of the exponential in (1.3.12) is proportional to the area τl enclosed by the curve C. It is then said that the Wilson loop obeys the *area law*, which, in turn, is usually taken as a definition of confinement.

The holographic prescription for computing the Wilson loop correlator $\langle W[C] \rangle$ was proposed in [81, 82] and states that $\langle W[C] \rangle$ is holographically computed by evaluating the gravity path integral with the insertion of a string worldsheet ending on C.[5] In the supergravity approximation, the leading contribution comes from the area of the minimal surface D that terminates on C, namely from the on-shell Nambu-Goto action S_{NG}

$$S_{NG}[D] = \frac{1}{2\pi\alpha'} \int d^2\sigma \sqrt{\det g_{|_D}} , \tag{1.3.13}$$

where $g_{|_D}$ indicates the pullback of the metric on the worldsheet D. Thus,

$$\langle W[C] \rangle \approx e^{-S_{NG}^{on\text{-}shell}[D]} . \tag{1.3.14}$$

We again see that, in the supergravity approximation, a challenging quantum field theory computation is mapped into a doable area-minimization computation. Similarly to (1.3.4), the on-shell Nambu-Goto action is usually divergent due to the infinite bulk volume. However, the divergence cancels after one considers a

---

[5]In fact, this prescription yields the correlator of a generalized (eventually supersymmetric) version of the Wilson loop (1.3.12) [81, 82].

boundary local term, motivated by the need to impose Neumann rather than Dirichlet boundary conditions [83].

In the $\mathcal{N} = 4$ SYM case, the leading order computation in the supergravity approximation $\lambda \to \infty$, $N \to \infty$ gives the quark/antiquark potential

$$V(l) = -\frac{4\pi^2}{\Gamma\left(\frac{1}{4}\right)^4}\frac{\sqrt{\lambda}}{l} \ . \tag{1.3.15}$$

The result at small λ reads [84]

$$V(l) = -\frac{\pi\lambda}{l} \ . \tag{1.3.16}$$

It is interesting to notice that the strongly-coupled result (1.3.15) is non-analytic in λ, a result that cannot be found with finite-order perturbation theory. Concerning the dependence on l, the fact that we do not get an area law from the computation of a minimal-surface area may be deemed as surprising. In fact, the Coulomb $1/l$ behavior of the potential is dictated by the theory's conformal symmetry. If we rescale the path C, we can rescale D so that its regularized area remains constant. Recalling that the scale transformations as in 1.2.2 involve the holographic coordinate, we see that such a rescaling is possible because the AdS holographic coordinate ranges from zero to infinity. The result changes if the background ends at a finite value z_0 of the holographic coordinate. In section 2.1, we will compute the quark/antiquark potential for the Witten-Sakai-Sugimoto model, which exhibits confining behavior in the low-temperature phase as a result of this fact.

Even though the ideas underlying the holographic dictionary hold in general in holography, so far we have implicitly assumed that the gauge theory inhabits $\mathbf{R}^{1,3}$ or, eventually, $\mathbf{R} \times S^3$.[6] Let us briefly comment on what happens when the gauge theory is defined on more general manifolds [33, 36]. This is relevant, for instance, when one studies the theory at finite temperature because, in that case, one compactifies the Euclidean time direction on a circle S^1. Moreover, to analogously compactify on a circle S^1 is a way of breaking conformal symmetry and supersymmetry, as one would like to do for QCD. We will come back to both these two points in chapter 2.

When the gauge theory is defined on a d-dimensional manifold M_d, in the supergravity limit, one has to consider all the backgrounds X that asymptotically become M_d (or $M_d \times W$ for some compact W manifold). It may occur that a manifold cannot be obtained as the boundary of another manifold. In this case, the holographic dual background might contain defects such as branes. Moreover, if a choice of spin structure is made in the boundary gauge theory, one must consider only bulk backgrounds on which the chosen spin structure can be extended.

---

[6]The first or the second case occurs depending on whether we consider, respectively, the AdS Poincaré patch or global AdS.

Let us consider $\mathcal{N} = 4$ SYM theory on $S^1 \times S^3$, and let us call $\beta = 1/T$ the length of S^1, which is interpreted as the inverse temperature. This manifold admits two different spin structures, depending on whether fermions obey periodic or antiperiodic boundary conditions. Imposing antiperiodic boundary conditions, we get the canonical ensemble partition function,

$$Z_{QFT} = \text{Tr}\, e^{-\beta H} = e^{-\beta F} \ , \tag{1.3.17}$$

where F is the free energy. In the supergravity approximation, the latter can be easily computed by evaluating on-shell the supergravity action. With periodic boundary conditions for the fermions, in contrast, the partition function reads

$$Z_{QFT} = \text{Tr}\, e^{-\beta H} (-1)^F \ , \tag{1.3.18}$$

where $(-1)^F$ is the fermion number operator.[7] Since the sphere S^n can be obtained as the boundary of the ball D_{n+1}, there are two backgrounds that are asymptotically $S^1 \times S^3$, namely $X_1 = S^1 \times D_4$ and $X_2 = D_2 \times S^3$. Since X_1 features a S^1 factor, both spin structures are consistent with it, and therefore it contributes to both (1.3.17) and (1.3.18). However, since X_2 is simply-connected, it is only consistent with antiperiodic boundary conditions for fermions on the boundary S^1, and therefore it can only contribute to (1.3.17).

When one studies a theory at finite temperature, if there are several contributing backgrounds, one has to compare their free energy contribution in order to establish which one dominates. By varying the temperature, two backgrounds may contribute by an equal amount. In this case, the system undergoes a first-order phase transition. In section 2.6, we will see this in the context of the Witten background relevant for QCD. This will be relevant for chapter 4, where two first-order phase transitions in the Witten-Sakai-Sugimoto model are studied in detail.

---

[7]We are using F for both the fermion number operator and the free energy. However, there should be no risk of confusion.

Chapter 2

The Witten-Sakai-Sugimoto model

In this chapter, we review the Witten-Sakai-Sugimoto model, the top-down holographic model that better resembles low-energy $4d$ QCD in the planar limit. It is a (3+1)-dimensional non-supersymmetric Yang-Mills theory with gauge group $SU(N)$ coupled to a tower of adjoint Kaluza-Klein (KK) fields and to N_f fundamental flavors (quarks) [36, 37] (see also [85] for a review). The model possesses five independent parameters. Two of them are actually dimensional quantities: M_{KK}, which represents the dynamically generated scale providing the mass of the first glueball and that of the first KK field, and L, which determines the scale of chiral symmetry breaking, as we will discuss. The other three dimensionless parameters are given by N, N_f, and the 't Hooft coupling λ at the scale M_{KK}. We will mainly consider the regime

$$N \gg 1 \ , \qquad \lambda \gg 1 \ , \qquad \frac{N_f}{N} \ll 1 \ . \qquad (2.0.1)$$

The model's properties at low energies are very similar to the real-world QCD ones since they include confinement, mass gap, and chiral symmetry breaking.

The model's phase diagram features two first-order phase transitions. The first separates the confining phase from the deconfined one, and one occurs at temperature $T_c = M_{KK}/2\pi$. The second one separates the chiral symmetry broken phase from the chirally symmetric one. As we will review in chapter 4, where the two first-order phase transitions are studied in detail, depending on the parameter L, the chiral symmetry phase transition coincides with the confinement phase transition or occurs at a higher critical temperature.

The holographic dual theory is obtained starting from a Type IIA string theory brane construction. A stack of N $D4$-branes wrapped on a circle S^1 yields the theory's gauge sector, whereas N_f pairs of $D8/\overline{D8}$ branes give the fields in the fundamental representation of $SU(N)$, namely quarks. In the $N_f \ll N$ limit, the $D8$-branes can be treated as probes in the background generated by the $D4$-branes, and therefore can be studied using the Dirac-Born-Infeld action (1.2.29) or, eventually, its non-Abelian generalization. The background's geometry encodes in a simple way confinement, mass-gap, and chiral symmetry breaking and provides analytical computation control on these highly non-trivial phenomena.

The chapter is organized as follows. In section 2.1, we study the Witten background that describes the WSS model's gauge sector in the low-temperature phase. We derive the relation between string and field theory parameters, and comment on the validity regime of the model's description via the Witten background. By computing the rectangular Wilson loop expectation value in the supergravity approximation, we will find a linear quark/antiquark potential, and therefore confinement. Finally, we argue that the background is dual to a theory that exhibits a mass gap.

In section 2.2, we show how the $D8$-branes introduce quarks in the gauge theory. We then study the embedding of the $D8$-branes on the Witten background.

In section 2.3, we derive from the DBI action of the $D8$-branes the effective chiral Lagrangian that describes the physics of pions. This also includes the Skyrme term that stabilizes the baryons. We then find the expression of the pion decay constant and the Skyrme coefficient in terms of the model's parameters.

Section 2.4 deals with a model's deformation dual to introducing a current-algebra quark mass term in the pion effective Lagrangian.

Section 2.5 deals with deforming the Witten background to include the θ-angle QCD term in the Lagrangian and with the chiral anomaly.

In section 2.6, we address the model at finite temperature. Applying holographic renormalization, we compute the model's free energy and find the above-mentioned confinement first-order phase transition. We then briefly discuss how different choices of boundary conditions for the $D8$-branes correspond to different phase diagrams for what concerns chiral symmetry.

Finally, in appendix 2.A, we briefly review the effective chiral Lagrangian approach to low-energy QCD, including the effects of the θ angle and the chiral anomaly and its generalization that includes the QCD axion.

2.1   Witten background

In chapter 1, we saw that a stack of N $D3$-branes has a low-energy dynamics described by four-dimensional $\mathcal{N} = 4$ Super-Yang-Mills theory, which exhibits superconformal symmetry. In order to build a model with at least the qualitative features of QCD, we would like to break these symmetries. A way to achieve this through a string theory brane construction was proposed by Witten in [36].

The idea is the following. Let us consider a stack of N $D4$-branes with worldvolume $\mathbf{R}^{1,3} \times S^1$, and let us call M_{KK} the inverse radius of S^1. A five-dimensional $U(N)$ gauge theory inhabits the worldvolume of the $D4$-branes. After compactification on the S^1, we have a four-dimensional vector A_μ, a scalar A_4 and five scalars φ^I, besides the fermionic partners. As we mentioned in section 1.3, when the gauge theory is studied on a manifold with a S^1 factor, we have to choose a spin structure. In order to break supersymmetry, we choose (anti)periodic boundary conditions for the bosonic (fermionic) fields. In this way, the fermions take a mass $\sim M_{KK}$ at tree level, whereas the traceless components of the scalars A_4 and φ^i are expected to take mass $\sim \lambda M_{KK}$ at one-loop level [36].

The trace components of the scalars remain massless due to the shift symmetry $\text{Tr}\, A_4 \to \text{Tr}\, A_4 + \alpha\mathbb{1}$. Nevertheless, their couplings with the other massless fields are IR-irrelevant, and therefore they are not expected to affect the low-energy dynamics.

At low energy, we are left with a massless gauge field, thus with $U(N)$ Yang-Mills theory. Since the $D4$-branes break $SO(1,9)$ into $SO(1,4) \times SO(5)$, the construction introduces a $SO(5)$ global symmetry, which QCD does not display. For the purpose of confronting the model with QCD, we will thus have to restrict our attention to $SO(5)$-singlet states. We will refer to the gauge theory devised as above as the *Witten-Yang-Mills (WYM) theory.*

Let us discuss the dual gravitational theory. According to the holographic prescription described in subsection 1.3, the dual gravitational background has to be topologically $\mathbf{R}^{1,3} \times D_2$, where D_2 is a disk such that $\partial D_2 = S^1$. Being simply-connected, D_2 admits only antiperiodic fermions, consistently with our choice of boundary conditions. Disk topologies arise in Euclidean black hole solutions, so let us look at the non-extremal solution (1.2.23) with $p = 4$. In fact, since we are looking for a solution with Lorentz signature and a disk topology, we have to perform two Wick rotations on (1.2.23), one along the time direction, and the other one along a spatial coordinate, which we call x_4. Taking the Maldacena limit[1] (1.2.45) of this solution, we obtain the background[2]

$$ds^2 = \left(\frac{u}{R}\right)^{3/2} \left[\eta_{\mu\nu}dx^\mu dx^\nu + f(u)dx_4^2\right] + \left(\frac{R}{u}\right)^{3/2} \left[\frac{du^2}{f(u)} + u^2 d\Omega_4^2\right]\,, \quad (2.1.1a)$$

with

$$e^\phi = g_s \left(\frac{u}{R}\right)^{3/4}\,, \qquad\qquad f(u) = 1 - \frac{u_0^3}{u^3}\,, \qquad\qquad (2.1.1b)$$

$$F_4 = dC_3 = \frac{3R^3}{g_s}\omega_4\,, \qquad\qquad R^3 = \pi g_s N l_s^3\,. \qquad\qquad (2.1.1c)$$

A notable difference with respect to the $\text{AdS}_5 \times S^5$ background is that (2.1.1) exhibits a running dilaton. This is related to the fact that the theory is non-conformal, as one can see by remembering that the dilaton gives the coupling to the $\text{Tr}\, F \wedge *F$ operator of the five-dimensional theory on the $D4$-branes. Below, we will come back to this point. The background (2.1.1) features a sphere S^4, whose isometries give the above-mentioned $SO(5)$ symmetry of the model.

The D_2 disk, usually called *cigar* in the WSS literature, is found in the (x_4, u) subspace. As we will see, it encodes the qualitative features of the gauge theory, namely mass-gap and confinement. Moreover, as we will see in sections 2.2 and 2.3, it enforces chiral symmetry breaking.[3]

---

[1]In the non-extremal case, r_0/α' is also kept fixed in the near-horizon limit.

[2]In conformity with the Witten-Sakai-Sugimoto literature, we rename $r \to u$ the holographic radial coordinate.

[3]The vice-versa of this statement is not true. Indeed, in section 2.6 we will see that the

Let us consider the region around $u = u_0$. The requirement of the absence of conical singularities imposes a relation between the parameter u_0 and the S^1 radius M_{KK}^{-1}. Expanding around $u = u_0$, the (x_4, u) part of the metric reads

$$ds^2_{(x_4,u)} = \frac{3u_0^{1/2}}{R^{3/2}}(u - u_0)dx_4^2 + \frac{R^{3/2}}{3u_0^{1/2}}\frac{du^2}{u - u_0} , \qquad (2.1.2)$$

By changing coordinates according to

$$\theta(x_4) = M_{KK}x_4 , \qquad r(u) = \frac{2}{\sqrt{3}}\left(\frac{R^3}{u_0}\right)^{1/4}\sqrt{u - u_0} , \qquad (2.1.3)$$

we find

$$ds^2_{(x_4,u)} = \frac{9u_0}{4R^3M_{KK}^2}r^2d\theta^2 + dr^2 . \qquad (2.1.4)$$

This is the metric of a cone with angle α given by $\sin\alpha = 9u_0/4R^3M_{KK}^2$. The conical singularity disappears if

$$u_0 = \frac{4}{9}R^3M_{KK}^2 . \qquad (2.1.5)$$

The coupling of the $(p+1)$-dimensional Yang-Mills theory living on the Dp-brane's worldvolume is related to the string coupling constant through (1.2.38), that is

$$g_{p+1}^2 = (2\pi)^{p-2}g_s l_s^{p-3} . \qquad (2.1.6)$$

The coupling of the four-dimensional gauge theory at the scale M_{KK} is obtained by g_5, after compactification on S^1. In particular, we will work with the 't Hooft coupling

$$\lambda = M_{KK}\frac{g_5^2}{2\pi}N = 2\pi g_s M_{KK}l_s N . \qquad (2.1.7)$$

The relation between the string theory parameters (R, u_0, g_s) and the field theory ones (M_{KK}, λ, l_s) is

$$g_s l_s = \frac{1}{2\pi}\frac{\lambda}{M_{KK}N} , \qquad \frac{R^3}{l_s^2} = \frac{1}{2}\frac{\lambda}{M_{KK}} , \qquad \frac{u_0}{l_s^2} = \frac{2}{9}\lambda M_{KK} . \qquad (2.1.8)$$

We will express some of the results in terms of the 't Hooft coupling

$$\lambda_{YM} \equiv 2\lambda = 4\pi g_s M_{KK}l_s N . \qquad (2.1.9)$$

This convention is suitable for comparison with the field theory results, which are customarily written using the conventions outlined in section 1.1.

We expect that the background (2.1.1) provides a reliable description of the WYM theory in the large-N, large-λ regime. Let us discuss this in more detail.

(x_4, u) subspace of the background describing the WSS at high temperatures is a cylinder (rather than a disk) and nonetheless admits a chiral symmetry breaking brane configuration.

The supergravity approximation works as long as the background's curvature is small in string units, namely when the curvature radius is large. The smallest value of the curvature radius is reached at $u = u_0$ and it is of order $(u_0 R^3)^{1/4}$. Using (2.1.8),

$$\frac{(u_0 R^3)^{1/2}}{l_s^2} \sim \lambda \ , \tag{2.1.10}$$

we see that the supergravity description is reliable as long as

$$\lambda \gg 1 \ . \tag{2.1.11}$$

Unfortunately, in the limit $\lambda \gg 1$, the spurious fields that make the Witten theory differ from Yang-Mills theory, namely the adjoint scalars and fermions, do not decouple from the dynamics. Their mass is expected to be of order M_{KK}. Thus, we would like to work in a regime where M_{KK} is greater than the Yang-Mills dynamical scale Λ_{QCD}. However, the relation between these two scales takes the form (1.1.5), that is

$$\Lambda_{QCD} \sim M_{KK} \exp\left(-\frac{c}{\lambda}\right) \ , \tag{2.1.12}$$

and therefore, in the supergravity limit $\lambda \gg 1$, the two scales coincide. As a consequence, asymptotic freedom will not appear in the supergravity approximation.

Furthermore, in the ultraviolet limit $u \to \infty$, the dilaton diverges. This reflects the non-renormalizability of the five-dimensional Yang-Mills theory living on the $D4$-brane worldvolume. The ultraviolet completion is provided by realizing the $D4$-branes of Type IIA string theory as M5-branes of $11d$ M-theory, compactified on a circle S^1 with supersymmetry-preserving spin structure [36]. The six-dimensional quantum field theory living on these branes is the so-called $\mathcal{N} = (2,0)$ superconformal theory. The Type IIA supergravity description is thus reliable as long as the dilaton does not become too large [86]. Let us define a critical value of the holographic coordinate u_{crit} through $e^{\phi_{crit}} = 1$, and let us demand $u_{crit} \gg u_0$. Recalling (2.1.1b) and (2.1.8),

$$u_{crit}^3 \sim N^4 l_s^6 M_{KK}^3 \lambda^{-3} \gg u_0^3 \sim \lambda^3 M_{KK}^3 l_s^6 \ , \tag{2.1.13}$$

and therefore

$$N^{2/3} \gg \lambda \ . \tag{2.1.14}$$

In order to perform computations in the large-N, large-λ limit beyond the bound (2.1.14), one has to work with the $\text{AdS}_7 \times S^4$ $11d$ supergravity solution dual to the $\mathcal{N} = (2,0)$ superconformal theory. We will use such a solution in subsection 3.3.2.

Confinement and mass gap

One of the most important features of $SU(N)$ Yang-Mills theory in four dimensions is confinement. We now show that the Witten-Yang-Mills theory is confining as well. As we discussed in section 1.3, confinement is defined through the

area–law behavior of the rectangular Wilson loop, which gives the amplitude of quark/antiquark probe pair separated by a distance l that propagate for a time interval τ. According to the Wilson loop's holographic prescription, in the supergravity approximation, we have to find the minimal surface Σ that ends on the Wilson loop path C at the boundary. In this case, C is the rectangle of lengths τ and l. The worldsheet area is computed by the Nambu-Goto action

$$S_{NG} = \frac{1}{2\pi\alpha'} \int d^2\sigma \sqrt{\det g_{|_\Sigma}} \, , \tag{2.1.15}$$

where $g_{|_\Sigma}$ indicates the pullback of the metric on the worldsheet Σ. Choosing x_0 and x_1 as worldsheet coordinates, it reads

$$ds^2_{\Sigma} = \left(\frac{u}{R}\right)^{3/2} dx_0^2 + \left(\frac{u}{R}\right)^{3/2} \left[1 + \left(\frac{R}{u}\right)^3 \frac{u'^2}{f(u)}\right] dx_1^2 \, , \tag{2.1.16}$$

so that

$$S_{NG} = \frac{\tau}{2\pi\alpha'} \int_{-l/2}^{+l/2} dx_1 \left(\frac{u}{R}\right)^{3/2} \sqrt{1 + \left(\frac{R}{u}\right)^3 \frac{u'^2}{f(u)}} \, , \tag{2.1.17}$$

where we have integrated along x_0. Since the integrand does not explicitly depend on x_1 we have a first integral, which allows us to write

$$\frac{\left(\frac{u}{R}\right)^{3/2}}{\sqrt{1 + \left(\frac{R}{u}\right)^3 \frac{u'^2}{f(u)}}} = \left(\frac{u_*}{R}\right)^{3/2} \, , \tag{2.1.18}$$

where u_* is the string's turning point, for which $u' = 0$. From this equation we find

$$u' = \pm\sqrt{f(u)} \left(\frac{u}{R}\right)^{3/2} \sqrt{\left(\frac{u}{u_*}\right)^3 - 1} \, . \tag{2.1.19}$$

Thus,

$$l = \int_{-l/2}^{l/2} dx_1 = 2 \int_{u_*}^{\infty} \frac{du}{u'} = \frac{2R^{3/2}}{u_*^{1/2}} \int_1^{\infty} dy \frac{1}{\sqrt{(y^3 - a^3)(y^3 - 1)}} \, , \tag{2.1.20}$$

where $a = u_0/u_*$. For large l, we have that $a \to 1$. It is useful to compare this behavior with the conformal case saw in section 1.3. In that case, the background displays a warp factor g_{00} that ranges from zero to infinity. Because of this, the worldsheet entering the holographic Wilson loop computation is allowed to probe bulk regions corresponding to arbitrarily small values of the gauge theory's energy scale.[4] As a result, it is allowed to keep constant the renormalized worldsheet

---

[4]Using the holographic coordinate r as in (1.2.19), in which infrared gauge theory's energy scales correpond to small values of r, $g_{00} \to 0$ for $r \to 0$. One finds [81] the the string's turning point r_* satisfies $r_* \sim L^2/l$. Since r ranges from zero to infinity, the string is allowed to go to arbitrarily small values of r.

area after rescalings of l. In contrast, the Witten background displays a warp factor that has a minimum given by $g_{00}(u_0) > 0$, which prevents the string to probe arbitrarily infrared regions. The more l grows, the more the worldsheet bends close to the $u = u_0$ surface. In the limit of very large l, the worldsheet takes a rectangular shape in the (u, x_1) plane. The two constant-x_1 lines are interpreted as the (infinite) rest mass of the quarks, which has to be subtracted in order to find the quark/antiquark potential. As a result, the latter is computed by the Nambu-Goto action evaluated on the $u = u_0$ surface,

$$S_{NG}^{class} = \frac{\tau l}{2\pi l_s^2}\left(\frac{u_0}{R}\right)^{3/2} . \tag{2.1.21}$$

The action goes as τl, which is the area enclosed by the Wilson loop, confirming that the Witten background is confining. Using (2.1.8), the quark/antiquark potential reads

$$V_{q\bar{q}} = \frac{2}{27\pi}\lambda M_{KK}^2 l . \tag{2.1.22}$$

From this, we read the string tension

$$\sigma = \frac{2}{27\pi}\lambda M_{KK}^2 . \tag{2.1.23}$$

We have seen that a crucial role for confinement is played by the fact that the warp factor $g_{00}(u)$ has a non-vanishing minimum. This is also the reason underlying the presence of a mass-gap. A theory exhibits a mass-gap when its lightest state has energy strictly greater than zero. The bound states of a pure gauge theory are called *glueballs*, and can be holographically studied by considering small fluctuations of the supergravity fields around the Witten background. For instance, for the dilaton ϕ we have to study

$$\Box\phi(x^\mu, u) = 0 . \tag{2.1.24}$$

Because of the Poincaré invariance along the $\{x^\mu\}$-subspace, we look for solutions of the form

$$\phi(x^\mu, u) = e^{ik\cdot x}\varphi(u) . \tag{2.1.25}$$

Since the spacetime is not compact, a discrete spectrum might be unexpected. In fact, if the time needed by a light-ray to travel in the holographic direction from one spacetime's extreme to the other is finite, the spectrum is discrete [87]. Indeed, using the time-of-flight coordinate s defined by

$$s(u) = \int_{u_0}^{u} du' \sqrt{\frac{g_{uu}}{|g_{00}|}} , \tag{2.1.26}$$

the Laplace equation (2.1.24) becomes the Schrodinger equation

$$\left[-\frac{d^2}{ds^2} + V(s) + k^2\right]\psi(s) = 0 , \tag{2.1.27}$$

where we redefined the field in order to cancel the terms with first derivatives. If s is bounded, (2.1.27) is the quantum mechanics problem of a particle in a box, for which the spectrum is discrete. From (2.1.26), we see that the presence of the mass gap depends on whether the warp factor $g_{00}(u)$ vanishes at its minimum value or not. For the Witten background, $g_{00}(u_0) > 0$ and therefore s turns out to be finite,[5]

$$\bar{s} = s(u \to \infty) = \frac{R^{3/2}}{u_0^{1/2}} \int_1^\infty \frac{dx}{\sqrt{x^3 - 1}} = 2\sqrt{\pi} \frac{\Gamma\left(\frac{7}{6}\right)}{\Gamma\left(\frac{2}{3}\right)} \frac{R^{3/2}}{u_0^{1/2}} \ . \qquad (2.1.28)$$

If one numerically solves (2.1.27) imposing normalizability and the regularity condition

$$\partial_s \psi(s)\big|_{s=0} = 0 \ , \qquad (2.1.29)$$

one indeed finds that the spectrum is discrete and exhibits only states with negative values of $k^2 = -m^2$. This proves the presence of the mass-gap. The detailed glueball spectrum was computed in [88], and exhibits features similar to those found with lattice methods [89]. For a detailed account of the quantitative predictions given by the Witten background and a comparison with the lattice findings, see [85].

2.2   Fundamental matter

The $D4$-branes discussed in section 2.1 provide adjoint fields coming from the 4-4 open string sector, where 4-4 indicates that both the endpoints of the strings lie on the $D4$-branes' worldvolume. In order to obtain a QCD-like theory, we would like to introduce fields transforming in the fundamental representation of the gauge group, namely quarks. This can be achieved by introducing N_f pairs of $D8/\overline{D8}$-branes, as shown by Sakai and Sugimoto in [37].

Let us consider the weak-coupling regime in which both $D4$ and $D8$ branes are thought of as hyperplanes where open strings end. Their configuration is such that the $D4$-branes extend over $\mathbf{R}^{1,3} \times S^1$ while the $D8$-branes extend over all the directions but x_4, the coordinate on the S^1. Along x_4, the $D8$-branes are separated from the $\overline{D8}$-branes by a distance $L \le \pi M_{KK}^{-1}$. On the worldvolume of the $D4$, $D8$ and $\overline{D8}$ branes there are, respectively, a $U(N)$, a $U(N_f)_{D8}$ and a $U(N_f)_{\overline{D8}}$ gauge symmetry.

After the introduction of the $D8$-branes we have new open string sectors: 8-8, $\bar{8}$-$\bar{8}$, 8-$\bar{8}$, 4-8, and 4-$\bar{8}$. The 4-8 sector provides fields that transform in the fundamental representation of $U(N)$ and in the fundamental representation of $U(N_f)_{D8}$. Analogously for the 4-$\bar{8}$ sector. The low-energy spectrum depends on the number ν of spacetime directions where mixed Dirichlet-Neumann conditions are imposed [90]. The zero-point energy of the Neveu-Schwarz sector a_{NS} is given

---

[5]The analogous calculation for the $\mathrm{AdS}_5 \times S^5$ background describing the conformal $\mathcal{N} = 4$ SYM theory yields a divergent result.

by

$$a_{NS} = -\frac{1}{2} + \frac{\nu}{8} \; . \tag{2.2.1}$$

The $D4/D8$ system of our interest is characterized by $\nu = 6$. As a result, a_{NS} is greater than zero and thus there are neither massless nor tachyonic bosonic fields. In contrast, the zero-point energy of the Ramond sector always vanishes. As a result, the spectrum displays two massless fermions of opposite chiralities from the 4-8 strings and two fermions of opposite chiralities from the 4-$\bar{8}$ sector. The GSO projection selects a fermion with a given chirality in the 4-8 sector and the fermion with the opposite chirality in the 4-$\bar{8}$ sector [91]. As a result, we are left with two Weyl fermions of opposite chiralities, placed at different points along S^1, since the massless fields live at the intersections of the $D4$ and the $D8$-branes.

The 8-8 and $\bar{8}$-$\bar{8}$ sectors, which define a $U(N_f)_{D8}$ and a $U(N_f)_{\overline{D8}}$ gauge theory, decouple in the Maldacena limit $\alpha' \to 0$ for the $D4$-branes, as can be seen from the ratio of their couplings [53]

$$\frac{g_9}{g_5} \sim \alpha'^2 \; . \tag{2.2.2}$$

As a consequence, $U(N_f)_{D8}$ and $U(N_f)_{\overline{D8}}$ will be global symmetries. Since the $D8$ and the $\overline{D8}$-branes provide fields with opposite chiralities, the global symmetry will be $U(N_f)_L \times U(N_f)_R$, as it occurs in classical massless QCD.

Finally, the 8-$\bar{8}$ sector is given by stretched strings and therefore does not provide local massless excitations. We will discuss its interpretation in section 2.4.

Let us consider the picture at strong coupling. We recall that the Witten background (2.1.1) that describes the backreaction of the N $D4$-branes is found from a solution of the equations of motion derived from the action S_{IIA} in (1.2.11). Since now we also have the $D8$-branes, in principle, we should find a solution of the equations of motion derived from the action

$$S = S_{IIA} + S_{D8} + S_{\overline{D8}} \; , \tag{2.2.3}$$

where S_{D8} and $S_{\overline{D8}}$ are given by the DBI action and their Chern-Simons coupling. In general, this is a difficult problem. However, in the regime $N_f \ll N$, we can work in the *probe approximation* where we neglect the backreaction of the $D8$-branes on the geometry [92] and embed them as probes in the Witten background (2.1.1).

At the end of section 1.1, in the context of the $1/N$ expansion of QCD, we pointed out that the diagrams that include quark loops are suppressed if we keep the number of quarks N_f fixed in the large-N limit. Indeed, they introduce boundaries into the diagrams. Consistently, quarks are holographically introduced through open string sectors, namely D-branes, and their backreaction is negligible if $N_f \ll N$.

In chapter 1, we saw that bulk closed string modes are dual to gauge-invariant local operators of the boundary theory. We now also have bulk open string

modes, the fluctuations of the probe branes. These are meant to be dual to gauge-invariant local operators involving fundamental fields [92], namely mesons operators.

In the probe approximation $N_f \ll N$, we can treat the $D8$-branes using the DBI action evaluated on the background (2.1.1) produced by the $D4$-branes. The $D8$-brane will be characterized by a profile $x_4 = x_4(u)$, which depends on the boundary conditions we impose. In general, we impose boundary conditions such that the $D8$-branes are separated from the $\overline{D8}$-branes by a distance $L \leq \pi M_{KK}^{-1}$ along the circle x_4 at the boundary. When the equality holds, the embedding is called *antipodal*.

The cigar geometry is a smooth disk, hence $D8$ and $\overline{D8}$ branes are bounded to join at a value $u_J \geq u_0$ of the holographic coordinate, where the equality holds in the antipodal case. We have said that the gauge symmetry on the $D8$ and $\overline{D8}$ worldvolume induces a global $U(N_f)_L \times U(N_f)_R$ flavor symmetry from the boundary gauge theory's point of view. In the joined configuration, a single gauge field appears and as a consequence, only the diagonal $U(N_f)_V$ transformations preserve the vacuum configuration. We will come back to this point in section 2.3.

Let us determine the $D8$-branes' embedding. The DBI action reads[6]

$$S_{D8} = -\frac{\mu_8 V_{3+1}}{g_s} V_4 \int dx_4 u^4 \sqrt{f(u) + \left(\frac{R}{u}\right)^3 \frac{u'^2}{f(u)}} \ , \qquad (2.2.4)$$

where V_{3+1} and V_4 are, respectively, the (infinite) spacetime volume and the S^4 volume and $\mu_8 = (2\pi)^{-8} l_s^{-9}$. The prime indicates the derivative with respect to x_4. Since the Lagrangian does not depend explicitly on x_4, there is a first integral,

$$\frac{u^4 \sqrt{f(u)}}{\sqrt{1 + \left(\frac{R}{u}\right)^3 \frac{u'^2}{f^2(u)}}} = u_J^4 \sqrt{f(u_J)} \ , \qquad (2.2.5)$$

where u_J is the point in which $u'(x_4) = 0$. Let us consider first the case $u_J \neq u_0$. From (2.2.5), we obtain the differential equation

$$\frac{du}{dx_4} = \pm f(u) \left(\frac{u}{R}\right)^{3/2} \sqrt{\left(\frac{u}{u_J}\right)^8 \frac{f(u)}{f(u_J)} - 1} \ . \qquad (2.2.6)$$

Solving the equation with one sign we find the profile for one branch. The other branch is found by symmetry. Figure 2.1 offers a pictorial representation of the branes' configuration for both the antipodal and the non-antipodal cases.

The profile reads

$$x_4(u) = R^{3/2} u_J^4 \sqrt{f_J} \int_{u_J}^u \frac{du}{u^{3/2} f(u) \sqrt{u^8 f(u) - u_J^8 f_J}} \ . \qquad (2.2.7)$$

---

[6]In the following, in order to avoid a proliferation of notations, we will write S_{D8} even though we may be focusing on a subset of its terms. We hope the reader will not be confused by this.
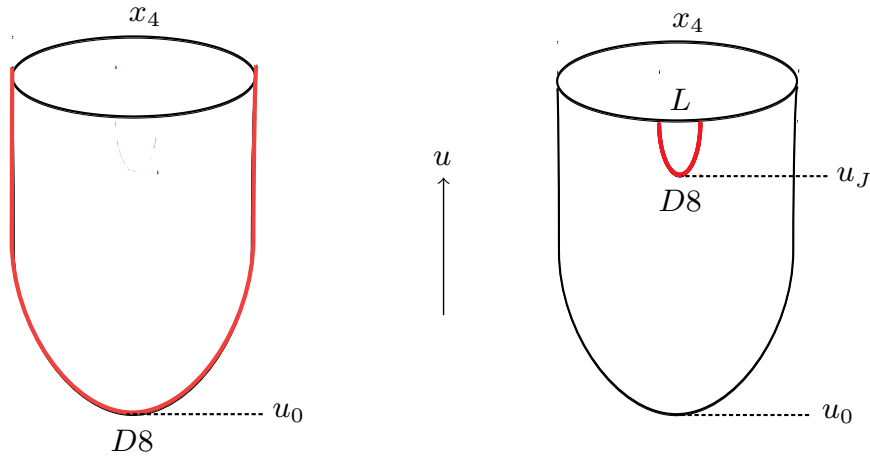
Figure 2.1. *Pictorial representation of the probe D8-brane's embedding in the cigar geometry with antipodal (left) and non-antipodal (right) boundary conditions.*

The brane separation L is computed through

$$L = \int dx_4 = 2 \int_{u_J}^{\infty} \frac{du}{u'} = 2R^{3/2} \int_{u_J}^{\infty} \frac{du\, u^{-3/2}}{f(u)\sqrt{\left(\frac{u}{u_J}\right)^8 \frac{f(u)}{f(u_J)} - 1}} \ . \tag{2.2.8}$$

Performing the change of variable $u = u_J v^{-1/3}$ and defining $b = u_0/u_J$, the brane separation reads

$$L = J(b)R^{3/2}u_J^{-1/2} \ , \tag{2.2.9}$$

where

$$J(b) = \frac{2}{3}\sqrt{1-b^3} \int_0^1 dv \, \frac{v^{1/2}}{(1-b^3v)\sqrt{1-b^3v-(1-b^3)v^{8/3}}} \ . \tag{2.2.10}$$

As a result, the value u_J decreases if L increases.

Let us consider the case $u_J = u_0$. From (2.2.6), we see that in this case $x_4(u)$ is a constant function. By symmetry, this corresponds to the case in which we take antipodal boundary conditions, so that

$$x_4(u) = \pm\frac{\pi}{2M_{KK}} \ . \tag{2.2.11}$$

The antipodal boundary conditions are those suitable for describing QCD. In the remaining of this chapter, we will consider this case. In chapter 3, we will show that by introducing in the WSS model an extra $D8/\overline{D8}$ pair with non-antipodal boundary conditions, the QCD axion appears in the low-energy spectrum.

In the antipodal case, it is useful to introduce new coordinates on the cigar:

$$y = r\cos\left(M_{KK}x_4\right) \ , \qquad z = r\sin\left(M_{KK}x_4\right) \ , \tag{2.2.12a}$$

where

$$u^3 = u_0^3 + u_0 r^2 \ . \tag{2.2.12b}$$

The metric of the cigar subspace reads

$$ds_{y,z}^2 = \frac{4}{9}\left(\frac{u}{R}\right)^{-3/2}\left[(1 - hz^2)dz^2 + (1 - hy^2)dy^2 - 2hyzdydz\right] \ , \tag{2.2.13}$$

where

$$h \equiv h(r) = \frac{1}{r^2}\left(1 - \frac{u_0}{u}\right) \ . \tag{2.2.14}$$

In these coordinates, the antipodal embedding reads

$$y(x^\mu, z) = 0 \ . \tag{2.2.15}$$

It can be shown that the embedding is stable with respect to small perturbations [37].

2.3   Low-energy WSS effective theory

We have seen that the gauge symmetry on the $D8/\overline{D8}$-branes realizes a global symmetry $U(N_f)_L \times U(N_f)_R$. The latter is the global symmetry of massless QCD. In fact, its $U(1)_A$ part is, notoriously, anomalous and thus does not represent a symmetry of the quantum theory. However, the anomaly is suppressed in the large-N expansion so that the symmetry is retrieved in the large-N limit.

As we discussed in section 2.2, the Witten background forces the $D8/\overline{D8}$-branes to join, realizing chiral symmetry breaking. As a result, N_f^2 Nambu-Goldstone bosons are expected. The structure of their low-energy theory is completely determined by the symmetry breaking pattern [93], as we review in appendix 2.A. In the present section, we show that the same theory is realized by the $D8$-branes.

In section 2.2, we mentioned that meson operators are holographically realized through the fluctuations of the probe $D8$-branes. Thus, let us look at the terms of the DBI action that depend on the gauge field $\mathcal{A}$ on the $D8$-branes,

$$S_{D_8} = -\frac{C\sqrt{u_0}}{3}\int d^4x dz\, \text{Tr}\left(\frac{R^3}{u}\mathcal{F}_{\mu\nu}\mathcal{F}^{\mu\nu} + \frac{9u^3}{2u_0}\eta^{\mu\nu}\mathcal{F}_{\mu z}\mathcal{F}_{\nu z}\right) \ , \tag{2.3.1}$$

where

$$C = \frac{\mu_8 V_4 R^{3/2}}{2g_s}(2\pi\alpha')^2 \ . \tag{2.3.2}$$

The gauge field $\mathcal{A}$ is valued in the $u(N_f)$ algebra, whose generators T^A are normalized according to $\text{Tr}\,T^A T^B = \delta^{AB}/2$.

The action is finite if the gauge field asymptotes to a pure gauge configuration,

$$\mathcal{A}_M(x^\mu, z) \to iU_\pm(x^\mu, z)^{-1}\partial_M U_\pm(x^\mu, z) \ , \qquad \text{for } z \to \pm\infty \ . \tag{2.3.3}$$

For $N_f > 2$, the topology of the symmetry group is such that $\pi_4(U(N_f)) = 0$, which guarantees the existence of a function $U(x^\mu, z)$ that asymptotes $U_\pm(x^\mu, z)$. We can then choose a gauge such that

$$\mathcal{A}_M(x_\mu, z) \to 0 , \qquad \text{for } z \to \pm\infty . \tag{2.3.4}$$

The condition (2.3.4) is not affected by residual gauge transformations $g(x^\mu, z)$ such that

$$\partial_M g \to 0 , \qquad \text{for } z \to \pm\infty . \tag{2.3.5}$$

The asymptotic values

$$\lim_{z \to \pm\infty} g(x, z) = g_\pm \tag{2.3.6}$$

are interpreted as elements (g_+, g_-) of the theory's global symmetry $U(N_f)_L \times U(N_f)_R$.

We have mentioned that the joining of $D8$ and $\overline{D8}$ branes is interpreted as the holographic realization of chiral symmetry breaking. Let us briefly explain why. Since in the Witten background $D8$ and $\overline{D8}$ branes are joined, we have a single gauge field $\mathcal{A}$ on the $D8$-branes' worldvolume, rather than two independent gauge fields associated to $D8$ and $\overline{D8}$. According to the holographic dictionary illustrated in section 1.3, the asymptotic values

$$\mathcal{A}_\pm(x) = \lim_{z \pm \infty} \mathcal{A}(x, z) \tag{2.3.7}$$

of the gauge field source the currents J_L and J_R associated to the chiral symmetry. Only the $U(N_f)_L \times U(N_f)_R$ transformations that belong to the diagonal subgroup $U(N_f)_V$ are symmetries of the vacuum. Indeed, a given vacuum configuration - say $\mathcal{A} = 0$ - is left invariant by a constant field transformation $g(x^\mu, z) = g_0$. In this case, $g_* = g_- = g_0$, so the transformation belongs to $U(N_f)_V$. In contrast, in order to obtain $g_+ \neq g_-$, a non-constant transformation $g(x^\mu, z) = g(z)$ is needed. This transformation will inevitably alter the chosen vacuum field configuration $\mathcal{A}$ and therefore does not constitute a symmetry of the vacuum.

As we review in appendix 2.A, the low-energy effective Lagrangian is usually written in terms of the meson matrix

$$U(x^\mu) = \exp\left(\frac{2i}{f_\pi} \pi^A(x) T^A\right) , \tag{2.3.8}$$

which transforms under $U(N_f)_L \times U(N_f)_R$ as

$$U(x^\mu) \to g_+ U(x^\mu) g_- . \tag{2.3.9}$$

The bulk object with the same transformation law is the line operator

$$U(x^\mu, z) = P \exp\left(i \int_{-\infty}^{+\infty} dz' \mathcal{A}_z(x^\mu, z')\right) , \tag{2.3.10}$$

where P denotes the path-ordering. We now show that this is indeed the holographic counterpart of the meson matrix (2.3.9). Let us define

$$\xi_{\pm}^{-1}(x^{\mu}, z) = P \exp\left(i \int_0^{\pm\infty} dz' \mathcal{A}_z(x^{\mu}, z')\right) . \qquad (2.3.11)$$

It is useful to work in the $\mathcal{A}_z = 0$ gauge, where mesons appear in the asymptotic behavior of the $\mathcal{A}_{\mu}$ components. The gauge field can be expanded using a complete basis as [37]

$$\begin{aligned}
\mathcal{A}_{\mu}(x^{\mu}, z) &= i\xi_+(x^{\mu})\partial_{\mu}\xi_+^{-1}(x^{\mu})\psi_+(z) + i\xi_-(x^{\mu})\partial_{\mu}\xi_-^{-1}(x^{\mu})\psi_-(z) + \\
&\quad + \sum_{n>1} B_{\mu}^{(n)}(x^{\mu})\psi_n(z) .
\end{aligned} \qquad (2.3.12)$$

where

$$\psi_{\pm}(z) = \frac{1}{2} \pm \frac{1}{\pi} \arctan\left(\frac{z}{u_0}\right) . \qquad (2.3.13)$$

Let us choose a gauge such that $\xi_-(x^{\mu}) = 1$ and $U(x^{\mu}) = \xi_-^{-1}(x^{\mu})$, hence

$$\mathcal{A}_{\mu}(x^{\mu}, z) = iU^{-1}(x^{\mu})\partial_{\mu}U(x^{\mu})\psi_+(z) + \sum_{n>1} B_{\mu}^{(n)}(x^{\mu})\psi_n(z) . \qquad (2.3.14)$$

Let us omit the vector mesons $B_{\mu}^{(n)}$. We have

$$\mathcal{F}_{z\mu} = iU^{-1}\partial_{\mu}U\hat{\phi}_0(z) , \qquad (2.3.15a)$$

where

$$\hat{\phi}_0(z) = \partial_z\psi_+(z) = \frac{1}{\pi}\frac{u_0}{u_0^2 + z^2} . \qquad (2.3.15b)$$

Plugging (2.3.15) into the action (2.3.1), we obtain

$$\begin{aligned}
S_{D_8} &= -\frac{3C}{2\sqrt{u_0}} \int d^4x\, dz\, u^3 \eta^{\mu\nu} \operatorname{Tr} \mathcal{F}_{\mu z}\mathcal{F}_{\nu z} \\
&= \frac{3C}{2\sqrt{u_0}} \int dz\, u^3 \hat{\phi}_0^2(z) \int d^4x \operatorname{Tr}(U^{-1}\partial_{\mu}U)^2 .
\end{aligned} \qquad (2.3.16)$$

This is the term that describes the pions' low-energy dynamics at the leading order in chiral perturbation theory, as discussed in appendix 2.A. Comparing with (2.A.5), we obtain the pion's decay constant,

$$f_{\pi}^2 = \frac{6C}{\sqrt{u_0}} \int dz\, u^3 \hat{\phi}_0^2(z) . \qquad (2.3.17)$$

Using (2.1.8) to express in terms of field-theory quantities, we obtain

$$f_{\pi}^2 = \frac{\lambda N}{54\pi^4} M_{KK}^2 . \qquad (2.3.18)$$

The action (2.3.1) includes also a $\mathcal{F}_{\mu\nu}\mathcal{F}^{\mu\nu}$ another term. We have

$$\mathcal{F}_{\mu\nu} = i[U^{-1}\partial_\mu U, U^{-1}\partial_\nu U]\psi_+(\psi_+ - 1) \ . \tag{2.3.19}$$

Plugging into the action (2.3.1),

$$
\begin{aligned}
S_{D_8} &= -\frac{CR^3\sqrt{u_0}}{3} \int d^4x\,dz\,\frac{1}{u} \operatorname{Tr} \mathcal{F}_{\mu\nu}\mathcal{F}^{\mu\nu} \\
&= \frac{CR^3\sqrt{u_0}}{3} \int dz\,\frac{\psi_+^2(\psi_+ - 1)^2}{u} \int d^4x\,\operatorname{Tr}[U^{-1}\partial_\mu U, U^{-1}\partial_\nu U]^2 \ . \tag{2.3.20}
\end{aligned}
$$

This is the Skyrme term that stabilizes the soliton solutions of the chiral Lagrangian, interpreted as baryons [94]. Comparing with (2.A.7), we find the expression for the Skyrme parameter,

$$e^2 = \frac{27\pi^7}{2b}\frac{1}{\lambda N} \ , \qquad b \approx 15.25 \ . \tag{2.3.21}$$

We have omitted the vector mesons $B_\mu^{(n)}$ appearing in (2.3.12). By keeping them, it is possible to obtain their couplings with the pions systematically [37].

We see that the low-energy theory derived from the $D8$-branes' fluctuations coincides with the massless chiral Lagrangian that describes low-energy QCD, as reviewed in appendix 2.A. In the effective field theory approach, each Lagrangian term enters with a coefficient that we have to determine by matching with the ultraviolet theory or using inputs from phenomenology. In the Witten-Sakai-Sugimoto model, all the coefficients are expressed in terms of the model's parameters M_{KK} and λ. The latter are determined by fitting the mass of the ρ meson and the value of the pion decay constant f_π, and read [37, 95]

$$\lambda \approx 16.63 \ , \qquad M_{KK} = 949 \text{ MeV} \ . \tag{2.3.22}$$

A detailed account of the WSS model's semi-quantitative results is provided in [85].

2.4 Quark masses

We have found that the $D4/D8/\overline{D8}$ brane system realizes at low energies the effective chiral Lagrangian that describes the pions. Since we have not found terms such as the second one in (2.A.6), the pions are massless, meaning that the current algebra quark masses vanish. We want to find a deformation of the model that gives mass to the pions.

From the boundary point of view, the WSS model is a five-dimensional theory where the left and right Weyl fermions are introduced as codimension-one defects placed at antipodal points along the $S_{x_4}^1$. As a result, a local Dirac mass term for the quarks is not allowed. The gauge-invariant boundary operator that better resembles the Dirac mass term is [96]

$$\psi_L(x^\mu, x_{4,+})e^{i\int_C \mathcal{A}}\psi_R(x^\mu, x_{4,-}) \ , \tag{2.4.1}$$

where $x_{4,\pm} = \pm\pi/M_{KK}$ and C represents a path that connects the two Weyl fermions. The operator (2.4.1) is an open Wilson line. We aim to find the corresponding bulk operator.

The first guess would involve the $D8$-brane holonomy $U(x^\mu)$. However, although the latter is gauge invariant under $D8$-brane gauge transformations, it is not gauge invariant under string-theory gauge transformations involving the Kalb-Ramond B field.[7] As a result, we have to consider the holonomy $U(x^\mu)$ multiplied by the phase $\exp(i\int B)$. This is the amplitude corresponding to the insertion of a fundamental string stretched between the $D8$ and the $\overline{D8}$ branes. In [96], it was proposed that the correlator insertion of the open Wilson line (2.4.1) is holographically dual to performing the gravity path integral over configurations that include a string worldsheet ending on the boundary line. In section 1.3, we saw that closed Wilson lines in the boundary theory are dual to closed-string worldsheets ending on the boundary lines. The proposal of [96] is therefore the open-line generalization. By considering such a worldsheet, we obtain the deformation

$$S_{mass} = c \int d^4x \operatorname{Tr} P\left[M \exp\left(-i\int_{-\infty}^{+\infty} A_z dz\right) + \text{c.c}\right] . \qquad (2.4.2)$$

Following different reasonings, the same term was found in [97], where the behavior of σ was also computed,

$$c \propto \lambda^{3/2} M_{KK}^3 . \qquad (2.4.3)$$

Recalling the definition of the pion matrix (2.3.10), we see that the term (2.4.2) is indeed the mass term discussed in appendix 2.A. As a result, the mesons take mass.

2.5   Theta angle and $U(1)_A$ anomaly

One of the many reasons that make non-Abelian Yang-Mills theories interesting is that the topological theta term

$$\mathcal{L}_\theta = \frac{\theta_0}{8\pi^2} \operatorname{Tr} F \wedge F \qquad (2.5.1)$$

introduces new physics. Let us consider $SU(N)$ Yang-Mills theory. Even though $\mathcal{L}_\theta$ is a total derivative, it is non-trivial due to the non-trivial topology of the gauge group, which is characterized by $\pi_3(SU(N)) = \mathbf{Z}$, so that instanton field configurations arise. As we will discuss in chapter 3, one of the open problems of the Standard Model is related to this term. In appendix 2.A, we show some of the effects of the term (2.5.1) in the chiral effective Lagrangian context.

---

[7]Indeed, as we mentioned in section 1.2.2, whenever we have a brane, the gauge-invariant quantity is not the field strength $\mathcal{F}$ of the inhabiting gauge field but, rather, the combination $B + 2\pi\alpha'\mathcal{F}$.

Let us discuss how the physics associated to the θ-angle is realized in the WSS model [38]. In this section, we work with Ramond-Ramond fields $\hat{C}_p$ normalized so that the Ramond-Ramond charges are integer multiples of 2π. These are related to the fields C_p used so far through

$$C_{p+1} = \frac{k_{10}^2 \mu_{6-p}}{\pi} \hat{C}_{p+1} . \tag{2.5.2}$$

With this convention, the Ramond-Ramond kinetic terms (1.2.12a) and the Chern-Simons couplings (1.2.39) read

$$S_{kin} = -\frac{(2\pi l_s)^{2(p-3)}}{4\pi} \int d\hat{C}_{p+1} \wedge {}^* d\hat{C}_{p+1} , \tag{2.5.3}$$

$$S_{CS} = \sum \int \hat{C}_{q+1} \wedge \text{Tr}\, e^{\mathcal{F}/2\pi} . \tag{2.5.4}$$

In the following, we will omit the hat on the Ramond-Ramond fields, understanding that they are normalized in this way.

We start with the weak-coupling description where we have N $D4$-branes as flat hyperplanes in flat Minkowski space. The $D4$-brane action includes the Chern-Simons coupling[8]

$$S_{CS} = \frac{1}{8\pi^2} \int_{D4} C_1 \wedge \text{Tr}\, F \wedge F . \tag{2.5.5}$$

We can choose a vacuum configuration with a flat holonomy

$$\int C_1 = \theta_0 . \tag{2.5.6}$$

The holonomy is gauge-invariant modulo $2\pi k$, so that θ_0 is an angle.

At strong coupling, the $D4$-branes are replaced by the geometry (2.1.1), which has topology $\mathbf{R}^{1,3} \times D_2 \times S^4$. In particular, the circle S^1 of the boundary theory is the boundary of the cigar-like disk D_2. From Stokes' theorem. the holonomy (2.5.6) cannot be obtained if the C_1 field strength vanishes. The field strength has to vanish just at the boundary, so that

$$\int_{D_2} \mathrm{d}C_1 = \lim_{u\to\infty} \int_{S^1} C_1 = \theta_0 + 2\pi k . \tag{2.5.7}$$

As we review in appendix 2.A, the theta term (2.5.1) is closely related to the $U(1)_A$ anomaly. If we consider QCD with massless flavors, a chiral rotation allows us to rotate the theta angle. Thus, if at least one of the quarks is massless, the theta angle does not carry physical meaning. This remark will play an

---

[8]In this section, several gauge fields appear. We use F and $\mathcal{F}$ for the field strengths of of the gauge fields on the $D4$ and $D8$ branes, respectively. We then use F_{p+2} for the field strengths of the Ramond-Ramond fields C_{p+1}.

important role in chapter 3, where the strong CP problem is discussed. Let us show how this physics is realized within the WSS model [37]. We recall that in the Sakai-Sugimoto model without deformations the quarks are massless. The $D8$-branes couple to the C_7 Ramond-Ramond field through the Chern.Simons coupling. Let us consider the C_7-dependent action terms,

$$S_{C_7} = -\frac{1}{4\pi}(2\pi l_s)^6 \int \mathrm{d}C_7 \wedge {}^*\mathrm{d}C_7 + \frac{1}{2\pi} \int C_7 \wedge \mathrm{Tr}\,\mathcal{F} \wedge \delta(y)\mathrm{d}y \ , \qquad (2.5.8)$$

where we added the form $\delta(y)\mathrm{d}y$ in order to integrate over the whole spacetime. From (2.5.8), we derive the equations of motion[9]

$$\mathrm{d}\tilde{F}_2 = \mathrm{Tr}\,\mathcal{F} \wedge \delta(y)\mathrm{d}y \ . \qquad (2.5.9)$$

The Chern-Simons coupling of the $D8$-branes spoils the Bianchi identity for the Ramond-Ramond field C_1. The right-hand side of (2.5.9) takes contributions only from the Abelian part of the field strength, since the generators of $SU(N_f)$ are traceless. Recalling that we work with the $U(N_f)$ generators normalized so that $\mathrm{Tr}(T^A T^B) = \delta^{AB}/2$, we can formally solve (2.5.9) by writing

$$\tilde{F}_2 = \mathrm{d}C_1 + \sqrt{\frac{N_f}{2}}\mathcal{A}^0 \wedge \delta(y)\mathrm{d}y \ . \qquad (2.5.10)$$

The field strength $\tilde{F}_2$ is invariant under gauge transformations on $\mathcal{A}$ only if $\mathrm{d}C_1$ transforms,

$$\delta_\Lambda \mathrm{d}C_1 = \sqrt{\frac{N_f}{2}}\mathrm{d}\Lambda \wedge \delta(y)\mathrm{d}y \ , \qquad \delta_\Lambda \mathcal{A}^0 = -\mathrm{d}\Lambda \ . \qquad (2.5.11)$$

Let us integrate on the cigar D_2. Recalling (2.5.7), we get

$$\delta_\Lambda \theta_0 = \sqrt{\frac{N_f}{2}}\left(\Lambda_{z\to+\infty} - \Lambda_{z\to-\infty}\right) \ . \qquad (2.5.12)$$

We can choose

$$\Lambda_{z\to\pm\infty} = \mp\sqrt{2N_f}\alpha \ , \qquad (2.5.13)$$

so that

$$\theta_0 \to \theta_0 - 2N_f\alpha \ . \qquad (2.5.14)$$

As we review in appendix 2.A, this is the way the θ_0 angle transforms under a chiral transformation on the quarks because of the chiral anomaly. This is consistent with the fact that the gauge transformation (2.5.13) asymptotes to opposite constants. Recalling the discussion at the beginning of section 2.3, this is indeed the definition of chiral transformation in the holographic set-up.

---

[9]We have put a tilde over the field strength because it is not $\mathrm{d}C_1$ due to the right-hand side of (2.5.9).

In appendix 2.A, we see that the θ_0 angle mixes with the complex phase of the meson matrix M. The same occurs in the WSS model. Indeed, if we try to cancel the θ_0 angle through

$$\delta_\Lambda \theta_0 = \sqrt{\frac{N_f}{2}} \left(\Lambda_{z\to+\infty} - \Lambda_{z\to-\infty} \right) = -\theta_0 \ , \tag{2.5.15}$$

from (2.5.12) we see that the Abelian component of the gauge field on the $D8$-branes transforms according to

$$\frac{1}{\sqrt{2N_f}} \int_{-\infty}^{+\infty} dz \, \mathcal{A}_z^0 \to \frac{1}{\sqrt{2N_f}} \int_{-\infty}^{+\infty} dz \, \mathcal{A}_z^0 - \frac{\theta_0}{N_f} \ . \tag{2.5.16}$$

But this is the object entering the holographic mass term (2.4.2). As a result, if all the quarks are massive, it is not possible to cancel the θ_0 angle because the combination

$$\theta = \theta_0 + \mathrm{Arg} \det M \ . \tag{2.5.17}$$

is left invariant by the chiral transformations.

In appendix 2.A, we show that the effects of the chiral anomaly are nicely taken into account by adding to the chiral Lagrangian a $1/N$ subleading operator (2.A.19). Let us show that the same term is reproduced by the WSS model. The action (2.5.8) is equivalent (on-shell) to the action

$$S_{\tilde{F}_2} = -\frac{1}{4\pi(2\pi l_s)^6} \int \tilde{F}_2 \wedge *\tilde{F}_2 \ . \tag{2.5.18}$$

Indeed, off-shell this action is

$$S_{\tilde{F}_2} = -\frac{1}{4\pi(2\pi l_s)^6} \int \tilde{F}_2 \wedge *\tilde{F}_2 + \frac{1}{2\pi} \int C_7 \wedge \left(\mathrm{Tr}\,\mathcal{F} \wedge \delta(y)\mathrm{d}y - \mathrm{d}\tilde{F}_2 \right) \ . \tag{2.5.19}$$

Varying $\tilde{F}_2$, the equations of motion are

$$*\tilde{F}_2 = -(2\pi l_s)^6 \mathrm{d}C_7 \ . \tag{2.5.20}$$

Then, the action $S_{\tilde{F}_2}$ evaluated on-shell reads

$$\begin{aligned} S_{\tilde{F}_2} &= \frac{1}{4\pi} \int \tilde{F}_2 \wedge \mathrm{d}C_7 + \frac{1}{2\pi} \int C_7 \wedge \left(\mathrm{Tr}\,\mathcal{F} \wedge \delta(y)\mathrm{d}y - \mathrm{d}\tilde{F}_2 \right) \\ &= -\frac{1}{4\pi} \int \mathrm{d}C_7 \wedge \tilde{F}_2 + \frac{1}{2\pi} \int C_7 \wedge \mathrm{Tr}\,\mathcal{F} \wedge \delta(y)\mathrm{d}y \\ &= -\frac{1}{4\pi}(2\pi l_s)^6 \int \mathrm{d}C_7 \wedge {}^*\mathrm{d}C_7 + \frac{1}{2\pi} \int C_7 \wedge \mathrm{Tr}\,\mathcal{F} \wedge \delta(y)\mathrm{d}y \ , \end{aligned} \tag{2.5.21}$$

which is the result we wanted to prove.

The solution of the equations of motion derived from (2.5.18) and consistent with (2.5.10) reads

$$\tilde{F}_2 = \frac{3M_{KK}}{2\pi} \frac{u_0^3}{u^4} \left(\theta + \frac{\sqrt{2N_f}}{f_\pi} \eta' \right) du \wedge dx_4 \ . \tag{2.5.22}$$

Plugging (2.5.22) into the action (2.5.18), we obtain

$$S_{\tilde{F}_2} = -\frac{\chi_{WYM}}{2} \int d^4x \left(\theta + \frac{\sqrt{2N_f}}{f_\pi} \eta' \right)^2 \ , \tag{2.5.23}$$

where

$$\chi_{WYM} = \frac{\lambda^3}{4(3\pi)^6} M_{KK}^4 \tag{2.5.24}$$

is the topological susceptibility of the Witten-Yang-Mills theory. The action (2.5.23) is precisely the term that takes into account the chiral anomaly effects within the low-energy effective theory. In particular, it yields the Witten-Veneziano formula [56, 98] that relates the mass of the η' to the topological susceptibility of the unflavored gauge theory.

$$m_{\eta'}^2 = \frac{2N_f}{f_\pi^2} \chi_{WYM} \ . \tag{2.5.25}$$

It is important to stress that the topological susceptibility (2.5.24) does not depend on N. Since $f_\pi^2 = O(N)$ we have $m_{\eta'}^2 = O(1/N)$. This is consistent with the fact that the anomaly is subleading in $1/N$.

2.6 The model at finite temperature

In order to study the WSS model at finite temperature T, let us compactify the Euclidean time direction on a circle S^1 with length $\beta = 1/T$. Choosing (anti-)periodic boundary conditions for the scalar (fermions) fields, the quantum field theory path integral computes the thermal partition function. The gauge theory is then defined on the manifold $M = \mathbf{R}^3 \times S_{x_0}^1 \times S_{x_4}^1$. As we pointed out in section 1.3, in order to holographically study a quantum field theory defined on a manifold M we have to consider all the backgrounds X such that $\partial X = M$. In our case, since M features two S^1 factors, there exist two gravitational backgrounds with boundary M:

$$X_4 \simeq \mathbf{R}^3 \times D_2 \times S_{x_0}^1 \ , \qquad X_0 \simeq \mathbf{R}^3 \times D_2 \times S_{x_4}^1 \ . \tag{2.6.1}$$

The background X_4 is the *solitonic* Witten background (2.1.1), except that it is taken with Euclidean signature and compactified time direction. The *black-hole*

background X_0 is simply obtained from X_4 by exchanging $x_4 \leftrightarrow x_0$. In Euclidean signature, this is just a relabeling of the coordinates. Thus, X_0 reads

$$ds^2 = \left(\frac{u}{R}\right)^{3/2} \left[f_T(u)dt^2 + dx^i dx^i + dx_4^2 \right] + \left(\frac{R}{u}\right)^{3/2} \left[\frac{du^2}{f_T(u)} + u^2 d\Omega_4^2 \right] \ , \quad (2.6.2a)$$

with

$$e^\phi = g_s \left(\frac{u}{R}\right)^{3/4} \ , \qquad\qquad f_T(u) = \tilde{f}(u) = 1 - \frac{u_T^3}{u^3} \ , \qquad (2.6.2b)$$

$$F_4 = \frac{3R^3}{g_s}\omega \ , \qquad\qquad R^3 = \pi g_s N l_s^3 \ . \qquad (2.6.2c)$$

For each value of the temperature, we have to check whether X_4 or X_0 dominates. This will depend on the radii of the two circles. It is then clear that when the two circles have equal radii, the backgrounds will exhibit the same free energy. This occurs at the critical temperature

$$T_c = \frac{M_{KK}}{2\pi} \ . \qquad (2.6.3)$$

At this temperature, there will be a first-order phase transition. As we will show in a moment, it turns out [99] that the dominant solution is always that in which the disk D_2 involves the circle with the smaller radius, so that:

- for $T < T_c$, X_4 dominates;

- for $T > T_c$, X_0 dominates.

In section 2.1, we studied the properties of the background X_4. In particular, we showed that, due to the fact that its warp factor $g_{00}(u)$ is always strictly positive, it describes a confining theory. In contrast, the background X_0 exhibits a warp factor that has a vanishing minimum, and therefore it describes a deconfined phase. Indeed, we have seen that in the background X_4, the string dual to the rectangular Wilson loop for large quark/antiquark separations l tends to go deep in the small-u region of the background. The Wilson loop's area law arises from the worldsheet surface at $u = u_0$. In contrast, the background X_0 given by (2.6.2) exhibits a horizon at $u = u_T$. The string dual to the Wilson loop can break into two pieces ending on the horizon [100], and the quark/antiquark potential will not be linear.

Let us compute the free energy given by the background (2.6.2). We have to evaluate on-shell the Type IIA supergravity action

$$S_{IIA} = -\frac{1}{2\kappa_{10}^2} \int d^{10}x \sqrt{g} \left[e^{-2\phi} \left(R + 4\partial_M\phi\partial^M\phi \right) - \frac{1}{2}|F_4|^2 \right] \ . \qquad (2.6.4)$$

The background (2.6.2) is characterized by

$$R = \frac{9}{4}\left(\frac{u}{R}\right)^{3/2}\frac{1}{u^5}\left(u_T^3 - 5u^3\right) \ , \tag{2.6.5a}$$

$$4\partial_M\phi\partial^M\phi = \frac{9}{4}\left(\frac{u}{R}\right)^{3/2}\frac{1}{u^2}f_T(u) \ , \tag{2.6.5b}$$

$$|F_4|^2 = = \frac{9}{g_s^2 u^2} \ . \tag{2.6.5c}$$

The action (2.6.4) is divergent, hence we regularize it by introducing a cut-off at $u = u_\Lambda$,

$$S_{IIA} = \frac{27}{4}\frac{V_{S^4}V_4\beta_4}{\kappa_{10}^2 g_s^2}\int_{u_T}^{u_\Lambda} du\, u^2 = \frac{9}{4}\frac{V_{S^4}V_4\beta_4}{\kappa_{10}^2 g_s^2}\left(u_\Lambda^3 - u_T^3\right) \ . \tag{2.6.6}$$

In order to have a well-defined variational principle, we need to include the Gibbons-Hawking boundary term

$$S_{GH} = -\frac{1}{\kappa_{10}^2}\int d^9x\sqrt{h}e^{-2\phi}K \ , \tag{2.6.7}$$

where h is the determinant of the metric's pullback on the surface $u = u_\Lambda$, whereas

$$K = \frac{1}{\sqrt{g}}\partial_u\left(\frac{\sqrt{g}}{\sqrt{g_{uu}}}\right) \tag{2.6.8}$$

is the extrinsic curvature of the surface $u = u_\Lambda$. In the background (2.6.2), it reads

$$K = \frac{1}{4u^4}\left(\frac{u}{R}\right)^{3/4}f_T^{-1/2}\left(19u_\Lambda^3 - 13u_T^3\right) \ , \tag{2.6.9}$$

so that

$$S_{GH} = -\frac{1}{4}\frac{V_{S^4}V_4\beta_4}{\kappa_{10}^2 g_s^2}\left(19u_\Lambda^3 - 13u_T^3\right) \ . \tag{2.6.10}$$

Summing (2.6.6) and (2.6.10) we obtain a divergent quantity. This is not unexpected. When we reviewed the holographic prescriptions in section 1.3, we mentioned that in general the on-shell gravitational action is divergent due to the infinite volume of the background. The divergences can be systematically canceled by introducing boundary counterterms [76, 77]. In our case, the divergence is canceled by the counterterm [99]

$$S_{ct} = \frac{1}{\kappa_{10}^2}\frac{g_s^{1/3}}{R}\int d^9x\sqrt{h}\frac{5}{2}e^{-7\phi/3} \ . \tag{2.6.11}$$

Its value is

$$S_{ct} = \frac{5}{2}\frac{V_{S^4}V_4\beta_4}{\kappa_{10}^2 g_s^2}f_T^{1/2}u_\Lambda^3 \ . \tag{2.6.12}$$

Since we need its value at $u = u_\Lambda$ and since at the end we will take $u_\Lambda \to \infty$ we can expand it,

$$S_{ct} = \frac{5}{2} \frac{V_{S^4} V_4 \beta_4}{\kappa_{10}^2 g_s^2} \left(u_\Lambda^3 - \frac{1}{2} u_T^3 \right) \ . \tag{2.6.13}$$

Summing all the contributions we obtain

$$S = S_{IIA} + S_{GH} + S_{ct} = -\frac{1}{4} \frac{V_{S^4} V_4 \beta_4}{\kappa_{10}^2 g_s^2} u_T^3 \ . \tag{2.6.14}$$

The free energy density of the background X_0 is therefore

$$f_{X_0} = -\frac{1}{2} \left(\frac{2}{3} \right)^7 \pi^4 \lambda_{YM} N^2 \frac{T^6}{M_{KK}^2} \ . \tag{2.6.15}$$

We see in this case that the free energy density goes as T^6, a behavior that is typical of six-dimensional conformal field theories. This reflects the fact that the ultraviolet completion of the WYM model is the six-dimensional $\mathcal{N} = (2, 0)$ superconformal theory, as pointed out in section 2.1.

Since X_0 and X_4 only differ for a relabeling $x_0 \leftrightarrow x_4$, the free energy of the background X_4 is easily obtained from (2.6.15) by substituting $T \to M_{KK}/2\pi$,

$$f_{X_4} = -\left(\frac{1}{3} \right)^7 \frac{1}{\pi^2} \lambda_{YM} N^2 M_{KK}^4 \ . \tag{2.6.16}$$

Let us take the difference between the two results,

$$f_{X_4} - f_{X_0} = \frac{\lambda_{YM} N^2}{\pi^2 M_{KK}^2} \left(\frac{1}{3} \right)^7 \left[-M_{KK}^6 + (2\pi T)^6 \right] \ . \tag{2.6.17}$$

We see that for temperatures $T < M_{KK}/2\pi$, X_4 is energetically favored, whereas for temperatures $T > M_{KK}/2\pi$, X_0 dominates.

From (2.6.15) and (2.6.16), we also notice that the entropy is independent on N for X_4 and goes as N^2 for X_0, confirming that the low-energy phase is confined and the high-temperature one is deconfined.

Let us now consider the $D8$-branes' embedding. In section 2.2, we saw that the zero-temperature background (2.1.1) forces $D8$ and $\overline{D8}$ branes to join. Above the critical temperature, the (x_4, u) subspace is a cylinder rather than a disk. As a result, the branes are not forced to join anymore. Whether they join or not depends on the separation L between $D8$ and $\overline{D8}$ along $S_{x_4}^1$ [43]. Let us recall that if the branes are connected, chiral symmetry is spontaneously broken. In contrast, a disconnected brane configuration signals that the vacuum preserves chiral symmetry.

As we will re-discuss in section 4.3.1 by using a variation approach [101], for $L > 0.97 M_{KK}^{-1}$, the branes do not join in the background X_0. Thus, the deconfinement phase transition implies the chiral symmetry breaking. In contrast, when $L < 0.97 M_{KK}^{-1}$, there exist a phase where the branes are connected even for

$T > T_c$. In this case, the branes get disconnected when the temperature reaches a greater critical temperature given by [43]

$$T_c^\chi \approx \frac{0.1538}{L} \ . \tag{2.6.18}$$

As a result, choosing boundary conditions such that $L < 0.97 M_{KK}^{-1}$, the scale of chiral symmetry breaking is strictly greater than the confinement scale. This fact will be pivotal in chapter 3.

To summarize, the phase diagram of the Witten-Sakai-Sugimoto model is such that:

- If $T < \frac{M_{KK}}{2\pi}$, the theory is confining and chiral symmetry is broken;

- If $T > \frac{M_{KK}}{2\pi}$, the theory is deconfined and:

    - if $T < \frac{0.1538}{L}$, chiral symmetry is broken;
    - if $T > \frac{0.1538}{L}$, chiral symmetry is preserved.

2.A   Low-energy QCD

In this appendix, we briefly review the chiral perturbation theory approach to low-energy QCD, describing how the symmetry breaking pattern determines the low-energy Lagrangian. We illustrate some basic aspects of the physics related to the QCD θ angle. After discussing the Witten-Veneziano formula that relates the mass of the η' meson to the topological susceptibility of the unflavored Yang-Mills theory, we discuss how to take it into account in chiral perturbation theory. Finally, we show how to generalize the effective Lagrangian in order to include the QCD axion.

QCD and effective chiral Lagrangian

QCD at low-energies is difficult to study due to the fact that the coupling parameter g_{YM} is a decreasing function of the energy scale, so that perturbative methods ceases to be reliable at low energies. Let us write the QCD ultraviolet Lagrangian,[10]

$$\mathcal{L}_{QCD} = -\frac{1}{2g_{YM}^2} \operatorname{Tr} F_{\mu\nu} F^{\mu\nu} + \sum_{i=1}^{N_f} \left[i\overline{\psi}^i \not{D}\psi_i - m_i{}^j \overline{\psi}^i \psi_j \right] \ , \tag{2.A.1}$$

where i and j are flavor indices. In real-world QCD, $N_f = 6$.

---

[10]We omit the terms related to the gauge fixing procedure as they do not play a relevant role in our discussion.

The theory possesses a $U(N_f)$ global symmetry acting on the flavor indices.[11] In the massless *chiral* limit $m_i^j \to 0$, the left and right components $\psi_{L,R}$ of the Dirac fermions are independent and the global symmetry is enhanced to

$$G = U(1)_V \times SU(N_f)_V \times SU(N_f)_A \ , \tag{2.A.2}$$

the axial $U(1)_A$ being anomalous. In the real world, the quarks' masses do not vanish. However, the masses of the up, down and strange quarks are smaller than the QCD dynamical scale $\Lambda_{QCD} \approx 300$ MeV so that, if we take $N_f = 2$ or $N_f = 3$, the chiral symmetry can be considered as an approximate symmetry.

Chiral symmetry is not seen in the low-energy QCD spectrum since its states are not organized in parity doublets. This means that the theory realizes spontaneous symmetry breaking according to the pattern

$$SU(N_f)_V \times SU(N_f)_A \to SU(N_f)_V \ . \tag{2.A.3}$$

As a consequence, there is a manifold of vacua parameterized by a $SU(N_f)$ matrix. Consistently with (2.A.3), the low-energy spectrum displays $N_f^2 - 1$ Nambu-Goldstone bosons, the pions. The low-energy degrees of freedom notably differ from the ultraviolet ones. It is indeed extremely hard to derive the low-energy effective theory starting from the ultraviolet theory in (2.A.1). However, the structure of the low-energy theory can be inferred from the symmetry breaking pattern [93].

The pions arise as long-wavelength fluctuations around a chosen vacuum. Expanding around the identity, we define the meson matrix

$$U(x) = \exp\left(\frac{2i\pi^a(x)}{f_\pi} T^a\right) \ , \tag{2.A.4}$$

where T^a are $SU(N_f)$ generators, normalized so that $\operatorname{Tr} T^a T^b = \delta^{ab}/2$. The parameter f_π is a scale introduced for dimensional reasons. It is called *pion decay constant*. Clearly, in the theory we are considering, the pions are the lightest states and are thus stable. However, they can decay when they are coupled to the electroweak sector. The scale f_π determines the pion's decay width, whence its name.

The idea underlying the chiral effective theory is to write down all operators that preserve Lorentz invariance and chiral symmetry. Since we are describing the long-wavelength fluctuations, the operators are organized according to the number of derivatives that they feature.

At lowest order, a single operator contributes,

$$\mathcal{L} = \frac{f_\pi^2}{4} \operatorname{Tr}(U^\dagger \partial_\mu U)^2 \ . \tag{2.A.5}$$

---

[11]In fact, the true global symmetry is $U(N_f)/\mathbf{Z}_N$ because the $\mathbf{Z}_N$ subgroup of $U(N_f)$ is part of the gauge group. However, our discussion will not be sensitive to these global aspects. Hence we neglect them for simplicity.

The effects of the small quark's masses can be taken into account by including a new term which possesses the same transformation properties of the mass term in (2.A.1),

$$\mathcal{L} = \frac{f_\pi^2}{4} \operatorname{Tr}(U\partial_\mu U)^2 + c \operatorname{Tr}(\mathcal{M}U + h.c.) \ , \tag{2.A.6}$$

where "$h.c.$" stands for Hermitian conjugation.

Although we have conceived the chiral Lagrangian by neglecting modes with high mass, it turns out that baryons can be considered as well. Indeed, for $N_f > 2$ the theory admits a topological symmetry associated to the fact that $\Pi_3(SU(N_f)) = \mathbf{Z}$.[12] The baryon's modes appear as solitonic field configurations with such a topological charge. We will not discuss how baryons are described in detail. We just mention that due to Derrick's theorem [103], stable configurations are found only if the chiral Lagrangian includes terms with more than two derivatives. In particular, a way to to do it is to introduce the *Skyrme term*

$$\mathcal{L}_{Skyrme} = \frac{1}{32g^2} \operatorname{Tr}\left([U^\dagger\partial_\mu, U^\dagger\partial_\nu U]^2\right) \ . \tag{2.A.7}$$

θ-angle effective Lagrangian

The QCD Lagrangian (2.A.1) is not the most general theory with the matter content that we have considered. Indeed, we can write another operator consistently with gauge symmetry and renormalizability,

$$\mathcal{L}_\theta = \frac{\theta_0}{32\pi^2}\epsilon^{\mu\nu\rho\sigma} \operatorname{Tr} F_{\mu\nu}F_{\rho s} = \frac{\theta_0}{8\pi^2} \operatorname{Tr} F \wedge F \ . \tag{2.A.8}$$

The parameter θ_0 is an angle $\theta_0 \sim \theta_0 + 2\pi$ since, given a closed four-dimensional manifold M_4,

$$\frac{1}{8\pi^2} \int_{M_4} \operatorname{Tr} F \wedge F \ \in \ \mathbf{Z} \ . \tag{2.A.9}$$

The Lagrangian $\mathcal{L}_\theta$ in general is not invariant under the P and T transformations. From CPT theorem, it also transforms under CP. These are symmetries only when $\theta_0 = 0$ and $\theta_0 = \pi$.

Due to the chiral anomaly, the θ_0 parameter is intimately related to the phase of the mass matrix $\mathbf{m}$ that appears in (2.A.1). Indeed, a $U(1)_A$ transformation

$$\psi_L \rightarrow e^{i\alpha}\psi_L \ , \qquad \psi_R \rightarrow e^{-i\alpha}\psi_R \ , \tag{2.A.10}$$

induces a transformation of the quarks' path integral's measure so that $\theta_0 \rightarrow \theta_0 - 2N_f\alpha$. Let us suppose that all the eigenvalues of the mass matrix are different from zero. The mass term in (2.A.1) transforms under (2.A.10). As a result, there is an invariant quantity,

$$\theta = \theta_0 + \operatorname{Arg}\det\mathbf{m} \ . \tag{2.A.11}$$

---

[12]See [102] for a proposal on how to describe baryons in the case $N_f = 2$.

This is the QCD θ-angle. As we will discuss in chapter 3, its unnaturally small value in Nature constitutes one of the open problems of the Standard Model, called *strong CP problem.*

Let us now suppose that at least one of the eigenvalues of the mass matrix vanishes. In that case, performing the transformation (2.A.10) for the corresponding massless field, it is possible to rotate away the θ-angle, which therefore becomes unphysical.

If we consider QCD at large-N, the θ term and thus the chiral anomaly are subleading. This is easily seen from the fact that $\mathcal{L}_\theta$ is not proportional to N, unlike the Yang-Mills term. Equivalently, we can look at the non-conservation of the axial current J_A associated to the transformation (2.A.10),

$$\partial_\mu J_A^\mu \propto g_{YM}^2 N_f \, \epsilon^{\mu\nu\rho\sigma} \, \text{Tr} \, F_{\mu\nu} F_{\rho\sigma} \; . \tag{2.A.12}$$

In the 't Hooft limit, $g_{YM} \to 0$ and therefore the right-hand side goes to zero. As a consequence, the $U(1)_A$ transformation (2.A.10) becomes a (spontaneously broken) symmetry and the low-energy spectrum displays an additional Nambu-Goldstone boson called η'. Its mass is thus expected to be suppressed by a $1/N$ factor.

The $1/N$ suppression of the η' mass can be inferred again with N-power counting using another argument [98]. As we discussed in section 1.1, the contribution to the vacuum energy $E(\theta)$ coming from the glue sector is proportional to N^2. The contribution coming from the quarks is order N. On the other hand, we showed that the introduction of a massless fermion allows us to rotate away the θ dependence of the vacuum energy. It seems that we have run into a contradiction. Let us look at the topological susceptibility

$$\chi = \frac{d^2 E(\theta)}{d\theta^2}\bigg|_{\theta=0} = \int d^4 x \langle Q(x) Q(0) \rangle \; , \tag{2.A.13}$$

where

$$Q(x) = \frac{1}{32\pi^2} \epsilon^{\mu\nu\rho\sigma} F_{\mu\nu} F_{\rho\sigma} \; . \tag{2.A.14}$$

Schematically, the topological susceptibility reads

$$\chi(k) = -\sum_{glue} \frac{N^2 a_i^2}{k^2 + M_i^2} - \sum_{mesons} \frac{N b_i^2}{k^2 + m_j^2} \tag{2.A.15}$$

At zero momentum, the second term on the right-hand side must cancel the first one. This can only happens if a meson has a mass squared proportional to $1/N$. It is then possible to relate the mass of this meson to the topological susceptibility of the unflavored Yang-Mills theory. Such a relation is called *Witten-Veneziano formula* and reads [56, 98]

$$m_{\eta'}^2 = \frac{2N_f}{f_\pi^2} \chi_{YM} \; . \tag{2.A.16}$$

Combining large-N expansion and chiral perturbation theory, we can include the η' meson in the discussion. We can even write a term that reproduces the

Witten-Veneziano formula (2.A.16). Let us work with a meson matrix that involves the Abelian component as well,

$$U(x) = \exp\left(\frac{2i\pi^A(x)}{f_\pi} T^A\right) \;, \qquad (2.A.17)$$

where $T^A = (\mathbb{1}, T^a)$ are $U(N_f)$ generators. We assumed $f_\pi = f_{\eta'}$, a result that is valid in the large-N limit. In principle, in the $U(N_f)$ case we should also consider the Lagrangian term

$$\left(\mathrm{Tr}\, U^\dagger \partial_\mu U\right)^2 \qquad (2.A.18)$$

that we did not consider in the $SU(N_f)$ case since the $SU(N_f)$ generators are traceless. However, in the large-N limit, this operator does not play a relevant role.

Since $U(x)$ is now a $U(N_f)$ matrix, its determinant is a phase, the η'. The introduction of the determinant as a Lagrangian term allows one to take into account the effects of the chiral anomaly. Using $\log \det U = \mathrm{Tr}\log U$, we write the Lagrangian

$$
\begin{aligned}
\mathcal{L} &= \frac{f_\pi^2}{4}\, \mathrm{Tr}\left(U^\dagger \partial_\mu U\right)^2 + c\, \mathrm{Tr}\left(\mathcal{M}U + \mathcal{M}^\dagger U^\dagger\right) + \\
&\quad - \frac{\chi_{YM}}{2}\left[-\frac{i}{2}\,\mathrm{Tr}\left(\log U - \log U^\dagger\right)\right]^2 .
\end{aligned}
\qquad (2.A.19)
$$

The new operator reproduces the Witten-Veneziano formula (2.A.16). Once we take into account the chiral anomaly, we take into account the QCD θ angle as follows. The mass matrix $\mathcal{M}$ in general is complex. Let us write it in terms of a real mass matrix M,

$$\mathcal{M} = e^{i\theta/N_f} M \;, \qquad (2.A.20)$$

so that

$$
\begin{aligned}
\mathcal{L} &= \frac{f_\pi^2}{4}\, \mathrm{Tr}\left(U^\dagger \partial_\mu U\right)^2 + c\, \mathrm{Tr}\left(e^{i\theta/N_f} MU + e^{-i\theta/N_f} M^\dagger U^\dagger\right) + \\
&\quad - \frac{\chi_{YM}}{2}\left[-\frac{i}{2}\,\mathrm{Tr}\left(\log U - \log U^\dagger\right)\right]^2 .
\end{aligned}
\qquad (2.A.21)
$$

Performing the transformation $U \to e^{-i\theta/N_f}U$ we finally find the low-energy effective theory that includes the η' and the physics associated to the QCD θ angle,

$$
\begin{aligned}
\mathcal{L} &= \frac{f_\pi^2}{4}\, \mathrm{Tr}\left(U^\dagger \partial_\mu U\right)^2 + c\, \mathrm{Tr}\left(MU + M^\dagger U^\dagger\right) + \\
&\quad - \frac{\chi_{YM}}{2}\left[-\frac{i}{2}\,\mathrm{Tr}\left(\log U - \log U^\dagger\right) - \theta\right]^2 .
\end{aligned}
\qquad (2.A.22)
$$

Starting from this Lagrangian, it is possible to check that the physics associated to the θ angle is reproduced. In particular, one finds that if the mass matrix M displays a vanishing eigenvalue the θ angle can be rotated away. If all the eigenvalues are non-zero, the θ angle affects meson physics. As we will discuss in chapter 3, experiments suggest that the θ angle, if not vanishing, is extremely small. We will see that within the Standard Model, this constitutes the strong CP problem. The most compelling solution of the strong CP problem requires the presence of a very light pseudoscalar particle called *axion*, which makes θ vanish dynamically. The axion can be easily implemented in the chiral Lagrangian by defining the $U(1)$ field

$$V(x) = \exp\left(\frac{i\sqrt{2}\,a(x)}{f_a}\right) , \tag{2.A.23}$$

where f_a is the axion decay constant, constrained by phenomenology to be within the range [48]

$$10^8 \text{ GeV} \lesssim f_a \lesssim 10^{12} \text{ GeV} . \tag{2.A.24}$$

The axion-dressed chiral Lagrangian reads [45]

$$
\begin{aligned}
\mathcal{L} &= \frac{f_\pi^2}{4}\operatorname{Tr}\left(U^\dagger \partial_\mu U\right)^2 + \frac{f_a^2}{4}\operatorname{Tr}\left(V^\dagger \partial_\mu V\right)^2 + c\operatorname{Tr}\left(MU + M^\dagger U^\dagger\right) + \\
&\quad - \frac{\chi_{YM}}{2}\left[-\frac{i}{2}\operatorname{Tr}\left(\log U - \log U^\dagger + \log V - \log V^\dagger\right) - \theta\right]^2 .
\end{aligned}
\tag{2.A.25}
$$

Chapter 3

The Holographic QCD Axion

The QCD axion is a spin-zero particle that solves one of the Standard Model's open problems called *strong CP problem*. The latter consists in the fact that experiments indicate that CP is to a very good approximation a symmetry of QCD. If CP were broken in the QCD sector, the neutron's electric dipole moment d_n would be non-zero. However, recent experiments have put a quite tight upper bound on its value: $|d_n| \leq 2.9 \cdot 10^{-26} e \cdot$ cm [3, 4].

Let us explain why this is deemed as a problem [104]. The Standard Model's global symmetries, such as the baryon and lepton number,[1] and the parity and charge conjugation of QED and QCD, are symmetries inherited by the gauge structure and the matter content of the model once one asks for renormalizability. The first operators that break these symmetries are not renormalizable and therefore can only come from new ultraviolet physics. In this case, the symmetries are called *accidental*. The strong CP problem stems from the fact that QCD admits a renormalizable gauge-invariant CP-breaking operator,

$$\mathcal{L} = \frac{\theta_0}{8\pi^2} \operatorname{Tr} F \wedge F \ , \tag{3.0.1}$$

and therefore CP cannot be thought of as an accidental symmetry of QCD. As we showed in appendix 2.A, the existence of a massless quark would automatically solve the problem because, in that case, the parameter θ_0 could be shifted away by means of a chiral rotation. However, there is evidence that none of the QCD quarks is massless [5]. The parameter θ_0 combines with the phases of the quark mass matrix $\mathbf{m}$ so that

$$\theta = \theta_0 + \operatorname{Arg} \det \mathbf{m} \tag{3.0.2}$$

is a physical quantity. Since CP is not an accidental symmetry of QCD, the unnaturally small value of θ constitutes a problem of the Standard Model.

The most compelling solution of the strong CP problem is then the *Peccei-Quinn mechanism* [6], which postulates the existence of an extra $U(1)$ global

---

[1]In fact, the baryon and the lepton numbers are not exactly conserved within the Standard Model because of an anomaly [105]. However, the breaking is very weak.

symmetry that is anomalous with respect to QCD. Such a symmetry gets spontaneously broken in order to cancel the θ angle and therefore a pseudoscalar light particle, called *axion*, must appear [7,8].

The importance of the axion is not limited to the solution of the strong CP problem. Indeed, it is also a good dark matter candidate [9], provided that its decay constant f_a falls in a specific range (see e.g. the review [106]).[2] For this reason, in the last years, there has been a renewed interest in building concrete axion models of different types and exploring their phenomenological consequences. Moreover, the study of axion-like particles is theoretically interesting since they are widespread in top-down particle physics models; for example, they are ubiquitous in string compactifications [16].

In this chapter, based on [107], we show how to construct the first (to our knowledge) top-down holographic model of an axion whose low-energy effective Lagrangian coincides with the axion-dressed chiral QCD one (2.A.25) (see e.g. [45]), in the planar limit. The model is built as a simple extension of the Witten-Sakai-Sugimoto model [36, 37] reviewed in chapter 2. It is a composite axion model falling in the KSVZ class [13, 14]. Its rationale is the following.

We have mentioned that a single massless quark is sufficient to solve the strong CP problem but that no quark seems to be massless. This problem can be avoided if an extra quark flavor condenses at a scale M_a that is much higher than the ordinary chiral symmetry breaking scale (f_a will be of the same order as M_a in the model). In this case, the extra quark does not enter perturbative corrections of Standard Model observables, and all the extra hadrons associated to this flavor have masses of order M_a, so they are not excluded by phenomenology for sufficiently large M_a. The one exception is the (pseudo) Goldstone boson of the extra chiral symmetry breaking. This is a natural candidate for the QCD axion since it automatically solves the CP problem by the standard Peccei-Quinn mechanism. The axial $U(1)_A$ symmetry of the extra flavor plays the role of the broken symmetry involved in the Peccei-Quinn mechanism.

Obviously, the main point of this scenario is how to induce condensation of the extra flavor at the scale M_a. In the model presented in this chapter, the condensation is induced by a strongly-coupled version of a (non-local) Nambu-Jona-Lasinio (NJL) quartic interaction between the extra quarks. The NJL condensation scale M_a is a genuine parameter of the model and can be made parametrically large. In fact, already the standard NJL interaction induces chiral symmetry breaking without confinement so that the two scales can be well separated.[3]

The quartic interaction requires a suitable UV completion. In the holographic model at hand, this is automatically provided by a higher dimensional theory. The whole QCD-like theory with axion, including its four-dimensional low energy

---

[2]The range of f_a goes from 10^8-10^9 GeV up to around 10^{17} GeV, see e.g. [48].

[3]Notice that the composite axion in our model is thus not a pseudo-Goldstone boson of some extra, hidden, gauge theory. In this respect the model differs from both standard composite axion models [13,108] and from more recent scenarios based on a large-N hidden sector [109].

phase, has, at strong coupling and in the planar limit, a dual gravitational description. As such, the construction provides a concrete, calculable strongly-coupled model for a composite axion. Needless to say, other UV embeddings of the quartic NJL operator, possibly not related to holographic models, are an interesting venue to explore in their own, but we will not pursue this issue in the present thesis.

The chapter is organized as follows. In section 3.1 we describe the model's construction and present the low-energy effective theory, discussing its parameter dependence and its main characteristics. Section 3.2 is devoted to the construction's technical details. In section 3.3, we consider the axion model in the deconfined phase, focusing, for simplicity, on the Yang-Mills-like theory without probe QCD $D8$-branes. As a first step, we compute the topological susceptibility of the Yang-Mills-like theory in the deconfined phase. As a second step, we also calculate the temperature dependence of the axion decay constant, and from these data, we extract the axion mass. As a bonus, we provide for the first time the result for the topological susceptibility of $\mathcal{N} = 4$ SYM at finite temperature.

The model will be employed in chapter 5 in the context of stochastic gravitational waves coming from first-order phase transitions.

3.1 The holographic axion

Let us discuss the holographic setting of the model. The introduction of N_f probe $D8/\overline{D8}$-branes at antipodal points on the circle S_{x_4}, corresponds to adding chiral quarks to the theory, as shown by Sakai and Sugimoto [37] and reviewed in chapter 2. The antipodal embedding is chosen so that chiral symmetry breaking and confinement occur at the same energy scale. This is not the only possibility. One can generically place the $D8/\overline{D8}$-branes at a separation distance $L < \pi R_4$, where R_4 is the radius of the circle [43] (see figure 3.1). In this case, the brane and the anti-brane join at a radial position $u_J > u_0$. Crucially, as shown in [44], this deformation of the theory does not correspond to giving a current algebra mass to the quarks – the pseudoscalar Goldstone bosons are still exactly massless [43]. Rather, the new parameter L (or equivalently u_J) is dual to the coefficient of a deformation of the theory that, at weak coupling, is a non-local quartic coupling between the quarks.[4] As such, this type of embedding is suitable to study the strongly-coupled phase of an NJL-like model. As a result, adding to the WSS model one extra $D8/\overline{D8}$-brane pair (a "PQ-brane", where PQ stands for Peccei-Quinn) with $L < \pi R_4$ corresponds to realizing the scenario outlined at the beginning of this section and therefore to adding the axion to the QCD-like theory.[5]

---

[4]The non-locality depends on the fact that the fermions are stuck at different points in the fifth dimension.

[5]An axion model with some similarities in a non holographic context can be found, for instance, in [110]. A five-dimensional orbifold model where the QCD axion is identified with the component of a $U(1)$ gauge field along the extra dimension has been proposed in [111].
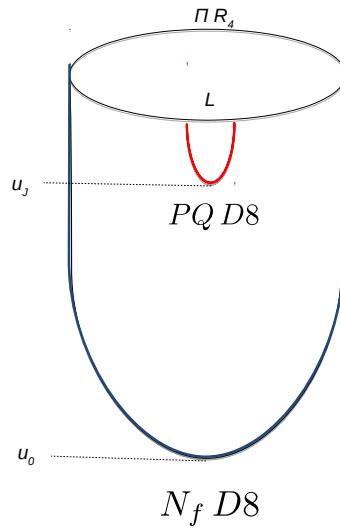
Figure 3.1. *Pictorial representation of the probe D8-branes' arrangement for the holographic axion model.*

The axion's low energy physics is dictated by symmetry: it couples in the Chiral Lagrangian just to the topological charge density operator $Q \sim \mathrm{Tr}\, F \wedge F$, precisely as the η'. However, crucially, its decay constant f_a is not related to f_π (not even in the planar limit we are discussing, where $f_{\eta'} = f_\pi$), since it is controlled by the new free parameter L.

In the following subsection, we will present the model's effective action, focusing on the axion plus pseudoscalar mesons sector. We will then discuss the axion couplings to matter. In subsection 3.1.4 we will extend some of the weak coupling considerations of [44] on the non-local NJL model to the case with two types of flavors. The reliability of these calculations requires that the separations of both flavors, L for the PQ quarks and L' for the QCD ones, is much smaller than πR_4. This is different from the WSS antipodal model (where the QCD quarks are at a distance πR_4), but allows to have an idea of the kind of quartic operators that are turned on and the relative strength of their couplings. In particular, it is found that, apart from the two quartic terms involving the QCD and PQ quarks separately, there are quartic terms involving both types of quarks. The strength of the latter interaction's coupling is of the same order as the one among the QCD quarks, so it is supposed to be much smaller than the one of the PQ quarks in the limit $L \ll L'$ we are interested in. Thus, the dominant term at weak coupling is the one causing the condensation of the PQ quarks at the scale f_a.

3.1.1 The effective action

To lowest order in derivatives, the $4d$ low energy effective Lagrangian on the N_f antipodal WSS $D8$-branes plus the extra non-antipodal PQ one, reduces to

$$\mathcal{L}_{\text{eff}} = -\frac{f_\pi^2}{4} \text{Tr} \left[\partial_\mu U \partial^\mu U^\dagger \right] - \frac{1}{2} \partial_\mu a \partial^\mu a + c \, \text{Tr} \left[MU^\dagger + \text{h.c.} \right] +$$
$$- \frac{\chi_{WYM}}{2} \left(\theta + \frac{\sqrt{2N_f}}{f_\pi} \eta' + \frac{\sqrt{2}}{f_a} a \right)^2 , \tag{3.1.1}$$

where a is the axion field,

$$U = \exp \left[\frac{2i}{f_\pi} \left(\Pi^a T^a + \frac{\eta'}{\sqrt{2N_f}} \right) \right] \tag{3.1.2}$$

is the $U(N_f)$ matrix for the pseudoscalar bosons Π^a and η', T^a are $SU(N_f)$ generators[6], f_π (resp. f_a) is the pion (resp. axion) decay constant and we set $f_\pi = f_{\eta'}$ since we work in the large-N limit and with small quark masses. Finally, M is the QCD flavor mass matrix, and χ_{WYM} is the topological susceptibility of the unflavored theory, discussed in section 2.5. To this Lagrangian one can add systematically other pieces, such as the Skyrme term and (axial) vector meson contributions. Notice that the physical axion, η' and pions will actually be given by linear combinations of the fields appearing above, as it can be easily realized by diagonalizing the related mass matrix. We will discuss this point in the next subsection.

Crucially, the interaction between the low energy modes on the WSS and PQ $D8$-branes is driven by the potential term proportional to χ_{WYM} in (3.1.1). When $N_f = 0$, the above mentioned potential term in (3.1.1) implies that the axion mass is given by the Witten-Veneziano formula

$$m_a^2 = \frac{2}{f_a^2} \chi_{WYM} . \tag{3.1.3}$$

discussed in appendix 2.A. In the flavored case, with massive flavors, χ_{WYM} is replaced by the full topological susceptibility. We will briefly discuss the mass spectrum in subsection 3.1.3.

All in all, by including both the N_f antipodal $D8/\overline{D8}$ pairs and the non-antipodal PQ one, we get precisely the Chiral Lagrangian of [45]. In order to see this explicitly, one can introduce an auxiliary field $Q(x)$ (that turns out to be the topological charge density) and rewrite the last term in (3.1.1) as follows

$$- \left(\theta + \frac{\sqrt{2N_f}}{f_\pi} \eta' + \frac{\sqrt{2}}{f_a} a \right) Q + \frac{1}{2\chi_{WYM}} Q^2 =$$
$$= \left[-\theta + \frac{i}{2} \text{Tr} \left(\log U - \log U^\dagger \right) + \frac{i}{2} \left(\log V - \log V^\dagger \right) \right] Q + \frac{1}{2\chi_{WYM}} Q^2 \tag{3.1.4}$$

---

[6]The normalization is chosen such that $\text{Tr}(T^a T^b) = \delta^{ab}/2$.

with $V = \exp\left(i\sqrt{2}a/f_a\right)$.[7]

As we will show in section 3.2, where details on the non-antipodally embedded flavor branes and the related meson spectrum are provided, the axion decay constant is given by

$$f_a^2 = \frac{N\lambda}{16\pi^3} \frac{J^3(b)}{I(b)} \frac{1}{M_{KK}L^3} \,, \qquad b \equiv \frac{u_0}{u_J} \,, \tag{3.1.5}$$

where

$$J(b) = \frac{2}{3}\sqrt{1-b^3} \int_0^1 dy \frac{y^{1/2}}{(1-b^3y)\sqrt{1-b^3y-(1-b^3)y^{8/3}}} \,, \tag{3.1.6a}$$

$$I(b) = \int_0^1 dy \; \frac{y^{-1/2}}{\sqrt{1-b^3y-(1-b^3)y^{8/3}}} \,, \tag{3.1.6b}$$

and

$$L = J(b)R^{3/2}u_J^{-1/2} \tag{3.1.7}$$

is the distance between the PQ asymptotic branches on the S_{x_4} circle, as described in section 2.2.

Let us complete our analysis with the implications for our model coming from the phenomenological constraints, which read

$$10^9 \lesssim r \equiv \frac{f_a}{f_\pi} \lesssim 10^{18} \,. \tag{3.1.8}$$

Recalling the expression (2.3.18) for f_π, we get

$$M_{KK}L = \frac{3}{2}\pi^{1/3}J(b)I(b)^{-1/3}r^{-2/3} \,. \tag{3.1.9}$$

This condition fixes the value of L which, in turn, fixes u_J. Using (3.1.7) and $u_0 = 4M_{KK}^2 R^3/9$, this condition becomes

$$b = \left(\frac{\pi}{r^2 I(b)}\right)^{2/3} \,. \tag{3.1.10}$$

Since $I(b) \approx 2.4$ for any value of $b < 10^{-1}$, we obtain

$$10^{-24} \lesssim b \lesssim 10^{-12} \,. \tag{3.1.11}$$

Throughout this interval, $J(b) \simeq 0.7$, so $L \simeq 0.7\,R^{3/2}u_J^{-1/2}$ and

$$f_a^2 \approx 0.1534 \frac{N\lambda}{16\pi^3} \frac{1}{M_{KK}L^3} \,. \tag{3.1.12}$$

---

[7]This is called N in [45].

We can compare the separation of the PQ-branes with the length of the cigar circle β_4. Recalling $\beta_4 = 4R^{3/2}u_0^{-1/2}/3$ we have $L/\beta_4 \simeq 0.5\, b^{1/2}$ and therefore

$$10^{-12} \lesssim \frac{L}{\beta_4} \lesssim 10^{-6} \ . \tag{3.1.13}$$

We know that the description of the gauge sector provided by the $D4$-branes is reliable as long as the holographic coordinate u is lower that a critical value u_{crit}, which can be identified as that value for which the dilaton e^ϕ becomes of order one. Recalling (2.1.1b), this value is given by

$$u_{crit} \sim Rg_s^{-4/3} \sim \frac{N^{4/3}l_s^2 M_{KK}}{\lambda} \ . \tag{3.1.14}$$

We therefore require the condition $u_J \ll u_{\text{crit}}$ to be valid. Recalling $2R^3 l_s^{-2} = \lambda/M_{KK}$, we can write this condition in terms of field theory quantities as

$$N^{2/3} \gg r^{2/3}\lambda \ . \tag{3.1.15}$$

3.1.2 Further properties of the model

In the setting outlined above, the PQ-brane is put at a macroscopic distance in the internal space from the N_f WSS branes. As a consequence, in the dual theory, the two types of degrees of freedom interact only through the gauge sector. Since we are in the planar limit, these interactions are quite suppressed. Thus, this model falls in the KSVZ class [13, 14]: the PQ symmetry is not realized on Standard Model fermions. As such, the UV dependent part - *i.e.* that not encoded in the low energy Lagrangian (3.1.1) - of the couplings of the axion with the nucleons is exactly zero, as reviewed, for instance, in [48]. In the next subsection, we will collect the known results for the "universal" IR part of these couplings [112].

Moreover, in the WSS model, the electromagnetic current is obtained by weakly gauging a vectorial part of the $U(N_f) \times U(N_f)$ chiral symmetry. As such, it pertains to the N_f WSS D-branes: the PQ quarks are automatically electrically uncharged.[8]

Thus, the axion's electromagnetic interactions just come from the mixing with the pion and the η' in the Chiral Lagrangian, with no UV contribution. Also in this respect, the model falls in the KSVZ class. Apart from the existence of a strongly coupled version of the NJL interaction in the UV, the extra information that the holographic picture seems to provide about the model is the co-existence of (at least) three quark condensates in the IR. In fact, suspended between each type of $D8$-branes there are string worldsheets whose areas provide the magnitude

---

[8]Strictly speaking, in the holographic model, the electromagnetic $U(1)$ symmetry is global on the QFT side since it corresponds to a gauge symmetry in the bulk. It is not clear whether our PQ quarks would stay uncharged also in a setup where a local $U(1)$ Maxwell symmetry is properly realized in the QFT.

of the fermion condensates [96]. Hence, if we denote as q, ψ respectively the standard and extra quarks, we expect to have both the $\langle \bar{q}q \rangle$, $\langle \bar{\psi}\psi \rangle$ condensates and a condensate of the form $\langle \bar{q}\psi\bar{\psi}q \rangle$. It would be interesting to investigate whether the latter influences the model both at weak and at strong coupling.

We have presented the simplest axion model with one extra flavor and a very symmetric configuration of branes. This is not the only possibility. For example, one can imagine a setting where one endpoint of the PQ-brane coincides with one endpoint of the QCD-branes so that one stack of branes contains $N_f + 1$ elements. Nevertheless, there is no enhancement of chiral symmetry (before spontaneous chiral symmetry breaking). This is because the QCD quarks have a mass term breaking explicitly chiral symmetry to $SU(N_f) \times U(1)_B \times U(1)_L \times U(1)_R$, where the last two terms refer to the PQ quarks.

In the dual holographic picture, this means that the N_f WSS $D8$-branes *must* join the N_f WSS $\overline{D8}$-branes. There is no possibility of joining one WSS $D8$ with the PQ $\overline{D8}$, for example. Then, the PQ $D8$ and $\overline{D8}$ have no possibility but joining among themselves.

3.1.3   Axion couplings to matter

In order to be self-contained, in this subsection we report on the results found in [112] on the couplings of the axion to the nucleons.[9] As we have stressed before, the UV part of these couplings is exactly zero. The couplings can then be extracted directly from the low energy action (3.1.1).

Let us consider the $N_f = 2$ case, where $M = \mathrm{diag}(m_u, m_d)$ and $2T^a = \tau^a$ are the Pauli matrices. Neglecting the mixing terms between pions and η', the mass eigenstates of the Lagrangian (3.1.1), to leading order in $1/f_a$ and absorbing the θ parameter in the VEV of $\sqrt{2}a/f_a$, turn out to be

$$\hat{\eta}' = \eta' + \frac{\chi f_\pi}{4c} \mathrm{Tr}[M^{-1}] \frac{\sqrt{2}a}{f_a} \ ,$$

$$\hat{\pi}^a = \pi^a + \frac{\chi f_\pi}{4c} \mathrm{Tr}[\tau^a M^{-1}] \frac{\sqrt{2}a}{f_a} \ ,$$

$$\hat{a} = a - \frac{\chi f_\pi}{4c} \mathrm{Tr}[M^{-1}] \frac{\sqrt{2}\eta'}{f_a} - \frac{\chi f_\pi}{4c} \mathrm{Tr}[\tau^a M^{-1}] \frac{\sqrt{2}\pi^a}{f_a} \ , \qquad (3.1.16)$$

where

$$\chi = \frac{4c\chi_{\mathrm{WYM}}}{4c + 2\chi_{\mathrm{WYM}} \mathrm{Tr}[M^{-1}]} \ , \qquad (3.1.17)$$

is the full topological susceptibility of the theory.

As it is shown in [112], the model allows to deduce the derivative as well as the non-derivative couplings of the axion to matter fields to leading order in the holographic limit. The most relevant ones are the couplings with nucleons. In

---

[9]Notice that the axion decay constant f_a in the present thesis differs from that in [112]: f_a [here] $= \sqrt{2}f_a$[there].

the WSS model, the latter correspond to instanton solutions for the gauge field $\mathcal{F}$ on the WSS $D8$-branes [113]. By carefully taking into account the mixing terms in (3.1.16), the axion couplings to nucleons can be derived from those of the pseudoscalar mesons.

The derivative axion-nucleon couplings defined by the effective interaction term

$$\delta\mathcal{L}_{aNN,\text{der}} = -\frac{\partial_\mu a}{\sqrt{2}f_a}c_N\bar{N}\gamma^\mu\gamma^5 N \ , \tag{3.1.18}$$

where $N = (p, n)$ is the nucleon field, are given by

$$c_p = -\frac{g_{\eta'NN}}{m_N}\frac{\chi f_\pi}{4c}\text{Tr}[M^{-1}] - \frac{g_{\pi NN}}{m_N}\frac{\chi f_\pi}{4c}\text{Tr}[M^{-1}\tau^3]$$

$$c_n = -\frac{g_{\eta'NN}}{m_N}\frac{\chi f_\pi}{4c}\text{Tr}[M^{-1}] + \frac{g_{\pi NN}}{m_N}\frac{\chi f_\pi}{4c}\text{Tr}[M^{-1}\tau^3] \ , \tag{3.1.19}$$

where m_N is the (large) nucleon mass and $g_{\eta'NN}$, $g_{\pi NN}$ are the CP-even couplings of the η' and the pions with the nucleons.

To leading order in the chiral limit $4c \ll 2\chi_{\text{WYM}}\text{Tr}[M^{-1}]$, which sets the pion mass to be much smaller than that of the η', the above expressions reduce to

$$c_p \approx -\frac{1}{2}\hat{g}_A - \frac{1}{2}g_A\frac{m_d - m_u}{m_d + m_u} \ ,$$

$$c_n \approx -\frac{1}{2}\hat{g}_A + \frac{1}{2}g_A\frac{m_d - m_u}{m_d + m_u} \ , \tag{3.1.20}$$

where we have used the generalized Goldberger-Treiman relations

$$g_{\eta'NN} = \frac{m_N}{f_\pi}\hat{g}_A \ , \quad g_{\pi NN} = \frac{m_N}{f_\pi}g_A \ , \tag{3.1.21}$$

between the isoscalar and isovector axial couplings and those of the η' and the pion. The couplings in (3.1.20) are independent on any UV parameter and precisely coincide with the ones obtained in any axion model in the KSVZ class [13, 14]. In the WSS model, the couplings g_A and $\hat{g}_A$ have been computed in [114]. To leading order in the holographic limit (and so in the classical limit for the instanton pseudo-moduli) they read

$$\hat{g}_A = \frac{27}{2\lambda} \ , \quad g_A = \frac{2N}{\pi}\sqrt{\frac{2}{15}} \ . \tag{3.1.22}$$

Non-derivative axion-nucleon couplings of the form

$$\delta\mathcal{L}_{aNN,\text{non-der}} = \bar{c}_N a\bar{N}N \ , \tag{3.1.23}$$

can be induced whenever the Peccei-Quinn mechanism is not precise and an effective θ parameter is left over. In [112] it has been found that

$$\bar{c}_p = -\bar{g}_{\eta'NN}\frac{\sqrt{2}\chi f_\pi}{4cf_a}\text{Tr}[M^{-1}] - \bar{g}_{\pi NN}\frac{\sqrt{2}\chi f_\pi}{4cf_a}\text{Tr}[M^{-1}\tau^3] \ ,$$

$$\bar{c}_n = -\bar{g}_{\eta'NN}\frac{\sqrt{2}\chi f_\pi}{4cf_a}\text{Tr}[M^{-1}] + \bar{g}_{\pi NN}\frac{\sqrt{2}\chi f_\pi}{4cf_a}\text{Tr}[M^{-1}\tau^3] \ , \tag{3.1.24}$$

where $\bar{g}_{\eta' NN}$ and $\bar{g}_{\pi NN}$ are the linear in θ CP-odd couplings of η' and pions with nucleons.[10] To leading order in the chiral limit they reduce to

$$\bar{c}_p \approx -\frac{1}{2}\bar{g}_{\eta' NN}\frac{f_\pi}{f_a} - \frac{1}{2}\bar{g}_{\pi NN}\frac{f_\pi}{f_a}\frac{m_d - m_u}{m_d + m_u}\,,$$
$$\bar{c}_n \approx -\frac{1}{2}\bar{g}_{\eta' NN}\frac{f_\pi}{f_a} + \frac{1}{2}\bar{g}_{\pi NN}\frac{f_\pi}{f_a}\frac{m_d - m_u}{m_d + m_u}\,. \tag{3.1.25}$$

To leading order in the holographic limit, in [112] it has been found that

$$\bar{g}_{\eta' NN} = -\left(\frac{54}{125}\right)^{1/4}\frac{m_\pi^2 N^{3/2}\gamma_1}{f_\pi^2 \pi^{7/2}}\theta\,, \qquad \bar{g}_{\pi NN} = \frac{9}{8}\left(\frac{3}{10}\right)^{1/4}\frac{m_\pi^2\sqrt{N}\gamma_2}{8f_\pi^2\sqrt{\pi}\lambda}\theta\,, \tag{3.1.26}$$

where $m_\pi^2 f_\pi^2 = 2c(m_u + m_d)$ and

$$\gamma_1 = \int_0^\infty dy\, y^2\left(1 + \cos\frac{\pi}{\sqrt{1 + 1/y^2}}\right) \approx 1.10\,,$$
$$\gamma_2 = \int_0^\infty dy(1 + y^{-2})^{-3/2}\sin\left(\frac{\pi}{\sqrt{1 + y^{-2}}}\right) \approx 1.05\,. \tag{3.1.27}$$

Recalling that $f_\pi^2 \sim N$, we see that $\bar{g}_{\eta' NN} \sim N^{1/2}$ and $\bar{g}_{\pi NN} \sim N^{-1/2}$. Numerical estimates and further details on the couplings can be found in [112].

3.1.4   Non-local Nambu-Jona Lasinio model

From the field theory point of view, the Witten-Sakai-Sugimoto model is a five-dimensional gauge theory with two Weyl fermions of opposite chiralities placed at two antipodal points along the fifth, compactified x_4-dimension. In this sense, the fermions are co-dimension one defects. In the previous subsections, we have extended the model in order to include the Peccei-Quinn axion. This has been achieved by introducing an additional pair of $D8$-branes, which amounts to adding two additional co-dimension one defects in the five-dimensional field theory. In order to disentangle the chiral symmetry breaking mechanism (whose associated Nambu-Goldstone boson we identified with the axion) from confinement, the additional Weyl fermions had to be taken in a non-antipodal configuration and in the regime $L \ll \pi R_4$, where L is the distance between fermions along the x_4 direction and R_4 is the compactification radius.

In the limit in which $R_4 \to \infty$ the gauge theory with two non-antipodal fermions reduces to the so-called non-local Nambu-Jona Lasinio model studied in [44]. It is not straightforward to extrapolate the considerations in [44] to the WSS confining case. If the separation L of the $D8/\overline{D8}$-branes is small compared to the length of the semi-circle, then the analysis is the same as in [44] to a very good accuracy. In [116], there is a first field theory analysis of the effects of the

---

[10]See for example [115] for a review on such terms in the chiral effective field theory.

compact circle, but still in the $L \ll \pi R_4$ case. The idea is that now the theory has a four-dimensional phase in the far IR, where the non-local model should reduce to the local one. As such, chiral symmetry breaking should be present only above a certain value of the coupling. A concrete realization of this idea is far from established.

In this subsection, we shall follow the analysis in [44] in order to extract information about the relative strengths of the interactions among the fermions. We shall consider the gauge theory in the linear approximation, treating the gauge field as an Abelian field and integrating it out. Since the gauge field is massless, its integration yields a Lagrangian with non-local quartic fermion interactions. We shall first consider the case with only one defect, then with two defects, and finally with four defects, as in the WSS model generalized by the axion's inclusion. The analysis is meant to be valid only when the distance between two fermions is much smaller than the radius of compactification of the fifth direction. This forces us to take in a non-antipodal configuration also the QCD quarks. Moreover, due to the non-locality of the model, we have to limit ourselves to the massless fermions case, as explained at the end of this subsection.

One defect case

Let us consider the gauge theory with a set of N_f left Weyl fermions q_L^i placed at $x_4 = 0$, where i is a flavor index. The system is invariant under global $U(N_f)_L$ transformations which act as

$$q_L^i \to (U_L)_j^i q_L^j , \qquad U_L \in U(N_f)_L . \qquad (3.1.28)$$

In the following we will omit the flavor indices. Capital latin letters will label the whole set of coordinates whereas greek letters will label all the coordinates except x_4. The classical action is

$$S = \int d^5 x \left[-\frac{1}{4g_5^2} F_{MN}^2 + \delta(x_4) q_L^\dagger \bar{\sigma}^\mu \left(i\partial_\mu + A_\mu \right) q_L \right] . \qquad (3.1.29)$$

Here, we use the standard notation $\sigma^\mu = (\mathbb{1}, \sigma^i)$, $\bar{\sigma}^\mu = (\mathbb{1}, -\sigma^i)$, where σ^i are the Pauli matrices. The gauge part of the Lagrangian is the Maxwell Lagrangian with a matter current

$$j^M(x, x_4) = \delta_\mu^M \delta(x_4) q_L^\dagger(x) \bar{\sigma}^\mu q_L(x) \qquad (3.1.30)$$

which transforms in the adjoint of the gauge group and it is a singlet under the global group $U(N_f)_L$. Let us integrate out the gauge field. In the Feynman gauge the propagator for the Abelian gauge field reads

$$\tilde{\Delta}_{MN}(p) = g_5^2 \tilde{G}(p) \eta_{MN} = -\frac{ig_5^2}{p^2} \eta_{MN} . \qquad (3.1.31)$$

In coordinate space the propagator $G(x)$ reads

$$G(x, x_4) = \frac{1}{8\pi^2} \frac{1}{|\eta_{\mu\nu} x^\mu x^\nu + x_4^2|^{3/2}} . \qquad (3.1.32)$$

We can use the propagator in order to express the gauge field in an integral form:

$$A_M(x, x_4) = -g_5^2 \int d^5y G(x - y, x_4 - y_4)\eta_{\mu M}\delta(y_4)q_L^\dagger(y)\bar{\sigma}^\mu q_L(y) \ . \qquad (3.1.33)$$

Inserting this result in (3.1.29) the interaction term becomes[11]

$$S_{\text{int}} = -g_5^2 \int d^4x d^4y \, G(x - y, 0) \left[q_L^\dagger(x)\bar{\sigma}_\mu q_L(y)\right] \left[q_L^\dagger(y)\bar{\sigma}^\mu q_L(x)\right] \ . \qquad (3.1.35)$$

The terms in square bracket in (3.1.35) are singlet under the (global part of the) gauge group and transform in the adjoint of the global flavor group. The interaction term S_{int} gives a correction to the free field propagator.

Two defects

Let us now consider the case in which we have N_f left Weyl fermions placed at $x_4 = L/2$ and N_f right Weyl fermions at $x_4 = -L/2$. In addition to the global symmetry $U(N_f)_L$ there is a symmetry under the global transformations $U(N_f)_R$ which act as

$$q_R^i \to (U_R)^i_j q_R^j \ , \qquad U_R \in U(N_f)_R \ . \qquad (3.1.36)$$

The classical action is then

$$\begin{aligned} S &= \int d^5x \left[-\frac{1}{4g_5^2}F_{MN}^2 + \delta\left(x_4 - L/2\right) q_L^\dagger \bar{\sigma}^\mu \left(i\partial_\mu + A_\mu\right) q_L + \right. \\ &+ \left. \delta(x_4 + L/2)q_R^\dagger \sigma^\mu \left(i\partial_\mu + A_\mu\right) q_R \right] \ . \end{aligned} \qquad (3.1.37)$$

In this case the matter current is

$$j^M(x, x_4) = \delta^M_\mu \delta(x_4 - L/2)q_L^\dagger(x)\bar{\sigma}^\mu q_L(x) + \delta^M_\mu \delta(x_4 + L/2)q_R^\dagger(x)\sigma^\mu q_R(x) \ , \qquad (3.1.38)$$

hence

$$\begin{aligned} A_M(x, x_4) &= -g_5^2 \int d^5y G(x - y, x_4 - y_4)\eta_{\mu M}\Big(\delta(y_4 - L/2)q_L^\dagger(y)\bar{\sigma}^\mu q_L(y) + \\ &+ \delta(y_4 + L/2)q_R^\dagger(y)\sigma^\mu q_R(y)\Big) \ . \end{aligned} \qquad (3.1.39)$$

Inserting this expression in the action (3.1.37) we are left with three interaction terms: two of them give corrections to the propagator of the left and right

---

[11]Here we use the Fierz identity

$$\left(\psi_{1L}^\dagger \bar{\sigma}^\mu \psi_{2L}\right)\left(\psi_{3L}^\dagger \bar{\sigma}_\mu \psi_{4L}\right) = \left(\psi_{1L}^\dagger \bar{\sigma}^\mu \psi_{4L}\right)\left(\psi_{3L}^\dagger \bar{\sigma}_\mu \psi_{2L}\right) \ . \qquad (3.1.34)$$

fermions, akin to the term derived in the previous subsection; the other one describes the interaction between left and right fermions and reads[12]

$$S_{\text{int}} = -4g_5^2 \int d^4x d^4y G(x-y, L) \left[q_L^\dagger(x) \cdot q_R(y) \right] \left[q_R^\dagger(y) \cdot q_L(x) \right] \ . \quad (3.1.41)$$

Each term in square bracket is a singlet under the (global part of the) gauge group and transforms in the adjoint under $U(N_f)_L \times U(N_f)_R$.

Four defects

Let us consider the case in which we have two "quark defects" separated by a distance L' as in the previous subsection and two "axion defects" separated by a distance $L \ll L'$. In particular we will consider a single left Weyl fermion $\psi_L(x)$ placed at $x_4 = -L/2$ and a single right Weyl fermion $\psi_R(x)$ placed at $x_4 = L/2$. In addition to the $U(N_f)_L \times U(N_f)_R$ there is also a symmetry under the $U(1)_L \times U(1)_R$ transformations which act on the axion quarks. The action reads

$$\begin{aligned}
S &= \int d^5x \left[-\frac{1}{4g_5^2} F_{MN}^2 + \delta\left(x_4 - L'/2\right) q_L^\dagger \bar{\sigma}^\mu \left(i\partial_\mu + A_\mu\right) q_L + \right. \\
&+ \delta\left(x_4 + L/2\right) \psi_L^\dagger \bar{\sigma}^\mu \left(i\partial_\mu + A_\mu\right) \psi_L + \delta(x_4 + L'/2) q_R^\dagger \sigma^\mu \left(i\partial_\mu + A_\mu\right) q_R \\
&+ \left. \delta\left(x_4 - L/2\right) \psi_R^\dagger \sigma^\mu \left(i\partial_\mu + A_\mu\right) \psi_R \right] \ .
\end{aligned} \quad (3.1.42)$$

The matter current in this case is

$$\begin{aligned}
j^M(x, x_4) &= \delta_\mu^M \delta(x_4 - L'/2) q_L^\dagger(x)\bar{\sigma}^\mu q_L(x) + \delta_\mu^M \delta(x_4 + L'/2) q_R^\dagger(x)\sigma^\mu q_R(x) + \\
&+ \delta_\mu^M \delta(x_4 + L/2)\psi_L^\dagger(x)\bar{\sigma}^\mu \psi_L(x) + \delta_\mu^M \delta(x_4 - L/2)\psi_R^\dagger(x)\sigma^\mu \psi_R(x) \ ,
\end{aligned}$$

hence the gauge field can be written as

$$\begin{aligned}
A_M(x, x_4) &= -g_5^2 \int d^5y G(x-y, x_4 - y_4)\eta_{M\mu}\Big(\delta(y_4 - L'/2)q_L^\dagger(y)\bar{\sigma}^\mu q_L(y) + \\
&+ \delta(y_4 + L/2)\psi_L^\dagger(y)\bar{\sigma}^\mu \psi_L(y) + \delta(y_4 + L'/2)q_R^\dagger(y)\sigma^\mu q_R(y) + \\
&+ \delta(y_4 - L/2)\psi_R^\dagger(y)\sigma^\mu \psi_R(y)\Big) \ .
\end{aligned} \quad (3.1.43)$$

Plugging this expression in (3.1.42) we obtain four kinds of terms:

- quartic terms which give corrections to the fermion propagators;

---

[12]In order to obtain this term we use the Fierz identity

$$\left(\psi_{1L}^\dagger \bar{\sigma}^\mu \psi_{2L} \right) \left(\psi_{3R}^\dagger \sigma_\mu \psi_{4R} \right) = 2 \left(\psi_{1L}^\dagger \psi_{4R} \right) \left(\psi_{3L}^\dagger \psi_{2R} \right) \ . \quad (3.1.40)$$

- quartic interactions involving both left and right quarks:

$$S_{\text{int}}^q = -4g_5^2 \int d^4x d^4y G(x-y, L') \left[q_L^\dagger(x) \cdot q_R(y)\right] \left[q_R^\dagger(y) \cdot q_L(x)\right] \; ; \quad (3.1.44)$$

- quartic interactions involving both left and right axion quarks:

$$S_{\text{int}}^{ax} = -4g_5^2 \int d^4x d^4y G(x-y, L) \left[\psi_L^\dagger(x) \cdot \psi_R(y)\right] \left[\psi_R^\dagger(y) \cdot \psi_L(x)\right] \; ; \quad (3.1.45)$$

- quartic interactions which involve two quarks and two axion quarks:

$$\begin{aligned}
S_{\text{int}}^{q,ax} &= -4g_5^2 \int d^4x d^4y G(x-y, L'/2 - L/2) \bigg\{ \left[q_L^\dagger(x) \cdot \psi_R(y)\right] \times \\
&\times \left[\psi_R^\dagger(y) \cdot q_L(x)\right] + \left[\psi_L^\dagger(y) \cdot q_R(x)\right] \left[q_R^\dagger(x) \cdot \psi_L(y)\right] \bigg\} + \\
&- 2g_5^2 \int d^4x d^4y G(x-y, L'/2 + L/2) \bigg\{ \left[q_L^\dagger(x)\bar{\sigma}^\mu \psi_L(y)\right] \times \\
&\times \left[\psi_L^\dagger(y)\bar{\sigma}_\mu q_L(x)\right] + \left[q_R^\dagger(x)\sigma^\mu \psi_R(y)\right] \left[\psi_R^\dagger(y)\sigma_\mu q_R(x)\right] \bigg\} \quad (3.1.46)
\end{aligned}$$

We expect the relative strengths between the different interactions to depend on the distance between the fields along the fifth direction. Thus, in order to estimate them let us consider

$$G(x - y, L) \sim \frac{1}{L^3} \; . \quad (3.1.47)$$

Recalling that $4\pi g_5^2 = M_{KK} g_{YM}^2$ and the result (3.2.30) for the axion decay constant, we have

$$S_{\text{int}}^{ax} \propto \frac{g_5^2}{L^3} \sim \frac{M_{KK}^2}{N^2} f_a^2 \; . \quad (3.1.48)$$

Analogously,

$$S_{\text{int}}^q \propto \frac{g_5^2}{L'^3} \sim \frac{M_{KK}^2}{N^2} f_q^2 \; , \quad (3.1.49)$$

where

$$f_q^2 = \frac{1}{16\pi^3} \frac{J^3(b)}{I(b)} \frac{\lambda}{M_{KK} L'^3} N \; . \quad (3.1.50)$$

In the regime $L \ll L'$,

$$S_{\text{int}}^{q,ax} \propto \frac{g_5^2}{L^3} \sim \frac{M_{KK}^2}{N^2} f_q^2 \; . \quad (3.1.51)$$

Thus, we expect the interaction involving two quarks and two axion quarks to be as relevant as the interactions between the quarks.

Finally, let us stress the fact that in this appendix we have been discussing the non-local NJL model assuming the quarks to be massless. Due to the non-locality of the model, we cannot add a Dirac mass term to the Lagrangian. The best we can do is to consider a Wilson line such as

$$S_{\text{mass}} = -m \int d^4x d^4y \, q_R^\dagger(x) P \exp\left(i \int_{-L/2}^{L/2} dx_4 A_4 \right) q_L(y) \; . \qquad (3.1.52)$$

Unfortunately, such a term makes the gauge field equations non-linear, thus preventing us from proceeding with the analysis.

3.2   Non-antipodally embedded $D8$-branes

Let us consider embedding in the WYM background (2.1.1) a PQ $D8$-brane with two asymptotic branches placed at non-antipodal points on the x_4 circle. Their distance on the circle is thus $L < \pi R_4$, *i.e.* $LM_{\text{KK}} < \pi$. In section 2.2, we wrote the equations that describe the branes' embedding also in the non-antipodal case. Let us recall that the branes join at a value u_J of the holographic coordinate, which is related to the paraemter L through

$$L = J(b)R^{3/2}u_J^{-1/2} \; , \qquad (3.2.1)$$

where

$$J(b) = \frac{2}{3}\sqrt{1-b^3} \int_0^1 dy \frac{y^{1/2}}{(1-b^3y)\sqrt{1-b^3y-(1-b^3)y^{8/3}}} \; . \qquad (3.2.2)$$

Let us now show that the Abelian gauge theory on the PQ-brane gives a pseudoscalar pseudo-Nambu-Goldstone boson (which we will identify with the axion field a) analogous to the η' mode of the antipodal configuration. On top of this, there will also be a tower of massive vector mesons. As we will show, the mass of the latter scales as $m^2 \sim L^{-2}$ and therefore the vector mesons decouple at low energy [43]. Expanding the $D8$-brane DBI action, we obtain the term

$$S_{\mathcal{F}\mathcal{F}} = -\frac{\mu_8}{4}(2\pi\alpha')^2 \int d^9x e^{-\phi}\sqrt{\det g_{MN}}g^{MR}g^{NS}\mathcal{F}_{MN}\mathcal{F}_{RS} \; . \qquad (3.2.3)$$

Integrating over S^4 with the assumption that the field strength $\mathcal{F}_{MN}$ does not depend on the S^4 coordinate, we get

$$S_{\mathcal{F}\mathcal{F}} = -C \int d^4x du \gamma^{-1/2}\left(R^3 u^{-1/2}\mathcal{F}_{\mu\nu}\mathcal{F}^{\mu\nu} + 2\gamma u^{5/2}\eta^{\mu\nu}\mathcal{F}_{\mu u}\mathcal{F}_{\nu u} \right) \; , \qquad (3.2.4)$$

where we defined

$$C = \frac{\mu_8 V_4 R^{3/2}}{2g_s}(2\pi\alpha')^2 \; , \qquad (3.2.5)$$

$$\gamma(u) = f(u) - f(u_J)\left(\frac{u_J}{u}\right)^8 \; . \qquad (3.2.6)$$

It is convenient to work with the coordinate z, defined by

$$u = \left(u_J^3 + u_J z^2\right)^{1/3} \ . \tag{3.2.7}$$

This coordinate takes values along the whole real axis, it is positive for $x_4 > L/2$ and negative for $x_4 < L/2$. The action then reads

$$S_{\mathcal{F}\mathcal{F}} \ = \ -\frac{C u_J}{3} \int d^4 x dz \Big(\frac{R^3 \gamma^{-1/2} |z|}{u^{5/2}} \mathcal{F}_{\mu\nu} \mathcal{F}^{\mu\nu} + \frac{9}{2} \gamma^{1/2} \frac{u^{9/2}}{u_J^2 |z|} \eta^{\mu\nu} \mathcal{F}_{\mu z} \mathcal{F}_{\nu z} \Big) \ . \tag{3.2.8}$$

Following [37], we expand the components of the gauge field as

$$A_\mu(x^\mu, z) \ = \ \sum_n B_\mu^{(n)}(x^\mu) \psi_n(z) \ , \tag{3.2.9a}$$

$$A_z(x^\mu, z) \ = \ \sum_n \varphi^{(n)}(x^\mu) \phi_n(z) \ . \tag{3.2.9b}$$

Accordingly,

$$\mathcal{F}_{\mu\nu}(x^\mu, z) \ = \ \sum_n F_{\mu\nu}^{(n)}(x^\mu) \psi_n(z) \ , \tag{3.2.10a}$$

$$\mathcal{F}_{\mu z}(x^\mu, z) \ = \ \sum_n \partial_\mu \varphi^{(n)}(x^\mu) \phi_n(z) - \sum_n B_\mu^{(n)}(x^\mu) \partial_z \psi_n(u) \ . \tag{3.2.10b}$$

3.2.1 PQ vector mesons

Let us first consider only the vector mesons. We have

$$S_{\mathcal{F}\mathcal{F}}^{\text{vec}} \ = \ -\frac{C u_J}{3} \sum_{n,m} \int d^4 x dz \Big(\frac{R^3 \gamma^{-1/2} |z|}{u^{5/2}} F_{\mu\nu}^{(n)} F^{(n)\mu\nu} \psi_m \psi_n +$$

$$+ \ \frac{9}{2} \gamma^{1/2} \frac{u^{9/2}}{u_J^2 |z|} B_\mu^{(n)} B^{(m)\mu} \partial_z \psi_n \partial_z \psi_m \Big) \ . \tag{3.2.11}$$

In order to obtain the kinetic term of the massive vector action we ask ψ_n to be normalized such that

$$\frac{4 C u_J R^3}{3} \int_{-\infty}^{+\infty} dz |z| \gamma^{-1/2} u^{-5/2} \psi_n \psi_m = \delta_{mn} \ . \tag{3.2.12}$$

Let us take the mass term

$$-\frac{3C}{2u_J} \sum_{n,m} \int dz \frac{\gamma^{1/2}}{|z|} u^{9/2} \partial_z \psi_n \partial_z \psi_m B_\mu^{(n)} B^{(m)\mu} =$$

$$= \ \frac{3C}{2u_J} \sum_{n,m} \int dz \partial_z \left(\frac{\gamma^{1/2}}{|z|} u^{9/2} \partial_z \psi_n \right) \psi_m B_\mu^{(n)} B^{(m)\mu} \ . \tag{3.2.13}$$

In order to obtain the mass term for the tower of mesons we ask

$$-\frac{9}{4u_J^2}\frac{\gamma^{1/2}u^{5/2}}{|z|}\partial_z\left(\frac{\gamma^{1/2}}{|z|}u^{9/2}\partial_z\psi_n\right) = m_n^2R^3\psi_n \ , \tag{3.2.14}$$

so that

$$\frac{3C}{2u_J}\int dz\frac{\gamma^{1/2}}{|z|}u^{9/2}\partial_z\psi_n\partial_z\psi_m = \frac{1}{2}m_n^2\delta_{m,n} \ . \tag{3.2.15}$$

By dimensional analysis, in the limit $u_J \gg u_0$ we have

$$m_n^2 \sim \frac{u_J}{R^3} \sim \frac{1}{L^2} \ . \tag{3.2.16}$$

3.2.2 Scalar sector: the holographic axion

From the second term in (3.2.8),

$$S_{\mathcal{FF}}^{\text{scal}} = -\frac{3C}{2u_J}\int d^4xdz\gamma^{1/2}\frac{u^{9/2}}{|z|}\eta^{\mu\nu}\mathcal{F}_{\mu z}\mathcal{F}_{\nu z} \ , \tag{3.2.17}$$

we read the kinetic term for the tower of scalar mesons:

$$S_{\mathcal{FF}}^{\text{scal}} = -\frac{3C}{2u_J}\sum_{m,n}\int d^4xdz\gamma^{1/2}\frac{u^{9/2}}{|z|}\partial_\mu\varphi^{(m)}\partial^\mu\varphi^{(n)}\phi_m\phi_n \ . \tag{3.2.18}$$

In order to canonically normalize the fields $\varphi^{(m)}$ we ask that ϕ_m satisfy the orthonormality condition

$$\frac{3C}{u_J}\int dz\gamma^{1/2}\frac{u^{9/2}}{|z|}\phi_m\phi_n = \delta_{m,n} \ . \tag{3.2.19}$$

Comparing (3.2.15) and (3.2.19), we see that it is possible to choose $\phi_n = m_n^{-1}\partial_z\psi_n$. There exists a zero mode,

$$\phi_0(z) = C_0|z|\gamma^{-1/2}u^{-9/2} \ , \qquad C_0 = \left(\frac{3C}{u_J}\int_{-\infty}^{+\infty}dz|z|\gamma^{-1/2}u^{-9/2}\right)^{-1/2} \ , \tag{3.2.20}$$

which is orthogonal to the other modes, since

$$\int dz\gamma^{1/2}\frac{u^{9/2}}{|z|}\phi_m\phi_0 \sim \int dz\partial_z\psi = 0 \ . \tag{3.2.21}$$

The field strength $\mathcal{F}_{\mu z}$ is then decomposed as

$$\mathcal{F}_{\mu z} = \partial_\mu\varphi^{(0)}\phi_0 + \sum_{n\geq 1}\left(m_n^{-1}\partial_\mu\varphi^{(n)} - B_\mu^{(n)}\right)\psi_n \ . \tag{3.2.22}$$

We can choose a gauge in which the second term vanishes, hence we are left with the action of a spinless massless field,

$$S_{\mathcal{F}\mathcal{F}}^{\text{scal}} = -\frac{1}{2} \int d^4x \, \partial_\mu \varphi^{(0)} \partial^\mu \varphi^{(0)} \ . \qquad (3.2.23)$$

Under parity transformation $P : (x^\mu, z) \rightarrow (-x^\mu, -z)$ we have $A_z \rightarrow -A_z$, so, since $\phi_0(z)$ is an even function, from (3.2.9b) we see that $\varphi^{(0)}$ must be a pseudoscalar field. We are thus led to identify $\varphi^{(0)}$ with the axion field a. As we will see, the axion field gets a Witten-Veneziano mass precisely as the η' in the previous section.

To summarize, the gauge field on the PQ $D8$-brane gives rise to the axion field and to a tower of PQ vector mesons,

$$S_{\mathcal{F}\mathcal{F}} = -\int d^4x \left[\frac{1}{2} \partial_\mu a \partial^\mu a + \sum_{n \geq 1} \left(\frac{1}{4} F_{\mu\nu} F^{\mu\nu} + \frac{1}{2} m_u^2 B_\mu^{(n)} B^{(n)\mu} \right) \right] \ . \qquad (3.2.24)$$

The axion decay constant f_a

In order to find the axion decay constant f_a, namely the analogous of f_π for the axion chiral Lagrangian, we define the holonomy for the axion field as

$$V(x^\mu) = \mathcal{P} \exp\left(i \int_{-\infty}^{\infty} dz \, A_z(x^\mu, z) \right) = \exp\left(\sqrt{2} i \frac{\varphi^{(0)}}{f_a} \right) \ . \qquad (3.2.25)$$

Expanding these exponentials up to the linear term and using the expression (3.2.9b) for A_z and (3.2.20) for the zero mode we have

$$V \sim 1 + i \int_{-\infty}^{+\infty} dz A_z = 1 + i C_0 \varphi^{(0)} \int_{-\infty}^{+\infty} dz |z| \gamma^{-1/2} u^{-9/2} \qquad (3.2.26)$$

and therefore

$$f_a^2 = \frac{3C}{u_J} \left(\int_0^\infty dz z \gamma^{-1/2} u^{-9/2} \right)^{-1} \ . \qquad (3.2.27)$$

Factorizing the dimensionful quantities by the change of variable $y = u_J^3/u^3$, we obtain

$$f_a^2 = \frac{6C}{I(b)} u_J^{3/2} \ , \qquad (3.2.28)$$

where

$$I(b) = \int_0^1 dy \, \frac{y^{-1/2}}{\sqrt{1 - b^3 y - (1 - b^3) y^{8/3}}} \ . \qquad (3.2.29)$$

The function $I(b)$ is of order one for any value of $b < 1$. Finally, in terms of field theory quantities the axion decay constant reads

$$f_a^2 = \frac{N\lambda}{16\pi^3} \frac{J^3(b)}{I(b)} \frac{1}{M_{KK} L^3} \ . \qquad (3.2.30)$$

Notice that, for $b \ll 1$,

$$f_a^2 \approx 0.1534 \frac{N\lambda}{16\pi^3} \frac{1}{M_{KK}L^3} + \mathcal{O}(b^3) \ . \tag{3.2.31}$$

As we have seen in section 3.1, phenomenological constraints actually require b to be tiny. Hence, the leading order term in (3.2.31) can be taken as the defining relation between the zero temperature axion coupling and the parameters of the WSS model. Using the Witten-Veneziano formula for the axion mass we can verify that in the regime in which we work the vector bosons masses are much bigger than the axion one:

$$\frac{m_a^2}{m_n^2} \sim \frac{\chi_{WYM}L^2}{f_a^2} \sim \frac{M_{KK}^5 L^5 \lambda^2}{N} \sim r^{-10/3} \frac{\lambda^2}{N} \ll 1 \ , \tag{3.2.32}$$

where we used (3.1.9).

Axion mass term and mixing with the η'

The combined presence of a θ-term and a PQ $D8$-brane affects the equation of motion and the Bianchi identity for $\tilde{F}_2$ precisely as in the case of the antipodal WSS branes. Actually, in [117] it has been shown that the action (2.5.23) is the same for the non-antipodal configuration, with the obvious substitutions $\eta' \to a$, $f_\pi \to f_a$

$$S_{\tilde{F}_2}^{(a)} = -\frac{\chi_{WYM}}{2} \int d^4x \left(\theta + \frac{\sqrt{2}}{f_a} a \right)^2 \ . \tag{3.2.33}$$

From this formula it follows that, in the pure Yang-Mills case, the axion mass is given by the Witten-Veneziano formula (3.1.3). By combining together the contribution from the N_f WSS $D8$-branes and that of the PQ one, we get a total action term

$$S_{\tilde{F}_2}^{\text{tot}} = -\frac{\chi_{WYM}}{2} \int d^4x \left(\theta + \frac{\sqrt{2N_f}}{f_\pi} \eta' + \frac{\sqrt{2}}{f_a} a \right)^2 \ . \tag{3.2.34}$$

The total action made up summing this term, the axion kinetic term (3.2.23), the effective WSS action (2.3.1) without the Skyrme term and the flavor mass term (2.4.2) exactly reproduces the axion-dressed chiral Lagrangian (3.1.1).

3.2.3 Axion Lagrangian in the deconfined phase

We now consider the Dirac-Born-Infeld action on the non-antipodal PQ $D8$-brane at finite temperature, in the regime where it keep on being connected whereas the QCD quark branes are disjoint, as depicted in Figure 3.2. Such action reads

$$\tilde{S}_{D8} = -\mu_8 \int d^9x \ e^{-\phi} \sqrt{\det \tilde{g}_{MN} + 2\pi\alpha' \mathcal{F}_{MN}} \ . \tag{3.2.35}$$
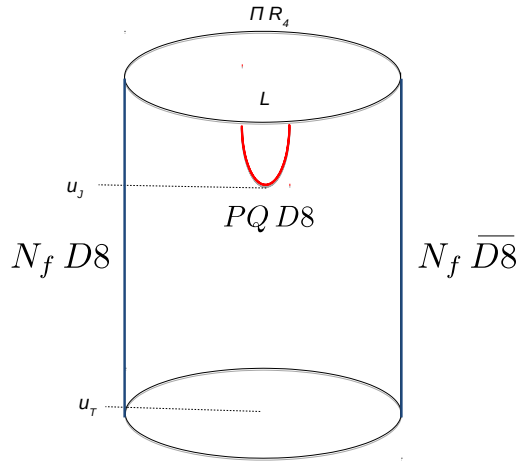
Figure 3.2. *Brane arrangement in the deconfined phase.*

The induced metric on the $D8$-brane can be derived from the ten-dimensional one (2.6.2), and reads

$$d\tilde{s}^2 = \left(\frac{u}{R}\right)^{\frac{3}{2}}\left[-\tilde{f}(u)\,dt^2 + dx_i dx^i + \left(\frac{1}{u'^2} + \left(\frac{R}{u}\right)^3\frac{1}{\tilde{f}(u)}\right)du^2\right] + \left(\frac{R}{u}\right)^{\frac{3}{2}}u^2 d\Omega_4^2 \ , \tag{3.2.36}$$

where $u' = \frac{du}{dx_4}$.

At the zeroth order, we have the usual action giving the first integral (which yet differs from the one at zero temperature, because of the blackening factor moving from dx_4 to dt)

$$u_J^4\sqrt{\tilde{f}(u_J)} = \frac{u^4\sqrt{\tilde{f}(u)}}{\sqrt{1 + \left(\frac{R}{u}\right)^3\frac{u'^2}{\tilde{f}(u)}}} \ . \tag{3.2.37}$$

The distance L is now given by

$$L = J_T(\tilde{b})R^{3/2}u_J^{-1/2} \ , \tag{3.2.38}$$

where $\tilde{b} = u_T/u_J$ and

$$J_T(\tilde{b}) = \frac{2}{3}\sqrt{1-\tilde{b}^3}\int_0^1 dy\frac{y^{1/2}}{\sqrt{1-\tilde{b}^3 y}\,\sqrt{1-\tilde{b}^3 y - (1-\tilde{b}^3)y^{8/3}}} \ . \tag{3.2.39}$$

At zero temperature, by fixing L we also fix u_J. When we turn on the temperature T, u_J becomes a non-trivial function of T. Indeed, recalling $9u_T = 16\pi^2 R^3 T^2$, we have

$$LT = \frac{3}{4\pi}\sqrt{\tilde{b}}\,J_T(\tilde{b}) \ . \tag{3.2.40}$$

In figure 3.3, we represent $LT = LT(\tilde{b})$. Notice that the solution we are focusing on only holds for $LT \leq LT_\chi \approx 0.154$. At $T = T_\chi$ there is a first order phase transition towards a configuration where the axion is dissolved since the Peccei-Quinn D8-brane splits into two disconnected branches [43]. The occurrence of this transition explains the behavior of $LT(\tilde{b})$ shown in figure 3.3. This function increases with $\tilde{b}$ up to a maximum value $LT_m(b_m) > LT_\chi$ above which the connected D8 brane solution does not exist anymore. For $\tilde{b} > \tilde{b}_m$ the function decreases with $\tilde{b}$ and this corresponds to an unstable branch.
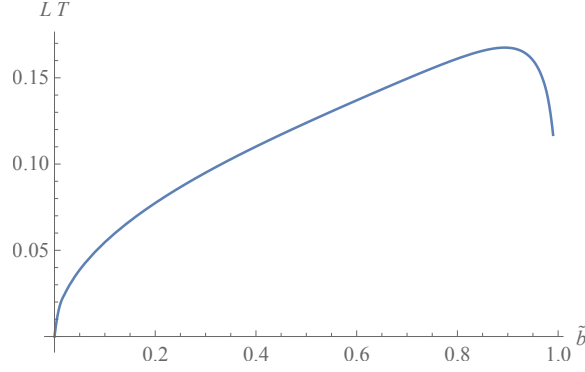

Figure 3.3. *LT as a function of $\tilde{b}$*

Going back to the action (3.2.35), at the quadratic order in α' we have

$$
\begin{aligned}
\tilde{S}_{\mathcal{FF}} &= -\frac{m_8}{4}(2\pi\alpha')^2 \int d^9x \; e^{-\phi}\sqrt{\det \tilde{g}} \; \tilde{g}^{MR}\tilde{g}^{NS}\mathcal{F}_{MN}\mathcal{F}_{RS} \\
&= -C \int d^4x \, du \, u^{5/2}\sqrt{\frac{\tilde{f}(u)}{\tilde{\gamma}(u)}} \; \tilde{g}^{MR}\tilde{g}^{NS}\mathcal{F}_{MN}\mathcal{F}_{RS} \;,
\end{aligned}
\tag{3.2.41}
$$

where

$$
\tilde{\gamma}(u) = \tilde{f}(u) - \frac{u_J^8}{u^8}\tilde{f}(u_J) \;,
\tag{3.2.42}
$$

and the constant C is the same as defined in eq. (3.2.5). We then use equation (3.2.37) to express

$$
\tilde{g}^{uu} = u'^2\tilde{g}^{44} = \left(\frac{u}{R}\right)^{3/2}\tilde{\gamma}(u) \;.
\tag{3.2.43}
$$

Using this and the expression of the metric (3.2.36), we are able to expand the action (3.2.41) as follows:

$$
\tilde{S}_{\mathcal{FF}} = -2C \int d^4x \int_{u_J}^{\infty} du \left\{ \frac{R^3 \, u^{-1/2}}{\sqrt{\tilde{\gamma}(u)\tilde{f}(u)}}\left[\quad -\mathcal{F}_{ti}\mathcal{F}_{ti} + \tfrac{1}{2}\tilde{f}(u)\,\mathcal{F}_{ij}\mathcal{F}_{ij}\right] \right.
$$
$$
\left. +u^{5/2}\sqrt{\frac{\tilde{\gamma}(u)}{\tilde{f}(u)}}\left[\quad -\mathcal{F}_{tu}\mathcal{F}_{tu} + \tilde{f}(u)\,\mathcal{F}_{iu}\mathcal{F}_{iu}\right] \right\} .
\tag{3.2.44}
$$

Notice that the temperature breaks Lorentz invariance on the four-dimensional boundary, as known. We now define a suitable base of functions, such that

$$\mathcal{F}_{tu} = \sum_n \left(\partial_t \varphi^{(n)}(t, \vec{x}) \, \tilde{\phi}_n(u) - A_t^{(n)}(t, \vec{x}) \partial_u \alpha_n(u) \right) \ , \tag{3.2.45a}$$

$$\mathcal{F}_{iu} = \sum_n \left(\partial_i \varphi^{(n)}(t, \vec{x}) \, \tilde{\phi}_n(u) - A_i^{(n)}(t, \vec{x}) \partial_u \beta_n(u) \right) \ , \tag{3.2.45b}$$

$$\mathcal{F}_{tj} = \sum_n \left(\partial_t A_j^{(n)}(t, \vec{x}) - \partial_j A_t^{(n)}(t, \vec{x}) \right) \alpha_n(u) \ , \tag{3.2.45c}$$

$$\mathcal{F}_{ij} = \sum_n \left(\partial_i A_j^{(n)}(t, \vec{x}) - \partial_j A_i^{(n)}(t, \vec{x}) \right) \beta_n(u) \ . \tag{3.2.45d}$$

In order to recover a four-dimensional action for a massive vector field, such that it satisfies the equation of motion $\partial_t^2 A_t^{(n)} = -m_n^2 A_t^{(n)}$, we have to require

$$4CR^{-3/2} \int_{u_J}^{\infty} du \left(\frac{R}{u} \right)^{9/2} \frac{u^4}{\sqrt{\tilde{\gamma}\tilde{f}}} \, \alpha_n \alpha_m = \delta_{nm} \ , \tag{3.2.46a}$$

$$\left(\frac{R}{u} \right)^3 \tilde{\gamma}\tilde{f} \, (\partial_u \beta_n)(\partial_u \beta_m) = m_n^2 \alpha_n \alpha_m \ . \tag{3.2.46b}$$

The scalar sector in (3.2.45a) and (3.2.45b) displays a zero-mode $\tilde{\phi}_0$ that should be normal to the higher modes, which in turn can be absorbed in redefinition of the vector fields by a gauge transformation on the boundary, as it is usual fashion in the Sakai-Sugimoto model. We then require the diagonal terms in the zero-mode scalar field and the gauge fields to vanish, that is

$$4C \int_{u_J}^{\infty} du \, u^{\frac{5}{2}} \tilde{f}^{-\frac{1}{2}} \, \tilde{\gamma}^{\frac{1}{2}} \, \tilde{\phi}_0 \, \partial_u \alpha_n \ = \ 0 \ , \tag{3.2.47a}$$

$$4C \int_{u_J}^{\infty} du \, u^{\frac{5}{2}} \sqrt{\tilde{\gamma}\tilde{f}} \, \tilde{\phi}_0 \, \partial_u \beta_n \ = \ 0 \ . \tag{3.2.47b}$$

These relations are satisfied by

$$\tilde{\phi}_0 = \frac{\tilde{C}_0}{2} \, u^{-5/2} \tilde{f}^{1/2} \tilde{\gamma}^{-1/2} \ , \tag{3.2.48}$$

(with $\tilde{C}_0$ a so far undetermined constant) if we take

$$\partial_u \alpha_n \equiv \tilde{f} \, \partial_u \beta_n \ . \tag{3.2.49}$$

With this last identity, the equation (3.2.46b) can be rewritten into a differential equation for the modes α_n's by themselves:

$$\partial_u \left[\left(\frac{R}{u} \right)^3 \tilde{f}^{-1} \tilde{\gamma} \, \partial_u \alpha_n \right] + m_n^2 \alpha_n = 0 \ . \tag{3.2.50}$$

Now, we have to normalize the zero-mode $\tilde{\phi}_0$ in order to have a canonically normalized kinetic term $\frac{1}{2}\left(\partial_t \varphi^{(0)}\right)^2$ in the four-dimensional Lagrangian. This is given by

$$4C \int_{u_J}^{\infty} du\; u^{5/2} \tilde{f}^{-1/2}\, \tilde{\gamma}^{1/2}\, \tilde{\phi}_0^2 \equiv C\tilde{C}_0^2 \int_{u_J}^{\infty} du\; u^{-5/2} \tilde{f}^{1/2}\, \tilde{\gamma}^{-1/2} = 1 \;, \qquad (3.2.51)$$

which thus fixes the constant $\tilde{C}_0$.

Using all these orthonormality relations, we can write down the part of the action (3.2.44) that concerns the scalar mode $\varphi^{(0)}$, that is the axion,

$$\int d^4 x \left[\frac{1}{2} \partial_t \varphi^{(0)} \partial_t \varphi^{(0)} - \left(1 - u_T^3\, C\tilde{C}_0^2 \int_{u_J}^{\infty} du\; u^{-11/2}\, \tilde{f}^{1/2}\, \tilde{\gamma}^{-1/2} \right) \frac{1}{2} \partial_i \varphi^{(0)} \partial_i \varphi^{(0)} \right] \;,$$
$$(3.2.52)$$

where we have used the explicit expression of the thermal form-factor $\tilde{f}$ in (2.6.2) in order to highlight the dependence on the temperature through u_T, which deforms the dispersion relation of the axion from the relativistic one, *i.e.*:

$$\omega_k^2 = \left(1 - u_T^3\, C\tilde{C}_0^2 \int_{u_J}^{\infty} du\; u^{-11/2}\, \tilde{f}^{1/2}\, \tilde{\gamma}^{-1/2} \right) k^2 \;. \qquad (3.2.53)$$

For $b \ll 1$, using (3.2.40), we obtain

$$\begin{aligned}
\omega_k^2 &\sim \left(1 - \frac{16\Gamma\left(\frac{9}{16}\right)\Gamma\left(\frac{11}{16}\right)}{\Gamma\left(\frac{1}{16}\right)\Gamma\left(\frac{3}{16}\right)} b^3 \right) k^2 \\
&\simeq \left[1 - 16383.2\, L^6 T^6 + \cdots \right] k^2 \;.
\end{aligned} \qquad (3.2.54)$$

Analogously, we can wonder what is the effect of the temperature on the axion decay constant f_a. To this purpose, we apply the same reasoning of equations (3.2.25) and (3.2.26) to the current finite-temperature model, and we obtain

$$\begin{aligned}
V &\sim 1 + 2i \int_{u_J}^{\infty} du\; \varphi^{(0)} \tilde{\phi}_0 = 1 + i\varphi^{(0)}\, \tilde{C}_0 \int_{u_J}^{\infty} du\; u^{-5/2} \tilde{f}^{1/2}\, \tilde{\gamma}^{-1/2} \\
&= 1 + \frac{i}{C\tilde{C}_0}\, \varphi^{(0)} \;,
\end{aligned} \qquad (3.2.55)$$

where in the last step we have used the normality relation (3.2.51). Then, having in mind the definition (3.2.25), we straightforwardly read the temperature-dependent decay constant

$$f_a^2(T) = 2C^2 \tilde{C}_0^2 \equiv 2C \left(\int_{u_J}^{\infty} du\; u^{-5/2} \tilde{f}^{1/2}\, \tilde{\gamma}^{-1/2} \right)^{-1} \;. \qquad (3.2.56)$$

In terms of the coordinate z, defined by $u^3 = u_J^3 + u_J z^2$, this result reads

$$f_a^2(T) = \frac{3C}{u_J} \left(\int_0^{\infty} dz\; z u^{-9/2} \tilde{f}^{1/2}\, \tilde{\gamma}^{-1/2} \right)^{-1} \;. \qquad (3.2.57)$$

This result agrees with the one that was found in [118] by another argument.

In terms of field theory quantities (and L). the axion decay constant at finite temperature reads

$$f_a^2(T) = 6C \, \frac{u_J^{3/2}}{I_T(\tilde{b})} = \frac{N\lambda}{16\pi^3} \frac{J_T^3(\tilde{b})}{I_T(\tilde{b})} \frac{1}{M_{\text{KK}}L^3} \ , \qquad (3.2.58)$$

where

$$I_T(\tilde{b}) = \int_0^1 dy \frac{y^{-1/2}\sqrt{1 - \tilde{b}^3 y}}{\sqrt{1 - \tilde{b}^3 y - y^{8/3}(1 - \tilde{b}^3)}} \ . \qquad (3.2.59)$$

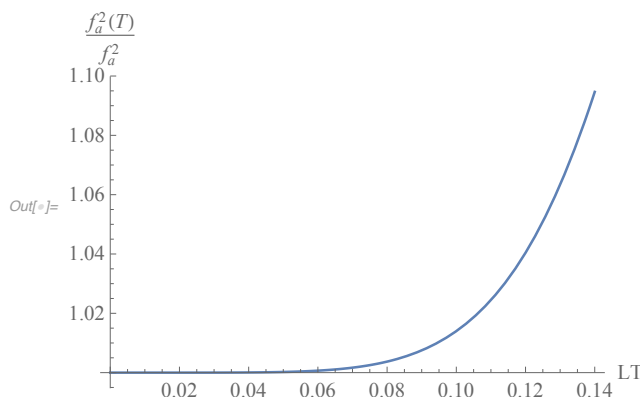A plot of $f_a^2(T)$ as a function of LT is given in figure 3.4. For $LT \ll 1$ we get

Figure 3.4. $f_a^2(T)$ *as a function of* LT

$$f_a^2(T) \approx f_a^2 \left[1 + 14247 \, L^6 T^6 + \cdots \right] \ , \qquad (3.2.60)$$

where the zero temperature axion coupling f_a is given in (3.2.31). The leading order term coincides with the one we found at zero temperature in the limit $u_J \gg u_0$, see eq. (3.2.31).

3.3   The holographic axion at large temperature

Interesting questions concerning axion phenomenology are posed at finite temperature. In the holographic model, turning on a temperature amounts to modify the dual gravity solutions in such a way that the Euclidean time coordinate is a circle of length $\beta = 1/T$, as discussed in section 2.6. Notice that the temperature dependence in the confined phase is typically trivial, *i.e.* no dependence is found, basically because of the absence of a horizon. This means that the main properties of the holographic axion will not be sensible to the temperature as far as $T < T_c$.

Before going on let us just recall that the black-brane solution presented above has, notoriously, two unwelcome features. To begin with, it has been

argued that the dual QFT phase is not in the same universality class of finite temperature Yang-Mills (or QCD for that matters)[13] - some discrete symmetries do not match [119].[14] Moreover, the deconfined phase dual solution reflects the six-dimensional nature of the holographic model in the UV; for example, the free energy density scales with the sixth power of the temperature. Nevertheless, the solution is very simple and allows us to get a lot of geometric intuition on chiral symmetry restoration and deconfinement transition, so we are going to use it as a proof of concept.

The main feature of the black brane solution (2.6.2) is that it can be obtained by a double Wick rotation of the solution in (2.1.1), exchanging the role of S_{x_4} with the Euclidean temporal circle. As such, the cigar in the geometry (2.1.1) is replaced by a semi-infinite cylinder originating at u_T, see figure 3.2. This makes it clear that the two branches of the N_f WSS antipodal $D8$-branes fall separately into the horizon and do not join anymore, realizing chiral symmetry restoration in the deconfined phase. Instead, the PQ brane is quite mildly affected by the presence of the horizon as long as $u_T \ll u_J$, that is $T \ll \mathcal{O}(10^{10})$ GeV (at that temperature the axion would melt in the plasma, revealing its composite nature). This means that the embedding of the PQ brane will have some quite small deformation due to the (distant) horizon [43].

Concerning the axion, a first important issue we want to focus on is the temperature dependence of its mass in the deconfined phase. The axion mass, in turn, is expected to be proportional to the topological susceptibility. In the flavored WSS setup we know that the latter can be different from zero only if all the quarks are massive. However, at present, there is no clear prescription on how to give finite masses to the flavors in the deconfined phase of the model. For this reason, we will only consider the unflavored WYM model in the following.

The topological susceptibility of the WYM model at $T > T_c$ is certainly strongly suppressed in the planar limit. This is reflected by the fact that the solution for the RR one-form potential C_1, such that $\int_{S_{x_4}} C_1 \sim \theta$, is now a constant on the black brane background. Thus, $F_2 = dC_1 = 0$, so that at leading order in N there are no effects of the θ angle in this phase.

In order to recover a non-trivial θ-dependence, it is necessary to go beyond the leading order gravity approximation. In Yang-Mills theory, we know that, at least for asymptotically large temperatures, the θ-dependence is captured by a dilute instanton gas. The leading one-instanton contribution to the topological susceptibility gives $\chi_{YM}(T) \sim T^4 e^{-8\pi^2/g_{YM}^2(T)}$, where the gauge coupling is evaluated at the scale T. Asymptotic freedom drives the exponentially suppressed term into $\chi(T) \sim T^4(T/\Lambda)^{-11N/3}$, which for $N = 3$ gives a susceptibility which is power-like suppressed $\chi_{YM} \sim T^{-7}$.

In the holographic WYM model, the one-instanton action corresponds to the action for a Euclidean $D0$-brane whose worldline is along the compact direction

---

[13]By contrast, the confined phase dual solution (2.1.1) is commonly believed to be in the same universality class of pure YM in the confined phase.

[14]In [119] there is an attempt to build the "correct" deconfined phase dual solution.

x_4. This brane is stable only in the deconfined phase, since in the confined case the cigar geometry tends to shrink the $D0$-brane to zero size. This nicely reproduces the field theory expectation that no (dilute) instanton gas can be defined in the confined phase. The Euclidean $D0$-brane action on the background (2.6.2) supported by a constant $C_1 \sim \theta dx_4$ potential, reads

$$S_{D0} = \frac{1}{l_s} \int e^{-\phi} \sqrt{g_{44}} dx_4 - \frac{i}{l_s} \int C_1 = \frac{8\pi^2}{g_{YM}^2} - i\theta \,, \qquad (3.3.1)$$

where $g_{YM}^2 \equiv 4\pi g_s l_s M_{KK}$. We thus expect instanton driven exponential corrections $e^{-S_{D0}} + $ c.c. to contribute to the topological susceptibility. Remarkably enough string theory allows to precisely compute these corrections. As we will see in the following, they arise when higher derivative (quartic) corrections to the gravity action are taken into account.

Before considering the WYM case, as a warm-up we present the calculation of the topological susceptibility of finite temperature $\mathcal{N} = 4$ SYM at strong coupling. To our knowledge, this result was missing in the literature. Then we will move to the WYM model showing how a non-trivial instanton-driven temperature-dependent topological susceptibility arises.

To complete our analysis of the temperature dependence of the axion mass in WYM we will also study how much the axion coupling f_a varies with T, referring to section 3.2 for details.

3.3.1   Topological susceptibility of finite temperature $\mathcal{N} = 4$ SYM

Let us consider the $\mathcal{N} = 4$ $SU(N)$ SYM theory in $3 + 1$ dimensions. This is a superconformal gauge theory where the complex coupling $\tau = (2\pi)^{-1}\theta + 4\pi i g_{YM}^{-2}$ is a modulus. There are no anomalies, hence, despite the fact that the theory contains massless (adjoint) fermions, the θ-dependence cannot be rotated away. At zero temperature, however, the topological susceptibility of the theory is zero. This can be immediately deduced from dimensional analysis: the theory has no scale, while the susceptibility is dimensionful. The same result can also be obtained by a direct computation

$$\chi_{SYM}(T = 0) \equiv \int d^4x \langle Q(x)Q(0)\rangle = 0 \,, \qquad (3.3.2)$$

where $Q(x) \sim \text{Tr} F \wedge F$ is the topological charge density operator, with protected conformal dimension $\Delta = 4$ and the Euclidean correlator is computed on the ground state at zero temperature.

At finite temperature, however, the above result can well be modified. The holographic dual description is provided by a $\text{AdS}_5 \times S^5$ black brane background

$$ds^2 = \frac{r^2}{l^2} \left(-f(r)dt^2 + dx_i\, dx_i\right) + \frac{l^2}{r^2} \left(\frac{dr^2}{f(r)} + r^2 d\Omega_5^2\right) \,, \quad f(r) = 1 - \frac{r_h^4}{r^4} \,, \ (3.3.3)$$

with constant dilaton $e^\phi = g_s$ and a five-form flux on S^5 proportional to the number of colors N. The radius of the horizon is related to the temperature by $r_h = \pi l^2 T$ and the AdS$_5$ radius is given by $l^4 = 4\pi g_s N \alpha'^2$.

The holographic picture suggests that the only possible contributions to the topological susceptibility can come from instanton corrections, *i.e.* D-instanton corrections on the gravity side [120]. The reason is that the type IIB axion C_0, which is dual to the field theory θ-angle according to the relation $\theta = 2\pi C_0$, is constant on the background. To leading order in derivatives, the (related, truncated) type IIB effective action only contains derivatives of C_0, so that the on-shell gravity action will not show any θ-dependent term. The situation changes if we include D-instanton corrections. As it was shown in [121] (see also [122]) these contribute to the first subleading correction (in α') to the type IIB effective action, *i.e.* to the so-called R^4 term. In Einstein frame and using the standard convention on the background value of the dilaton $e^\phi = g_s$, the latter can be written as (see *e.g.* [123] and [124])

$$\delta S = -\frac{1}{16\pi G_{10}} \int d^{10}x \sqrt{g}\, \alpha'^3 f(\tau, \bar{\tau}) g_s^{3/2} e^{-3\phi/2} W \ , \qquad (3.3.4)$$

where W contains quartic terms in the Riemann tensor,

$$\tau = C_0 + i e^{-\phi} \ , \qquad (3.3.5)$$

and the non-holomorphic function $f(\tau, \bar{\tau})$, in the $e^\phi \to 0$ limit, is given by

$$f(\tau, \bar{\tau}) = \frac{\zeta(3)}{8} + \frac{\pi^2}{24} e^{2\phi} + \frac{e^{2\phi}}{16} \sum_{N=1}^{\infty} G_{N,4} \ , \qquad (3.3.6)$$

where the first term arises at tree level, the second one at one loop and the third one contains the non-perturbative D-instanton corrections (the summation runs over the N-instanton contributions). The leading order, one-instanton term reads [122]

$$G_{1,4} = 4\pi e^{-\phi/2} e^{2\pi i \tau} + c.c. \ . \qquad (3.3.7)$$

The action term (3.3.4) has been computed at tree level in [123], to obtain the first subleading correction (in inverse powers of the 't Hooft coupling) to the free energy of $\mathcal{N} = 4$ SYM at finite temperature in the holographic limit. As discussed in [123] there exists a scheme where the quartic term W can be written in terms of just the Weyl tensor

$$W = C^{hmnk} C_{pmnq} C_h^{rsp} C_{rsk}^q + \frac{1}{2} C^{hkmn} C_{pqmn} C_h^{rsp} C_{rsk}^q \ . \qquad (3.3.8)$$

With this choice, the term (3.3.4) does not modify the zero-temperature AdS$_5 \times S^5$ solution. However, it does perturb the finite temperature black brane solution [123]. Nevertheless, if one is interested in just the leading corrections to the field theory free energy, it is enough to compute the action term (3.3.4) on the unperturbed

black brane solution. The related on-shell value of the quartic term W has been computed in [123] with the result

$$W = \frac{180}{l^8} \frac{r_h^{16}}{r^{16}} . \tag{3.3.9}$$

Integrating over S^5, the on-shell action reduces to

$$\delta S = -\frac{1}{16\pi G_5} \int d^5 x \sqrt{g_5} \alpha'^3 f(\tau, \bar{\tau}) W , \tag{3.3.10}$$

where

$$16\pi G_5 = \frac{16\pi G_{10}}{\pi^3 l^5} , \quad \sqrt{g_5} = \frac{r^3}{l^3} . \tag{3.3.11}$$

Crucially, in view of the on-shell value of eq. (3.3.9), one immediately realizes that the integral in δS is perfectly convergent at large r so that one does not need to add any counterterm to the computation.

Using the holographic relation $F = T S_{\text{on-shell}}$ between the field theory free energy and the on-shell gravity action, we thus get that the correction to the free energy density corresponding to the δS term reads[15]

$$\delta f = -\frac{15}{8} \pi^2 N^2 T^4 f(\tau, \bar{\tau}) \lambda_{YM}^{-3/2} . \tag{3.3.12}$$

The leading order θ-dependent term arises from the one-instanton contribution to $f(\tau, \bar{\tau})$ and reads (see eq. (3.3.6) and (3.3.7))

$$\delta f^{(\theta)} = -\frac{15}{128} \pi^{3/2} \sqrt{N} \, T^4 e^{-8\pi^2/g_{YM}^2} \cos\theta , \tag{3.3.13}$$

so that the topological susceptibility is given by

$$\chi_{SYM}(T) = \frac{d^2 \delta f^{(\theta)}}{d\theta^2}|_{\theta=0} = \frac{15}{128} \pi^{3/2} \sqrt{N} \, T^4 e^{-8\pi^2/g_{YM}^2} . \tag{3.3.14}$$

Notice that, apart from the overall factors, it has the same form as can be obtained for a dilute instanton gas. A crucial difference w.r.t. to pure non supersymmetric Yang-Mills is that the gauge coupling does not run to leading order in $1/\lambda_{\text{YM}}$ in the thermal case (actually the quartic term makes the dilaton running with r [123]). As a result, the topological susceptibility increases with T.

Notice that the overall factor $\sqrt{N}$ is typical of instanton corrections in the present setup, see e.g. [125].

---

[15]In this section, we use different conventions w.r.t. those in [123] for what concerns the holographic definitions of the couplings. Here we use $\lambda_{YM} = g_{YM}^2 N = 4\pi g_s N$, while in [123] $g_{YM}^2 = 2\pi g_s$.

3.3.2 Topological susceptibility in the deconfined phase of WYM

The WYM black brane solution (2.6.2) in Type IIA string theory can be obtained starting from the $\text{AdS}_7 \times S^4$ black brane solution

$$ds^2 = G_{MN}dx^M dx^N = \frac{y^2}{R^2}\left[-f(y)dt^2 + \sum_{i=1}^{4} dx_i^2 + dx_{10}^2\right] + \frac{4R^2}{f(y)y^2}dy^2 + R^2 d\Omega_4^2, \tag{3.3.15}$$

arising as the near horizon limit of the background sourced by N non-extremal $M5$-branes. Here,

$$f(y) = 1 - \frac{y_0^6}{y^6} , \qquad y_0 = \frac{4}{3}\pi R^2 T . \tag{3.3.16}$$

The background (2.6.2) is obtained by reducing the above solution on a two-dimensional torus $S_{x_{10}} \times S_{x_4}$ with circles of radii $R_4 = M_{KK}^{-1}$ and $R_{10} = g_s l_s$ [36]. The solution also supports N units of four-form flux along S^4. The flux quantization condition fixes $R^9/\kappa_{11}^2 = N^3/(2^7\pi^5)$, where $2\kappa_{11}^2 = 16\pi G_N^{(11)} = (2\pi)^8 l_{11}^9$ gives the 11-dimensional Newton constant. The 11-dimensional Planck length is related to the Type IIA string scale by $l_{11} = g_s^{1/3} l_s$.

Quite remarkably, quartic corrections to the 11d supergravity action compactified on a torus are known, see e.g. [126, 127]. With the conventions used in [123, 127] they read

$$\delta S = -\frac{1}{\kappa_{11}^{2/3}}\int d^{11}x\sqrt{-G}\, W\left[\frac{2\pi^2}{3} + \mathcal{V}_2^{-3/2}f(\rho,\bar{\rho})\right] , \tag{3.3.17}$$

where W can be expressed as in (3.3.8), so that the extremal $\text{AdS}_7 \times S^4$ solution is not modified by the action term (3.3.17) [123]. Moreover, (recalling that $R_4 = M_{KK}^{-1}$ and $g_{YM}^2 = 4\pi g_s l_s M_{KK}$),

$$\mathcal{V}_2 = \frac{4\pi^2 R_{10}R_4}{\kappa_{11}^{4/9}}\sqrt{G_{(2)}} = \frac{4\pi^2 g_s l_s M_{KK}^{-1}}{\kappa_{11}^{4/9}}\frac{y^2}{R^2} \equiv \frac{g_{YM}^2}{M_{KK}^2}\frac{\pi}{\kappa_{11}^{4/9}}\frac{y^2}{R^2} , \tag{3.3.18}$$

is related to the volume V_T of the torus by

$$V_T = \kappa_{11}^{4/9}\mathcal{V}_2 = \int dx_4 dx_{10}\sqrt{G_{(2)}} , \tag{3.3.19}$$

with $G_{(2)} = G_{44}G_{10\,10}$. In the $\mathcal{V}_2 \to \infty$ limit the action term (3.3.17) reduces to that considered in [123] in the non-compact 11d case.

The modular function appearing in (3.3.17) is defined as [126]

$$f(\rho,\bar{\rho}) = 2\zeta(3)\rho_2^{3/2} + \frac{2\pi^2}{3}(\rho_2)^{-1/2} + 4\pi(e^{2\pi i\rho} + e^{-2\pi i\bar{\rho}}) + \cdots , \tag{3.3.20}$$

where we neglect corrections with instanton number higher than one and we take the $\rho_2 \to \infty$ limit with

$$\rho \equiv \rho_1 + i\rho_2 = (2\pi)^{-1}\theta + 4\pi i g_{YM}^{-2} \ , \tag{3.3.21}$$

being proportional to the action (3.3.1) of a Euclidean $D0$-brane wrapped along the x_4 circle [126]. The quartic term W on the background (3.3.15) has been computed in [123] and reads

$$W = \frac{3285}{64R^8} \frac{y_0^{24}}{y^{24}} \ . \tag{3.3.22}$$

Using the above expressions we get that the free energy density of the WYM theory at $T > T_c$ receives the following contributions from the quartic term (3.3.17)

$$\delta f = \delta f_{GKT} + \delta f_{\mathcal{V}_2} \ , \tag{3.3.23}$$

where

$$\delta f_{GKT} = -730 \left(\frac{2\pi}{3}\right)^8 \left(\frac{\pi}{2}\right)^{4/3} \lambda_{\text{eff}}(T)T^4 \ , \tag{3.3.24}$$

can be obtained by a simple compactification of the related M5-brane result found in [123] and

$$\lambda_{\text{eff}}(T) \equiv g_{YM}^2 N \frac{T^2}{M_{KK}^2} \equiv \lambda_{YM} \frac{T^2}{M_{KK}^2} \ . \tag{3.3.25}$$

The novel contribution is

$$\begin{aligned}
\delta f_{\mathcal{V}_2} &= -\frac{3285}{42} \left(\frac{2\pi}{3}\right)^4 M_{KK}T^3 \left[\frac{32\pi^2 N^2}{\lambda_{YM}^2}\zeta(3) + \frac{2\pi^2}{3} + \right. \\
&+ \left. 16\pi^{3/2}\frac{\sqrt{N}}{\sqrt{\lambda_{YM}}}e^{-8\pi^2/g_{YM}^2}\cos\theta\right] \ .
\end{aligned} \tag{3.3.26}$$

Thus, from the θ-dependent term, we see that, to leading order in the instanton expansion, the topological susceptibility of the WYM model in the deconfined phase reads

$$\chi_{WYM}(T) = \frac{3285\pi^{3/2}}{42} \left(\frac{4\pi}{3}\right)^4 \frac{\sqrt{N}}{\sqrt{\lambda_{\text{eff}}(T)}} \ T^4 e^{-8\pi^2/g_{YM}^2} \ . \tag{3.3.27}$$

Notice that we get the same overall $\sqrt{N}$ factor as in the SYM case and that the scaling with the temperature is given by $\chi_{WYM} \sim M_{KK}T^3$.

Let us conclude, for completeness, by recalling the status of the analogous computation in the alternative background, dual to the deconfined phase, presented in [119]. In [128], it is pointed out that extracting the instanton action for generic instanton size is not possible at present. So, a complete estimate of the topological susceptibility for that background is lacking. What can be done is to check that, in this case, the dual instanton action is peaked at a specific size, where the temperature behavior is of the form $S_{inst} \sim \frac{8\pi^2}{g_{YM}^2}(1 - \text{const}\sqrt{T_c/T})$.

3.3.3 Temperature dependence of the axion mass in WYM

The temperature dependence of the axion mass in the deconfined phase of WYM can be read from a suitable generalization of (3.1.3)

$$m_a^2(T) = \frac{2}{f_a^2(T)} \chi_{WYM}(T) \; . \tag{3.3.28}$$

If the temperature is much smaller than f_a (the zero-temperature axion coupling) but higher than the deconfinement temperature T_c, the temperature dependence of the axion coupling is usually neglected. In the WYM model, the coupling $f_a(T)$ can be deduced by a careful extension to the deconfined WYM background of the computations reviewed in section 3.2 for deducing f_a. The details are provided at the end of that appendix. The result is that, in the $T_c < T \ll f_a$ regime, *i.e.* for $LT_c < LT \ll 1$,

$$f_a^2(T) \approx f_a^2 \left[1 + \frac{1.3}{\pi^6} \lambda^2 N^2 \frac{T^6}{M_{KK}^2 f_a^4} + \cdots \right] \; , \tag{3.3.29}$$

where we used (3.1.12) for the zero temperature axion coupling f_a. Thus, the decay constant $f_a(T)$ slightly increases with temperature in that regime. Just as for the topological susceptibility, this behavior differs from what is expected in QCD. At very high temperatures, instead, (more precisely at $LT \geq LT_\chi \approx 0.154$ [43]) the axion melts as a result of the fact that the energetically favoured configuration for the PQ D8-brane corresponds to two disconnected branches.

Thus, in the $LT \ll 1$ regime, the temperature dependence of f_a can be neglected and that of the axion mass in the deconfined phase of the WYM model is driven by that of the topological susceptibility (3.3.27). The result is that m_a^2 increases like T^3 in that regime. This behavior is of course very different from the power-like suppression of the axion mass with temperature, which can be extracted, from asymptotic freedom, in Yang-Mills in the dilute instanton gas approximation. The peculiar higher dimensional UV completion of the WYM model is at the basis of this expected discrepancy.

Chapter 4

Phase transitions in the WSS model

The WSS model studied in this thesis exhibits two first-order phase transitions, one associated to confinement and another one associated to chiral symmetry breaking. Recently, first-order phase transitions occurring in the early stages of the Universe's cosmological evolution have been receiving attention because they might have produced a stochastic background of gravitational waves that can be measured in the near future by the newborn gravitational wave astronomy (see e.g. [19–21]). Within the Standard Model, the electroweak and the QCD phase transitions (at small baryon density) are crossovers rather than first-order [23, 24]. By contrast, first-order phase transitions arise in many beyond-Standard-Model (BSM) scenarios for the early Universe. They are often combined with dynamical mechanisms explaining, for instance, the baryon-antibaryon matter asymmetry or the nature of dark matter. Several such scenarios involve strongly-coupled gauge sector. In particular, in chapter 5, based on [129], we will compute the stochastic gravitational wave spectrum produced in cosmological first-order phase transitions having the WSS model as underlying beyond-Standard-Model theory. The computations require studying in more detail the model's phase transitions, which is the aim of this chapter, based on [101].

The gauge/gravity duality provides unique tools to study the properties of strongly-coupled gauge theories, including their phase structure. First-order phase transitions have been thoroughly analyzed in many different models, following the seminal papers [33] for theories with only adjoint matter, and [130] for cases with fundamental matter. Once the threshold for the phase transition is crossed, the former minimal energy configuration becomes a "false vacuum" and is expected to decay to the new ground state, the "true vacuum".

This kind of vacuum decay was first studied long ago in a simple one-scalar field model [25], where a first-order phase transition occurs when the scalar potential has two minima, one of which is metastable. The decay of the latter can proceed through quantum tunneling or via thermal fluctuations (or, more generally, by a combination of the two effects). Dynamically, the transition happens through the nucleation of bubbles of true vacuum in the metastable phase [25–27, 131, 132].

In general, the decay rate of a metastable vacuum per unit volume in the semiclassical limit is given by an expression of the form $\Gamma = A\,e^{-S_B}$, where A and S_B depend on the underlying quantum field theory. The first coefficient is usually very hard to compute in closed form: it is given in terms of a certain functional determinant and it is often estimated by dimensional analysis. The exponential term is the so-called *bounce* action. For a scalar field Φ in 3+1 dimensions, with potential having an absolute minimum (the true vacuum) at Φ_t and a local minimum (the false vacuum) at Φ_f, the bounce action is defined by $S_B = S_E(\Phi_B) - S_E(\Phi_f)$, where S_E is the Euclidean action for the scalar field and Φ_B is called "the bounce". The latter is a non-trivial "bubble-like" solution of the Euclidean equation of motion which approaches the false vacuum Φ_f at Euclidean infinity and a constant Φ_0 at the center of the bubble.[1] When the transition proceeds through quantum tunneling, the bounce is $O(4)$ symmetric and Φ_B only depends on the radial coordinate $\rho = \sqrt{t^2 + x_i x_i}$, where t is the Euclidean time and x_i are the space coordinates. When the transition is dominated by thermal fluctuations, the bounce is $O(3)$ symmetric [26, 27] and $\Phi_B = \Phi_B(\rho)$, with $\rho = \sqrt{x_i x_i}$. The configuration for which the rate Γ has the larger value is the one that dominates the decay process.

The main aspects of the above mentioned simple scalar model can be generalized to vacuum decay in gravitational dual descriptions of quantum field theories, a process that has been studied in various papers in the past. Nevertheless, as far as we know, this literature is focused on bottom-up models with AdS geometries, like those relevant for Randall-Sundrum (RS)-like setups [46, 133–144].[2]

In this chapter, based on [101], we try to proceed a step further, studying, for the first time, the dynamics of first-order phase transitions in gauge theories with a precise string embedding. We will mainly focus on the WSS model. This top-down perspective allows for a precise identification of the gauge theories under investigation and for an understanding of the approximations leading to the dual classical gravitational descriptions. As a result, computations performed in the planar limit at strong coupling are reliable, without uncontrolled approximations as the ones plaguing effective models (such as sigma models, NJL, etc.) or bottom-up holographic models.

The confinement/deconfinement phase transition of the WSS model occurs at a critical temperature $T_c = M_{KK}/2\pi$. In the dual gravity picture, it corresponds to a Hawking-Page transition between a solitonic background and a black-brane solution. Finding the full-fledged configuration that interpolates between the two backgrounds in ten-dimensional supergravity is an extremely interesting but complicated open problem, see e.g. [147]. Following a prescription developed in bottom-up RS-AdS models in [46], we will use an off-shell description of the phase transition, modeling it with a single scalar effective action which we will compute

---

[1]As discussed in [25, 132], this Euclidean solution is meant to represent the bubble at time zero in Minkowskian signature.

[2]See also [145] for a holographic superfluid setup and [146] for some considerations on backgrounds dual to confining theories.

using holographic renormalization techniques. From this, we will compute the aforementioned bounce, effectively interpolating between the two vacua, and its on-shell action. This will allow us to determine the bubble nucleation rate in terms of the parameters of the model.

The phase transition associated to chiral symmetry breaking depends on choice of the flavor branes' boundary conditions, namely on the value of the parameter L which measures the distance between branes and anti-branes along the compactification circle $S_{x_4}^1$. With antipodal boundary conditions, i.e. when $LM_{KK} = \pi$, chiral symmetry breaking and confinement occur at the same energy scale. In particular, when $T < T_c$ chiral symmetry is broken and the theory confines, while at $T > T_c$ the theory enters a deconfined phase with chiral symmetry restoration. However, for non-antipodal configurations with $LM_{KK} < 0.966$, an intermediate phase with deconfinement but broken chiral symmetry arises [43]. In the second part of this chapter, we will examine this kind of separate first-order phase transition. The bubble nucleation dynamics is described by the Dirac-Born-Infeld (DBI) action for the $D8$-branes on the fixed black-brane background. In this case, even the numerical analysis is challenging due to the non-linearities inherent to the DBI action. We will develop a variational approach (which could be hopefully useful to study further static and dynamical issues in the model) to solve the problem. This will allow us to compute the (approximate) bounce solution interpolating between the chiral symmetry broken and restored configurations, corresponding to connected and disconnected brane embeddings, and ultimately the actions and decay rates.

The chapter is organized as follows. In section 4.1, we revisit the compact Randall-Sundrum model at finite temperature examined in [46]. Making use of standard holographic renormalization techniques, we compute the kinetic term in the single scalar effective action for the bounce in the deconfined phase. This kinetic term was missing in the literature. In section 4.2 we present the derivation of the effective action for the scalar field modeling the confinement/deconfinement phase transition. Using holography, we compute both the potential and the kinetic term for the scalar. As in the compact Randall-Sundrum example, holographic renormalization techniques play a crucial role in the process. We compute the bubble nucleation rate both in the small temperature regime, where quantum tunneling is driven by $O(4)$-symmetric bubbles, and in the high temperature regime, where $O(3)$-symmetric bubbles are relevant. In section 5.3 we study the chiral symmetry breaking/restoration phase transition in the deconfined phase. Using a powerful variational method we compute the bounce action and the related bubble nucleation rates. In section 4.4, we present the thin and thick wall approximations for the confinement/deconfinement phase transition.

4.1 Revisiting the Randall-Sundrum transition

In this section, as a warm-up, we revisit the analysis performed in [46] of the compact Randall-Sundrum (RS) model with two relevant scales, given by the

temperature T and the radial distance between a Standard-Model brane (the TeV brane) and a Planck brane. The system experiences a first-order phase transition at some critical temperature T_c. At low temperatures, it is described by the RS solution with stabilized radion, while at large temperatures its (bottom-up) holographic description is captured by an AdS$_5$ Schwarzschild black hole whose horizon replaces the TeV brane. A cosmological scenario is considered where the system evolves cooling down from a large temperature stage. The nucleation rate of bubbles of RS vacuum is then estimated. In the process, the horizon radius of the AdS black hole and the radion are promoted to space-dependent fields whose effective action, describing the bounce, is then estimated. Actually, both fields are seen as two different realizations of a single scalar field, whose effective potential can be obtained, in some suitable limit, by gluing the effective potentials in the two phases. In the following section, we will apply the same strategy to model the dynamics of the confinement/deconfinement transition in the top-down WSS model.

Before going on, let us recall that a missing piece in the analysis of [46] was the computation of the effective derivative term for the horizon radius field. We present a proposal to fill this gap. Although in [46] the horizon radius field is ultimately not employed, essentially because its contribution is argued to be subleading with respect to the radion, in the subsequent literature on the gravitational wave spectra in this type of models this field is commonly included in the calculations, so the precise normalization of its derivative term is important (see e.g. [134, 139]).

Let us work in Euclidean signature, with Einstein-Hilbert gravity action given by

$$S_{EH} = -2M^3 \int d^5x \sqrt{g} \left[\mathcal{R} + \frac{12}{L^2} \right] \, , \qquad (4.1.1)$$

where M is the 5d Plank mass. The (Euclidean) AdS$_5$ Schwarzschild solution is given by

$$ds^2 = \left(\frac{u}{L} \right)^2 \left[f_T(u)dt^2 + dx^i dx^i \right] + \left(\frac{u}{L} \right)^{-2} \frac{du^2}{f_T(u)} \, , \qquad (4.1.2\text{a})$$

where L is the AdS radius and

$$f_T(u) = 1 - \frac{u_T^4}{u^4} \, . \qquad (4.1.2\text{b})$$

The real-time (Minkowski) metric has an event horizon at $u = u_T$. In the near-horizon ($u \to u_T$) limit, the metric of the (t, u)-subspace becomes

$$ds^2_{(t,u)} = \frac{4u_T}{L^2}(u - u_T)dt^2 + \frac{L^2}{4u_T} \frac{du^2}{u - u_T} \, . \qquad (4.1.3)$$

By performing the change of variables

$$r(u) = \frac{L}{\sqrt{u_T}} \sqrt{u - u_T} \, , \qquad \theta(t) = 2\pi T t \, , \qquad (4.1.4)$$

we see that the metric is that of a cone

$$ds^2_{(t,u)} = (\sin\alpha)^2 r^2 d\theta^2 + dr^2 \ , \tag{4.1.5}$$

with

$$\sin\alpha = T_h/T \ , \qquad T_h \equiv \frac{u_T}{\pi L^2} \ . \tag{4.1.6}$$

When $T_h = T$, there is no conical singularity and the metric is a proper solution of S_{EH}. In this case, the free energy density of the black hole is given by

$$f_{BH} = -2\pi^4 (ML)^3 T^4 \ . \tag{4.1.7}$$

The above result can be obtained in at least three equivalent ways. The fastest one consists in integrating the thermodynamic relation $s = -\partial_T f$, where s is the Bekenstein-Hawking entropy density. Alternatively, one can use the holographic relation

$$F \equiv f V_3 = S_{ren} T \ , \tag{4.1.8}$$

where F is the free energy, $V_3 = \int d^3x$ is the infinite flat 3d space volume and S_{ren} is the renormalized on-shell Euclidean action. The latter, as reviewed in [46], can be obtained as the difference between the on-shell value of the action (4.1.1) on the black hole solution (4.1.2) and its on-shell value on a pure AdS spacetime with the same boundary. Alternatively, it can be obtained by the procedure of holographic renormalization (see e.g. [77] for a review). In the present setup, it amounts to writing

$$
\begin{aligned}
S_{ren} &= \lim_{u_\Lambda \to \infty} [S_{EH} + S_{GH} + S_{ct}] \\
&= \lim_{u_\Lambda \to \infty} \left[S_{EH} + 2M^3 \int_{u=u_\Lambda} d^4x \sqrt{h} \left(-2K + \frac{6}{L} \right) \right] \ .
\end{aligned} \tag{4.1.9}
$$

Here, u_Λ is a radial cut-off introduced to regularize the on-shell actions and h is the determinant of the metric at the boundary $u = u_\Lambda$. The first piece in round parenthesis is due to the Gibbons-Hawking term S_{GH}, K being the trace of the extrinsic curvature of the boundary. The second piece is due to the counterterm action S_{ct} which precisely cancels the divergent terms (in powers of u_Λ) from the on-shell value of $S_{EH} + S_{GH}$. As a result, S_{ren} turns out to be finite. Let us recall that a generic counterterm is required to be covariant with respect to the boundary metric.

According to the holographic correspondence, eq. (4.1.7) can be seen as the free energy density of a dual strongly coupled (3+1)-dimensional conformal field theory (CFT), at finite temperature $T = T_h$, in the planar limit. In top-down holography, an infinite class of explicit examples of such CFT arises by considering the low-energy dynamics of N D3-branes at the tip of a six-dimensional (Calabi-Yau) cone. The dual description is provided by $AdS_5 \times X_5$ backgrounds where X_5 is the base of the cone. The master example is provided by $X_5 = S^5$, in which

case the six-dimensional transverse space is flat and the dual CFT is $\mathcal{N} = 4$ $SU(N)$ Yang-Mills, as we discussed in chapter 1. For all such CFT,

$$(ML)^3 = \frac{N^2}{16\pi^2}\, p\ , \quad p = \frac{\pi^3}{V(X_5)}\ , \tag{4.1.10}$$

where $V(X_5)$ is the volume of X_5. In the $\mathcal{N} = 4$ SYM case, $p = 1$.

When $T_h \neq T$, the conical singularity contributes to the free energy. It is useful to consider this possibility since, as it will be clear in a moment, it can provide a natural "off-shell" description for the background along the phase transition. As described in [148], it is possible to regularize the singularity with a two-dimensional spherical cap of radius $r \to 0$, such that its Ricci scalar $\mathcal{R}_{S^2}$ is $2/r^2$ and its area[3] is $2\pi r^2(1 - T_h/T)$. As a result, the contribution of the spherical cap to the on-shell Euclidean gravity action turns out to be given by

$$S_{cone} = -2M^3 \int d^5x \sqrt{g}\, \mathcal{R}_{S^2} = -8\pi M^3 \left(1 - \frac{T_h}{T}\right) V_3 \frac{u_T^3}{L^3}\ . \tag{4.1.11}$$

Correspondingly, the contribution to the free energy density is given by

$$f_{cone} = 8\pi^4 (ML)^3 T_h^4 \left(1 - \frac{T}{T_h}\right)\ . \tag{4.1.12}$$

Thus, the total free energy density reads

$$f = f_{BH} + f_{cone} = 2\pi^4 (ML)^3 \left(3T_h^4 - 4TT_h^3\right)\ , \tag{4.1.13}$$

which is the result obtained in [46]. A crucial idea in that paper was to model the dynamics of the first-order phase transition by means of an effective action for a single scalar field. In the deconfined phase, the latter is realized by promoting the parameter T_h to a space-dependent field. This is the reason why we need to develop an "off-shell" formalism where we allow T_h to vary taking general values different from T. Within this scheme, eq. (4.1.13) provides the effective potential for the scalar field T_h. Consistently, the potential has a minimum in the homogeneous equilibrium configuration with $T_h = T$.

To proceed further, let us first rewrite the AdS-BH metric (4.1.2) in terms of the radial coordinate r defined in (4.1.4) without restricting the change of variables between u and r to the near horizon limit. As a result

$$\begin{aligned}
ds^2 &= \frac{u_T^2}{L^2}\left(1 + \frac{r^2}{L^2}\right)^2 \left[f_T(r)dt^2 + dx_i dx_i\right] + \frac{4}{L^2}\left(1 + \frac{r^2}{L^2}\right)^{-2} \frac{r^2 dr^2}{f_T(r)}\ , \\
f_T(r) &= 1 - \frac{L^8}{(L^2 + r^2)^4}\ ,
\end{aligned} \tag{4.1.14}$$

---

[3]The sphere is glued to the cone in a way such that their tangent vectors match. As a result the area of the spherical cap reads $2\pi r^2 \int_{\pi/2+\alpha}^{\pi} d\theta \sin\theta = 2\pi r^2(1 - \sin\alpha)$ where $\sin\alpha$ is given in (4.1.6).

with r ranging from zero (at the horizon) to infinity. In this coordinate system, the constant u_T factorizes in a very simple way. Let us now consider a simple $O(3)$ symmetric deformation of this metric, allowing just u_T to become a function of the 3d radial variable $\rho = \sqrt{x_i x_i}$,

$$ds^2 = \frac{u_T(\rho)^2}{L^2} \left(1 + \frac{r^2}{L^2}\right)^2 \left[f_T(r)dt^2 + d\rho^2 + \rho^2 d\Omega_2^2\right] + \frac{4}{L^2} \left(1 + \frac{r^2}{L^2}\right)^{-2} \frac{r^2 dr^2}{f_T(r)} \,. \tag{4.1.15}$$

This deformation is built to holographically account for $O(3)$ symmetric defects (bubbles) in the dual QFT. Consistently, only an $O(3)$ symmetry is preserved at the boundary $r \to \infty$. The metric (4.1.15) is not the exact, proper dual to the bounce state, which would require solving the full set of supergravity equations, a complicated task which has not been achieved in the literature yet. Rather, the background (4.1.15) has to be interpreted as an "off-shell" effective way of interpolating between black hole backgrounds with different values of T_h as ρ is varied. It is meant to represent a sequence of such metrics, each with its conical singularity with different deficit angle, giving the potential (4.1.13) according to the proposal of [46]. As such, it is a convenient way of calculating the derivative term for the effective field T_h.

In order to compute the effective $4d$ action for the field $u_T(\rho)$, one can evaluate the total gravity action (including the contribution (4.1.11) from the conical singularity) on the background (4.1.15) and then integrate over the $5d$ radial variable r.[4] The deformation gives rise to terms which depend on the derivatives of $u_T(\rho)$. The terms that do not depend on these derivatives are not affected by the deformation, since the latter amounts to a coordinate transformation for them. As a result, the expression (4.1.13), which gives the effective potential for the field $T_h(\rho) = u_T(\rho)/\pi L^2$, is unchanged.

The derivative term in the effective action arises from the on-shell value of

$$S_{kin} = -2M^3 \int d^5 x \sqrt{g}\, \mathcal{R} \,. \tag{4.1.16}$$

Actually, this gives rise to contributions proportional to $(\partial_\rho u_T)^2$ which diverge as $r \to \infty$. Implementing the holographic renormalization procedure, these divergences can be removed by regularizing the above action term with a cut-off r_Λ, adding the counterterm

$$S_{kin\,ct} = -2M^3 \left(-\frac{L}{2}\right) \int_{r=r_\Lambda} d^4 x \sqrt{h}\, \mathcal{R}_h \,, \tag{4.1.17}$$

and taking the $r_\Lambda \to \infty$ limit. In the above expression, h_{mn} is the boundary metric at $r = r_\Lambda$ and $\mathcal{R}_h$ is the corresponding Ricci scalar. The renormalized

---

[4]This way of proceeding is analogous to what is done to obtain the effective action for the radion, see e.g. [149]. Here, we are just turning off any fluctuation corresponding to the $4d$ graviton, according to the semiclassical approximation of [46] where the bounce is modeled by a single-scalar-field action.

derivative term is thus given by

$$S_{kin\,ren} = 6M^3 \frac{4\pi}{TL} \int d\rho \rho^2 (\partial_\rho u_T)^2 \ . \tag{4.1.18}$$

Rewriting the above result in terms of the field $T_h(\rho)$ and taking into account the potential term from (4.1.13), we get the total effective Euclidean action

$$S_{eff} \equiv \frac{S_3}{T} = \frac{4\pi}{T} \frac{N^2}{16\pi^2} p \int d\rho \, \rho^2 \left[6\pi^2 (\partial_\rho T_h)^2 + 2\pi^4 (3T_h^4 - 4T_h^3 T) \right] \ . \tag{4.1.19}$$

This formula is the main result of this section: our analysis determines the relative coefficient between the derivative and the potential term in the effective action for the "temperature field" $T_h(\rho)$, for the entire class of strongly coupled planar $(3+1)$-dimensional CFT with an AdS_5 black hole holographic dual.[5]

4.2   Confinement/deconfinement phase transition

In this section, we study bubble nucleation in the confinement/deconfinement phase transition in the WSS model. We consider a scenario where the WSS theory starts at a high temperature and then cools down. Due to the first-order phase transition, bubbles of confining (solitonic) vacuum will start to nucleate within the deconfined (black hole) vacuum.

4.2.1   Free energies of the Witten backgrounds

In section 2.6, we studied the WSS at finite temperature. We saw that once one compacfies the temporal circle, two gravitational backgrounds enter the computation of the free energy. For temperatures $T < M_{KK}/2\pi$ the solitonic solution (2.1.1) is energetically favored, while for temperatures $T > M_{KK}/2\pi$ the black hole solution (2.6.2) dominates. At $T = T_c = M_{KK}/2\pi$ the system features a first-order phase transition.

Following section 4.1, we define M_h and T_h by

$$u_0 = \frac{4}{9} R^3 M_h^2 \ , \qquad u_T = \frac{16\pi^2}{9} R^3 T_h^2 \ . \tag{4.2.1}$$

As we mentioned in section 2.1, if $T_h \neq T$ and $M_h \neq M_{KK}$, the backgrounds display a conical singularity and the latter contributes to the free energy. For the black hole background, we regularize the (t, u) subspace smoothing it with a two-dimensional spherical cap precisely as done in the RS-AdS case revisited in section 4.1. The contribution of the spherical cap to the action is therefore

$$\begin{aligned} S_{BH}^{cone} &= -\frac{1}{2\kappa_{10}^2} \int d^{10}x \sqrt{g} e^{-2\phi} \mathcal{R}_{S^2} \\ &= -\frac{2\pi V_3 V_{S^4}}{2\kappa_{10}^2 g_s^2 M_{KK}} 4\pi \left(1 - \frac{T_h}{T} \right) \left(\frac{u_T}{R} \right)^{-3/2} u_T^4 \ . \end{aligned} \tag{4.2.2}$$

---

[5]Comparing with the notations of e.g. [139], we see that our analysis allows to determine their derivative term coefficient as $c_3 = 48c_2 = 6\pi^2 p$.

Analogously, for the solitonic background we have

$$
\begin{aligned}
S_{solitonic}^{cone} &= -\frac{1}{2\kappa_{10}^2}\int d^{10}x\sqrt{g}e^{-2\phi}\mathcal{R} \\
&= -\frac{1}{2\kappa_{10}^2}\frac{V_3 V_{S^4}\beta}{g_s^2}4\pi\left(1-\frac{M_h}{M_{KK}}\right)\left(\frac{u_0}{R}\right)^{-3/2}u_0^4\,.
\end{aligned}
\tag{4.2.3}
$$

The contribution of the conical singularity then reads

$$
f_{BH}^{cone} = 3\left(\frac{2}{3}\right)^7\pi^4\lambda_{YM}N^2\frac{T_h^6}{M_{KK}^2}\left(1-\frac{T}{T_h}\right)\,,
\tag{4.2.4}
$$

$$
f_{solitonic}^{cone} = 6\left(\frac{1}{3}\right)^7\frac{1}{\pi^2}\lambda_{YM}N^2\frac{M_h^6}{M_{KK}^2}\left(1-\frac{M_{KK}}{M_h}\right)\,.
\tag{4.2.5}
$$

As a result, recalling[6] (2.6.15) and (2.6.16), the total free energies read

$$
\begin{aligned}
f_{BH} &= f_{X_0}+f_{BH}^{cone} \\
&= \frac{1}{2}\left(\frac{2}{3}\right)^7\pi^4\lambda_{YM}N^2\frac{1}{M_{KK}^2}\left(5T_h^6-6TT_h^5\right)\,,
\end{aligned}
\tag{4.2.6}
$$

$$
\begin{aligned}
f_{solitonic} &= f_{X_4}+f_{solitonic}^{cone} \\
&= \left(\frac{1}{3}\right)^7\frac{1}{\pi^2}\lambda_{YM}N^2\frac{1}{M_{KK}^2}\left(5M_h^6-6M_{KK}M_h^5\right)\,.
\end{aligned}
\tag{4.2.7}
$$

4.2.2 Holographic bubbles

In order to describe the bubble's nucleation, we should find a solution of the equations of motion that interpolates between the confined and the deconfined backgrounds. Unfortunately, this is a very difficult task to pursue. The idea is then to take an effective approach in which the interpolation is mediated by a single effective degree of freedom [46]. Since the two backgrounds differ only for the fact that the blackening factor sits in front of dx_4^2 or dt^2, we might try to promote the parameters u_T and u_0 to fields $u_T(\rho)$ and $u_0(\rho)$, where ρ is the radial coordinate for the bubble. We will consider either $O(3)$ symmetric bubbles, for which $\rho^2 = x_i x_i$, or $O(4)$ symmetric ones, where $\rho^2 = t^2 + x_i x_i$. For instance, in the black hole case, one could start from a $O(3)$-symmetric ansatz of the form

$$
ds^2 = \left(\frac{u}{R}\right)^{3/2}\left[f_T(u,\rho)dt^2+d\rho^2+\rho^2 d\Omega_2^2+dx_4^2\right]+\left(\frac{R}{u}\right)^{3/2}\left[\frac{du^2}{f_T(u,\rho)}+u^2 d\Omega_4^2\right]\,,
\tag{4.2.8}
$$

with

$$
f_T(u,\rho) = 1-\frac{u_T(\rho)^3}{u^3}\,,
\tag{4.2.9}
$$

---

[6]Notice that, because of the definition (4.2.1), the results (2.6.15) and (2.6.16) have to be taken with T and M_{KK} replaced, respectively, by T_h and M_h.

and the other fields left unchanged. In this setup, the temperature of the horizon T_h is promoted to a field as well,

$$u_T(\rho) = \frac{16\pi^2}{9} R^3 T_h(\rho)^2 \ . \tag{4.2.10}$$

The effective action for this field will now include a contribution from its derivative term. This comes from the Ricci scalar and reads

$$
\begin{aligned}
\mathcal{R}_{kin} &= -\frac{9}{2}\left(\frac{u}{R}\right)^{3/2} \frac{R^3 u_T^4}{u^3(u^3 - u_T^3)^2} (\partial_\rho u_T)^2 \\
&= -\frac{9}{2}\left(\frac{32\pi^2}{9}\right)^2 \left(\frac{u}{R}\right)^{3/2} \frac{R^9 u_T^4}{u^3(u^3 - u_T^3)^2} T_h^2 (\partial_\rho T_h)^2 \ .
\end{aligned}
\tag{4.2.11}
$$

Thus, we see that using the ansatz (4.2.8) the Ricci scalar (4.2.11) displays a divergence for $u \to u_T(\rho)$ which deviates from the conical singularity. Indeed, if we expand the metric around $u = u_T(\rho)$, we do not find the metric of a cone, because the change of coordinates (2.1.3) becomes non-trivial when u_T is a function of ρ. This background is not satisfactory, because we would like it to display a conical singularity with a ρ-dependent cone angle.

Let us consider another ansatz. We start from the background (2.1.1) and we perform the coordinate change between u and r as in (2.1.3). Then we promote u_T to be a function of ρ. In this way, the metric expanded around $r = 0$ is the metric of a cone for any value of ρ. In general, it reads

$$ds^2 = \left(\frac{u}{R}\right)^{3/2}\left[f_T(u)dt^2 + d\rho^2 + \rho^2 d\Omega_2^2 + dx_4^2\right] + \left(\frac{R}{u}\right)^{3/2}\left[\frac{9\,u_T\,r^2 dr^2}{4R^3 f_T(u)} + u^2 d\Omega_4^2\right] ,$$
$$\tag{4.2.12}$$

where

$$u = u(r, \rho) = u_T(\rho) + \frac{3}{4}\sqrt{\frac{u_T(\rho)}{R^3}} r^2 \ . \tag{4.2.13}$$

The dilaton and the RR four form will be taken as in the original background. In particular, due to eq. (4.2.13), the dilaton will now be a function of both r and ρ.

The effective four-dimensional action for $u_T(\rho)$ will be obtained by plugging the ansatz above in the renormalized action $S_{ren} = S_{IIA} + S_{ct} + S_{GH}$ as defined in section 4.2.1 and integrating over r, x_4 and the transverse four-sphere. The background deformation described above affects only the quantities which depend on the derivatives of $u_T(\rho)$. Thus, the potential term in the effective action will be read from eq. (4.2.6), where $T_h(\rho)$ is expressed in terms of $u_T(\rho)$ by means of eq. (4.2.10).

The derivative term in the effective action for $u_T(\rho)$ requires some care. In principle, it is obtained from the on-shell value of

$$S_{kin\,eff} = -\frac{1}{2\kappa_{10}^2} \int d^{10}x \sqrt{g} \left[e^{-2\phi}\left(\mathcal{R} + 4\partial_\rho\phi\partial^\rho\phi\right)\right] \ . \tag{4.2.14}$$

Actually, this gives rise to contributions proportional to $(\partial_\rho u_T(\rho))^2$ which diverge as $r \to \infty$. Remarkably enough, the above divergences can be removed by adding to the action above the counterterm

$$S_{kin\,ct} = -\frac{1}{2\kappa_{10}^2} \left(-\frac{40R}{9g_s^{1/3}} \right) \int_{r=r_{UV}} d^9x \, \sqrt{h} \, e^{-5\phi/3} \, h^{mn} \, \partial_m\phi \, \partial_n\phi \;, \qquad (4.2.15)$$

where h_{mn} is the boundary metric at fixed $r = r_{UV}$. All in all we get a quite simple effective action for $u_T(\rho)$.

It is possible to show that precisely the same results (and the same expression for the renormalized derivative term) can be obtained using an alternative counterterm action that is built having in mind the structure of the first two terms of the counterterm action in eq. (5.78) of [150]. It reads

$$\begin{aligned} S_{kin\,ct\,alt} &= -\frac{1}{2\kappa_{10}^2} \left(-\frac{5R}{7g_s^{1/3}} \right) \int_{r=r_{UV}} d^9x \, \sqrt{h} \, e^{-5\phi/3} \, \mathcal{R}_{[h]} + \\ &\quad -\frac{1}{2\kappa_{10}^2} \left(\frac{60}{7R\,g_s^{-1/3}} \right) \int_{r=r_{UV}} d^9x \, \sqrt{h} \, e^{-7\phi/3} \;. \end{aligned} \qquad (4.2.16)$$

The second, "volume" counterterm, cancels all the divergences and the finite terms - which do not depend on derivatives of $u_T(\rho)$ - coming from the first one. The structure of this term is analogous to that of the "volume" counterterm we have added to renormalize the bulk on-shell action.

With the same procedure we can get an effective action for $u_0(\rho) \sim M_h(\rho)^2$ in the confined phase.

The ansatz we have chosen in our discussion above is $O(3)$ symmetric. This is what is expected to hold at large enough temperatures. For smaller temperatures, one should expect a $O(4)$-symmetric ansatz to hold. This ansatz would be perfectly consistent with the symmetries of the solitonic background dual to the confined phase. In fact, even on the black hole background, which has only $O(3)$ symmetry, at a small enough temperature, the radius of the bubble can be much smaller than the length of the time circle. In this case, the configuration can effectively enjoy an enlarged $O(4)$ symmetry including the Euclidean time direction [26, 27]. We will present the related effective actions in the following subsection.

4.2.3 Effective actions and solutions

Let us now write the effective actions for $u_T(\rho)$ or $u_0(\rho)$ in terms of the field

$$Y = -Y_T \text{(deconfined phase)} \;, \quad Y = Y_0 \text{(confined phase)} \;, \qquad (4.2.17)$$

where

$$Y_T = T_h(\rho)^2 \;, \qquad Y_0 = \left(\frac{M_h(\rho)}{2\pi} \right)^2 \;. \qquad (4.2.18)$$

In the $O(3)$-symmetric case, the effective action in the deconfined phase reads

$$\frac{S_3(Y)}{T} = \frac{16\pi^3 \lambda_{YM} N^2}{3^5 M_{KK}^2 T} \int d\rho \rho^2 \left[\left(5 - \frac{\pi}{2\sqrt{3}} \right) Y'^2 - \frac{16\pi^2}{9} \left(5Y^3 + 6T(-Y)^{5/2} \right) \right] ,$$

(4.2.19)

where the prime denotes derivative with respect to ρ, and Y is supposed to take negative values. In the confined phase the action is

$$\frac{S_3(Y)}{T} = \frac{16\pi^3 \lambda_{YM} N^2}{3^5 M_{KK}^2 T} \int d\rho \rho^2 \left[\left(5 - \frac{\pi}{2\sqrt{3}} \right) Y'^2 + \frac{16\pi^2}{9} \left(5Y^3 - \frac{3}{\pi} M_{KK} Y^{5/2} \right) \right] ,$$

(4.2.20)

where now Y takes positive values. The full problem is simply the junction of the two regimes. By passing to dimensionless quantities

$$\Phi \equiv \frac{Y}{M_{KK}^2} , \qquad \bar{\rho} \equiv M_{KK} \rho , \qquad \bar{T} \equiv \frac{2\pi T}{M_{KK}} , \qquad (4.2.21)$$

such that the critical temperature T_c corresponds to $\bar{T} = 1$, one factorizes the parametric dependences out of the Lagrangians and the whole action reads

$$\frac{S_3(\Phi)}{T} = \frac{32\pi^4 g}{3^5 \bar{T}} \int_0^\infty d\bar{\rho}\bar{\rho}^2 \left[\left(5 - \frac{\pi}{2\sqrt{3}} \right) \Phi'^2 + \Theta(\Phi) V_c(\Phi) + \Theta(-\Phi) V_d(\Phi) \right] ,$$

(4.2.22)

where $\Theta(\cdot)$ is the Heaviside step function,

$$V_c(\Phi) = \frac{16\pi^2}{9} \left(5\Phi^3 - \frac{3}{\pi} \Phi^{5/2} \right) ,$$
$$V_d(\Phi) = -\frac{16\pi^2}{9} \left(5\Phi^3 + \frac{3}{\pi} \bar{T}(-\Phi)^{5/2} \right) , \qquad (4.2.23)$$

and

$$g \equiv \lambda_{YM} N^2 . \qquad (4.2.24)$$

Formula (4.2.22) is the main result of this section, providing the action for the scalar field effectively describing the interpolation between the black brane and solitonic backgrounds. Note that there is a single parameter g which enters multiplicatively the action.

Figure 4.1 depicts the full potential for three different values of the reduced temperature $\bar{T}$. The two minima are $V_d = -\bar{T}^6/(36\pi^4)$ for $\Phi_d = -\bar{T}^2/(4\pi^2)$ and $V_c = -1/(36\pi^4)$ for $\Phi_c = 1/(4\pi^2)$. We will focus on the case $\bar{T} \in [0,1]$, where the true vacuum is the confining one at $\Phi = \Phi_c$.

We are going to find a bubble-like solution Φ_B of the equation of motion derived from the action (4.2.22) in the following way. We start inside the bubble, i.e. for $\bar{\rho} \in [0, \bar{\rho}_w]$ (where $\bar{\rho}_w$ is the location of the bubble wall), i.e. in the confined case with $\Phi > 0$. The equation is solved with boundary conditions

$$\Phi_B(0) = \Phi_0 , \qquad \Phi_B'(0) = 0 , \qquad (4.2.25)$$
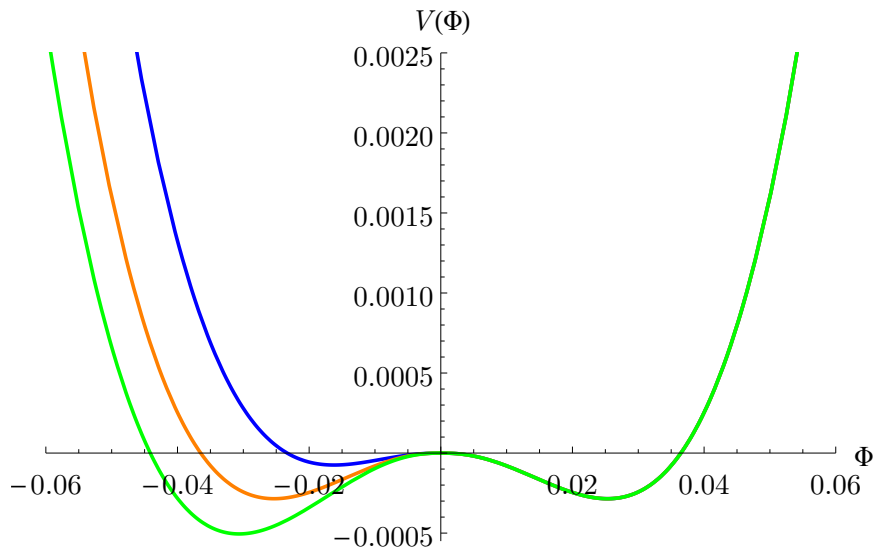
Figure 4.1. *Representative curves of the potential for three different values of the dimensionless temperature: $\bar{T} = 0.8$ (blue), $\bar{T} = 1$ (orange), $\bar{T} = 1.1$ (green). The region where Φ takes positive values does not depend on the temperature, hence the curves overlap.*

for some positive value Φ_0; the second condition corresponds to the request of regularity. The solution Φ_B is going to vanish at a finite position of the radius, which is identified with $\bar{\rho}_w$. There we calculate the derivative $\Phi'_B(\bar{\rho}_w) \equiv \Phi'_{B,w}$.

Then we solve the equation outside the bubble, i.e. for $\bar{\rho} \in [\bar{\rho}_w, \infty]$, i.e. in the deconfined case where $\Phi < 0$. The boundary conditions we use are the ones enforcing continuity of Φ_B and Φ'_B at the junction,

$$\Phi_B(\bar{\rho}_w) = 0 \ , \qquad \Phi'_B(\bar{\rho}_w) = \Phi'_{B,w} \ . \tag{4.2.26}$$

Finally, we search for the initial value Φ_0 at the center of the bubble such that the solution for large $\bar{\rho}$ goes to the false vacuum, Φ_d. Thus, the whole solution is such that at the center of the ball it goes to a positive constant[7] with vanishing derivative and at infinity it goes to the false vacuum solution. Examples of solutions corresponding to different choices of $\bar{T}$ are given in figure 4.2. The amplitude of the configuration is reduced as the temperature gets smaller and smaller.

Once the solution is calculated, one can plug it back into the action. As mentioned in the introduction, the bounce action S_B that enters the formula $\Gamma = A \, e^{-S_B}$ for the rate of the vacuum decay is, in the $O(3)$-symmetric case, $S_B = S_{3,B}$ given by [25]

$$\frac{S_{3,B}}{T} = \frac{S_3(\Phi_B) - S_3(\Phi_d)}{T} \ . \tag{4.2.27}$$

---

[7]Note that the constant Φ_0 is typically different from the true vacuum Φ_c, because the equation of motion derived from (4.2.22) contains a friction term.
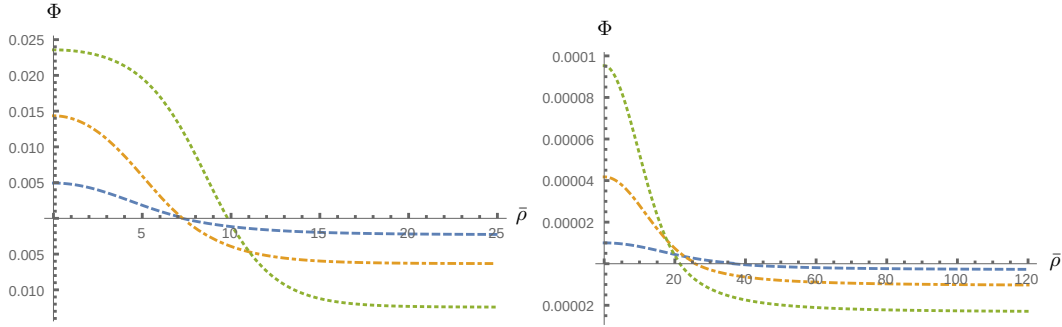
Figure 4.2. *Solutions for the bubble profile in the $O(3)$ case (left) with $\bar{T} = 0.3$ (dashed), 0.5 (dash-dotted), 0.7 (dotted) and in the $O(4)$ case (right) with $\bar{T} = 0.01$ (dashed), 0.02 (dash-dotted), 0.03 (dotted).*

For small temperatures, one could have also $O(4)$ symmetric bounces. Notice that in the present setup this symmetry is also preserved by the solitonic background (2.1.1) describing the low temperature phase of the model. The action for the $O(4)$ symmetric configuration is almost the same as (4.2.22), but for the fact that the four-dimensional measure d^4x is now given by $d\Omega_3 d\rho\rho^3$, where $d\Omega_3$ is the measure of the three-sphere. As a result, the action does not display the overall $M_{KK}/T = 2\pi/\bar{T}$ factor that in the $O(3)$ case came from the integration over t,

$$S_4(\Phi) = \frac{8\pi^4 g}{3^5} \int_0^\infty d\bar{\rho}\, \bar{\rho}^3 \left[\left(5 - \frac{\pi}{2\sqrt{3}} \right) \Phi'^2 + \Theta(\Phi)V_c(\Phi) + \Theta(-\Phi)V_d(\Phi) \right] \, . \tag{4.2.28}$$

Then, proceeding as above, one obtains solutions for the bubbles as in figure 4.2. The bounce action is defined as $S_{4,B} = S_4(\Phi_B) - S_4(\Phi_d)$.

We underline that these $O(4)$ and $O(3)$ symmetric configurations have to be considered as reliable approximations in the following sense. At $T = 0$, $O(4)$ symmetric bubbles with radius ρ_w are produced. At $T > 0$, where the Euclidean time direction is compact and has period $\beta = 1/T$, exact $O(4)$ symmetric configurations are generically forbidden. However, if $T \ll \rho_w^{-1}$ the solution may be still approximated by a periodic array of $O(4)$ symmetric configurations separated by a distance β along the Euclidean time direction. At $T \sim \rho_w^{-1}$ these bubbles start overlapping and finally at $T \gg \rho_w^{-1}$ the solution looks like a cylinder along the Euclidean time direction with $O(3)$ symmetric spatial cross section. For this configuration, integration over the Euclidean time direction in the effective action naively reduces to multiplication by $1/T$. Due to the exponential dependence of the decay rate on the value of the bounce action, the transition region from the low-temperature regime ($T \ll \rho_w^{-1}$) to the high-temperature one ($T \gg \rho_w^{-1}$) usually turns out to be very narrow: hence the related configurations actually provide a good estimate for the effective bounce in the whole temperature range [27].

In section 4.4, we report on the use of the thin and thick wall approximations, which allow us to study semi-analytically the problem at large and small temperatures, respectively. There it is also shown that the bubble is unlikely to have
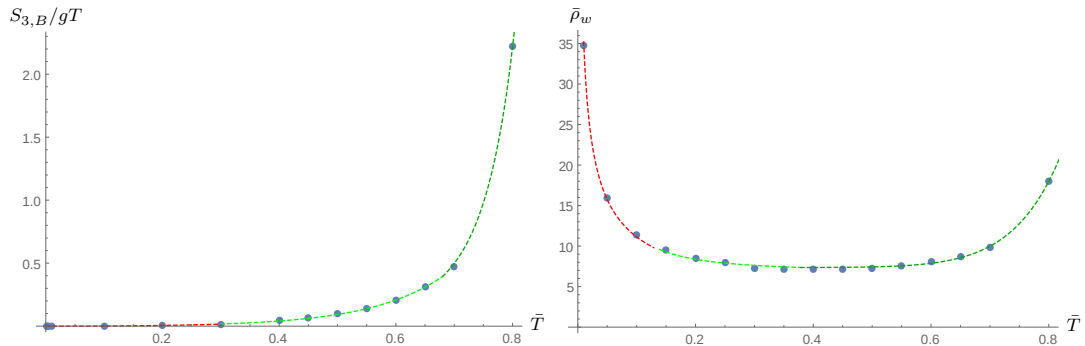
Figure 4.3. *The action $S_{3,B}/gT$ and dimensionless radius $\bar{\rho}_w$ of the $O(3)$ symmetric bubble as a function of $\bar{T}$. Dots correspond to numerical results, the dotted lines to eqs. (4.2.29), (4.2.30). Different colors correspond to different expressions of the piecewise functions.*

an even larger symmetry than $O(4)$. In fact, in principle in the dual description, the bubble could happen to be small as compared to the four-sphere and the x_4 circle of the background. In section 4.4 we show that this is never the case for temperatures below T_c, justifying the ansatze adopted in this section.

Based on the numerical results and inspired by the functional form of the thin and thick wall approximations studied in section 4.4, a continuous analytic approximation to the action for the $O(3)$ bubble can be provided as follows,

$$\frac{S_{3,B}}{gT} \approx \begin{cases} 0.32\ \bar{T}^{5/2} & (\bar{T} \leq 0.3) \\ 1.8 \times 10^{-3}\exp(7.9\ \bar{T}) - 2 \times 10^{-3} & (0.3 \leq \bar{T} \leq 0.68) \\ 5.4 \times 10^{-2}\exp(8.8\ \bar{T}^{3.8}) & (0.68 \leq \bar{T} \leq 0.87) \\ 2.6/\bar{T}(1 - \bar{T}^6)^2 & (\bar{T} \geq 0.87) \end{cases} \qquad (4.2.29)$$

while its radius can be approximated as

$$\bar{\rho}_w \approx \begin{cases} 3.5/\bar{T}^{1/2} & (\bar{T} \leq 0.13) \\ 6.8 + 0.13/\bar{T}^{1.5} & (0.13 \leq \bar{T} \leq 0.38) \\ 7.4 + 110\ \bar{T}^{10} & (0.38 \leq \bar{T} \leq 0.84) \\ 16/(1 - \bar{T}^6) & (\bar{T} \geq 0.84) \end{cases} \qquad (4.2.30)$$

Figure 4.3 shows a comparison between the latter fits and numerical data.

For the $O(4)$ bubble, since it is only defined for small temperatures, it is sufficient to consider the functional form of the thick wall approximation, giving

$$\frac{S_{4,B}}{g} \approx 0.39\ \bar{T}^3\ , \qquad \bar{\rho}_w \approx \frac{4.0}{\bar{T}^{1/2}} \qquad (\bar{T} < 0.06)\ . \qquad (4.2.31)$$

The comparison with numerical data is shown in figure 4.4. We only plot $S_{4,B}/g$ for small $\bar{T}$ because of its range of validity. In fact, the $O(4)$ bubble radius must be much smaller than $1/T$, otherwise one cannot have this enlarged symmetry
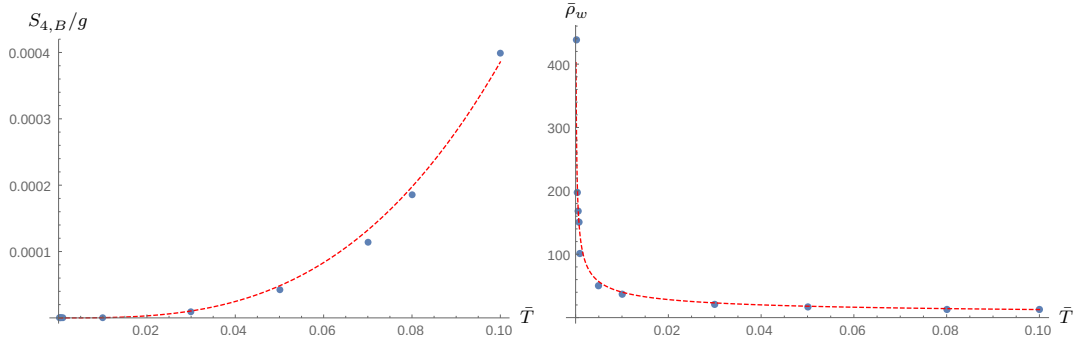
Figure 4.4. *The action $S_{4,B}/g$ and dimensionless radius $\bar{\rho}_w$ of the $O(4)$ symmetric bubble as a function of $\bar{T}$. Dots correspond to numerical results, the dotted lines to eq. (4.2.31).*

configuration on the thermal circle [26, 27].[8] We choose to place the discriminant bubble radius value, above which we do not consider $O(4)$ configurations, at the conventional point where $\rho_w = 1/2\pi T$ (the radius of the thermal circle). In our case, this happens for $\bar{T} \approx 0.06$.

4.2.4 Bubble nucleation rate

The bubble nucleation rate is the maximum of the rates of the $O(3)$ and $O(4)$ symmetric bubbles [25–27, 131, 132][9]

$$
\begin{aligned}
\Gamma &= \text{Max}\left[T^4 \left(\frac{S_{3,B}}{2\pi T}\right)^{3/2} e^{-S_{3,B}/T}, \left(\frac{S_{4,B}}{2\pi \rho_w^2}\right)^2 e^{-S_{4,B}} \right] \\
&= M_{KK}^4 \text{Max}\left[\frac{\bar{T}^4}{(2\pi)^4} \left(\frac{S_{3,B}}{2\pi T}\right)^{3/2} e^{-S_{3,B}/T}, \left(\frac{S_{4,B}}{2\pi \bar{\rho}_w^2}\right)^2 e^{-S_{4,B}} \right] . \quad (4.2.32)
\end{aligned}
$$

Some examples of the rates in the $O(3)$ case are provided in figure 4.5. Since the rate is exponentially suppressed with the action, it is more and more suppressed as the parameter g is increased. Also, the peak of the rate is shifted to smaller temperatures by increasing g, so that for large values of this parameter the theory features what is called *supercooling*. In this case, the rate is so small that the theory is trapped in the false vacuum, below the critical temperature of the first-order transition, for a long time.

Similar features are present in the $O(4)$ case, shown again in figure 4.5. As can be appreciated by comparing the left and right plots in figure 4.5, which correspond to the same values of g, the rate for the $O(4)$ bubble dominates on

---

[8]The $O(4)$ bubble does not fit the thermal circle for $2\rho_w > 1/T$. But even if $2\rho_w < 1/T$, if the radius is close to the extremal value $1/2T$, the assumption that there is an enlarged $O(4)$ symmetry is hardly consistent.

[9]The prefactors T^4 and $1/\rho_w^4$ in (4.2.32) are essentially determined by dimensional analysis and heuristic considerations [27, 131]. We verified that changing e.g. T^4 into T^6/M_{KK}^2 has very small impact on the numerical values found in this thesis.
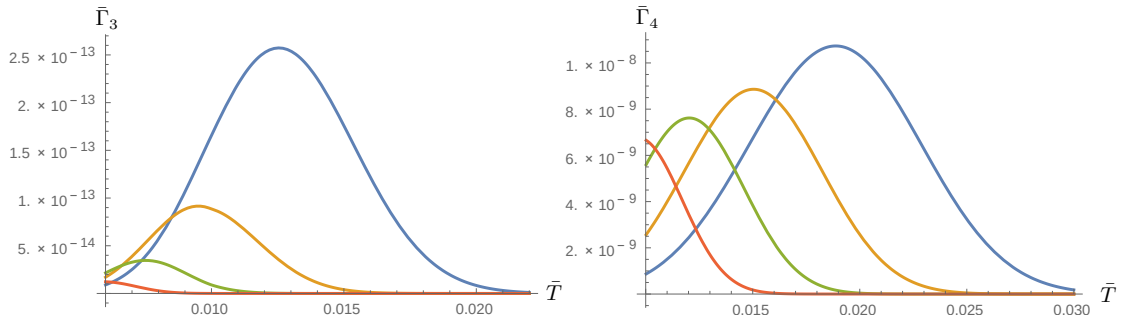
Figure 4.5. *Representative plots of the decay rate $\bar{\Gamma} \equiv \Gamma/M_{KK}^4$ for $g/10^6 = 1$ (blue), 2 (orange), 4 (green), 8 (red), for the $O(3)$ (left) and $O(4)$ (right) configurations.*

the one for the $O(3)$ bubble for those values of $\bar{T}$ for which it is defined, namely for $\bar{T} \lesssim 0.06$. Thus, at such small temperatures, the decay is much more likely to happen via quantum rather than thermal fluctuations.

4.3 Chiral symmetry phase transition

4.3.1 Revisiting the transition

As already mentioned in chapter 3, the authors of [43] showed that in the Witten-Sakai-Sugimoto model the deconfinement phase transition and the chiral symmetry breaking phase transition can take place at different temperatures for certain values of the model's parameters. Thus, apart from the vacuum decay studied in section 4.2, there is a different type of vacuum decay associated to the embedding of the flavor branes. In this section we will briefly review the analysis of [43] and then put forward a simple analytic expression that approximates with good accuracy the brane embedding profiles. This expression will be a useful tool in subsection 4.3.2 where we will discuss the bubble configurations that mediate the chiral symmetry breaking phase transitions in the deconfined phase.

We want to study probe brane embedding profiles in the (Euclidean) background (2.6.2). The Dirac-Born-Infeld action reads

$$S_{DBI} = \frac{T_8}{g_s} \int d^9x \left(\frac{u}{R}\right)^{-3/2} u^4 \sqrt{1 + f_T(u)\left(\frac{u}{R}\right)^3 (\partial_u x_4)^2} \ . \tag{4.3.1}$$

We have a conserved quantity,

$$u^4 \frac{f_T(u)\left(\frac{u}{R}\right)^{3/2}(\partial_u x_4)}{\sqrt{1 + f_T(u)\left(\frac{u}{R}\right)^3(\partial_u x_4)^2}} = \text{constant} \ . \tag{4.3.2}$$

The simplest solution is that of a straight brane-antibrane pair each at constant x_4. That would be the phase with unbroken chiral symmetry. On the other hand, there are U-shaped solutions that connect the brane and the antibrane somewhere

in the bulk, leading to a breaking of chiral symmetry. Any solution of that kind has a tip, where the brane and antibrane are joined, located at some position of the holographic direction $u = u_J$ such that $x_4'(u_J) = \infty$. For this case, we can rewrite (4.3.2) as

$$\frac{u^4 \sqrt{f_T(u)}}{\sqrt{1 + \left(f_T(u) \left(\frac{u}{R} \right)^3 (\partial_u x_4)^2 \right)^{-1}}} = u_J^4 \sqrt{f_T(u_J)} \; . \tag{4.3.3}$$

We can rescale the coordinate to factor out the dimensionful parameters,[10]

$$x_4 = x \, u_T^{-1/2} R^{3/2} = x \frac{3}{4\pi T} \; , \qquad u = y \, u_T \; , \qquad u_J = y_J \, u_T \; , \tag{4.3.4}$$

such that

$$f_T(u) \equiv f_T = 1 - y^{-3} \; , \qquad f_T(u_J) \equiv f_{TJ} = 1 - y_J^{-3} \; . \tag{4.3.5}$$

The periodicity of the cigar coordinate is

$$x \sim x + \frac{2\pi \sqrt{u_T}}{M_{KK} R^{\frac{3}{2}}} = x + \frac{8\pi^2 T}{3 M_{KK}} \; . \tag{4.3.6}$$

In these coordinates, equation (4.3.3) can be rewritten as

$$\partial_y x = \left[f_T y^3 \left(\frac{y^8 f_T}{y_J^8 f_{TJ}} - 1 \right) \right]^{-1/2} \; . \tag{4.3.7}$$

Recalling that L is the distance between the brane and the antibrane along x_4 in the $u \to \infty$ limit, for the U-shaped configuration, it can be computed as

$$\begin{aligned} L &= \int_{worldvolume} dx_4 = 2 \int_{u_J}^{\infty} \frac{dx_4}{du} du \\ &= 2 \frac{3}{4\pi T} \int_{y_J}^{\infty} \left[f_T y^3 \left(\frac{y^8 f_T}{y_J^8 f_{TJ}} - 1 \right) \right]^{-1/2} dy \; , \end{aligned} \tag{4.3.8}$$

where the factor of 2 arises from adding up both sides of the "U". Thus, for each value of u_J (or, equivalently, of y_J), there is a unique solution with a given value of LT that can be numerically computed by integrating (4.3.8). This is represented in figure 4.6. The figure also displays some profiles for different values of y_J.

The next step is to understand in which cases the U-shaped profile is energetically preferred to the disconnected brane-antibrane pair. We have to compare the on-shell actions of both cases. Let us first express (4.3.1) in terms of the

---

[10]Notice that the y defined here does not coincide with the one defined by [43].
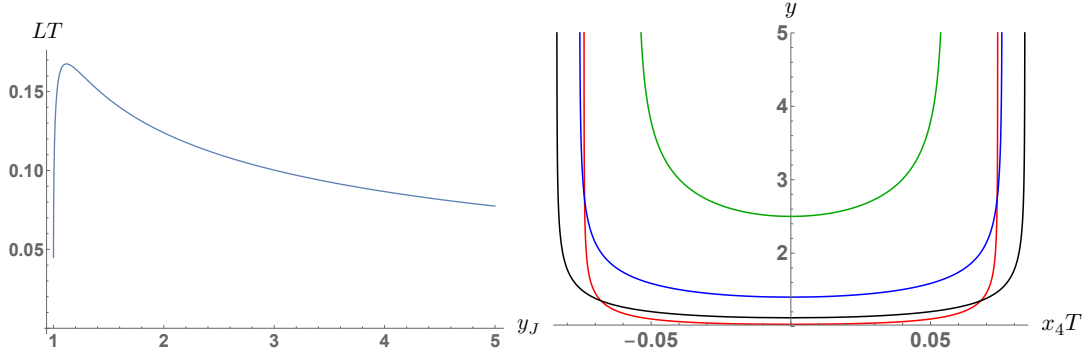
Figure 4.6. *Left: Separation in x_4 times the temperature as a function of $y_J = u_J/u_T$ for the U-shaped configuration in the deconfined background. The maximum value of LT in the plot is $LT \approx 0.1675$ and occurs for $y_J \approx 1.119$. Right: Profiles for different values of y_J: $y_J = 1.03$ (red), $y_J = 1.119$ (black), $y_J = 1.4$ (blue), $y_J = 2.5$ (green). We have assumed, without loss of generality, that the tip of the brane is located at $x_4 = 0$.*

dimensionless constants. We write $V_{1,3}$ for the (infinite) volume of Minkowski space and V_{S^4} for the volume of the internal four-sphere. We get

$$S_{DBI} = K \int y^{5/2} \sqrt{1 + f_T y^3 (\partial_y x)^2} dy \ , \qquad (4.3.9)$$

where $K = \frac{T_8}{g_s} V_{1,3} V_{S^4} R^{3/2} u_T^{7/2}$ is a constant factor, common to all brane configurations. For the disconnected configuration, taking into account the factor of 2 for the brane-antibrane pair and inserting a UV cut-off,

$$S_{DBI}|_d = 2K \int_1^{y_{cut}} y^{5/2} dy \ . \qquad (4.3.10)$$

For the connected configuration, we can insert the value of $(\partial_y x)$ for the solution, as given in (4.3.7),

$$S_{DBI}|_c = 2K \int_{y_J}^{y_{cut}} y^{5/2} \left(1 - \frac{y_J^8 f_{TJ}}{y^8 f_T}\right)^{-1/2} dy \ . \qquad (4.3.11)$$

We are interested in the difference $\Delta S_{DBI} = S_{DBI}|_c - S_{DBI}|_d$. This difference is not divergent and the UV cut-off can be safely removed. Splitting $S_{DBI}|_d$ into two integrals below and above y_J, we have

$$\frac{\Delta S_{DBI}}{K} = 2 \int_{y_J}^{\infty} y^{5/2} \left[\left(1 - \frac{y_J^8 f_{TJ}}{y^8 f_T}\right)^{-1/2} - 1\right] dy - \frac{4}{7}(y_J^{7/2} - 1) \ . \qquad (4.3.12)$$

The value of ΔS_{DBI} can be computed numerically as a function of y_J. It turns out that $\Delta S_{DBI} > 0$ for $y_J < y_{\chi SB} \approx 1.3592$, a case in which the disconnected configuration is preferred and chiral symmetry is preserved. Conversely, $\Delta S_{DBI} <$

0 for $y_J > y_{\chi SB}$ and the connected configuration is preferred. The value of $y_{\chi SB}$ corresponds to $(LT)_{\chi SB} \approx 0.1538$.

We now demonstrate that a variational approach can provide a good approximation to these results. Let us consider a family of profiles for a length L of the form

$$y = y_J + B \left[\text{arctanh} \left(\frac{2x}{\tilde{L}} \right) \right]^2 , \qquad (4.3.13)$$

where $\tilde{L}$ is the distance between the brane and the antibrane in the coordinate x, which, taking (4.3.4) into account, is related to L as

$$\tilde{L} = \frac{4\pi}{3} LT . \qquad (4.3.14)$$

The expression (4.3.13) can be inverted,

$$x = \frac{\tilde{L}}{2} \tanh \left(\frac{\sqrt{y - y_J}}{\sqrt{B}} \right) . \qquad (4.3.15)$$

The parameters y_J and B are here variational constants that can take values $1 \leq y_J < \infty$, $0 < B < \infty$. It is important to remark that the variational profile smoothly interpolates between a U-shaped profile and the chiral symmetry preserving profile that is recovered in the limit $y_J = 1$, $B \to 0$. For a particular $\tilde{L}$, the values of y_J and B have to be determined by minimizing the on-shell action attained after inserting (4.3.15) in

$$\frac{\Delta S_{DBI}}{K} = 2 \int_{y_J}^{\infty} y^{5/2} \left[\sqrt{1 + f_T y^3 (\partial_y x)^2} - 1 \right] dy - \frac{4}{7}(y_J^{7/2} - 1) , \qquad (4.3.16)$$

where we have used (4.3.9) and subtracted the straight brane-antibrane pair. Figure 4.7 depicts two examples of the behavior of ΔS_{DBI} as a function of the variational parameters.

With this procedure, a variational approximation to the lowest energy profile can be found for any value of $\tilde{L}$. Figure 4.8 shows that the approximation is quite accurate. To further emphasize that this variational approach captures the physics very well, we can compute the value of $\tilde{L}$ at which the phase transition occurs. Numerically solving the exact equations (namely finding from eq. (4.3.12) the value of y_J for which ΔS_{DBI} vanishes and inserting it in (4.3.8)), we obtain $\tilde{L}_{\chi SB} = 0.6444$. From the variational approach, we find $\tilde{L}_{\chi SB} = 0.6442$. We have introduced this analytic approximation to the brane profiles in order to simplify the computation of vacuum decay that will be discussed below. Nevertheless, it is natural to expect that it may also prove useful to study other properties of the WSS as, e.g., the relation between the excitations of the branes in the connected and disconnected phases [151].

4.3.2   Flavor brane bubbles

We have seen that for $\tilde{L} = \frac{4\pi}{3} LT < 0.644$, the chiral symmetry breaking configuration is energetically preferred (it is the "true vacuum") and therefore for
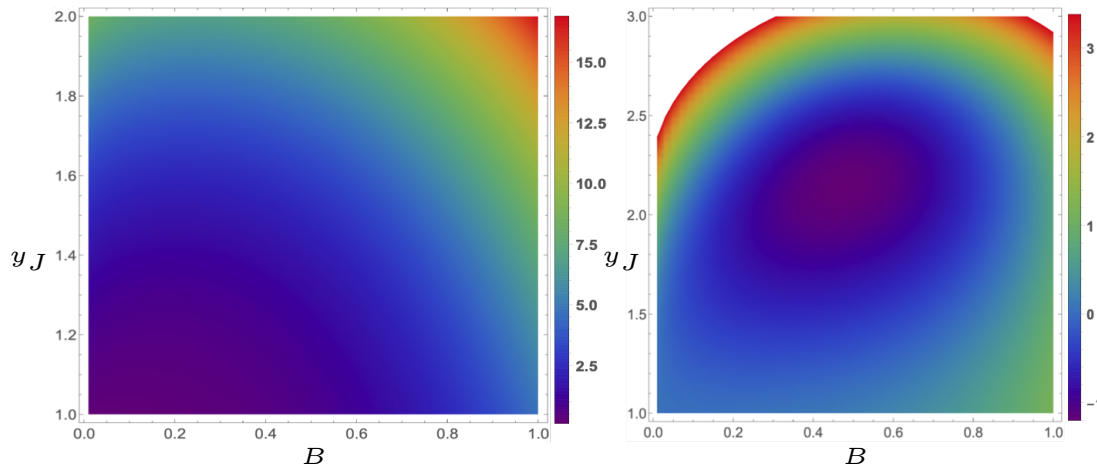
Figure 4.7. *Numerically computed values of $K^{-1}\Delta S_{DBI}(y_J, B)$ for two different values of $\tilde{L}$. On the left ($\tilde{L} = 1$), the minimum is at $y_J = 1$, $B \to 0$ and therefore the disconnected solution is preferred. On the right ($\tilde{L} = 0.5$), the minimum is at $y_J = 2.15$, $B = 0.48$, the connected solution has lower energy and chiral symmetry breaking is to be expected. It is interesting to notice that the disconnected solution ($y_J = 1$, $B \to 0$) remains a local minimum of the action in all the cases.*

lower temperatures the chirally symmetric vacuum (the "false vacuum") can decay through bubble nucleation [25–27, 132]. The bubble would correspond to a "bounce solution". Namely, we look for a regular solution of the equations of motion obtained from the Euclidean action that interpolates between a configuration related to the true vacuum at the center of the bubble and the false vacuum far away from it.[11] Our goal is to produce estimates for the production rate of vacuum decay bubbles. As in the deconfinement phase transition case, we will discuss ansatze with $O(3)$ [25, 132] and $O(4)$ [26, 27] symmetries.

$O(3)$-symmetric bubbles

We start by rewriting the metric with the Euclidean physical space in spherical coordinates, with ρ as the radial coordinate,

$$ds_E^2 = \left(\frac{u}{R}\right)^{3/2}\left[f_T(u)dt^2 + d\rho^2 + \rho^2 d\Omega_2^2 + dx_4^2\right] + \left(\frac{R}{u}\right)^{3/2}\left[\frac{du^2}{f_T(u)} + u^2 d\Omega_4^2\right] .$$
(4.3.17)

Considering an ansatz in which $x_4(u, \rho)$, the DBI action reads

$$S_{DBI} = \frac{T_8}{g_s}\int d^9x \rho^2 \left(\frac{u}{R}\right)^{-3/2} u^4 \sqrt{1 + f_T(u)\left(\frac{u}{R}\right)^3 (\partial_u x_4)^2 + (\partial_\rho x_4)^2} .$$
(4.3.18)

---

[11]A bounce solution mediated by a complex tachyon field for a brane-antibrane pair in flat space was analyzed in [152].
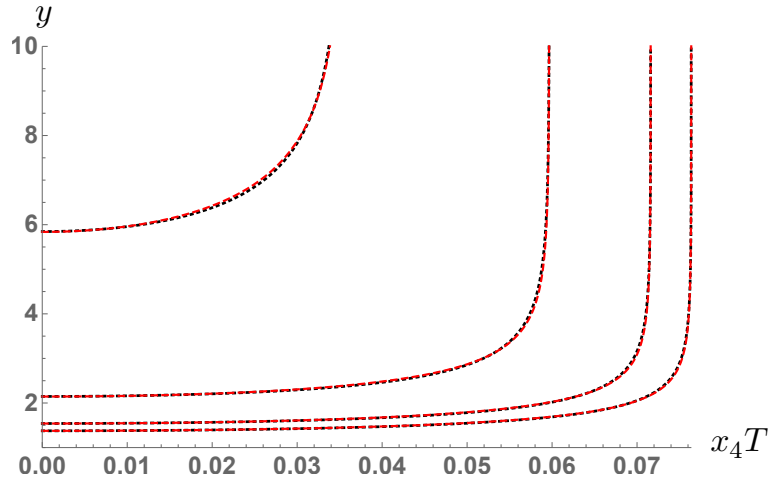
Figure 4.8. *Comparison of the numerical profiles (red dashed lines) with the variational profiles (black dotted lines) for four cases: $\tilde{L} = 0.64$, $\tilde{L} = 0.6$, $\tilde{L} = 0.5$ and $\tilde{L} = 0.3$. The lines are hardly distinguishable, showing that the variational profile is a very good approximation to the exact profile.*

We can use (4.3.4), (4.3.5) together with

$$\rho = \sigma \, u_T^{-1/2} R^{3/2} = \sigma \frac{3}{4\pi T} \, , \tag{4.3.19}$$

in order to extract all the dimensionful factors from the integral. In terms of quantities of the dual field theory (2.1.8), we find

$$S_{DBI} = \frac{N T^3 \lambda_{YM}^3}{486 M_{KK}^3} \, \tilde{S} \, , \tag{4.3.20}$$

where

$$\tilde{S} = \int \int \sigma^2 y^{5/2} \sqrt{1 + (y^3 - 1)(\partial_y x)^2 + (\partial_\sigma x)^2} d\sigma dy \, . \tag{4.3.21}$$

Once extracted the factor written in (4.3.20), the renormalized on-shell action is

$$\Delta \tilde{S} = 2 \int_0^\infty d\sigma \, \sigma^2 \left(\int_{y_J(\sigma)}^\infty y^{5/2} \left[\sqrt{1 + (y^3 - 1)(\partial_y x)^2 + (\partial_\sigma x)^2} - 1 \right] dy + \right.$$

$$\left. - \frac{2}{7} (y_J(\sigma)^{7/2} - 1) \right) \, , \tag{4.3.22}$$

where we have subtracted the straight brane-antibrane pair. We can derive the Euler-Lagrange equation for $x(y, \sigma)$ from the Lagrangian density,

$$\partial_y \left(\frac{\sigma^2 y^{5/2} (y^3 - 1)(\partial_y x)}{\sqrt{1 + (y^3 - 1)(\partial_y x)^2 + (\partial_\sigma x)^2}} \right) + \partial_\sigma \left(\frac{\sigma^2 y^{5/2} (\partial_\sigma x)}{\sqrt{1 + (y^3 - 1)(\partial_y x)^2 + (\partial_\sigma x)^2}} \right) = 0 \, . \tag{4.3.23}$$

Numerically solving (4.3.23) is a daunting task, due to the non-linear nature of the partial differential equation. A much simpler possibility is to look for approximate solutions by using a reasonable variational ansatz. Taking into account the discussion of the previous section, the natural choice is to promote the y_J and B constants in (4.3.15) to functions of σ, namely

$$x = \frac{\tilde{L}}{2} \tanh\left(\frac{\sqrt{y - y_J(\sigma)}}{\sqrt{B(\sigma)}}\right) . \qquad (4.3.24)$$

We will use a further simplification, assuming that the bounce is a straight line in the y_J, B plane. This simplifies the computations because there is only one function of one variable that is unknown. Take

$$
\begin{aligned}
y_J(\sigma) &= y_{J,tv} - (y_{J,tv} - 1)\alpha(\sigma) , \\
B(\sigma) &= B_{tv}(1 - \alpha(\sigma)) ,
\end{aligned}
\qquad (4.3.25)
$$

where the tv labels mean "true vacuum". This true vacuum corresponds to $\alpha(\sigma) = 0$ and the false vacuum to $\alpha(\sigma) = 1$. Therefore, we insert (4.3.24), (4.3.25) into (4.3.22), derive the Euler-Lagrange equation for $\alpha(\sigma)$ and, in analogy with [25], look for the solution that satisfies $\alpha'(0) = 0$ and $\lim_{\sigma\to\infty} \alpha(\sigma) = 1$. The idea is simple but the procedure is somewhat tricky, so we explain it here in some detail. First, we change variables in order to have fixed limits in the integrals,

$$z = \frac{y - y_J(\sigma)}{B(\sigma)} . \qquad (4.3.26)$$

The Lagrangian can be expressed as

$$\mathcal{L} = \int_0^\infty F \, dz + G , \qquad (4.3.27)$$

where

$$
\begin{aligned}
F &= 2\sigma^2 B(\sigma)(B(\sigma)z + y_J(\sigma))^{5/2}\left(\sqrt{1 + (y^3 - 1)(\partial_y x)^2 + (\partial_\sigma x)^2} - 1\right) , \\
G &= -\frac{4}{7}\sigma^2\left(y_J(\sigma)^{7/2} - 1\right) .
\end{aligned}
\qquad (4.3.28)
$$

Notice that, once $\tilde{L}$ is fixed, $y_{J,tv}$ and B_{tv} can be computed as detailed in section 4.3.1. Then F is a function of $z, \sigma, \alpha(\sigma), \alpha'(\sigma)$ and G is a function of $\sigma, \alpha(\sigma)$. Thus, $\partial_{\alpha'(\sigma)}\mathcal{L} = \int_0^\infty \partial_{\alpha'(\sigma)}F \, dz$ and we can write

$$\frac{d}{d\sigma}\left[\partial_{\alpha'(\sigma)}\mathcal{L}\right] \equiv \int_0^\infty H \, dz + \alpha''(\sigma)\int_0^\infty J \, dz , \qquad (4.3.29)$$

where H and J depend on $z, \sigma, \alpha(\sigma), \alpha'(\sigma)$ but not on $\alpha''(\sigma)$. Then, the Euler-Lagrange equation for $\alpha(\sigma)$ yields

$$\alpha''(\sigma) = \left(\int_0^\infty J \, dz\right)^{-1}\left[-\int_0^\infty H \, dz + \int_0^\infty \left(\frac{\partial F}{\partial\alpha(\sigma)}\right) dz + \left(\frac{\partial G}{\partial\alpha(\sigma)}\right)\right] .$$
$$(4.3.30)$$

Having this explicit expression for $\alpha''(\sigma)$, we set up a standard explicit fourth-order Runge-Kutta integration method for the ordinary differential equation. The initial conditions are provided near the center,

$$\alpha(0) = \alpha_0 \ , \qquad \alpha'(0) = 0 \ . \tag{4.3.31}$$

The goal is to determine $\alpha_0 \in (0, 1)$ in order to have $\lim_{\sigma \to \infty} \alpha(\sigma) = 1$. It turns out that if α_0 is chosen to be too small, $\alpha(\sigma)$ becomes larger than 1 at some value of σ and it subsequently acquires an imaginary part. On the other hand, if α_0 is chosen to be too large, $\alpha(\sigma)$ eventually starts decreasing without reaching 1. Taking these observations into account, we set up a shooting method to determine the sought value of α_0. Once the profiles are known, we can compute the value of $\Delta\tilde{S}$ by inserting them in (4.3.22). Figure 4.9 presents some numerical results for the variational function $\alpha(\sigma)$, its value at the center of the bubble α_0, the on-shell action of the bounce solution and the radius of the bubble. In particular, the dimensionless radius $\tilde{R}$ is defined as the value of σ for which α is halfway between its value at the center and its value in the false vacuum, namely $\alpha(\tilde{R}) = (\alpha_0 + 1)/2$. For illustrative purposes, we depict in figure 4.10 two examples of the brane profiles $x(y, \sigma)$ for bounce solutions.

It is useful to have some analytic approximation for the functions $\Delta\tilde{S}(\tilde{L})$, $\tilde{R}(\tilde{L})$. We propose the following expressions, that match quite precisely the numerical results:[12]

$$\Delta\tilde{S} \approx \begin{cases} 0.555\tilde{L}^5 & (\tilde{L} \leq 0.31) \\ 4.61 \times 10^{-6} \exp(18.8\tilde{L}) & (0.31 \leq \tilde{L} \leq 0.57) \\ \frac{0.000467}{(0.6442 - \tilde{L})^2} + \frac{0.00937}{0.6442 - \tilde{L}} & (\tilde{L} \geq 0.57) \end{cases} \tag{4.3.32}$$

$$\tilde{R} \approx \begin{cases} 1.081\tilde{L} & (\tilde{L} \leq 0.2) \\ 0.0777 \exp(5.11\tilde{L}) & (0.2 \leq \tilde{L} \leq 0.55) \\ \frac{0.0872}{(0.6442 - \tilde{L})} + 0.369 & (\tilde{L} \geq 0.55) \end{cases} \tag{4.3.33}$$

$O(4)$-symmetric bubbles

When the radius of the bubble is much smaller than the inverse of the temperature, one expects to have bubbles with $O(4)$-symmetry in the Euclidean spacetime [26, 27]. However, the blackening factor $f_T(u)$ in (2.6.2) breaks the $O(4)$-symmetry and an ansatz of the form $x_4(u, \rho)$ where ρ is a radial coordinate in the $t - x_i$ four-dimensional space is not consistent with the equations of motion. Still, it is natural to expect bubble solutions with non-trivial behavior along the time coordinate, for instance with an ansatz of the type $x_4(u, \rho, t)$. Solving the

---

[12]For values of $\tilde{L}$ near 0.6442, the numerics becomes very delicate and we have not been able to obtain reliable results for $\tilde{L} > 0.63$. However, we assume in (4.3.32), (4.3.33) that $\Delta\tilde{S}$ diverges as $(0.6442 - \tilde{L})^2$ and $\tilde{R}$ as $(0.6442 - \tilde{L})$, as it should be expected from a thin wall approximation similar to [25], and find good agreement.
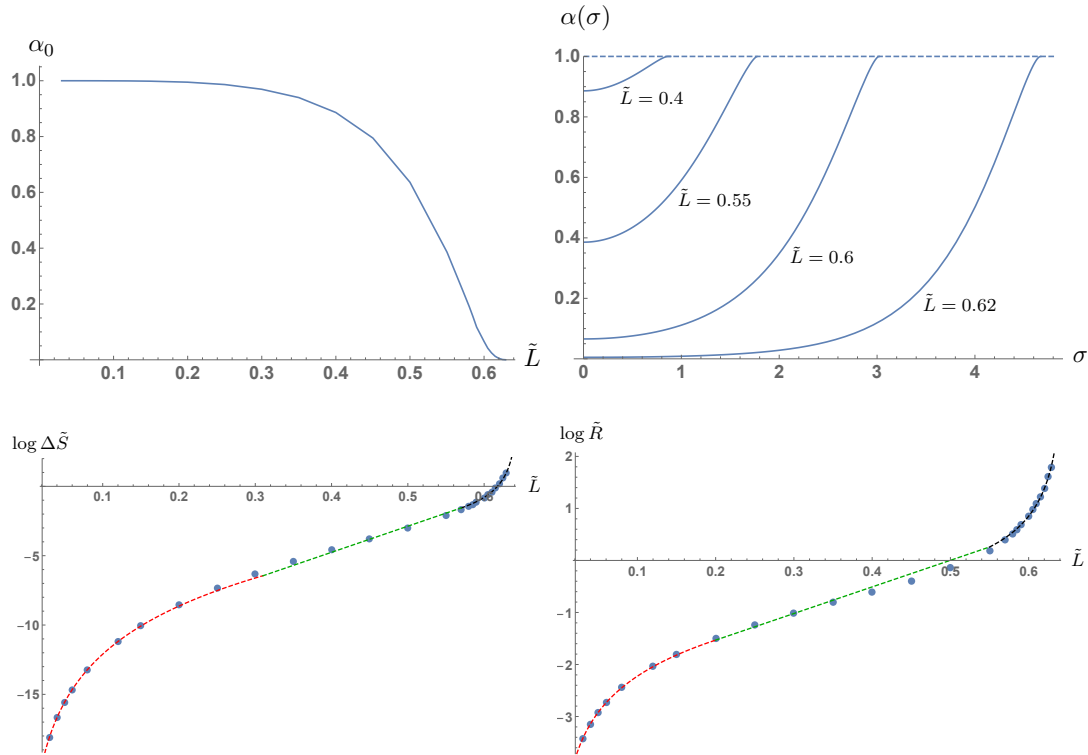
Figure 4.9. *On the top left, we depict the values of α_0 in the variational approximation to the bounce solution as a function of $\tilde{L}$. Notice that $\alpha_0 \to 0$ for $\tilde{L} \to 0.6442$ and the interior of the bubble is very close to the true vacuum. On the other hand $\alpha_0 \to 1$ as $\tilde{L} \to 0$. On the top right, we depict the numerically found profiles for four values of $\tilde{L}$. On the bottom, we depict the on-shell action and the radius of the $O(3)$-bubble as a function of $\tilde{L}$ in a semilogarithmic scale. The dots represent numerically computed data and the dashed lines correspond to the analytic approximation given in eqs. (4.3.32) and (4.3.33). Different colors correspond to different expressions of the piecewise functions.*

problem with this ansatz, either integrating the exact equation or with a reliable approximation seems extremely difficult and is beyond the scope of the present work. Nevertheless, we can get an order of magnitude estimate by considering a "naive $O(4)$ configuration" in which we just neglect the $O(4)$ breaking due to the blackening factor.[13] As discussed in section 4.2.3, we do this by simply considering the measure d^4x to be given by $d\Omega_3 d\rho \rho^3$, where $d\Omega_3$ is the measure of the three-sphere. By changing accordingly (4.3.22) and (4.3.28), we can follow the steps explained in the previous section and find the following approximate

---

[13]Notice that the results will produce an underestimation of the action since the presence of the blackening factor tends to increase it.
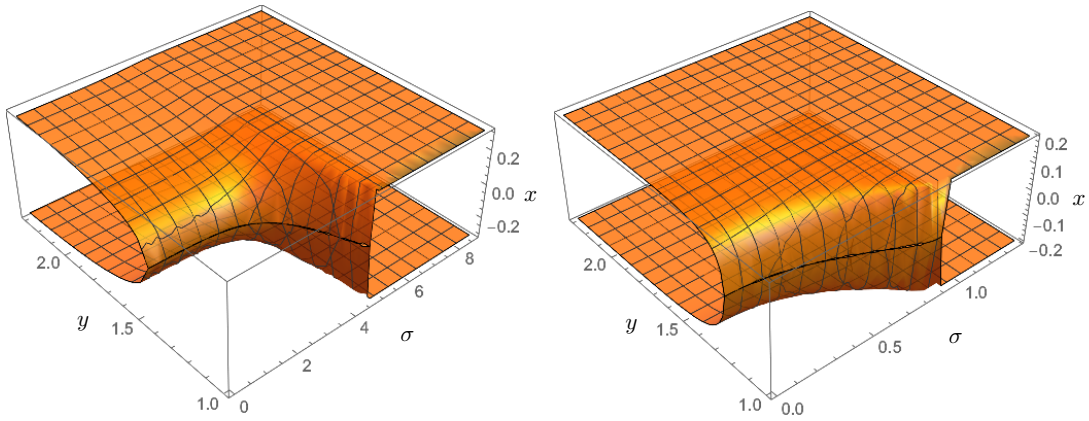
Figure 4.10. *Plots for the bounce profile $x(y, \sigma)$ in two cases: $\tilde{L} = 0.62$ (left) and $\tilde{L} = 0.4$ (right). The configurations smoothly interpolate between U-shaped profiles at $\sigma = 0$ and disconnected branes at $\sigma \to \infty$. The solution on the left can be regarded as a thin wall bubble: a U-shaped configuration very close to the true vacuum exists for a finite range of σ which then rapidly evolves into the false vacuum. On the other hand, the embedding on the right can be considered as a thick wall configuration.*

expression for the on-shell action:

$$\Delta\tilde{S} \approx \begin{cases} 0.638\tilde{L}^6 & (\tilde{L} \leq 0.22) \\ 3.91 \times 10^{-7}\exp(23.8\tilde{L}) & (0.22 \leq \tilde{L} \leq 0.54) \\ \frac{0.0000432}{(0.6442 - \tilde{L})^3} + \frac{0.00118}{(0.6442 - \tilde{L})^2} & (\tilde{L} \geq 0.54) \end{cases} \tag{4.3.34}$$

We can also study the radius of the bubble. Defining $\tilde{R}$ as above, we find the approximate expressions

$$\tilde{R} \approx \begin{cases} 1.34\tilde{L} & (\tilde{L} \leq 0.21) \\ 0.101\exp(4.89\tilde{L}) & (0.21 \leq \tilde{L} \leq 0.49) \\ \frac{0.151}{(0.6442 - \tilde{L})} + 0.131 & (\tilde{L} \geq 0.49) \end{cases} \tag{4.3.35}$$

Figure 4.11 depicts some numerical results compared to their fits given in eqs. (4.3.34), (4.3.35).

It is important to recall that the $O(4)$ configuration could start playing a role only if the bubble radius is smaller than the radius of the time circle. It is easy to verify that this condition can be satisfied only for $\tilde{L} \lesssim 0.386$.
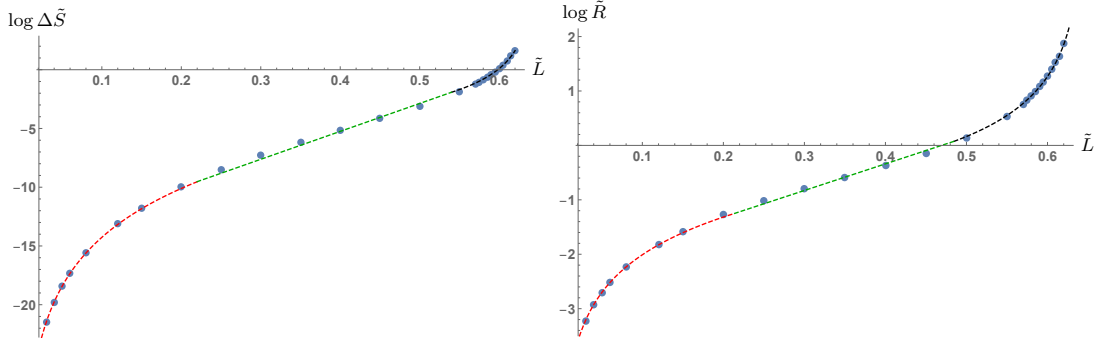
Figure 4.11. *The on-shell action and the radius of the $O(4)$-bubble as a function of $\tilde{L}$ in a semilogarithmic scale. The dots represent numerically computed data and the dashed lines correspond to the analytic approximation given in eqs. (4.3.34) and (4.3.35). Different colors correspond to different expressions of the piecewise functions.*

4.3.3 Bubble nucleation rate

In principle, the rates for the bubble nucleations are provided by formula (4.2.32)

$$
\begin{aligned}
\Gamma &= \mathrm{Max}\left[T^4\left(\frac{S_{3,B}}{2\pi T}\right)^{3/2} e^{-S_{3,B}/T}, \left(\frac{S_{4,B}}{2\pi \rho_w^2}\right)^2 e^{-S_{4,B}} \right] \\
&= M_{KK}^4 \mathrm{Max}\left[\left(\frac{\tilde{T}\bar{f}_\chi^{2/3}}{0.35\lambda_{YM}^{1/3} N^{1/3}}\right)^4 \left(\frac{S_{3,B}}{2\pi T}\right)^{3/2} e^{-S_{3,B}/T}, \left(\frac{S_{4,B}}{2\pi \bar{\rho}_w^2}\right)^2 e^{-S_{4,B}} \right],
\end{aligned}
$$

where we have introduced the dimensionless quantities

$$
\tilde{T} \equiv \frac{TL}{0.1538} \simeq 0.35(\lambda_{YM}N)^{1/3}\frac{T}{M_{KK}^{1/3} f_\chi^{2/3}} , \tag{4.3.36a}
$$

$$
\bar{f}_\chi \equiv \frac{f_\chi}{M_{KK}} , \qquad \bar{\rho}_w \equiv \rho_w M_{KK} \simeq 0.35(\lambda_{YM}N)^{1/3}\frac{3\tilde{R}}{4\pi\tilde{T}\bar{f}_\chi^{2/3}} , \tag{4.3.36b}
$$

so that the critical temperature for the chiral symmetry breaking transition corresponds to $\tilde{T} = 1$ and the chiral symmetry breaking scale is given, as a function of the asymptotic brane separation L, by [43, 107]

$$
f_\chi^2 \simeq 0.1534\frac{\lambda_{YM}N}{32\pi^3}\frac{1}{M_{KK}L^3} . \tag{4.3.37}
$$

As we have outlined before, the symmetries of the black hole background do not allow for (simple) $O(4)$ solutions, so that the analysis of the previous subsection can, at best, be considered as providing a rough estimate of some limiting value of the corresponding bounce action. Hence, here, we will just focus on the $O(3)$ bounce.

The rate for the $O(3)$ bubble depends on three distinct parameters: λ_{YM}, N and $\bar{f}_\chi$. Its behavior when these parameters are separately varied is shown
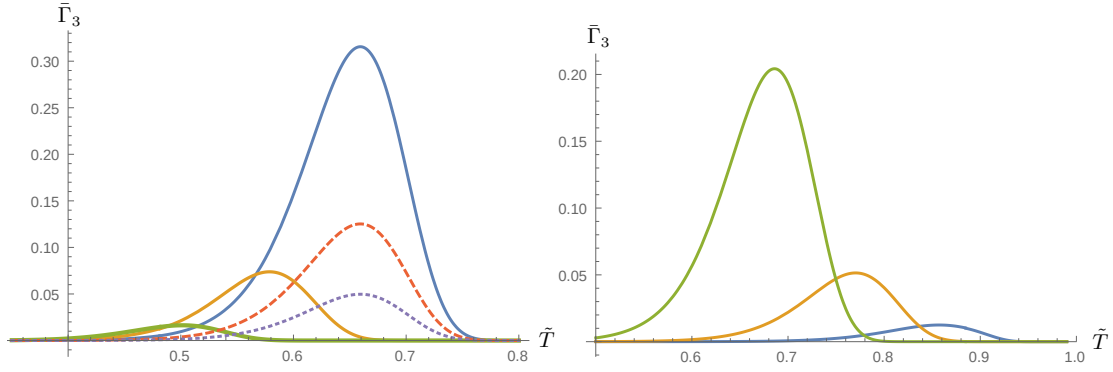
Figure 4.12. *Plots of $\bar{\Gamma}_3 \equiv \Gamma_3/M_{KK}^4$ for different values of parameters. On the left, the rate magnitude is quenched as N is increased (solid blue, dashed and dotted lines correspond to $N = 10, 20, 40$ with $\lambda_{YM} = 10, \bar{f}_\chi = 10$) and as λ_{YM} is increased (solid blue, orange, green lines correspond to $\lambda_{YM} = 10, 20, 40$ with $N = 10, \bar{f}_\chi = 10$). On the right, the magnitude increases as $\bar{f}_\chi$ is increased (blue, orange and green lines correspond to $\bar{f}_\chi = 2, 4, 8$ with $\lambda_{YM} = 10, N = 10$).*

in figure 4.12. Increasing λ_{YM} both quenches the rate and shifts the peak to smaller temperatures while increasing N has essentially only a quenching effect. Instead, the rate magnitude is enhanced if the chiral symmetry breaking scale $\bar{f}_\chi$ is increased, while the peak is shifted to smaller temperatures.

4.4   Semi-analytical estimates

In this section, we provide some analytical estimates of the bounce action, of the radius of the bubbles and of the vacuum decay rate related to the confinement/deconfinement phase transition. We adopt the two standard thick and thin wall approximations.

4.4.1   The $O(4)$ bubble

We follow the procedure discussed in [134]. Let us assume that the nucleation temperature is much smaller than T_c. In such a regime, if the bubble radius is smaller than $1/(2\pi T)$, the system has $O(4)$ symmetry and its physics can be captured by the thick wall approximation. We recall that, in our setup, the Euclidean action with $O(4)$ symmetry reads

$$S_4(\Phi) = \frac{8\pi^4 g}{3^5} \int_0^\infty d\bar{\rho}\, \bar{\rho}^3 \left[a\, \Phi'^2 + \Theta(\Phi)V_c(\Phi) + \Theta(-\Phi)V_d(\Phi) \right] \,, \qquad (4.4.1)$$

where

$$a = 5 - \frac{\pi}{2\sqrt{3}} \qquad (4.4.2)$$

and

$$
\begin{aligned}
V_c(\Phi) &= \frac{16\pi^2}{9}\left(5\Phi^3 - \frac{3}{\pi}\Phi^{5/2}\right) , \\
V_d(\Phi) &= -\frac{16\pi^2}{9}\left(5\Phi^3 + \frac{3}{\pi}\bar{T}(-\Phi)^{5/2}\right) .
\end{aligned}
\tag{4.4.3}
$$

Let us consider a bubble of true vacuum and (dimensionless) radius $\bar{\rho}_w$ nucleated in the false vacuum. What we need is the on-shell value of the action S_4 on the bounce solution, or, more precisely, the difference between the latter and the action computed on the false vacuum,

$$
S_{4,B} = S_4(\Phi_B) - \frac{8\pi^4 g}{3^5}\int_0^\infty d\bar{\rho}\,\bar{\rho}^3 V_d(\Phi_d) .
\tag{4.4.4}
$$

More explicitly, it reads

$$
S_{4,B} = \frac{8\pi^4 g}{3^5}\left[\int_0^\infty d\bar{\rho}\,\bar{\rho}^3[a\,\Phi_B'^2 - V_d(\Phi_d)] + \int_0^{\bar{\rho}_w} d\bar{\rho}\,\bar{\rho}^3 V_c(\Phi_B) + \int_{\bar{\rho}_w}^\infty d\bar{\rho}\,\bar{\rho}^3 V_d(\Phi_B)\right] .
\tag{4.4.5}
$$

If $\bar{\rho}_w \to \infty$, we can approximate the above expression as

$$
S_{4,B} \approx \frac{8\pi^4 g}{3^5}\int_0^\infty d\bar{\rho}\,\bar{\rho}^3\left[a\,\Phi_B'^2 + V_c(\Phi_B) - V_d(\Phi_d)\right] .
\tag{4.4.6}
$$

Just as in [134], let us roughly estimate this action as

$$
S_{4,B} \approx \frac{8\pi^4 g}{3^5}\left[\bar{\rho}_w^3 a\left(\frac{\delta\Phi_B}{\delta\bar{\rho}_w}\right)^2 \delta\bar{\rho}_w + \frac{1}{4}\left(V_c(\Phi_0) - V_d(\Phi_d)\right)\bar{\rho}_w^4\right] ,
\tag{4.4.7}
$$

where $\delta\Phi_B = \Phi_B(0) - \Phi_B(\infty) = \Phi_0 - \Phi_d$. In the thick wall approximation

$$
\delta\bar{\rho}_w \approx \bar{\rho}_w ,
\tag{4.4.8}
$$

so that, extremizing (4.4.7) w.r.t. $\bar{\rho}_w$ we find the critical bubble radius squared

$$
\bar{\rho}_w^2 \approx -\frac{2a(\delta\Phi_B)^2}{[V_c(\Phi_0) - V_d(\Phi_d)]} .
\tag{4.4.9}
$$

Now, numerical analysis shows that $\Phi_0 \approx c_0\bar{T}^2$ at small $\bar{T}$ so that

$$
\delta\Phi_B = \Phi_0 - \Phi_d \approx \left(c_0 + \frac{1}{4\pi^2}\right)\bar{T}^2
\tag{4.4.10}
$$

and

$$
V_c(\Phi_0) - V_d(\Phi_d) = \frac{16\pi^2}{9}\left(5\Phi_0^3 - \frac{3}{\pi}\Phi_0^{5/2}\right) + \frac{\bar{T}^6}{36\pi^4} \approx -\frac{16\pi}{3}c_0^{5/2}\bar{T}^5 .
\tag{4.4.11}
$$

Hence, from (4.4.9), we get

$$\bar{\rho}_w^2 \approx \frac{3a}{16\pi c_0^{5/2}} \left(c_0 + \frac{1}{4\pi^2} \right)^2 \frac{1}{\bar{T}} \equiv \frac{b^2}{\bar{T}} \ . \tag{4.4.12}$$

Thus, the bubble radius goes like $\bar{\rho}_w \sim \bar{T}^{-1/2}$ when $\bar{T} \ll 1$: this relation qualitatively reproduces what we have obtained numerically in the small $\bar{T}$ regime.

Recalling that $\bar{\rho} \equiv M_{KK}\rho$ and $M_{KK}\bar{T} = 2\pi T$, the above results imply that the dimensionful bubble radius in the small temperature regime scales like

$$\rho_w \approx \frac{b}{\sqrt{2\pi\, T\, M_{KK}}} \ . \tag{4.4.13}$$

An important question regarding our holographic model is whether in the limit of small enough bubble radius a $O(5)$ symmetric bubble should be used instead of the $O(4)$ symmetric one. This should be unavoidable if the bubble radius turns out to be smaller than $1/(2\pi T)$ (the length of the radius of the time circle) and, at the same time, smaller than $1/M_{KK}$ (the length of the radius of the x_4 circle). Let us study whether these two conditions are mutually compatible in the regime where the approximations used since now hold. The first condition implies

$$\rho_w \ll \frac{1}{2\pi T} \quad \text{hence} \quad T \ll \frac{M_{KK}}{2\pi b^2} \ , \tag{4.4.14}$$

while the second one implies

$$\rho_w \ll \frac{1}{M_{KK}} \quad \text{hence} \quad T \gg b^2 \frac{M_{KK}}{2\pi} \ . \tag{4.4.15}$$

At least parametrically, the two above conditions are not mutually compatible. Hence we argue that in the regime of parameters where the bubble is $O(4)$ symmetric, an $O(5)$ configuration cannot be consistent. The very same considerations can be done for the directions along the four-sphere of the background.

Let us now try to see whether, in the thick wall approximation, it is possible to deduce some qualitative information about the nucleation rate. For this aim, it is enough to notice that the action (4.4.7) at the critical radius (4.4.9) reads

$$S_{4,B} \approx -\frac{2\pi^4 g}{3^5} \bar{\rho}_w^4 [V_c(\Phi_0) - V_d(\Phi_d)] \approx c_4\, g\, \bar{T}^3 \ . \tag{4.4.16}$$

From the fit of numerical data and the previous relations we get

$$c_4 \approx 0.39 \ , \qquad b \approx 6.6 \ . \tag{4.4.17}$$

The nucleation rate is given by

$$\Gamma_4 = M_{KK}^4 \frac{c_4^2}{(2\pi)^2\, b^4} g^2 \bar{T}^8 e^{-c_4\, g\, \bar{T}^3} \ . \tag{4.4.18}$$

4.4.2 The $O(3)$ bubble

As explained in section 4.2.3, the radius of the $O(4)$ bubble is much smaller than the dimensionless parameter $1/\bar{T}$ only for very small $\bar{T}$, i.e. $\bar{T} \lesssim 0.06$. Hence the use of the $O(4)$ symmetric bounce for larger values of $\bar{T}$ is questionable and it should be replaced by the $O(3)$ symmetric one.

The $O(3)$ bounce arises as a solution of the action $S = S_3(T)/T$ where S_3 is the Euclidean action with $O(3)$ symmetry,

$$\frac{S_3(\Phi)}{T} = \frac{32\pi^4 g}{3^5 \bar{T}} \int_0^\infty d\bar{\rho}\bar{\rho}^2 \left[a\Phi'^2 + \Theta(\Phi)V_c(\Phi) + \Theta(-\Phi)V_d(\Phi) \right] \ . \quad (4.4.19)$$

As already mentioned, we need the difference between the on-shell action on the bounce solution and the action evaluated on the false vacuum configuration,

$$\frac{S_{3,B}}{T} = \frac{S_3(\Phi_B)}{T} - \frac{32\pi^4 g}{3^5 \bar{T}} \int_0^\infty d\bar{\rho}\, \bar{\rho}^2 V_d(\Phi_d) \ . \quad (4.4.20)$$

Explicitly,

$$\frac{S_{3,B}}{T} = \frac{32\pi^4 g}{3^5 \bar{T}} \left[\int_0^\infty d\bar{\rho}\, \bar{\rho}^2 [a\, \Phi_B'^2 - V_d(\Phi_d)] + \right.$$
$$\left. + \int_0^{\bar{\rho}_w} d\bar{\rho}\, \bar{\rho}^2 V_c(\Phi_B) + \int_{\bar{\rho}_w}^\infty d\bar{\rho}\, \bar{\rho}^2 V_d(\Phi_B) \right] \ . \quad (4.4.21)$$

Small temperatures

It is worth to consider the case in which for some range of values of $\bar{T} \ll 1$ the $O(3)$ configuration is the relevant one. In this case, we could try to use the thick wall approximation.

In this approximation, following the same steps described in the previous subsection and using the fact that $\Phi_0 \sim \bar{T}^2$ for small $\bar{T}$, we find the dimensionless bubble radius

$$\bar{\rho}_w^2 \approx -\frac{a(\delta\Phi_B)^2}{[V_c(\Phi_0) - V_d(\Phi_d)]} \approx \frac{\tilde{b}^2}{\bar{T}} \ , \quad (4.4.22)$$

for some constant $\tilde{b}$. The action at the critical radius above reads

$$\frac{S_{3,B}}{T} \approx -\frac{64\pi^4 g}{3^6 \bar{T}}[V_c(\Phi_0) - V_d(\Phi_d)]\bar{\rho}_w^3 \approx c_3\, g\, \bar{T}^{5/2} \ . \quad (4.4.23)$$

The S_4 action is parametrically smaller than S_3/T. From the fit of numerical data and the previous relations we get

$$c_3 \approx 0.32 \ , \qquad \tilde{b} \approx 9.3 \ . \quad (4.4.24)$$

When the $O(3)$ configuration dominates, the nucleation rate is given by

$$\Gamma_3 = M_{KK}^4 \frac{c_3^{3/2}}{(2\pi)^{11/2}} g^{3/2} \bar{T}^{31/4} e^{-c_3\, g\, \bar{T}^{5/2}} \ . \quad (4.4.25)$$

Large temperatures

At large enough temperatures, the $O(3)$ configuration is definitely the dominant one. We can try to get some intuition about its physical properties using the thin wall approximation, which is expected to be valid around T_c, i.e. in the $\bar{T} \to 1$ limit [25]. In the thin wall approximation, the bounce action can be estimated as

$$\frac{S_{3,B}}{T} \approx \frac{32\pi^4 g}{3^5 \bar{T}} \left[\frac{\bar{\rho}_w^3}{3} \Delta V + \bar{\rho}_w^2 S_1 \right] , \qquad (4.4.26)$$

where $S_1 \approx S_1(T_c)$ is the bubble surface tension

$$S_1 = 2\sqrt{a} \int_{\Phi_d}^{\Phi_c} d\Phi \sqrt{\frac{16\pi^2}{9} \left(5|\Phi|^3 - \frac{3}{\pi} |\Phi|^{5/2} \right) + \frac{1}{36\pi^4}} \approx 0.0023 , \qquad (4.4.27)$$

and

$$\Delta V = V_c(\Phi_c) - V_d(\Phi_d) = -\frac{1}{36\pi^4}(1 - \bar{T}^6) . \qquad (4.4.28)$$

Extremizing the action above, we get the critical bubble radius

$$\bar{\rho}_w \approx -\frac{2S_1}{\Delta V} \approx \frac{16}{1 - \bar{T}^6} . \qquad (4.4.29)$$

This is increasing for $\bar{T} \to 1$, in qualitative agreement with our numerical results.

In the $\bar{T} \to 1$ limit, the action (4.4.26) at the critical radius (4.4.29) goes like

$$\frac{S_{3,B}}{T} \approx \frac{\tilde{c}_3 g}{\bar{T}(1 - \bar{T}^6)^2} , \qquad \tilde{c}_3 \approx 2.6 , \qquad (4.4.30)$$

so that in the same limit the nucleation rate (4.4.25) goes as

$$\Gamma_3 \approx \frac{M_{KK}^4}{(2\pi)^4} \frac{\tilde{c}_3^{3/2}}{(2\pi)^{3/2}} \frac{g^{3/2}}{\bar{T}^{3/2}(1 - \bar{T}^6)^3} e^{-\frac{\tilde{c}_3 g}{\bar{T}(1 - \bar{T}^6)^2}} . \qquad (4.4.31)$$

Chapter 5

Dark Holograms and Gravitational Waves

The measurement of the first direct gravitational wave (GW) signal by LIGO in 2015 [18] has started a new era in observational astrophysics. Not only the observation of black hole and neutron star mergers are tremendously important discoveries, but current and future experiments are now expected to be able to measure GW signals from several different sources. This promises to give experimental access to physics which would be challenging to investigate with other types of observations. Not surprisingly, there are currently several experiments in the developing phase, which will considerably extend the accessible GW frequency and sensitivity ranges in the near future. In this situation, it is of clear interest to study possible sources of GWs which could be detected in these facilities.

In this chapter, based on [129], we consider stochastic GW spectra produced in first-order cosmological phase transitions. As we mentioned at the beginning of chapter 4, these observables allow us to investigate beyond-Standard-Model physics. The generation of GWs in first-order phase transitions is determined by the dynamics of bubbles of true vacuum nucleated in the metastable phase once the temperature of the Universe descends below the phase transition temperature [25–27, 131, 132]. The bubbles can generate GWs either by their collisions or by their interaction with the plasma medium, through sound waves or turbulence. We refer to [19–22] for reviews.

It is a challenging task to connect the qualitative picture of the bubble dynamics to solid predictions for the power spectra of GWs that can be observed in experimental devices. Luckily, there are general formulae in the literature that estimate the GW spectra once some parameters characterizing the phase transition are known. These parameters depend on the details of the microscopic model describing the transition. The evaluation of the parameters and the formulae for the spectra typically rely on a series of controlled and less controlled approximations. It is a crucial goal to reduce to zero the number of uncontrolled approximations such that the theoretical predictions can be reliably tested in experiments.

In this chapter, we make a step in this direction for cosmological transitions in sectors described by strongly-coupled Yang-Mills or QCD-like theories. The latter appear in many dark matter models (see, e.g., [17, 28, 153]). We consider scenarios where the dark matter is constituted e.g. by dark glueballs, pions or baryons.

Whenever the theory is confining, one expects a confinement/deconfinement transition as the Universe cools below the theory's dynamical scale. If the transition is first order, it may generate GWs.

When the gauge theory includes (approximately) massless quarks, the strongly-coupled dynamics is such that the (approximate) chiral symmetry is broken at a scale that might or might not coincide with the gauge theory's dynamical scale. We consider both the case in which the confinement phase transition implies the chiral symmetry phase transition and the case in which it does not. The first case also includes the Peccei-Quinn transition in the simplest composite axion model with hidden gauge group [13, 47, 108]. The second case includes the Peccei-Quinn first-order phase transition of the holographic axion model [107, 112] analyzed in chapter 3, where the axion appears as a pseudo-Nambu-Goldstone boson associated with the chiral symmetry breaking of an extra pair of quark/antiquark fields.

In particular, we study these scenarios by utilizing the WSS model. In most of the cases, we use it not as a proxy for QCD but as a model for a dark sector. Being a so-called top-down model, the WSS has the advantage that computations performed in the planar limit at strong coupling are reliable, in the sense that there is a precise control on the validity regime of the various approximations, something which usually does not occur in effective phenomenological models or bottom-up holographic theories. In fact, this property eliminates one of the sources of uncertainty in the calculation of the parameters for the GWs spectra when dealing with strongly-coupled theories, and it constitutes the main motivation for [129].

In chapter 4, we addressed the problem of the nucleation of bubbles of true vacuum associated with both the confinement/deconfinement phase transition and the chiral symmetry breaking/restoration phase transition in the WSS model.

In this chapter, we use those results to compute the stochastic GW spectra, due to bubble collisions and sound waves, in several beyond Standard Model scenarios featuring the WSS model. As we will see, the main conclusion of our analysis is that there is a large window of the WSS parameter space where the GW signals may be accessible in near-future experiments. Moreover, the model allows for the generation of GWs compatible with the possible observation recently reported by NANOGrav [49].

The chapter is organized as follows. In section 5.1, we summarize the steps of the analysis needed to find the GW spectra. In section 5.2, we consider three different dark matter scenarios. These are cases where the chiral symmetry transition, if present, is implied by the confinement one. In subsection 5.2.4, we discuss the results for the GW spectra. Figure 5.1 encodes in a global view some

benchmark results of the investigation.

In section 5.3, we consider two scenarios where GWs come from the chiral symmetry breaking/restoration phase transition. In one of them, the chiral transition is followed by a separated confinement/deconfinement one. We thus investigate the fascinating possibility of detecting a GW spectrum with two peaks. In this case, moreover, we outline the fact that the usual assumption of adiabatic expansion of the Universe from the first phase transition to present times cannot be used anymore: the presence of a second phase transition requires a refinement of the usual redshift factors in the formulae for the GW spectra. The results for the GW spectra are reported in subsection 5.3.3 and in figure 5.4.

Appendix 5.A provides an overview of all of the relevant formulae used to obtain the GW spectra. In particular, in 5.A.1, we discuss how the occurrence of two separated phase transitions affects the quantities that determine the GW spectra, providing explicit formulae for the modified redshift factors advocated in section 5.3.

5.1 The WSS model in cosmology

In this section, we describe the features of the Witten-Sakai-Sugimoto model and the general framework needed to calculate the GW spectra, also fixing our notation. We leave most of the technical details, which are quite standard, to appendix 5.A, for the benefit of the reader who is not familiar with this type of computations.

Let us start with the WSS model's phase diagram. As we discussed in chapter 4, it exhibits two first-order phase transitions. The first one separates the low-temperature confined phase of the theory from the high-temperature deconfined one. The critical temperature for the transition is [43]

$$T_c = \frac{M_{KK}}{2\pi} \ .$$

(5.1.1)

The second first-order phase transition separates the chirally symmetric phase from the phase where chiral symmetry is broken [43]. In the general case, L, the distance of the branes from the antibranes along $S^1_{x_4}$, is a free parameter that can be used to separate the confinement scale from the chiral symmetry breaking one, as seen in chapter 3. When $L > 0.97 M_{KK}^{-1}$ the confinement/deconfinement transition implies the chiral symmetry breaking/restoration one. In contrast, when $L < 0.97 M_{KK}^{-1}$, the two transitions are independent, with the chiral symmetry breaking/restoration one occurring at the temperature

$$T_c^\chi \approx \frac{0.1538}{L} \ .$$

(5.1.2)

To summarize,

- If $T < \frac{M_{KK}}{2\pi}$, the theory is confining and chiral symmetry is broken;

- If $T > \frac{M_{KK}}{2\pi}$, the theory is deconfined and:

    - if $T < \frac{0.1538}{L}$, chiral symmetry is broken;
    - if $T > \frac{0.1538}{L}$, chiral symmetry is preserved.

We will consider a cosmological setting where the Universe starts at some high temperature, in which the WSS is in the deconfined phase, and then cools down. Depending on the scenario that we consider, the WSS sector will undergo one or two first-order phase transitions. They are triggered by the nucleation of bubbles of *true* vacuum (confined phase or chirally broken phase, depending on the transition) in the plasma, which is in the metastable *false* vacuum (deconfined or chirally symmetric). These bubbles will expand and eventually fill all the Universe, leaving it in the true vacuum state. The *percolation* temperature T_p is defined as the temperature of the Universe when this process completes. We will compute it case by case, using the formulae discussed in appendix 5.A.1.

The cosmological evolution of the Universe is described, as usual, by the Friedmann-Lemaitre-Robertson-Walker (FLRW) metric[1]

$$ds^2 = -dt^2 + R(t)^2 dx^i dx^i \ , \tag{5.1.3}$$

where $R(t)$ is the cosmic scale which defines the Hubble scale $H(t) = \dot{R}(t)/R(t)$. The latter is determined by the total energy density through the Friedmann equation

$$H^2 = \frac{\rho}{3M_{Pl}^2} \ , \tag{5.1.4}$$

with $M_{Pl} \approx 2.4 \cdot 10^{18}$ GeV. The energy density ρ takes contributions from the Standard Model and from the dark sector.

In the sector described by the WSS model, the energy density in the deconfined and in the confined phase at order $\mathcal{O}(N^2)$ can be derived from (2.6.15) and (2.6.16) and reads, respectively,

$$\rho_{rad,glue} \ = \ 5\frac{2^6\pi^4}{3^7}\lambda_{YM}N^2\frac{T^6}{M_{KK}^2} \ . \tag{5.1.5a}$$

$$\rho_{conf,glue} = -\rho_{0,glue} \ = \ -\frac{1}{3^7\pi^2}\lambda_{YM}N^2M_{KK}^4 \ . \tag{5.1.5b}$$

In the limit

$$\epsilon_f \equiv \frac{1}{12\pi^3}\lambda_{YM}^2\frac{N_f}{N} \ll 1 \ , \tag{5.1.6}$$

the contribution of N_f quarks to the energy density in the high-temperature regime and in the low-temperature one at order $\mathcal{O}(N_f N)$, in the case $L = \pi M_{KK}^{-1}$,

---

[1]The WSS model features extra dimensions. The cosmic scale factor is meant to be present just in front of the spatial three-dimensional space.

read (see e.g. [154, 155])

$$\rho_{rad,\chi} = \frac{2^6\pi^2}{7\cdot 3^7}\lambda_{YM}^3 N_f N\frac{T^7}{M_{KK}^3} \ , \tag{5.1.7a}$$

$$\rho_{conf,\chi} = -\rho_{0,\chi} = -\frac{1}{7\cdot 3^7\pi^{7/2}\Gamma\left(-\frac{2}{3}\right)\Gamma\left(\frac{1}{6}\right)}\lambda_{YM}^3 N_f N M_{KK}^4 \ . \tag{5.1.7b}$$

As mentioned above, when $L \ll \pi M_{KK}^{-1}$, there is an intermediate phase where the gauge theory is deconfined and the quarks are condensed. In this case, the energy density is not known analytically. However, it can be computed numerically starting from the energy density of the chirally-unbroken configurations. In particular, it reads,

$$\rho_{b,\chi} = \rho_{rad,\chi} + (1 - T\partial_T)(TP\Delta\tilde{S}) \ , \tag{5.1.8a}$$

where $\Delta\tilde{S}$ is defined in (4.3.22) and

$$TP = \frac{2^3\pi^2}{3^8}\lambda_{YM}^3 N\frac{T^7}{M_{KK}^3} \ . \tag{5.1.8b}$$

In fact, $TP\Delta\tilde{S}$ gives exactly the difference of free energies of the flavors in the broken and unbroken phases. Using the fact that the energy is the derivative of the free energy w.r.t. the temperature, the second term on the r.h.s. of the first relation (5.1.8) is the difference of the energies in the two phases, so that adding the known contribution of the unbroken phase, one is left with that of the broken phase. As we will comment on in section 5.3.2, the energy density of condensed quarks with $L = \pi M_{KK}^{-1}$ in the confined phase will always be subleading and can be neglected.

From (5.1.5) and (5.1.7), we see that the confined phase of the WSS model carries a temperature-independent contribution to the energy, which would act as a cosmological constant after the phase transition. Since the measured cosmological constant almost vanishes, the zero-point energy has to be shifted accordingly. As a result, the energy density in the deconfined and chirally symmetric phase reads[2]

$$\rho_{unbroken}^{deconf} = \rho_{rad,glue} + \rho_{rad,SM} + \rho_{rad,\chi} + \rho_{0,glue} + \rho_{0,\chi} \ , \tag{5.1.9}$$

where

$$\rho_{rad,SM} = \frac{\pi^2}{30}g_*^{SM}(T)\frac{T^4}{\xi^4} \tag{5.1.10}$$

is the Standard Model contribution, given by the temperature-dependent number of relativistic degrees of freedom g_*^{SM}. The factor

$$\xi \equiv \frac{T}{T_V} \ , \tag{5.1.11}$$

---

[2]In the most general case, we have quarks of both $L = \pi M_{KK}^{-1}$ and $L \ll \pi M_{KK}^{-1}$ kind. Hence, the contribution $\rho_{0,\chi}$ is not simply given by (5.1.7b), because the latter holds only for the $L = \pi M_{KK}^{-1}$. The $L \ll \pi M_{KK}^{-1}$ contribution is suppressed by a $M_{KK}/f_{\chi,L}$ factor and can be usually neglected.

is defined as the ratio between the temperature T of the dark sector and that of the Standard Model T_V. As we will see, ξ can (and in some cases must) be different from 1.

The energy density in the deconfined and chirally broken phase reads

$$\rho_{broken}^{deconf} = \rho_{rad,glue} + \rho_{rad,SM} + \rho_{b,\chi} + \rho_{0,glue} \; , \qquad (5.1.12)$$

whereas in the confined and chirally broken phase it is

$$\rho_{broken}^{conf} = \frac{\pi^2}{30} \left(g_*^{SM}(T) \frac{T^4}{\xi^4} + g_*(T) T^4 \right) \; , \qquad (5.1.13)$$

where $g_*(T)$ accounts for possible contributions of relativistic particles from the dark sector.

We will investigate several scenarios where (5.1.9), (5.1.12) and (5.1.13) will be used. The cases will differ for the values of the parameters N_f, N, λ_{YM}, and the number of degrees of freedom involved.

Away from the phase transitions, the universe evolves adiabatically, i.e. according to the conservation of the entropy

$$S \sim R^3 g_*^S(T) T^3 \; , \qquad (5.1.14)$$

where, in general, $g_*^S(T) \neq g_*(T)$, see appendix 5.A.1. During the phase transition, an amount of energy is released and the plasma gets heated up. The temperature T_R of the plasma at the end of the transition is called *reheating* temperature and is found via the conservation of energy. This point will play an important role in section 5.3, where we will consider the case in which the universe undergoes two first-order phase transitions. As we will see, the presence of the second phase transition modifies the redshift of the GW signal compared to the adiabatic evolution one, usually assumed to be valid after the single phase transition.

As we detail in appendix 5.A, the efficiency of the phase transition depends on the ratio Γ/H^4, where Γ is the bubble nucleation rate. In the case in which a single field describes the transition, the bubble nucleation rate Γ can be computed in the semiclassical approximation using the formalism developed in [25–27,131,132]. The confining phase transition of the WSS model involves several fields. In chapter 4, based on [101], we took an effective approach inspired by [46] where only a single field is involved. The formula for the bubble nucleation rate is reported in (5.A.1), which involves a comparison between the efficiency of quantum and thermal fluctuations. The former are given by the $O(4)$-symmetric solution, and the latter by the $O(3)$-symmetric one. In the analysis, we always have to verify which kind of bubble dominates.

Depending on the phase transition's efficiency, the universe may remain trapped in the false vacuum for a long time after it reaches the critical temperature, featuring supercooling. In this case, the energy density may include a temperature-independent contribution, which may start to dominate, acting as

an effective cosmological constant that makes the universe inflate.[3] As a result, it is not guaranteed that the phase transition completes, hence in the analysis, we will always have to check that it actually does. Technically, this is done through formula (5.A.21) discussed in appendix 5.A. Depending on whether percolation enters the vacuum-dominated phase or not, the percolation temperature is computed, respectively, by (5.A.13) or (5.A.16). In performing these and the following calculations, we use the Chapman-Jouguet formula (5.A.25) for the velocity of the bubble.[4]

Gravitational waves are produced during the propagation of nucleated bubbles in the plasma in three ways: collisions among bubbles, collisions of plasma sound waves, and turbulence in the plasma. Unfortunately, the turbulence contribution to the gravitational waves spectra is currently not well-understood. Typically it is deemed as subdominant. We will only consider the contributions coming from bubble collision and from the sound waves for these reasons. The formulae for the spectra in these two cases are given, respectively, by (5.A.39) and (5.A.40).

As we discuss in appendix 5.A, it is not easy to estimate how the energy is distributed among the various contributions. Comprehension of the bubble dynamics and, most importantly, interaction with the plasma is one of the major open problems in the field so that the results are affected by huge incertitudes. For this reason, in this chapter, the results for the spectra are presented separately for the bubble collision and sound waves contributions, pretending that all of the energy is concentrated in one of them in turn. The true spectra will obviously be in between these two "extremal" cases.

The GW spectrum depends crucially on a parameter, usually called α, which accounts for the amount of energy released in the transition. We are going to use its expression in terms of the trace of the energy-momentum tensor (formula (5.A.24)), adjusting in any place the number of relativistic d.o.f. at the relevant temperature scale.[5] As we will see, the spectrum with a larger magnitude is that associated with sound waves.

In the next two sections, we present the analysis in the various scenarios. From the WSS model perspective, the main difference among them is given by the choice of the parameters M_{KK}, $f_{\chi,L}$, N_f, N, and λ_{YM}. Actually, for what concerns the next section, the latter two enter through the combination

$$g \equiv \lambda_{YM} N^2 \ . \tag{5.1.15}$$

As a general framework, although both N and λ_{YM} are required to be large parameters, it is natural not to introduce a huge hierarchy of scales. Thus, we tend to prefer (but not limit ourselves) to consider not-too-large values of the parameter g, starting from $g \gtrsim 100$.

---

[3]We recall, indeed, that the radiation and the vacuum contributions to the energy density scale, respectively, as $R(t)^{-4}$ and $R(t)^0$.

[4]The friction with the plasma puts some upper bound on the velocity (see, e.g., [156]). In our cases, an estimate of these upper bounds along the lines of [143] turns out to be always larger than the velocity calculated with (5.A.25).

[5]Table I in [157] turns out to be a useful tool for this task.

5.2   GWs from deconfinement phase transition

In this section, we present the GW spectra produced in three possible dark scenarios, which we name *Dark HQCD 1*, *Dark glueballs* and *Dark axion*. The "H" in HQCD stands for "Holographic", to underline the fact that there are extra modes w.r.t. standard QCD-like theories. In these scenarios, gravitational waves are always associated with the confinement/deconfinement phase transition. It is important to outline that the WSS model realizes explicitly, in a specific regime of parameters, scenarios which have been previously proposed in the literature (see e.g. [158] and [17, 28, 153] for reviews). Even though it would be very interesting to further study the phenomenological implications of this regime of parameters, in this thesis we just concentrate on the gravitational waves spectra. Thus, in the following subsections we are going to sketch the different scenarios, discussing the main information needed for the computation of the GW spectra. The latter are determined with the formulae collected in appendix 5.A and the results are presented in subsection 5.2.4.

5.2.1   Dark HQCD 1

QCD-like theories with N_f flavors can provide different dark matter candidates. Depending on the details of the models, the main fraction of dark matter can come from dark baryons, nuclei, mesons, and so on. Analogously, the dynamically generated scale, which in the WSS model is denoted as M_{KK}, varies considerably among the various theories, typically from about 100 MeV to about 100 TeV. In this subsection we consider the WSS model with N_f flavors, in the regime

$$N \gg 1 \ , \qquad \lambda_{YM} \gg 1 \ , \qquad \frac{N_f}{N} \ll 1 \ , \qquad (5.2.1)$$

as providing a strongly-correlated large N dark QCD-like sector. Previous studies of gravitational wave spectra in similar scenarios include [159–164].

We have analyzed the spectra of GW produced in the phase transition for the dynamical scale values

$$M_{KK} = 10^n \text{ GeV} \ , \qquad n = -1, 0, ..., 6 \ , \qquad (5.2.2)$$

and for

$$g = 10^m \ , \qquad m = 2, 3, 6, 10 \ . \qquad (5.2.3)$$

The case $g = 10^2$ is the only one where the Universe at the time of bubble percolation is in a radiation domination phase, hence we employ formula (5.A.16) to determine the percolation temperature; in all the other cases, the Universe is in a vacuum domination era and we have to employ formula (5.A.13). For $g = 10^{2,3,6}$, the relevant bounce solution is the $O(3)$-symmetric one, while for $g = 10^{10}$ the $O(4)$-symmetric configuration dominates.

In determining the reheating temperature according to formula (5.A.23), care must be taken to count the correct number of degrees of freedom both in the

Standard Model and in the dark sector. In fact, in the confined phase of the dark sector there can be glueballs, KK-modes and mesons which become relativistic at the reheating temperature. This happens for $g = 10^6$ and $g = 10^{10}$. In the first case, only the lightest glueball and KK mode must be included, together with the lightest mesons. In contrast, in the second case, the reheating temperature is about seven times M_{KK}. At this scale, many glueballs from Table 2 in [88] as well as many mesons must be included, giving hundreds of d.o.f. Unfortunately, the spectrum of KK modes is not known in detail. The first KK modes have mass of one M_{KK}, but we have no definite information on the number of degrees of freedom at $7M_{KK}$. We give a very rough estimate of this number assuming that the density of KK modes has the same dependence on the energy as the spectrum of glueballs. We then double the number of degrees of freedom to account for the fermionic glueballs and KK modes. The same is done for the mesons. However, we underline that the incertitude associated to the number of degrees of freedom introduces an error that does not spoil the order of magnitude of our results.

5.2.2 Dark Glueballs

Another well-motivated class of dark matter candidates is represented by stable glueballs, the bound states of $SU(N)$ Yang-Mills theory. The WSS model with $N_f = 0$ is therefore suitable for describing such a scenario and for performing in this context reliable calculations. Being derived in the quenched approximation, the results of section 5.2.1 can be seen as also concerning a scenario where the non-interacting dark sector is constituted by a $SU(N)$ Yang-Mills theory without flavors.

The latter can also model the case where the dark matter is actually self-interacting, a possibility which helps softening the problems of the ΛCDM model with small-scale structures [165]. In this scenario, phenomenology can be satisfied for glueball masses ranging from keV to fraction of GeV. When the order of the latter is around one MeV or smaller, one has to take care of phenomenological constraints related to the effective number of neutrino species and coming from Cosmic Microwave Background (CMB) measurements, and from measurements of the relative abundance of elements in Big Bang Nucleosynthesis (BBN). They imply that the dark sector cannot be in thermal equilibrium with the visible sector. In particular, the dark sector temperature T has to be smaller than T_V, the visible sector one [166, 167]. As a result, non-gravitational couplings among the two sectors have to be absent or extremely small. Whenever this is the case, gravitational waves produced in first-order transitions can be one of the few means at our disposal in order to observe direct signals coming from the dark sector. Previous studies of the GW spectra in similar cases within the context of simple effective models can be found in [166, 167].

In this section we will investigate cases with dynamical scale values

$$M_{KK} = 10^n \, \text{keV} \, , \qquad n = 0, 1, 2, 3, 4 \, . \tag{5.2.4}$$

The other main difference with respect to the analysis performed in section 5.2.1

is given by the fact that the ratio $\xi = T/T_V$ can be smaller than one. We assume that ξ stays constant during the bubble nucleation and GW observation process. We explicitly explore benchmark cases where

$$\xi = 10^{-1} \ , \qquad g = 10^{3,5,10} \ . \tag{5.2.5}$$

Moreover, we have considered the case where $M_{KK} = 100$ keV, $g = 5 \cdot 10^3$ and $\xi = 0.1$. We have also checked that the smaller the value of ξ is, the more the signal is suppressed. For $\xi = 10^{-5}$, for example, the signal will be completely invisible in near-future facilities.

We estimate the constraints from the CMB and the BBN on the number of relativistic degrees of freedom by parameterizing them as an extra contribution to the effective number of neutrino species ΔN_{eff} [166]. The constraint from the BBN, which turns out to be the most stringent one, dictates that $\Delta N_{eff} \lesssim 0.5$. We use the formula [166]

$$\Delta N_{eff} = \frac{4}{7} \left(\frac{11}{4} \right)^{4/3} g_* \, \xi^4 \ . \tag{5.2.6}$$

The constraint has to be imposed around $T_{V,BBN} \sim 100$ keV. Whenever the percolation temperature is such that the dark sector is in the confining regime at $T_{V,BBN}$, g_* just counts the number of relativistic glueballs and the constraint is automatically satisfied for our range of parameters because of the ξ factor in (5.2.6). If instead the dark sector is in the deconfined phase at $T_{V,BBN}$, the relevant formula for g_* is, from the energy density of section 5.1,

$$g_* = \frac{5^2 \cdot 2^7 \pi^2}{3^6} g \frac{T^2}{M_{KK}^2} \ . \tag{5.2.7}$$

In this case large values of g can overcome the ξ^4 suppression in (5.2.6). In fact, for $g = 10^{10}$ the constraint from the BBN is never satisfied in the range of energies (5.2.4), and it restricts the allowed regimes to $M_{KK} \geq 100$ keV for $g = 10^3$ (and for $g = 5 \cdot 10^3$), $M_{KK} \geq 1$ MeV for $g = 10^5$.

Let us briefly describe the main features of the spectra. The decoupling of the dark and visible sectors implies that whenever we consider plasma effects, the plasma in question is just the one of the dark sector. As a consequence, there are two relevant α parameters (formula (5.A.26)), denoted as α and α_D, measuring respectively the energy released in the transition w.r.t. the *visible* sector energy density only and w.r.t. the *dark* sector energy density only. The velocity of the bubble wall is determined by formula (5.A.25) with α replaced by α_D. The same is true for the efficiency parameter κ_v (formula (5.A.41)) for the sound wave spectra.

For $g = 10^3$ (and $g = 5 \cdot 10^3$), in all the cases the Universe is found to be in a radiation domination era at the time of percolation. In fact, values of $\xi < 1$ enhance the contribution of the SM energy density of radiation against the dark sector vacuum energy density. The bubbles in these cases have $O(3)$

symmetry. Only for the cases of $g = 10^{5,10}, \xi = 10^{-1}$ the Universe is in a vacuum domination era, the percolation temperature is very small due to supercooling and $O(3)$ ($O(4)$) bubbles dominate for $g = 10^5$ ($g = 10^{10}$). Moreover, in the cases of $g = 10^3, \xi = 10^{-5}$ and $g = 10^{10}, \xi = 10^{-1}$ the reheating temperature is considerably different from T_p, so that we have to consider many glueball and KK modes from the dark sector. However, due to the damping factor ξ, the contribution of the dark degrees of freedom is quite suppressed w.r.t. the contribution of the SM particles.

5.2.3 Dark Axion

In this section, we analyze a third range of dark sector dynamical scales, relevant for composite QCD axion models. The benchmark model is the one discussed in [108] building on the model in [13] (see also [47], and [10, 168] for recent reviews).

In its simplest realization, the model comprises a dark $SU(N)$ Yang-Mills sector and four massless flavors in its fundamental representation. Three of them form a triplet of the QCD $SU(3)_c$ gauge group, whereas the fourth constitutes a singlet. The global symmetry includes an axial $U(1)_A$, which plays the role of the Peccei-Quinn symmetry. In fact, the latter is anomalous and spontaneously broken by the flavor condensation due to the strong dynamics of the dark $SU(N)$. The associated pseudo-Nambu-Goldstone boson is then a composite axion. In this scenario, the confinement/deconfinement transition of the dark $SU(N)$ theory implies the Peccei-Quinn phase transition, which is of the first order. Previous studies of GW spectra from Peccei-Quinn transitions in effective theories (possibly of bottom-up Randall-Sundrum type) can be found in [142, 143, 169].

In the model of [13], the axion decay constant f_a is related to f_χ by

$$f_a = \frac{\sqrt{6}}{N} f_\chi \ . \tag{5.2.8}$$

In the WSS model, the decay constant f_χ is given by (2.3.18), so that

$$f_a = \frac{1}{3\pi^2} \sqrt{\frac{\lambda_{YM}}{2N}} M_{KK} \ . \tag{5.2.9}$$

Consistency with phenomenology requires $f_a \gtrsim 10^8$ GeV. Moreover, formula (5.1.6) with $N_f = 4$ gives the constraint

$$\lambda_{YM} \lesssim 3\sqrt{N} \ , \tag{5.2.10}$$

and therefore we are led to consider dynamical scales $M_{KK} \gtrsim 10^9$ GeV. We will consider two benchmark values of g,

$$g = 10^3 \ , \qquad g = 10^8 \ . \tag{5.2.11}$$

The details of the calculations are very similar to the ones in section 5.2.1. In all the cases, the Universe is in an energy domination era at the time of

percolation. For $g = 10^3$ ($g = 10^8$) the $O(3)$ ($O(4)$) bounce dominates. In order to determine the reheating temperature for $g = 10^8$, we have to take into account glueball, KK and mesonic degrees of freedom.

5.2.4   Results for the spectra

In this section, we describe the results for the GW spectra generated by the first-order confinement/deconfinement transition of the holographic model. As we have already mentioned, we do not consider the contribution from turbulence in the plasma and we separately consider the contributions from bubble collisions and sound waves.

For what concerns the sound waves contribution, there is a further incertitude due to the unknown source duration. Until very recently, the source was expected to last for a long time in Hubble units. Under this assumption, most of the literature has employed the formulae reviewed in [20, 170]. However, it has been recently pointed out that the source can be quite short, see e.g. [21, 171–174]. Accordingly, the power spectrum is quenched by the short time factor (5.A.42). In [129], an agnostic attitude is taken and both spectra, with and without quenching factor, are presented. This allows us to have an idea of the possible range of the signal and to compare the results with previous literature.

In summary, three types of spectra are calculated: the one from bubble collisions Ω_c, the one from sound waves without quenching factor Ω_{sw} and the one from sound waves with quenching factor $\Omega_{sw,q}$. As a general trend, Ω_c is found to give the smallest peak signal. Moreover, the peak frequency increases with M_{KK} and the amplitude of the signal increases with g.

In figure 5.1 we report examples of power spectra. In the plot, a few benchmark values of the parameters M_{KK}, g are chosen to show the detectability potential of the GW emissions. A number of experimental sensitivities are shown for comparison.

The first clear result is that in various cases the GW signals are going to be detectable in near future experiments, with the possible exception of the composite axion model.

Notice that Ω_c and $\Omega_{sw,q}$ approximately span an order of magnitude in power of the signal around the peak, represented in the figure by the regions in between the dashed and continuous curves. Notice, moreover, that the upper value of the signal for the Ω_{sw} spectra (dotted lines) is greatly amplified w.r.t. the quenched case $\Omega_{sw,q}$ (continuous lines); the true signal from sound waves is expected to be in between the two types of lines. The total signal is expected to be a combination of the one from sound waves and the one from collisions.

The blue lines at the left of the plot show a representative case for a small dynamical scale value, $M_{KK} = 100$ keV, relevant for the Dark Glueballs scenario, for $g = 5 \cdot 10^3$ and for the value $\xi = 0.1$ of the ratio between the dark and the visible sector temperatures. It is clear that the signal is potentially detectable by pulsar timing array experiments such as IPTA and SKA. Actually, the most
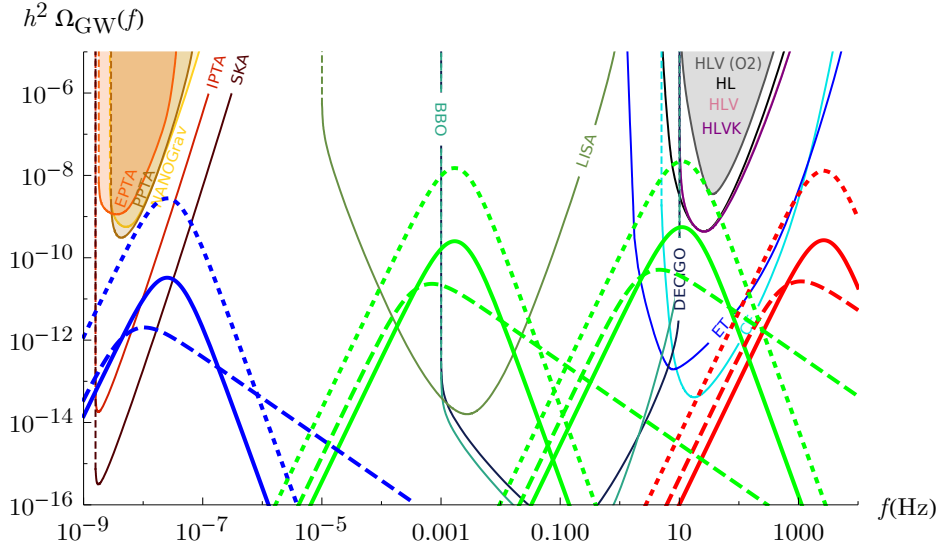
Figure 5.1. *Examples of GW power spectra $h^2\Omega_{GW}$ due to bubble collisions (Ω_c, dashed lines) and sound waves in the case of* short *source duration ($\Omega_{sw,q}$, continuous lines) and long source duration (Ω_{sw}, dotted lines). Expected sensitivities (PLISCs) for a number of experimental facilities are reported for comparison [175]. From left to right, the spectra correspond to the following parameters: $(M_{KK}/\text{GeV}, g) = (10^{-4}, 5 \cdot 10^3)$ (blue lines), $(10^2, 10^6), (10^6, 10^6)$ (green lines), $(10^9, 10^3)$ (red lines).*

"optimistic" scenario where almost all the energy of the process goes into GWs from sound waves is of great experimental interest. In fact, in this case the signal could be visible in current single experiments such as NANOGRAV, EPTA and PTTA. Actually, very recently, the results of 12.5 years observations by NANOGRAV have been reported in [49], showing strong evidence for a stochastic spectrum compatible with GW signals with frequency peak around $10^{-9} - 10^{-8}$ Hz and average energy density $\langle h^2\Omega_{GW}\rangle \sim 10^{-10}$. If, among the possible sources of this signal, there is space for a cosmological strongly first-order phase transition in a dark sector - as it has been recently suggested in [176–178] - our Dark Glueball model could be viewed as a possible candidate.

Although it is not shown in the figure, the same possibility of detection happens if $g = 10^{3,5}$ (again for $\xi = 0.1$) for M_{KK} around $0.1 - 1$ MeV, at least in the SKA experiment.

The two sets of green lines at the center of the plot correspond to the parameter value $g = 10^6$ and energies respectively of $M_{KK} = 10^2$ and $M_{KK} = 10^6$ GeV, relevant for the Dark HQCD 1 scenario. The first case is going to be detectable already by LISA and clearly by the more sensitive experiments such as BBO and DECIGO. The same remains true down to $M_{KK} \sim 10$ GeV and $g \sim 10^2$ (not shown in the plot). The second case of $M_{KK} = 10^6$ GeV is detectable by ET or CE facilities. Of course, all the intermediate energies can be detected, and this remains true even for smaller values of g down to 10^2 and larger values of $M_{KK} \lesssim 10^7$ GeV. For $g = 10^{10}$ the signal is visible at LISA starting from

$M_{KK} \sim 1$ GeV. Thus, a few near future experiments (LISA and ET for example) are going to be able to fully probe strongly coupled dark QCD-like sectors (with large ranks) in the energy range $M_{KK} \sim 1 - 10^7$ GeV.

Finally, the three red lines at the right of the plot correspond to $g = 10^3$ and $M_{KK} = 10^9$ GeV, and are relevant for the Dark Axion scenario with $f_a \sim 10^8$ GeV. Only in the optimistic case in which the duration of the sound waves' source is long, the spectrum falls within the sensitivity curve of CE. Since we expect the real signal to be in the region between the three curves, this case is unlikely to be detectable in near-future experiments. Moreover, if M_{KK} increases, such that $f_a > 10^8$ GeV, the curves are shifted to larger values of the peak frequencies. As a result, the Dark Axion scenario is not favorable for producing detectable gravitational waves.

Figure 5.2 illustrates some of the results, depicting the regions of parameter space that could be explored by five facilities projected for the near future (CE, ET, BBO, DECIGO and LISA). The current capabilities of LIGO and VIRGO are insufficient for detection, although they come quite close for 10^6 GeV $< M_{KK} < 10^7$ GeV and $g > 10^4$ and, therefore, these facilities and KAGRA have been left out of the plot. In the figure, only the dark HQCD 1 and the dark axion scenarios are considered because the dark glueballs model would require introducing the extra parameter ξ. As a benchmark case, we have chosen to make the plot using the predicted spectrum of GWs produced by sound waves, taking into account the suppression factor due to short pulse duration. For the plot, we just consider the spectrum at the frequency f_{det} at which each detector attains its best sensitivity and compare it to $h^2\Omega_{sw}(f_{det})$. This is certainly a simplification which, together with all the approximations and assumptions involved in the derivation of $h^2\Omega_{sw}(f)$, implies that the contours of the figure should be considered only as very rough estimations.

However, the picture that emerges is clear: facilities in the near future should be able to investigate the GW spectrum stemming from large regions of the parameter space of holographic theories with a first-order phase transition in the early Universe. Moreover, in various (optimistic) scenarios, stochastic GW background generated in this type of models can be detectable by the advanced version of currently running experiments. Large M_{KK} is probed by devices that concentrate in large GW frequencies. In fact, the small values of M_{KK} of the dark glueballs scenario can only be observed through pulsar timing arrays, as shown in figure 5.1. The dependence on the coupling of the gauge theory g is only mild, provided that it is large enough for the holographic description to apply.

5.3   GWs from chiral phase transition

In this section, we consider scenarios that display a chiral symmetry breaking/restoration phase transition separated from the eventual confinement one. This implies the fascinating consequence of having two distinct peaks in the spectrum of stochastic GWs. Firstly, we discuss the possible scenarios and then
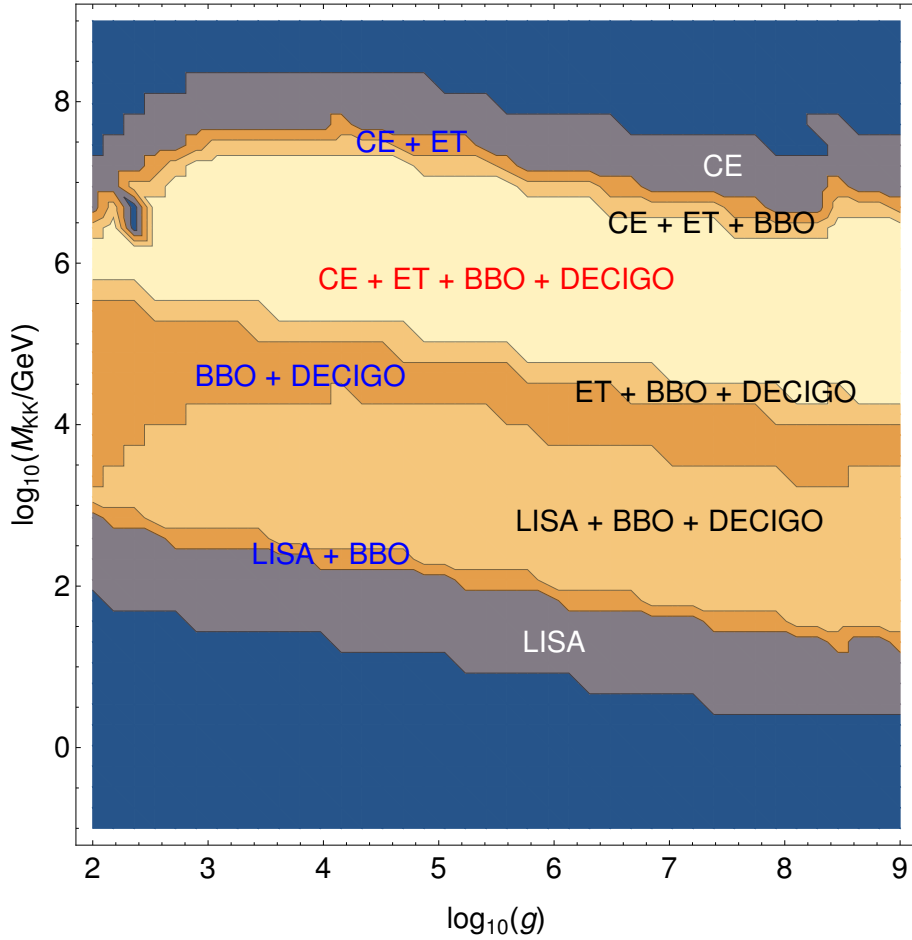
Figure 5.2. *Rough estimate of the possibility of detection in future facilities of GWs produced by holographic first-order confinement phase transitions. The plot explores the parameter space of the dark HQCD 1 and dark axion scenarios and considers GWs produced by sound waves, eq. (5.A.40), including the suppression factor (5.A.42). The color code indicates the number of facilities that could measure the signal for a particular value of the parameters: none (blue), one (grey), two (dark orange), three (light orange) or four (yellow).*

we present the results for the spectra.

5.3.1 Dark HQCD 2

The scenario that we consider in this subsection is a close cousin of the Dark HQCD 1 scenario of subsection 5.2.1: the WSS model describes a dark sector, very weakly interacting with the Standard Model (in the most extreme case, even interacting with the Standard Model only gravitationally). The difference with respect to what has been discussed in section 5.2.1 concerns the choice of the WSS parameter L. In section 5.2.1, the latter was taken to be $L = \pi M_{KK}^{-1}$, corresponding to the chiral symmetry breaking scale f_χ given in (2.3.18). In

contrast, here we will consider cases with $L \ll \pi M_{KK}^{-1}$, for which the chiral symmetry breaking scale $f_{\chi,L}$ is given by (3.1.12). As said, this implies that the chiral phase transition is separated from the confinement one.

An important difference with respect to the scenario of section 5.2.1 is that the evolution of the Universe cannot be considered to be adiabatic from the time of the chiral symmetry breaking transition to the present time, since there is a second first-order phase transition. This calls for a correction of the standard formulae for the redshift of the signal, which are derived under the assumption of adiabatic evolution. In fact, the adiabatic assumption holds from the time of the chiral symmetry breaking transition to the percolation time of the confinement transition. Then, assuming fast reheating in the confinement transition, the temperature has a sudden jump from the percolation temperature to the reheating temperature. Finally, from this time to the present day, the Universe continues to evolve adiabatically. In appendix 5.A.1 this behavior is reflected in formulae (5.A.34), (5.A.35) for the frequency and power spectrum redshifts.

A consequence of these formulae is that the magnitude of the chiral symmetry breaking transition signal decreases if the value of $g = \lambda_{YM} N^2$ increases. This is due to powers of the ratio of the percolation and reheating temperatures of the confining transition, $T_{p,conf}, T_{R,conf}$, appearing in formulae (5.A.34), (5.A.35) (in a coefficient which we have called δ in (5.A.36)). As we semi-analytically estimate in appendix 5.B, an increase of g implies more supercooling, hence $T_{p,conf}$ decreases and at the same time $T_{R,conf}$ increases, resulting in a suppression of the GW signal. For this reason, in the present scenario we are going to describe the case where λ_{YM} and N are such that g has a "*small*" value. In particular, we will investigate the representative case

$$\lambda_{YM} = N = 10 \, , \qquad g = 10^3 \, . \tag{5.3.1}$$

It is convenient to introduce dimensionless quantities,

$$\tilde{f}_\chi \equiv \frac{f_{\chi,L}}{M_{KK}} \, , \qquad \tilde{T} \equiv \frac{TL}{0.1538} \sim 0.35 (\lambda_{YM} N)^{1/3} \frac{T}{M_{KK}^{1/3} f_{\chi,L}^{2/3}} \, , \tag{5.3.2}$$

such that the critical temperature for the chiral symmetry breaking transition corresponds to $\tilde{T} = 1$. The condition that the chiral symmetry breaking transition happens above the deconfinement transition gives the constraint

$$\tilde{f}_\chi > 0.013 \lambda_{YM}^{1/2} N^{1/2} \, , \tag{5.3.3}$$

that with the choice (5.3.1) corresponds to $\tilde{f}_\chi > 0.13$.

In fact, the signal is enhanced if the chiral symmetry breaking scale $\tilde{f}_\chi$ is large. The validity of the quenched approximation we are assuming for the flavors constrains the magnitude of this parameter. In particular, the requirement that the approximation works at the percolation temperature and at the reheating temperature sets the limit $\tilde{f}_\chi \leq 60$ for the choice of parameters (5.3.1). This comes from the requirement that the energy density of the flavors is subleading

with respect to the one of the gluonic degrees of freedom.Thus, we will consider the benchmark values

$$\tilde{f}_\chi = 30 \ , \qquad \tilde{f}_\chi = 60 \ . \tag{5.3.4}$$

A noticeable difference with respect to the cases analyzed in section 5.2 is that the energy released in the transition is much smaller than the energy of radiation, since the former comes from the flavors, which are quenched, while the latter mostly comes from the gluons. As a result, the parameter α is much smaller than one in this case and the bubble velocity sometimes is not very close to unity. Since the energy released in the transition is small as compared to the total energy, we expect the reheating temperature to be close to the percolation temperature.

Regarding the counting of degrees of freedom, in the case at hand, by normalizing the entropy density as

$$s = \frac{2\pi^2}{45} g_*^S T^3 \ , \tag{5.3.5}$$

at the time of emission we have the three contributions from the Standard Model, gluons and flavors

$$g_*^S = g_{*,SM} + g_{*,glue}^S + g_{*,\chi}^S \ , \tag{5.3.6}$$

with [43]

$$g_{*,glue}^S \quad = \quad \frac{5 \cdot 2^6 \pi^2}{3^4} \lambda_{YM} N^2 \frac{T^2}{M_{KK}^2} \ , \tag{5.3.7a}$$

$$g_{*,\chi}^S \quad = \quad \frac{5 \cdot 2^4}{3^6} \lambda_{YM}^3 N_f N \frac{T^3}{M_{KK}^3} \ . \tag{5.3.7b}$$

From the energy density of section 5.1 we read

$$g_* = g_{*,SM} + g_{*,glue} + g_{*,\chi} \ , \tag{5.3.8}$$

with

$$g_{*,glue} \quad = \quad \frac{5^2 \cdot 2^7 \pi^2}{3^6} \lambda_{YM} N^2 \frac{T^2}{M_{KK}^2} \ , \tag{5.3.9a}$$

$$g_{*,\chi} \quad = \quad \frac{5 \cdot 2^7}{7 \cdot 3^6} \lambda_{YM}^3 N_f N \frac{T^3}{M_{KK}^3} \ . \tag{5.3.9b}$$

5.3.2 Holographic Axion

Another scenario where a chiral symmetry breaking/restoration takes place is the holographic QCD axion model of [107], studied in chapter 3, which we call *HoloAxion* in the following. The WSS theory is considered as a model for the strong interactions of the Standard Model, including the QCD axion physics. The axion arises as a composite particle, analogous to the η', coming from an extra flavor with $L \ll \pi M_{KK}^{-1}$ so that it condenses at a large scale $f_a = f_{\chi,L} \gg \Lambda_{QCD}$. In contrast, the SM quarks are embedded in such a way that the related chiral

symmetry breaking scale is given by (3.1.12). The condensation of the axion is a Peccei-Quinn first-order transition which can therefore generate gravitational waves.

The energy density of the false vacuum configuration in this case reads formally as (5.1.9). Let us briefly comment on each contribution. Since the QCD sector of the theory, gluons and quarks, is described by the WSS model, the related relativistic degrees of freedom are not counted in g_*^{SM} (which then has 27.75 as its maximal value) in $\rho_{rad,SM}$. Concerning $\rho_{rad,\chi}$, the number of flavors in (5.1.7a) is $N_f = 7$, because we have six QCD quarks plus an extra flavor that provides the axion. The contribution $\rho_{0,\chi}$ is given by (5.1.7b) with $N_f = 6$, because the latter holds only for the case $L = \pi M_{KK}^{-1}$. The remaining flavor gives a contribution analogous to (5.1.7b) but suppressed by a factor of $M_{KK}/f_{\chi,L}$, hence it can be neglected.

Since in this scenario the WSS model describes the strong sector, the usual, uncontrolled extrapolation of the regime of validity of these formulae to the real world parameter values is performed. This amounts to quitting the planar regime by setting $N = 3$. As mentioned in section 2.3, the parameters λ_{YM} and M_{KK} are determined by fitting the ρ-meson mass and the value of $f_\pi = f_\chi$, giving [37, 95]

$$\lambda_{YM} = 33.26 \ , \qquad M_{KK} = 0.949 \text{ GeV} \ . \qquad (5.3.10)$$

The probe approximation is also dropped in this regime of parameters, as usual in the WSS model. The choice of the parameter L which sets f_a is constrained by the requirement

$$10^8 \text{ GeV} \lesssim f_a \lesssim 10^{17} \text{ GeV} \ . \qquad (5.3.11)$$

coming from axion phenomenological constraints.

5.3.3 Results for the spectra

Let us comment on the behavior of the spectra that we find in the scenarios where a chiral symmetry breaking/restoration transition occurs.

In the Dark HQCD 2 scenario, two separated phase transitions occur and the signal is given by the sum of the signals of the two phase transitions. Since we work in the quenched approximation (5.1.6), the chiral symmetry phase transition is characterized by smaller released energies and therefore smaller signal magnitudes with respect to the confinement/deconfinement one. The peak of the signal of the chiral symmetry transition is at higher frequencies than that due to the confinement/deconfinement transition. Being smaller, the former might be negligible with respect to the tail of the confinement signal and therefore the chiral symmetry phase transition would be effectively unobservable.[6] Since the signals associated to bubble collisions are suppressed with respect to the ones due to sound modes, we discuss only the latter.

---

[6]Indeed, we recall that the formulae for the spectra are affected by the incertitudes mentioned in the introduction, hence a big chiral symmetry signal is needed in order to be significant.

Examples of the signals for different values of the parameters, with and without the correcting factor (5.A.42) for the duration of the transition, are reported in figure 5.3. Clearly, larger values of $\tilde{f}_\chi$ are more effective in separating the peak due to the chiral symmetry transition from that due to confinement.
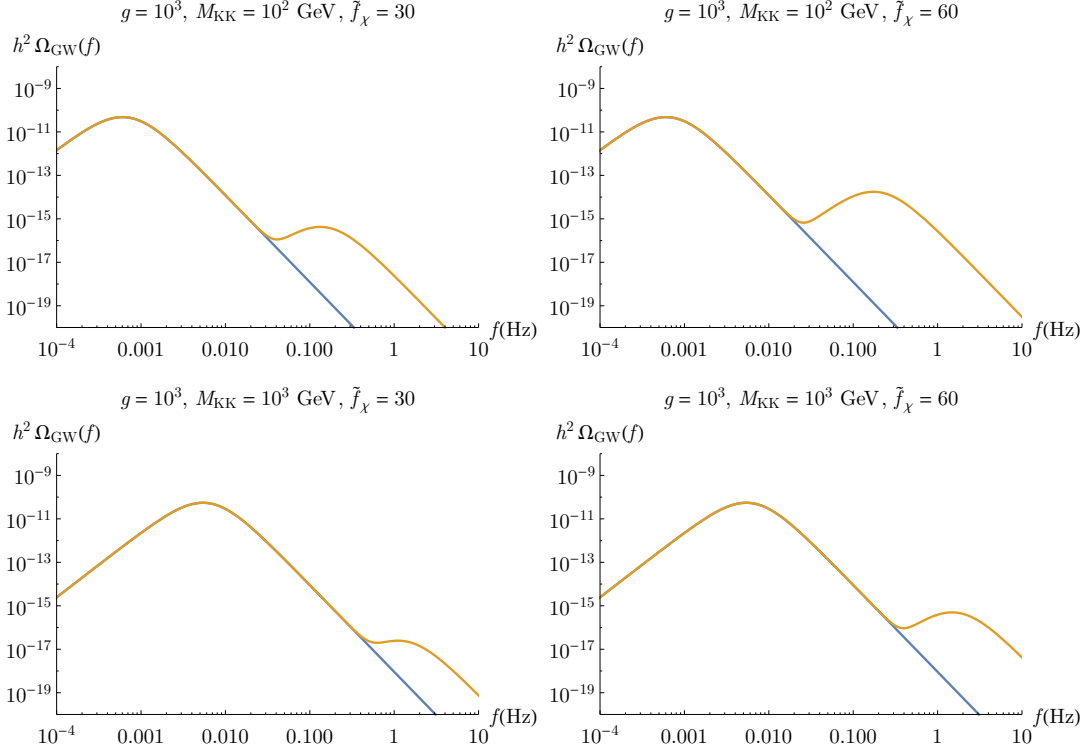

Figure 5.3. *The GW power spectra from the confinement transition (blue lines, sound modes) and from the sum of the confinement and chiral symmetry transitions (orange lines, sound modes), for different values of the parameters. The spectra on the first (second) line are calculated without (with) the correction factor (5.A.42) for the chiral transition.*

Figure 5.4 offers an example of the scenarios that we have been discussing in this section, presenting the comparison of the computed spectra with the sensitivity curves of experiments. The green curves correspond to a representative two-peak case in the Dark HQCD 2 scenario, namely that where $M_{KK} = 100$ GeV and $\tilde{f}_\chi = 60$. It displays a large peak due to the confinement/deconfinement transition at frequency $f \sim 10^{-3}$ Hz which fits into the sensitivity curve of LISA, and a smaller peak due to the chiral symmetry transition at frequency $f \sim 10^{-1}$ Hz which does not fit into the LISA sensitivity curve but is expected to be visible by the next generation facilities such as BBO and DECIGO. The conclusion is that the two-peak signal is certainly within reach of the next generation facilities at least for a certain region of parameter space.

Concerning the HoloAxion case, the result for the extremal case where the axion decay constant takes the lower allowed value $f_a \sim 10^8$ GeV is displayed in red in figure 5.4. The frequencies of the peak of these curves are too large and
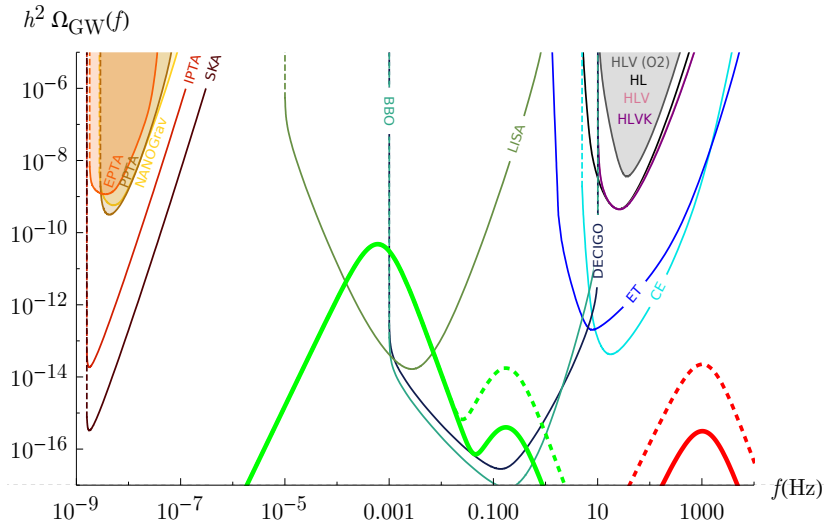
Figure 5.4. *Experimental sensitivity curves (PLISCs from [175]) and examples of theoretical GW power spectra from sound waves. In green, the sum of the signal from the confinement transition with $\lambda_{YM} = N = 10, M_{KK} = 100$ GeV and that from the chiral symmetry transition with $N_f = 1, \tilde{f}_\chi = 60$. In red, the spectra for the HoloAxion case with $f_a \sim 10^8$ GeV. Continuous (dashed) curves correspond to the signal with (without) suppression factor (5.A.42) for the short duration of the chiral transition.*

their magnitudes are too small to be captured by near-future facilities like ET or CE, even in the optimistic case in which we do not include the quenching factor (5.A.42) due the duration of the sound waves. Moreover, as f_a increases, the peak frequencies increase as well, hence going further away from the sensitivity curves of the experiments. Thus, we conclude that the Peccei-Quinn transition in the HoloAxion scenario cannot be seen in near future experiments.

5.A   Calculation of the gravitational wave spectra

In this appendix, we review all the formulae needed to calculate the gravitational wave spectra produced by cosmological first-order phase transitions. The formulae for the spectra are reported in section 5.A.2. They require the knowledge of some crucial parameters which we discuss in section 5.A.1. These are essentially given by the temperature (and hence the related value of the Hubble parameter) at which the phase transition completes, the phase transition duration β^{-1}, computed starting from the bubble nucleation rate Γ, the strength α, i.e., the energy budget of the transition and the bubble wall speed v.

5.A.1 Parameters

Bubble nucleation rate

First-order phase transitions are triggered by the nucleation of true vacuum bubbles on the false vacuum state. Such nucleation can occur through thermal or quantum fluctuations. As we will discuss in the following subsections, whether the transition actually takes place depends on the ratio Γ/H^4, where Γ is the bubble nucleation rate per unit of volume and H is the Hubble scale. The latter is determined by the energy density ρ through the Friedmann equation $H^2 = \rho/3M_{Pl}^2$, where $M_{Pl} \approx 2.4 \cdot 10^{18}$ GeV.

The bubble nucleation rate can be computed using the well-known formalism developed in [25–27] for models where the transition is described by a single field Φ. One has to find a particular solution Φ_B of the Euclidean equation of motion usually called *bounce*. The latter satisfies the following boundary conditions: it approaches the false vacuum Φ_f at Euclidean infinity and a constant Φ_0 at the center of the bubble.[7] When the transition from the false to the true vacuum is due to quantum tunneling, the bounce is $O(4)$ symmetric: in this case Φ_B only depends on the radial coordinate $\rho = \sqrt{t^2 + x_i x_i}$, where t is the Euclidean time and x_i are the space coordinates. When the transition is (mostly) driven by thermal fluctuations, the bounce is $O(3)$ symmetric: in this case $\Phi_B = \Phi_B(\rho)$, with $\rho = \sqrt{x_i x_i}$. The configuration which dominates the process is the one for which the rate Γ has the larger value. As a result, the formula for the bubble nucleation rate reads

$$\Gamma = \text{Max} \left[T^4 \left(\frac{S_{3,B}}{2\pi T} \right)^{3/2} e^{-S_{3,B}/T}, \left(\frac{S_{4,B}}{2\pi \rho_w^2} \right)^2 e^{-S_{4,B}} \right], \qquad (5.A.1)$$

where ρ_w is the size of the $O(4)$ bubble. The bounce action $S_{3,B}$ appearing in (5.A.1) is defined by $S_{3,B}/T = (S_3(\Phi_B) - S_3(\Phi_f))/T$, where $S_3(\Phi)$ is the $O(3)$-symmetric Euclidean action for the scalar field. The action $S_{4,B}$ is defined analogously.

The relevant temperatures

In order to calculate the spectrum of GWs, the first datum to determine is the temperature at which the waves are produced. Since from the time of nucleation, which happens at plasma temperature T_n, to the time where most of the collisions take place and most of the sound waves collide there could be a sizable difference, the percolation temperature T_p is considered to be the relevant one for the production of gravitational waves [21]. In the following, we are going to discuss both T_n and T_p.

---

[7]In [25, 132], it is discussed how this Euclidean solution is meant to represent the bubble at time zero in Minkowskian signature.

Nucleation temperature

The nucleation time t_n is defined as the time at which the total number of nucleated bubbles per Hubble patch from $t = t_c$ (the time when the Universe is at the critical temperature T_c) to $t = t_n$ is order one,

$$\int_{t_c}^{t_n} dt \frac{\Gamma}{H^3} \sim 1 \; , \tag{5.A.2}$$

where $H = \dot{R}(t)/R(t)$ is the Hubble scale. We can write this condition in terms of the temperature of the Universe. Assuming[8] $R(T) \sim T^{-r}$, we have

$$r \frac{dT}{T} = -H dt \; , \tag{5.A.3}$$

and therefore (5.A.2) becomes

$$r \int_{T_n}^{T_c} \frac{dT}{T} \frac{\Gamma}{H^4} \sim 1 \; . \tag{5.A.4}$$

We can get analytical insight by noticing that the integral is dominated by the region very close to T_n. The general form of the nucleation rate is

$$\Gamma(T) = f(T) \exp(-S_B(T)) \; , \tag{5.A.5}$$

where $f(T)$ is a polynomial function, usually assumed to be T^4 by dimensional analysis. Let us write the Taylor expansion of the exponent as

$$S_B(T) \sim S_B(T_n) + (T - T_n) \frac{\tilde{\beta} r}{HT} |_{T_n} \; , \tag{5.A.6}$$

where

$$\tilde{\beta} \equiv -\frac{dS_B}{dt} = \frac{HT}{r} \frac{dS_B}{dT} \; . \tag{5.A.7}$$

Thus, the condition (5.A.4) can be approximately computed as

$$1 \sim r \left(\frac{\Gamma}{H^4 T} \right) |_{T_n} \int_{T_n}^{\infty} dT \, e^{-\left(\frac{\tilde{\beta} r}{HT} \right) |_{T_n} (T - T_n)} \; , \tag{5.A.8}$$

where we extended the integration domain to infinity, and therefore it reads

$$\frac{\Gamma}{H^4} |_{T_n} \sim \frac{\tilde{\beta}}{H} |_{T_n} \; . \tag{5.A.9}$$

---

[8]When the energy density behaves as $\rho \sim g_* T^4$ with a time-independent number of relativistic degrees of freedom g_*, $r = 1$. In general, g_* may depend on the temperature. In the WSS model, in the regime where the contribution from the glue sector dominates, $r = 5/3$.

Percolation temperature

The percolation temperature T_p is defined as the Universe temperature when the fraction of space sitting in the true vacuum takes a benchmark conventional value. We choose the latter to be one.[9] In order to compute the percolation temperature, we have to estimate the size of a bubble as a function of time, which involves the knowledge of the bubble wall speed v. We follow [171]. The fraction of space in the true vacuum reads

$$I(t) = \frac{4\pi}{3} \int_{t_c}^{t} dt' \Gamma(t') R(t')^3 r_b(t,t')^3 \ , \qquad (5.A.10)$$

where $r_b(t,t')$ is the size of the bubble in comoving coordinates as a function of time, which can be obtained by

$$r_b(t,t') = \int_{t'}^{t} \frac{d\tilde{t}\, v}{R(\tilde{t})} \ . \qquad (5.A.11)$$

Here, v is the velocity of the bubble wall. Using $R(T) \sim T^{-r}$ and (5.A.3), we have

$$I(T) = \frac{4\pi r^4}{3} \int_{T}^{T_c} \frac{dT' \Gamma(T')}{H(T') T'^{1+3r}} \left(\int_{T}^{T'} \frac{d\tilde{T}\, v}{H(\tilde{T})\tilde{T}^{1-r}} \right)^3 \ . \qquad (5.A.12)$$

We therefore define the percolation temperature T_p by

$$I(T_p) = 1 \ . \qquad (5.A.13)$$

In the scenarios considered in this thesis, the energy density includes a radiation term and a vacuum term. Adopting the notation of [171], we therefore write $H = H_R + H_V$. Let us consider approximate solutions to (5.A.12). Firstly, let us consider the case in which the vacuum contribution H_V can be neglected. This is expected to give a good approximation when supercooling is not significant. Assuming $H_R = c_R T^s$, and constant velocity v, we obtain

$$I(T) = \frac{4\pi r^4 v^3}{3 c_R^4 (s-r)^3} \int_{T}^{T_c} \frac{dT' \Gamma(T')}{T'^{1+3r+s}} \left(\frac{1}{T^{s-r}} - \frac{1}{T'^{s-r}} \right)^3 \ . \qquad (5.A.14)$$

The formulae of reference [171] are retrieved putting $s = 2$, $r = 1$, and $c_R = (\sqrt{3} M_{Pl} \xi_g)^{-1}$. In the WSS model (see (5.1.5)),

$$s = 3 \ , \qquad r = 5/3 \ , \qquad c_R = \sqrt{5} \frac{2^3 \pi^2}{3^4} \frac{\sqrt{g}}{M_{Pl} M_{KK}} \ . \qquad (5.A.15)$$

Evaluating the integral (5.A.14) as done above for the nucleation temperature, we find an approximate formula for the percolation temperature T_p, which does not depend on the coefficients r and s,

$$\frac{\Gamma}{H^4}|_{T_p} \approx \frac{1}{8\pi v^3} \left(\frac{\tilde{\beta}}{H} \right)^4 |_{T_p} \ . \qquad (5.A.16)$$

---

[9]Another value that is often taken in the literature is 0.34. We have verified that in our cases the gravitational wave spectra are not significantly sensitive to such a difference.

When there is supercooling, the vacuum term H_V may become dominant before percolation. Defining the temperature T_V by $H_R(T_V) = H_V(T_V)$, let us approximate the Hubble scale with

$$H(T) = H_R\Theta(T - T_V) + H_V\Theta(-T + T_V) \ , \tag{5.A.17}$$

where $\Theta(\cdot)$ is the Heaviside step function. In this case, the factor $R(T')r_b(T, T')$ appearing in (5.A.10) takes two contributions, reading

$$R(T')r_b(T, T') = \frac{v}{H_V}\left[1 - \left(\frac{T}{T'}\right)^r\right] \tag{5.A.18}$$

for $T \leq T' \leq T_V$, and

$$R(T')r_b(T, T') = \frac{v}{H_V}\left[\frac{s}{s-r}\left(\frac{T_V}{T'}\right)^r - \frac{r}{s-r}\left(\frac{T_V}{T'}\right)^s - \left(\frac{T}{T'}\right)^r\right] \tag{5.A.19}$$

for $T \leq T_V \leq T'$. As a result, the fraction of volume in the true vacuum takes the form,

$$
\begin{aligned}
I(T) &= \frac{4\pi r v^3}{3H_V^4}\left\{\int_{T_V}^{T_c}\frac{dT'\Gamma(T')}{T'^{1+s}T_V^{-s}}\left[\frac{s}{s-r}\left(\frac{T_V}{T'}\right)^r - \frac{r}{s-r}\left(\frac{T_V}{T'}\right)^s - \left(\frac{T}{T'}\right)^r\right]^3 + \right. \\
&\quad + \left. \int_T^{T_V}\frac{dT'\Gamma(T')}{T'}\left[1 - \left(\frac{T}{T'}\right)^r\right]^3\right\} \ .
\end{aligned}
\tag{5.A.20}
$$

Notice that if $T_p = T_V$, $I(T_p)$ from (5.A.20) precisely reduces to the value computed using (5.A.14). Hence, in general, when $T_p \approx T_V$ we can still use formula (5.A.16) to estimate the percolation temperature. The same conclusion holds in the different limit $T_p \ll T_V \approx T_c$. In all the cases examined in this thesis we have found no notable numerical differences between the percolation temperature computed using formula (5.A.14) and that computed using (5.A.20).

Finally, when the Universe is inflating due to vacuum energy domination, it is not guaranteed that the transition can complete at all, since the bubbles can never percolate with the required velocity. One needs to check explicitly that the probability of finding a fraction of space occupied by the false vacuum, $V_{false} \propto R(t)^3 \exp(-I_{RV})$, is decreasing at the supposed percolation temperature. This translates into the condition

$$\frac{1}{V_{false}}\frac{dV_{false}}{dt} = H(T_p)\left(3 + \frac{T_p}{r}\frac{dI_{RV}(T)}{dT}\Big|_{T_p}\right) < 0 \ . \tag{5.A.21}$$

Once the percolation temperature has been determined, one can derive a crucial parameter for the spectrum

$$\frac{\beta}{H_*} = \frac{1}{H_*\Gamma}\frac{d\Gamma}{dt}\Big|_{T_p} = -\frac{1}{\Gamma}\frac{T}{r}\frac{d\Gamma}{dT}\Big|_{T_p} \ . \tag{5.A.22}$$

Reheating temperature

During a first-order phase transition, entropy is released and therefore the Universe gets heated. Assuming that the entropy release is approximately instantaneous, we define the reheating temperature T_R as the temperature of the Universe after the release. By exploiting the conservation of the energy density during the transition, we find the reheating temperature through the formula

$$\rho_t(T_R) = \rho_f(T_p) \,, \tag{5.A.23}$$

where ρ_f and ρ_t are, respectively, the total energy density in the false and true vacua.

Especially in the case of strong first-order transitions, the reheating temperature may be greater than the critical temperature T_c (see e.g. [134]). In this case, one should check whether the inverse phase transition could take place or not. In our cases, this does not happen essentially because the distance in field space between the two minima of the effective potential at $T = T_R \gg T_c$ is "large" enough to drastically suppress the rate of the inverse transition w.r.t. the Hubble scale.

Released energy and wall velocity

Another crucial parameter for the gravitational wave spectra is the ratio of the energy released in the transition to the energy of the radiation bath [21]. In particular, the formulae for the spectra include the parameter α defined as

$$\alpha = \frac{\Delta\theta}{\rho_{rad}} \,, \tag{5.A.24}$$

where $\theta = (\rho - 3p)/4$ is the trace of the energy-momentum tensor, and the Δ indicates the difference between the false and true vacua.

The knowledge of the parameter α allows us to estimate the velocity of the bubble walls according to the Chapman-Jouguet formula

$$v = \frac{1/\sqrt{3} + \sqrt{\alpha^2 + 2\alpha/3}}{1 + \alpha} \,. \tag{5.A.25}$$

Formula (5.A.25) has a limited range of validity; in particular, it has to be corrected when the friction in the bubble interactions with the plasma is significant. However, to provide better estimates of the wall speed is still one of the big open problems in determining the bubble dynamics.

In the case in which we consider a dark sector that is not in thermal equilibrium with the visible one, we have to define two separated α parameters for the two sectors,

$$\alpha = \frac{\Delta\theta}{\rho_{rad,SM}} \,, \qquad \alpha_D = \frac{\Delta\theta}{\rho_{rad,glue}} \,, \tag{5.A.26}$$

which take into account the fact that the relevant radiation could be only the one of the visible (dark) sector, $\rho_{rad,SM}$ ($\rho_{rad,glue}$). Note that if the Standard Model

plasma is not interacting with the dark sector one, in formula (5.A.25) one has to replace α with α_D.

Redshift

Once we know the parameters that we have discussed so far, we can compute the spectrum of gravitational waves as it appears at the time of production. From this time to the time of detection, the signal gets redshifted due to the cosmological expansion. We are going to discuss how to take into account the redshift of the signal in two different circumstances, both occurring in the scenarios that we study in the present thesis.

Let us start with the case in which the Universe evolves adiabatically from gravitational waves emission to the detection time [179]. This is the case in which only one first-order phase transition occurs. Thus, it includes all the scenarios that we consider in this thesis but the Dark HQCD 2 one. Let us call T_e and T_d the temperature of the Universe, respectively, at the emission and at the detection times. The detection temperature is $T_d \approx 2.35 \cdot 10^{-13}$ GeV. The adiabatic evolution is characterized by the conservation of the entropy

$$S \sim R^3 g_*^S(T) T^3 \,, \tag{5.A.27}$$

from which we find the ratio of the scale factors between the two temperatures

$$\frac{R_d}{R_e} = \left(\frac{g_{*,e}^S}{g_{*,d}^S} \right)^{1/3} \frac{T_e}{T_d} \,. \tag{5.A.28}$$

In this expression, $g_{*,e}^S$ and $g_{*,d}^S$ are the number of relativistic degrees of freedom at the time of emission and detection, respectively; they are computed in the free case using the general formula

$$g_*^S(T) = \sum_{i=\text{bosons}} g_i \left(\frac{T_i}{T} \right)^3 + \frac{7}{8} \sum_{i=\text{fermions}} g_i \left(\frac{T_i}{T} \right)^3 \,, \tag{5.A.29}$$

where T_i represents the temperature of the i-th species.

The frequency f and the energy density[10] Ω of the GWs get redshifted as R^{-1} and R^{-4} respectively, hence

$$f_d = f_e \frac{R_e}{R_d} \,, \tag{5.A.30a}$$

$$H_d^2 \Omega_d = H_e^2 \Omega_e \left(\frac{R_e}{R_d} \right)^4 \,. \tag{5.A.30b}$$

The Hubble scale H is given by the energy density via the Friedmann equation

$$H^2 = \frac{\rho}{3M_{Pl}^2} = \frac{1}{3M_{Pl}^2} \frac{\pi^2}{30} g_*(T) T^4 \,. \tag{5.A.31}$$

---

[10]As customary in cosmology, Ω is defined as the energy density divided by the critical density $\rho_{crit,0} = 3M_{Pl}^2 H_0^2$, where H_0 is the Hubble scale computed in the present epoch.

Here, g_* is defined in the free case as[11]

$$g_*(T) = \sum_{i=\text{bosons}} g_i \left(\frac{T_i}{T}\right)^4 + \frac{7}{8} \sum_{i=\text{fermions}} g_i \left(\frac{T_i}{T}\right)^4 . \tag{5.A.32}$$

As a result, using (5.A.28) and (5.A.31), we find

$$f_d = \frac{\pi}{\sqrt{90 M_{Pl}^2}} \frac{f_e}{H_e} T_e T_d \frac{(g_{*,d}^S)^{1/3}(g_{*,e})^{1/2}}{(g_{*,e}^S)^{1/3}} , \tag{5.A.33a}$$

$$H_d^2 \Omega_d = \frac{\pi^2}{90 M_{Pl}^2} \Omega_e T_d^4 \frac{(g_{*,d}^S)^{4/3}(g_{*,e})}{(g_{*,e}^S)^{4/3}} . \tag{5.A.33b}$$

Let us now consider the case in which two first-order phase transitions occur. Among the scenarios studied in this thesis, this happens in the Dark HQCD 2 scenario of section 5.3.1, where a chiral symmetry breaking/restoration transition is followed by a confinement/deconfinement one. We will refer to this case, even though the discussion will be valid for two generic separated first-order phase transitions.

When we compute the redshift of the gravitational waves spectrum associated with the chiral symmetry transition, we have to take into account that adiabaticity is violated during the confinement/deconfinement one. As a result, conservation of entropy can be used from the time of the chiral symmetry breaking transition, where the temperature T_e is taken to be the reheating temperature, to the percolation time of the confinement transition $T_{p,conf}$. Then, assuming fast reheating in the confinement transition, the temperature has a sudden jump from the percolation temperature $T_{p,conf}$ to the reheating temperature $T_{R,conf}$. Finally, from this time to the present, the Universe evolves adiabatically, and we can again use the conservation of entropy. All in all, the redshifted frequency and energy density read

$$f_d = f_e \frac{R_e}{R_{p,conf}} \frac{R_{R,conf}}{R_d} = f_e \left(\frac{g_{*,p,conf}^S}{g_{*,e}^S}\right)^{1/3} \frac{T_{p,conf}}{T_e} \left(\frac{g_{*,d}^S}{g_{*,R,conf}^S}\right)^{1/3} \frac{T_d}{T_{R,conf}}$$

$$= \frac{\pi}{\sqrt{90 M_{Pl}^2}} \frac{f_e}{H_e} T_e T_d \frac{(g_{*,d}^S)^{1/3}(g_{*,e})^{1/2}}{(g_{*,e}^S)^{1/3}} \cdot \frac{(g_{*,p,conf}^S)^{1/3} T_{p,conf}}{(g_{*,R,conf}^S)^{1/3} T_{R,conf}} . \tag{5.A.34}$$

and

$$H_d^2 \Omega_d = \frac{\pi^2}{90 M_{Pl}^2} \Omega_e T_d^4 \frac{(g_{*,d}^S)^{4/3}(g_{*,e})}{(g_{*,e}^S)^{4/3}} \cdot \left(\frac{(g_{*,p,conf}^S)^{1/3} T_{p,conf}}{(g_{*,R,conf}^S)^{1/3} T_{R,conf}}\right)^4 . \tag{5.A.35}$$

---

[11]Notice that if some species are decoupled from the bath, $g_* \neq g_*^S$. This, notoriously, occurs in the cosmological evolution because of neutrino decoupling when electrons and positrons become non-relativistic. Neutrino and photon relic temperatures do not coincide. They are related by $T_\nu = (4/11)^{1/3} T_\gamma$. As a result, today $g_* \approx 3.36$ is different from $g_*^S = 3.91$.

With respect to the single-transition case, the difference is encoded in the parameter

$$\delta \equiv \frac{(g_{*,p,conf}^S)^{1/3} T_{p,conf}}{(g_{*,R,conf}^S)^{1/3} T_{R,conf}} . \tag{5.A.36}$$

In models with multiple, separated phase transitions, a δ factor for each transition after the first one must be included in the formulae for the GW spectra.

5.A.2 Formulae for the spectra

Let us finally discuss the formulae that allow us to find the gravitational wave spectrum. In linear approximation, the spectrum is given by the sum of three contributions, coming from the collisions of the bubbles, from collisions of plasma sound waves and plasma turbulence,

$$h^2 \Omega_{GW} \approx h^2 \Omega_c(f) + h^2 \Omega_{sw} + h^2 \Omega_{turb} . \tag{5.A.37}$$

Here, h is defined from today's value of the Hubble scale through

$$H_0 = 100 \, h \text{Km/s/Mpc} . \tag{5.A.38}$$

Following [21], we are going to neglect the turbulence contribution because it is still not well-understood and because it is expected that only a small fraction of the transition energy is converted to turbulence.

Let us first consider the collision contribution. Using the so-called *envelope approximation*, a formula for the signal of gravitational waves coming from bubble collisions was numerically found in [179]. An improved version of such a formula (see, e.g., the review [170]) reads

$$h^2 \Omega_c(f) \sim 1.67 \cdot 10^{-5} \left(\frac{\beta}{H_*}\right)^{-2} \left(\frac{\kappa\alpha}{1+\alpha}\right)^2 \left(\frac{100}{g_*}\right)^{1/3} \left(\frac{0.48v^3}{1+5.3v^2+5v^4}\right) S_{env}(f) , \tag{5.A.39a}$$

where f denotes the frequency of the waves, and v the average velocity of the bubbles. The factor κ quantifies the fraction of available energy converted into gravitational waves coming from bubble collision. Finally, the spectral form S_{env} and the peak frequency f_{env} are given by

$$S_{env}(f) \sim \left[0.064 \left(\frac{f}{f_{env}}\right)^{-3} + 0.456 \left(\frac{f}{f_{env}}\right)^{-1} + 0.48 \left(\frac{f}{f_{env}}\right)\right]^{-1} , \tag{5.A.39b}$$

$$f_{env} \sim 16.5 \cdot 10^{-6} \text{Hz} \left(\frac{f_*}{\beta}\right) \left(\frac{\beta}{H_*}\right) \left(\frac{T_*}{100 \text{GeV}}\right) \left(\frac{g_*}{100}\right)^{1/6} , \tag{5.A.39c}$$

where

$$\frac{f_*}{\beta} \sim \frac{0.35}{1 + 0.069v + 0.69v^4} . \tag{5.A.39d}$$

In these formulae, β/H_*, g_*, and α are evaluated at the percolation temperature T_p, whereas T_* in (5.A.39c) is identified with the reheating temperature.[12]

Until recently, the sound wave contribution Ω_{sw} was expected to be subleading with respect to Ω_c in the $v \sim 1$ limiting case. Indeed, scenarios with $v \sim 1$ are expected to be characterized by large supercooling, which causes the plasma to be very diluted, and friction effects to be suppressed. Such a scenario was challenged in [180], where it was pointed out that even in these conditions, there is a so-called *transition radiation* given by the emission of particles that change mass across the bubble walls, which cause a friction pressure. This friction causes (at least part of) the energy to be transmitted to the plasma rather than stored in the bubble-wall kinetic energy. As a result, whether Ω_c or Ω_{sw} dominates the spectrum depends on the energy fraction that gets dispersed in the plasma. This is a highly non-trivial quantity to calculate.

The spectrum due to sound waves is given by[13] [170, 182]

$$h^2 \Omega_{sw}(f) \sim 8.5 \cdot 10^{-6} \left(\frac{\beta}{H_*} \right)^{-1} \left(\frac{\kappa_v \alpha}{1 + \alpha} \right)^2 \left(\frac{100}{g_*} \right)^{1/3} v \, S_{sw}(f) \ . \qquad (5.A.40a)$$

The spectral shape and peak frequency today in this case are

$$S_{sw}(f) \sim \left(\frac{f}{f_{sw}} \right)^3 \left(\frac{7}{4 + 3(f/f_{sw})^2} \right)^{7/2} \ , \qquad (5.A.40b)$$

$$f_{sw} \sim 8.9 \cdot 10^{-6} \text{Hz} \frac{1}{v} \left(\frac{\beta}{H_*} \right) \left(\frac{z_p}{10} \right) \left(\frac{T_*}{100\text{GeV}} \right) \left(\frac{g_*}{100} \right)^{1/6} \qquad (5.A.40c)$$

where we are going to use the approximate value $z_p \sim 10$, and the efficiency factor in the case $v \sim 1$ is

$$\kappa_v = \frac{\alpha}{0.73 + 0.083\sqrt{\alpha} + \alpha} \ . \qquad (5.A.41)$$

If the Standard Model plasma is not in thermal equilibrium with the dark sector, in this formula one has to use α_D instead of α [167].

In fact, formula (5.A.40a) is valid under the assumption that the source of GWs lasts for a period longer than a Hubble time. If the source's duration is short, turbulence effects can be sizable and one can estimate that the net effect is to multiply formula (5.A.40a) by a factor [21]

$$(8\pi)^{1/3} v \left(\frac{\beta}{H_*} \right)^{-1} \left(\frac{\kappa_v \alpha}{1 + \alpha} \right)^{-1/2} \ . \qquad (5.A.42)$$

---

[12]If supercooling is small, reheating is small as well, and therefore the reheating and nucleation temperatures approximately coincide. This is why, in the literature, T_* is often taken to be the nucleation temperature.

[13]A word of caution is in order. The known formulae for Ω_{sw} have been derived under the hypothesis that $\alpha \lesssim 0.1$ and that the speed is far from the Chapman-Jouguet one. Lacking better estimates, these formulae are usually employed even when α is larger than this value. A first study of the spectrum for $\alpha \sim 1$ has highlighted a further suppression of the signal [181]. Nevertheless, this suppression is more important in the case of deflagration, which is not relevant in our cases.

This term tends to reduce the amplitude of the signal. On the other hand, one should add the contribution due to turbulence, which is very uncertain and as stated it is ignored in this thesis. Thus, Ω_{sw} including the term (5.A.42) really corresponds to a lower bound on the contribution of the plasma to the GW spectrum. See also [174] for a discussion of this topic.

5.B   Semi-analytical estimates of GW parameters

It is instructive to give an estimate of how the relevant parameters entering the computation of the stochastic GW spectra depend on the WSS parameters. In this subsection we focus on the confinement/deconfinement phase transition and neglect the flavor contributions.

In the small-temperature regime, when the $O(4)$ symmetric bounce dominates the transition, the bubble nucleation rate (5.A.1) can be easily computed using the relations (4.2.31) giving

$$\Gamma(T) = M_{KK}^4 \frac{(S_{4,B})^2}{4\pi^2 \bar{\rho}_w^4} e^{-S_{4,B}} \approx M_{KK}^4 \frac{c_4^2 g^2 \bar{T}^8}{4\pi^2 b^4} e^{-c_4 g \bar{T}^3} , \qquad (5.B.1)$$

where $c_4 \approx 0.39$ and $b \approx 4$. The rate has a peak at $\bar{T} = \bar{T}_m = [8/(3c_4 g)]^{1/3}$ where $\Gamma(T_m) \sim M_{KK}^4 g^{-2/3}$. Hence, increasing g, both $\bar{T}_m$ and $\Gamma(T_m)$ decrease. This qualitative behavior holds in general, beyond the small-temperature regime, as can be appreciated by the analysis of the rates done in [101].

The nucleation temperature can be estimated using eq. (5.A.7) with $r = 5/3$ and (5.A.9), giving the relation

$$\frac{\Gamma(T_n)}{H(T_n)^4} \approx \frac{9}{5} c_4 g \bar{T}_n^3 , \qquad (5.B.2)$$

where, since we are working in a small-temperature regime $\bar{T} \ll 1$, the Hubble parameter is dominated by the vacuum energy contribution

$$H(T_n)^4 \approx \frac{g^2}{3^{16}\pi^4} M_{KK}^4 \left(\frac{M_{KK}}{M_{pl}} \right)^4 . \qquad (5.B.3)$$

Hence, from (5.B.2) we get

$$\bar{T}_n^5 e^{-c_4 g \bar{T}_n^3} \approx \frac{4b^4 g}{3^{14}5\pi^2 c_4} \left(\frac{M_{KK}}{M_{pl}} \right)^4 . \qquad (5.B.4)$$

Now, if, for $\bar{T}_n \ll 1$ and $g \gg 1$, we have

$$c_4 \, g \, \bar{T}_n^3 \gg \frac{5}{3} |\log(c_4 g \bar{T}_n^3)| , \qquad (5.B.5)$$

i.e. if $c_4 g \bar{T}_n^3 \gg 1.7$, from (5.B.4) we get

$$\bar{T}_n^3 \approx \frac{4}{c_4 \, g} \log \left(\frac{M_{pl}}{g^{2/3} M_{KK}} \right) + \mathcal{O}(1/g) . \qquad (5.B.6)$$

The nucleation temperature, in the limit where the above approximations hold, decreases when g and M_{KK} increase and keeps being much smaller than the critical temperature. Supercooling is thus enhanced when g and M_{KK} grow.

In the same limits we can estimate the percolation temperature from eq. (5.A.16). If $v \sim 1$ we find that

$$\bar{T}_p^3 \approx \bar{T}_n^3 + \mathcal{O}(1/g) . \tag{5.B.7}$$

Using the above results and approximations we can also estimate the other relevant parameter, defined in (5.A.22), as

$$\begin{aligned}
\frac{\beta}{H_*}|_{T_p} &= -\frac{3}{5} T_p \frac{d \log \Gamma}{dT}|_{T_p} \approx \frac{3}{5} \left(3 c_4\, g\, \bar{T}_p^3 - 8\right) \\
&\approx \frac{3}{5} \left[12 \log \left(\frac{M_{pl}}{g^{2/3} M_{KK}} \right) - 8 \right] ,
\end{aligned} \tag{5.B.8}$$

up to a velocity dependent term. In the small-temperature regime, we thus find that β/H_* slightly decreases as M_{KK} and g increase.

When the $O(3)$ configuration dominates, using the small $\bar{T}$ expression in the first row of eq. (4.2.29), and taking the large g limit, we can analogously get the nucleation and percolation temperatures. In this case the bubble nucleation rate is given by

$$\Gamma(T) = M_{KK}^4 \frac{\bar{T}^4}{(2\pi)^4} \left(\frac{S_{3,B}}{2\pi T} \right)^{3/2} e^{-S_{3,B}/T} \approx M_{KK}^4 \frac{\bar{T}^{31/4}}{(2\pi)^{11/2}} (c_3 g)^{3/2} e^{-c_3 g \bar{T}^{5/2}} , \tag{5.B.9}$$

where $c_3 \approx 0.32$. It has a peak at $\bar{T}_m = [31/(10 c_3 g)]^{2/5}$, where $\Gamma(T_m) \sim M_{KK}^4 g^{-8/5}$. Again, both $\bar{T}_m$ and $\Gamma(T_m)$ decrease while increasing g, in agreement with the more general numerical analysis done chapter 4.

The relation (5.A.9) determining the nucleation temperature now reads

$$\frac{\Gamma(T_n)}{H(T_n)^4} \approx \frac{3}{2} c_3 g \bar{T}_n^{5/2} , \tag{5.B.10}$$

where, again, the Hubble parameter is approximated by (5.B.3). If, for $\bar{T}_n \ll 1$ and $g \gg 1$, we have

$$c_3\, g\, \bar{T}_n^{5/2} \gg \frac{21}{10} |\log(c_3 g \bar{T}_n^{5/2})| , \tag{5.B.11}$$

i.e. if $c_3 g \bar{T}_n^{5/2} \gg 2.1$, we get

$$\bar{T}_n^{5/2} \approx \frac{4}{c_3\, g} \log \left(\frac{M_{pl}}{M_{KK} g^{9/10}} \right) + \mathcal{O}(1/g) . \tag{5.B.12}$$

Again, $\bar{T}_n$ decreases as g and M_{KK} increase.

In the same limits as before, the percolation temperature approximately coincides with the nucleation temperature and

$$\frac{\beta}{H_*}|_{T_p} \approx \frac{3}{5} \left(\frac{5}{2} c_3 g \bar{T}_p^{5/2} - \frac{31}{4} \right) \approx \frac{3}{5} \left[10 \log \left(\frac{M_{pl}}{M_{KK} g^{9/10}} \right) - \frac{31}{4} \right] , \tag{5.B.13}$$

up to a velocity dependent term. This parameter decreases as g and M_{KK} increase.

For strong supercooling, in both the $O(3)$ and the $O(4)$-symmetric cases, the reheating temperature calculated from (5.A.23) reads

$$\bar{T}_R \approx \left(\frac{160}{3^6 g_{SM}^*} \right)^{1/4} g^{1/4} \, , \tag{5.B.14}$$

where $g_{SM}^* = g_{SM}^*(T_R) = \mathcal{O}(100)$. The reheating temperature is thus independent from M_{KK} and increases with g. When $g \gg 1$, it is parametrically larger than the critical temperature.

Finally, using the definition (5.A.24), it is possible to estimate the parameter α, measuring the relative energy released during the transition. In the small temperature regime it reads

$$\alpha(T_p) \approx \frac{1}{5\bar{T}_p^6} \gg 1 \, . \tag{5.B.15}$$

Conclusions and outlook

In this thesis, we have employed the Witten-Sakai-Sugimoto (WSS) model to address two different, but not unrelated, problems: the strong CP problem and the gravitational wave production in cosmological first-order phase transition predicted by hidden strongly-coupled gauge sectors. In the following, we summarize the main findings of our original work illustrated in chapters 3, 4 and 5 and point out some possible future directions.

In chapter 3, we have put forth a new calculable, strongly-coupled UV completion of the low-energy QCD axion physics in the planar limit. The completion is provided by the five-dimensional theory (and then by the six-dimensional (2,0) theory in the M-theory limit) in the UV of the holographic WSS model. The construction seems to evade the phenomenologically unsatisfactory constraints on the allowed values of f_a commonly encountered in string theory axion models [16].

Often a higher dimensional embedding of the axion physics provides a natural protection against higher-dimensional operators which could spoil the PQ mechanism (see e.g. [183]). It would be interesting, for the future, to check if this is the case in the present model.

Since in the construction the Peccei-Quinn symmetry is not realized on the Standard Model fields, the model falls in the KSVZ class. The axion couplings with the nucleons and the photon have no UV contributions and are entirely determined by the low-energy action and the mixing with the pseudoscalars.

In the deconfined phase, we have evaluated the topological susceptibility, the temperature dependence of f_a and that of the axion mass. The latter is found to be an increasing function of the temperature. The setting seems to be less reliable as a QCD model in this phase, for it exhibits a higher dimensional completion and absence of asymptotic freedom.

As an aside, we have calculated for the first time the topological susceptibility of $\mathcal{N} = 4$ SYM theory at strong coupling and finite temperature.

An interesting task for the future would be to study axionic strings and domain walls, since the holographic model geometrizes these topological objects [39]. It would also be interesting to investigate the consequences of more than one extra flavor in the axion sector.

In chapter 4, we have studied the dynamics of first-order phase transitions in strongly-coupled planar gauge theories. Using the holographic correspondence as a tool, we have been able to compute the decay rate of the false vacuum which proceeds through the nucleation of bubbles in the metastable phase. As discussed

in the seminal papers [25–27], the decay probability per unit time and unit volume in the semiclassical limit is obtained by the on-shell action evaluated on the bounce, a solution of the Euclidean equations of motion found with boundary conditions that enforce the interpolation between the false and the true vacua.

In holographic models such as the WSS and the Randall-Sundrum models, a first-order phase transition can be related, in the dual picture, either to a change of the gravity background (a Hawking-Page transition for instance) or to a change of the embedding of some probe brane on a fixed background, which can be studied through the Dirac-Born-Infeld (DBI) action.

When the background changes from a soliton-like solution to a black-hole one, the dual quantum gauge theory experiences a first-order (de)confinement transition. Describing the dynamics of the transition in the gravity side requires developing an off-shell formalism that may allow to follow the jump from a black hole solution describing the deconfined phase to a "solitonic" solution describing the confined one. Deriving the complete solution for the mixed fluctuations of the metric and the other background fields would be a daunting task. Thus we have adopted a simplified practical approach, introduced in [46] for Randall-Sundrum models with an AdS_5 dual description.

We have revisited the compact Randall-Sundrum model examined in [46]. In this seminal paper, and in the following literature, a missing piece in the analysis of the bounce action in the deconfined phase (dual to an AdS_5 black hole) was the derivative term for the field $T_h(\rho)$ related to the horizon radius. Using holographic renormalization, we have been able to compute this term.

Holographic renormalization has also been the relevant tool we have adopted in studying the dynamics of the confinement/deconfinement transition in the WSS model. To the best of our knowledge, this is the first time the phase transition dynamics is studied in a full-fledged top-down holographic model. We have been able to extract the effective bounce action and to compute the bubble nucleation rate as a function of the model's parameters. Analytic expressions have also been provided in the thick and thin wall approximations.

The second kind of transition we have examined is the very special chiral symmetry breaking/restoration one, which, provided certain parameters of the WSS model are opportunely tuned, occurs in the deconfined phase, with a critical temperature that is larger than the one for deconfinement. In this case, the two phases are related to two different solutions for the embedding of probe $D8$-branes in the black hole background describing the deconfined phase. In principle, the DBI action for the branes is enough to deduce the on-shell action for this field. However, the non-linearities inherent to the DBI action render the complete analysis very challenging. We have been able to tackle the problem by using a powerful variational approach that could hopefully be useful for treating more general (static and dynamical) problems related to flavor-brane dynamics in WSS and similar models. Again this has allowed us to compute the bubble interpolating between the two configurations and the nucleation rate.

It would be interesting to apply the techniques employed in this study to

investigate other holographic first-order transitions, for example involving finite density states.

In chapter 5, we have used the WSS model to compute the spectrum of gravitational waves coming from cosmological first-order phase transitions. Dark sectors, as hidden sectors very weakly interacting with the Standard Model, could well display such transitions. Indeed, in many cases, they are realized as Yang-Mills or QCD-like theories. If the gauge group's rank of these theories is sufficiently large, the planar limit constitutes a good approximation to their dynamics. We have considered the scenario where a dark sector admits a top-down holographic dual description in the gravity regime. In such a case, at least in principle, we have full control on its strongly-coupled dynamics, without the need to employ effective models. More generally, one can view the holographic description as an effective tool to model the strong-coupling dynamics - this latter approach has been used extensively for QCD.

Making use of the results obtained in chapter 4, we have been able to calculate all the relevant parameters necessary for the determination of the GW spectra. The results of our investigation are partially in line with other studies in the literature. In table 5.1 we report the benchmark cases displayed in figures 5.1 and 5.4. In the case of the single confinement transition, there is a large part of the parameter space of the theory where the GW signal is going to be detectable in the next generation facilities (see figure 5.1 for examples). These include pulsar timing arrays as well as space- and ground-based interferometers, depending on the dynamical scale of the theory. Interestingly, a window of parameter space can produce a signal within the current NANOGrav sensitivity, explaining the recent potential observation in this experiment [49].

When the chiral symmetry breaking transition is separated from the confinement one, the model predicts two distinct peaks in the GW spectra. Detection of both peaks would represent an exciting smoking gun for the models with two transitions. The gravity regime allows us to faithfully explore a branch of parameter space where the chiral symmetry signal is smaller than the confinement one. Nevertheless, we have shown that there are certain values of parameters allowing for observation of the two peaks, for example by space-based interferometers (figure 5.4). It would be interesting to study the correlations of the two peaks, which could distinguish the holographic model from other models with two phase transitions.

Finally, we have considered Peccei-Quinn transitions in two distinct axion models: a standard composite axion from a hidden sector [13, 47, 108] and the holographic axion model presented in chapter 3. Unfortunately, in both cases, the lower bound on the axion decay constant around 10^8 GeV corresponds to a peak frequency that is too large for detection in the near future. In this respect, the model is distinct from the holographic bottom-up (phenomenological) ones recently investigated in [142, 143], where the possibility of tuning a very small parameter, measuring the departure from conformality, allows producing signals within the sensitivity of ET or CE.

In this thesis, we have started to use top-down holographic models to study dark (hidden) sectors. It will be clearly interesting to better constrain the models' parameter space taking into account current observational constraints and to produce predictions for observables in the theory's strong-coupling regime.

Summary of the benchmark cases			
Scenario	Dynamical scale	Chiral scale	Experiment
Dark HQCD 1	$10^2, 10^6$	$10^2, 10^6$	LISA-BBO, ET-LIGO
Dark Glueballs	10^{-6}	-	NANOGrav-IPTA-SKA
Dark Axion	10^9	10^8	(ET-CE)
Dark HQCD 2	10^2	$6 \cdot 10^3$	LISA-BBO-DECIGO
HoloAxion	0.949	10^8	-

Table 5.1. *Values of the dynamically generated scale and the chiral symmetry breaking scale (or axion decay constant) of the WSS model for the benchmark cases considered in figures 5.1 and 5.4. In the last column we report some experiments with the potential of detecting the corresponding signals. In the Dark Axion case the experiments are in brackets because the detectability is marginal. All the energies are expressed in GeV.*

Bibliography

[1] **ATLAS** Collaboration, G. Aad *et al.*, "Observation of a new particle in the search for the Standard Model Higgs boson with the ATLAS detector at the LHC," *Phys. Lett. B* **716** (2012) 1–29, `arXiv:1207.7214 [hep-ex]`.

[2] **CMS** Collaboration, S. Chatrchyan *et al.*, "Observation of a New Boson at a Mass of 125 GeV with the CMS Experiment at the LHC," *Phys. Lett. B* **716** (2012) 30–61, `arXiv:1207.7235 [hep-ex]`.

[3] J. M. Pendlebury *et al.*, "Revised experimental upper limit on the electric dipole moment of the neutron," *Phys. Rev. D* **92** no. 9, (2015) 092003, `arXiv:1509.04411 [hep-ex]`.

[4] C. Baker *et al.*, "An Improved experimental limit on the electric dipole moment of the neutron," *Phys. Rev. Lett.* **97** (2006) 131801, `arXiv:hep-ex/0602020`.

[5] **MILC** Collaboration, C. Aubin, C. Bernard, C. E. DeTar, J. Osborn, S. Gottlieb, E. Gregory, D. Toussaint, U. Heller, J. Hetrick, and R. Sugar, "Light pseudoscalar decay constants, quark masses, and low energy constants from three-flavor lattice QCD," *Phys. Rev. D* **70** (2004) 114501, `arXiv:hep-lat/0407028`.

[6] R. Peccei and H. R. Quinn, "CP Conservation in the Presence of Instantons," *Phys. Rev. Lett.* **38** (1977) 1440–1443.

[7] S. Weinberg, "A New Light Boson?," *Phys. Rev. Lett.* **40** (1978) 223–226.

[8] F. Wilczek, "Problem of Strong P and T Invariance in the Presence of Instantons," *Phys. Rev. Lett.* **40** (1978) 279–282.

[9] J. Preskill, M. B. Wise, and F. Wilczek, "Cosmology of the Invisible Axion," *Phys. Lett. B* **120** (1983) 127–132.

[10] L. Di Luzio, M. Giannotti, E. Nardi, and L. Visinelli, "The landscape of QCD axion models," *Phys. Rept.* **870** (2020) 1–117, `arXiv:2003.01100 [hep-ph]`.

[11] A. Zhitnitsky, "On Possible Suppression of the Axion Hadron Interactions. (In Russian)," *Sov. J. Nucl. Phys.* **31** (1980) 260.

[12] M. Dine, W. Fischler, and M. Srednicki, "A Simple Solution to the Strong CP Problem with a Harmless Axion," *Phys. Lett. B* **104** (1981) 199–202.

[13] J. E. Kim, "Weak Interaction Singlet and Strong CP Invariance," *Phys. Rev. Lett.* **43** (1979) 103.

[14] M. A. Shifman, A. Vainshtein, and V. I. Zakharov, "Can Confinement Ensure Natural CP Invariance of Strong Interactions?," *Nucl. Phys. B* **166** (1980) 493–506.

[15] D. J. Marsh, "Axions and ALPs: a very short introduction," in *13th Patras Workshop on Axions, WIMPs and WISPs*, pp. 59–74. 2018. arXiv:1712.03018 [hep-ph].

[16] P. Svrcek and E. Witten, "Axions In String Theory," *JHEP* **06** (2006) 051, arXiv:hep-th/0605206.

[17] S. Profumo, L. Giani, and O. F. Piattella, "An Introduction to Particle Dark Matter," *Universe* **5** no. 10, (2019) 213, arXiv:1910.05610 [hep-ph].

[18] **LIGO Scientific, Virgo** Collaboration, B. Abbott *et al.*, "Observation of Gravitational Waves from a Binary Black Hole Merger," *Phys. Rev. Lett.* **116** no. 6, (2016) 061102, arXiv:1602.03837 [gr-qc].

[19] M. Maggiore, *Gravitational Waves. Vol. 2: Astrophysics and Cosmology*. Oxford University Press, 3, 2018.

[20] C. Caprini *et al.*, "Science with the space-based interferometer eLISA. II: Gravitational waves from cosmological phase transitions," *JCAP* **04** (2016) 001, arXiv:1512.06239 [astro-ph.CO].

[21] C. Caprini *et al.*, "Detecting gravitational waves from cosmological phase transitions with LISA: an update," *JCAP* **03** (2020) 024, arXiv:1910.13125 [astro-ph.CO].

[22] M. B. Hindmarsh, M. Lüben, J. Lumma, and M. Pauly, "Phase transitions in the early universe," arXiv:2008.09136 [astro-ph.CO].

[23] Y. Aoki, G. Endrodi, Z. Fodor, S. Katz, and K. Szabo, "The Order of the quantum chromodynamics transition predicted by the standard model of particle physics," *Nature* **443** (2006) 675–678, arXiv:hep-lat/0611014.

[24] K. Kajantie, M. Laine, K. Rummukainen, and M. E. Shaposhnikov, "Is there a hot electroweak phase transition at m(H) larger or equal to m(W)?," *Phys. Rev. Lett.* **77** (1996) 2887–2890, arXiv:hep-ph/9605288.

[25] S. R. Coleman, "The Fate of the False Vacuum. 1. Semiclassical Theory," *Phys. Rev. D* **15** (1977) 2929–2936. [Erratum: Phys.Rev.D 16, 1248 (1977)].

[26] A. D. Linde, "Fate of the False Vacuum at Finite Temperature: Theory and Applications," *Phys. Lett. B* **100** (1981) 37–40.

[27] A. D. Linde, "Decay of the False Vacuum at Finite Temperature," *Nucl. Phys. B* **216** (1983) 421. [Erratum: Nucl.Phys.B 223, 544 (1983)].

[28] G. D. Kribs and E. T. Neil, "Review of strongly-coupled composite dark matter models and lattice simulations," *Int. J. Mod. Phys. A* **31** no. 22, (2016) 1643004, `arXiv:1604.04627 [hep-ph]`.

[29] C. Michael and M. Teper, "The Glueball Spectrum in SU(3)," *Nucl. Phys. B* **314** (1989) 347–362.

[30] M. E. Peskin, "Mandelstam 't Hooft Duality in Abelian Lattice Models," *Annals Phys.* **113** (1978) 122.

[31] C. Dasgupta and B. Halperin, "Phase Transition in a Lattice Model of Superconductivity," *Phys. Rev. Lett.* **47** (1981) 1556–1560.

[32] J. M. Maldacena, "The Large N limit of superconformal field theories and supergravity," *Int. J. Theor. Phys.* **38** (1999) 1113–1133, `arXiv:hep-th/9711200`.

[33] E. Witten, "Anti-de Sitter space and holography," *Adv. Theor. Math. Phys.* **2** (1998) 253–291, `arXiv:hep-th/9802150`.

[34] S. Gubser, I. R. Klebanov, and A. M. Polyakov, "Gauge theory correlators from noncritical string theory," *Phys. Lett. B* **428** (1998) 105–114, `arXiv:hep-th/9802109`.

[35] O. Aharony, S. S. Gubser, J. M. Maldacena, H. Ooguri, and Y. Oz, "Large N field theories, string theory and gravity," *Phys. Rept.* **323** (2000) 183–386, `arXiv:hep-th/9905111`.

[36] E. Witten, "Anti-de Sitter space, thermal phase transition, and confinement in gauge theories," *Adv. Theor. Math. Phys.* **2** (1998) 505–532, `arXiv:hep-th/9803131`.

[37] T. Sakai and S. Sugimoto, "Low energy hadron physics in holographic QCD," *Prog. Theor. Phys.* **113** (2005) 843–882, `arXiv:hep-th/0412141 [hep-th]`.

[38] E. Witten, "Theta dependence in the large N limit of four-dimensional gauge theories," *Phys. Rev. Lett.* **81** (1998) 2862–2865, `arXiv:hep-th/9807109 [hep-th]`.

[39] S. Dubovsky, A. Lawrence, and M. M. Roberts, "Axion monodromy in a model of holographic gluodynamics," *JHEP* **02** (2012) 053, `arXiv:1105.3740 [hep-th]`.

[40] F. Bigazzi, A. L. Cotrone, and R. Sisca, "Notes on Theta Dependence in Holographic Yang-Mills," *JHEP* **08** (2015) 090, `arXiv:1506.03826 [hep-th]`.

[41] L. Bartolini, F. Bigazzi, S. Bolognesi, A. L. Cotrone, and A. Manenti, "Theta dependence in Holographic QCD," *JHEP* **02** (2017) 029, `arXiv:1611.00048 [hep-th]`.

[42] L. Bartolini, F. Bigazzi, S. Bolognesi, A. L. Cotrone, and A. Manenti, "Neutron electric dipole moment from gauge/string duality," *Phys. Rev. Lett.* **118** no. 9, (2017) 091601, `arXiv:1609.09513 [hep-ph]`.

[43] O. Aharony, J. Sonnenschein, and S. Yankielowicz, "A Holographic model of deconfinement and chiral symmetry restoration," *Annals Phys.* **322** (2007) 1420–1443, `arXiv:hep-th/0604161 [hep-th]`.

[44] E. Antonyan, J. A. Harvey, S. Jensen, and D. Kutasov, "NJL and QCD from string theory," `arXiv:hep-th/0604017 [hep-th]`.

[45] P. Di Vecchia, G. Rossi, G. Veneziano, and S. Yankielowicz, "Spontaneous *CP* breaking in QCD and the axion potential: an effective Lagrangian approach," *JHEP* **12** (2017) 104, `arXiv:1709.00731 [hep-th]`.

[46] P. Creminelli, A. Nicolis, and R. Rattazzi, "Holography and the electroweak phase transition," *JHEP* **03** (2002) 051, `arXiv:hep-th/0107141`.

[47] K. Choi and J. E. Kim, "DYNAMICAL AXION," *Phys. Rev. D* **32** (1985) 1828.

[48] G. Grilli di Cortona, E. Hardy, J. Pardo Vega, and G. Villadoro, "The QCD axion, precisely," *JHEP* **01** (2016) 034, `arXiv:1511.02867 [hep-ph]`.

[49] **NANOGrav** Collaboration, Z. Arzoumanian *et al.*, "The NANOGrav 12.5-year Data Set: Search For An Isotropic Stochastic Gravitational-Wave Background," `arXiv:2009.04496 [astro-ph.HE]`.

[50] G. 't Hooft, "Dimensional reduction in quantum gravity," *Conf. Proc. C* **930308** (1993) 284–296, `arXiv:gr-qc/9310026`.

[51] L. Susskind, "The World as a hologram," *J. Math. Phys.* **36** (1995) 6377–6396, `arXiv:hep-th/9409089`.

[52] G. 't Hooft, "A Planar Diagram Theory for Strong Interactions," *Nucl. Phys. B* **72** (1974) 461.

[53] M. Ammon and J. Erdmenger, *Gauge/gravity duality: Foundations and applications.* Cambridge University Press, Cambridge, 4, 2015.

[54] S. R. Coleman, "1/N," in *17th International School of Subnuclear Physics: Pointlike Structures Inside and Outside Hadrons*, p. 0011. 3, 1980.

[55] E. Witten, "Baryons in the 1/n Expansion," *Nucl. Phys. B* **160** (1979) 57–115.

[56] G. Veneziano, "U(1) Without Instantons," *Nucl. Phys. B* **159** (1979) 213–224.

[57] I. Klebanov and A. Polyakov, "AdS dual of the critical O(N) vector model," *Phys. Lett. B* **550** (2002) 213–219, `arXiv:hep-th/0210114`.

[58] J. D. Bekenstein, "Black holes and entropy," *Phys. Rev. D* **7** (1973) 2333–2346.

[59] L. Susskind and E. Witten, "The Holographic bound in anti-de Sitter space," `arXiv:hep-th/9805114`.

[60] A. W. Peet and J. Polchinski, "UV / IR relations in AdS dynamics," *Phys. Rev. D* **59** (1999) 065011, `arXiv:hep-th/9809022`.

[61] J. Polchinski, "Dirichlet Branes and Ramond-Ramond charges," *Phys. Rev. Lett.* **75** (1995) 4724–4727, `arXiv:hep-th/9510017`.

[62] J. Callan, Curtis G., E. Martinec, M. Perry, and D. Friedan, "Strings in Background Fields," *Nucl. Phys. B* **262** (1985) 593–609.

[63] J. Polchinski, *String theory. Vol. 2: Superstring theory and beyond*. Cambridge Monographs on Mathematical Physics. Cambridge University Press, 12, 2007.

[64] G. T. Horowitz and A. Strominger, "Black strings and P-branes," *Nucl. Phys. B* **360** (1991) 197–209.

[65] M. R. Garousi and R. C. Myers, "Superstring scattering from D-branes," *Nucl. Phys. B* **475** (1996) 193–224, `arXiv:hep-th/9603194`.

[66] P. Di Vecchia, M. Frau, I. Pesando, S. Sciuto, A. Lerda, and R. Russo, "Classical p-branes from boundary state," *Nucl. Phys. B* **507** (1997) 259–276, `arXiv:hep-th/9707068`.

[67] M. Bertolini, P. Di Vecchia, M. Frau, A. Lerda, R. Marotta, and R. Russo, "Is a classical description of stable nonBPS D-branes possible?," *Nucl. Phys. B* **590** (2000) 471–503, `arXiv:hep-th/0007097`.

[68] I. R. Klebanov, "World volume approach to absorption by nondilatonic branes," *Nucl. Phys. B* **496** (1997) 231–242, `arXiv:hep-th/9702076`.

[69] S. S. Gubser, I. R. Klebanov, and A. A. Tseytlin, "String theory and classical absorption by three-branes," *Nucl. Phys. B* **499** (1997) 217–240, `arXiv:hep-th/9703040`.

[70] J. Polchinski, "Introduction to Gauge/Gravity Duality," in *Theoretical Advanced Study Institute in Elementary Particle Physics: String theory and its Applications: From meV to the Planck Scale*, pp. 3–46. 10, 2010. `arXiv:1010.6134 [hep-th]`.

[71] E. Witten, "AdS / CFT correspondence and topological field theory," *JHEP* **12** (1998) 012, `arXiv:hep-th/9812012`.

[72] J. M. Maldacena, G. W. Moore, and N. Seiberg, "D-brane charges in five-brane backgrounds," *JHEP* **10** (2001) 005, `arXiv:hep-th/0108152`.

[73] D. M. Hofman and N. Iqbal, "Generalized global symmetries and holography," *SciPost Phys.* **4** no. 1, (2018) 005, `arXiv:1707.08577 [hep-th]`.

[74] U. Gursoy and E. Kiritsis, "Exploring improved holographic theories for QCD: Part I," *JHEP* **02** (2008) 032, `arXiv:0707.1324 [hep-th]`.

[75] U. Gursoy, E. Kiritsis, and F. Nitti, "Exploring improved holographic theories for QCD: Part II," *JHEP* **02** (2008) 019, `arXiv:0707.1349 [hep-th]`.

[76] M. Henningson and K. Skenderis, "The Holographic Weyl anomaly," *JHEP* **07** (1998) 023, `arXiv:hep-th/9806087`.

[77] K. Skenderis, "Lecture notes on holographic renormalization," *Class. Quant. Grav.* **19** (2002) 5849–5876, `arXiv:hep-th/0209067`.

[78] P. Breitenlohner and D. Z. Freedman, "Positive Energy in anti-De Sitter Backgrounds and Gauged Extended Supergravity," *Phys. Lett. B* **115** (1982) 197–201.

[79] P. Breitenlohner and D. Z. Freedman, "Stability in Gauged Extended Supergravity," *Annals Phys.* **144** (1982) 249.

[80] K. G. Wilson, "Confinement of Quarks,".

[81] J. M. Maldacena, "Wilson loops in large N field theories," *Phys. Rev. Lett.* **80** (1998) 4859–4862, `arXiv:hep-th/9803002`.

[82] S.-J. Rey and J.-T. Yee, "Macroscopic strings as heavy quarks in large N gauge theory and anti-de Sitter supergravity," *Eur. Phys. J. C* **22** (2001) 379–394, `arXiv:hep-th/9803001`.

[83] N. Drukker, D. J. Gross, and H. Ooguri, "Wilson loops and minimal surfaces," *Phys. Rev. D* **60** (1999) 125006, `arXiv:hep-th/9904191`.

[84] J. Erickson, G. Semenoff, R. Szabo, and K. Zarembo, "Static potential in N=4 supersymmetric Yang-Mills theory," *Phys. Rev. D* **61** (2000) 105006, `arXiv:hep-th/9911088`.

[85] A. Rebhan, "The Witten-Sakai-Sugimoto model: A brief review and some recent results," *EPJ Web Conf.* **95** (2015) 02005, `arXiv:1410.8858 [hep-th]`.

[86] N. Itzhaki, J. M. Maldacena, J. Sonnenschein, and S. Yankielowicz, "Supergravity and the large N limit of theories with sixteen supercharges," *Phys. Rev. D* **58** (1998) 046004, `arXiv:hep-th/9802042`.

[87] H. Nastase, *Introduction to the ADS/CFT Correspondence.* Cambridge University Press, 9, 2015.

[88] R. C. Brower, S. D. Mathur, and C.-I. Tan, "Glueball spectrum for QCD from AdS supergravity duality," *Nucl. Phys. B* **587** (2000) 249–276, `arXiv:hep-th/0003115`.

[89] B. Lucini, A. Rago, and E. Rinaldi, "Glueball masses in the large N limit," *JHEP* **08** (2010) 119, `arXiv:1007.3879 [hep-lat]`.

[90] C. V. Johnson, *D-branes.* Cambridge Monographs on Mathematical Physics. Cambridge University Press, 2005. `http://books.cambridge.org/0521809126.htm`.

[91] S. Sugimoto and K. Takahashi, "QED and string theory," *JHEP* **04** (2004) 051, `arXiv:hep-th/0403247`.

[92] A. Karch and E. Katz, "Adding flavor to AdS / CFT," *JHEP* **06** (2002) 043, `arXiv:hep-th/0205236 [hep-th]`.

[93] S. Weinberg, *The quantum theory of fields. Vol. 2: Modern applications.* Cambridge University Press, 8, 2013.

[94] I. Zahed and G. Brown, "The Skyrme Model," *Phys. Rept.* **142** (1986) 1–102.

[95] T. Sakai and S. Sugimoto, "More on a holographic dual of QCD," *Prog. Theor. Phys.* **114** (2005) 1083–1118, `arXiv:hep-th/0507073`.

[96] O. Aharony and D. Kutasov, "Holographic Duals of Long Open Strings," *Phys. Rev.* **D78** (2008) 026005, `arXiv:0803.3547 [hep-th]`.

[97] K. Hashimoto, T. Hirayama, F.-L. Lin, and H.-U. Yee, "Quark Mass Deformation of Holographic Massless QCD," *JHEP* **07** (2008) 089, `arXiv:0803.4192 [hep-th]`.

[98] E. Witten, "Current Algebra Theorems for the U(1) Goldstone Boson," *Nucl. Phys. B* **156** (1979) 269–283.

[99] M. Kruczenski, D. Mateos, R. C. Myers, and D. J. Winters, "Towards a holographic dual of large N(c) QCD," *JHEP* **05** (2004) 041, `arXiv:hep-th/0311270`.

[100] S.-J. Rey, S. Theisen, and J.-T. Yee, "Wilson-Polyakov loop at finite temperature in large N gauge theory and anti-de Sitter supergravity," *Nucl. Phys. B* **527** (1998) 171–186, `arXiv:hep-th/9803135`.

[101] F. Bigazzi, A. Caddeo, A. L. Cotrone, and A. Paredes, "Fate of false vacua in holographic first-order phase transitions," *JHEP* **12** (2020) 200, `arXiv:2008.02579 [hep-th]`.

[102] Z. Komargodski, "Baryons as Quantum Hall Droplets," `arXiv:1812.09253 [hep-th]`.

[103] G. Derrick, "Comments on nonlinear wave equations as models for elementary particles," *J. Math. Phys.* **5** (1964) 1252–1254.

[104] E. Witten, "Symmetry and Emergence," *Nature Phys.* **14** no. 2, (2018) 116–119, `arXiv:1710.01791 [hep-th]`.

[105] G. 't Hooft, "Symmetry Breaking Through Bell-Jackiw Anomalies," *Phys. Rev. Lett.* **37** (1976) 8–11.

[106] I. G. Irastorza and J. Redondo, "New experimental approaches in the search for axion-like particles," *Prog. Part. Nucl. Phys.* **102** (2018) 89–159, `arXiv:1801.08127 [hep-ph]`.

[107] F. Bigazzi, A. Caddeo, A. L. Cotrone, P. Di Vecchia, and A. Marzolla, "The Holographic QCD Axion," *JHEP* **12** (2019) 056, `arXiv:1906.12117 [hep-th]`.

[108] D. B. Kaplan, "Opening the Axion Window," *Nucl. Phys. B* **260** (1985) 215–226.

[109] P. Anastasopoulos, P. Betzios, M. Bianchi, D. Consoli, and E. Kiritsis, "Emergent Axions," *PoS* **CORFU2019** (2020) 114.

[110] G. Shiu and W. Staessens, "Phases of Inflation," *JHEP* **10** (2018) 085, `arXiv:1807.00888 [hep-th]`.

[111] K.-w. Choi, "A QCD axion from higher dimensional gauge field," *Phys. Rev. Lett.* **92** (2004) 101602, `arXiv:hep-ph/0308024`.

[112] F. Bigazzi, A. L. Cotrone, M. Järvinen, and E. Kiritsis, "Non-derivative Axionic Couplings to Nucleons at large and small N," *JHEP* **01** (2020) 100, `arXiv:1906.12132 [hep-ph]`.

[113] H. Hata, T. Sakai, S. Sugimoto, and S. Yamato, "Baryons from instantons in holographic QCD," *Prog. Theor. Phys.* **117** (2007) 1157, `arXiv:hep-th/0701280`.

[114] K. Hashimoto, T. Sakai, and S. Sugimoto, "Holographic Baryons: Static Properties and Form Factors from Gauge/String Duality," *Prog. Theor. Phys.* **120** (2008) 1093–1137, `arXiv:0806.3122 [hep-th]`.

[115] P. Di Vecchia and F. Sannino, "The Physics of the θ-angle for Composite Extensions of the Standard Model," *Eur. Phys. J. Plus* **129** (2014) 262, `arXiv:1310.0954 [hep-ph]`.

[116] A. Dhar and P. Nag, "Intersecting branes and Nambu−Jona-Lasinio model," *Phys. Rev.* **D79** (2009) 125013, `arXiv:0901.4942 [hep-th]`.

[117] O. Bergman and G. Lifschytz, "Holographic U(1)(A) and String Creation," *JHEP* **04** (2007) 043, `arXiv:hep-th/0612289 [hep-th]`.

[118] O. Aharony, K. Peeters, J. Sonnenschein, and M. Zamaklar, "Rho meson condensation at finite isospin chemical potential in a holographic model for QCD," *JHEP* **02** (2008) 071, `arXiv:0709.3948 [hep-th]`.

[119] G. Mandal and T. Morita, "Gregory-Laflamme as the confinement/deconfinement transition in holographic QCD," *JHEP* **09** (2011) 073, `arXiv:1107.4048 [hep-th]`.

[120] M. Bianchi, M. B. Green, S. Kovacs, and G. Rossi, "Instantons in supersymmetric Yang-Mills and D instantons in IIB superstring theory," *JHEP* **08** (1998) 013, `arXiv:hep-th/9807033`.

[121] M. B. Green and M. Gutperle, "Effects of D instantons," *Nucl. Phys. B* **498** (1997) 195–227, `arXiv:hep-th/9701093`.

[122] M. B. Green and M. Gutperle, "D instanton partition functions," *Phys. Rev. D* **58** (1998) 046007, `arXiv:hep-th/9804123`.

[123] S. S. Gubser, I. R. Klebanov, and A. A. Tseytlin, "Coupling constant dependence in the thermodynamics of N=4 supersymmetric Yang-Mills theory," *Nucl. Phys. B* **534** (1998) 202–222, `arXiv:hep-th/9805156`.

[124] A. Buchel, R. C. Myers, M. F. Paulos, and A. Sinha, "Universal holographic hydrodynamics at finite coupling," *Phys. Lett. B* **669** (2008) 364–370, `arXiv:0808.1837 [hep-th]`.

[125] N. Dorey, T. J. Hollowood, V. V. Khoze, M. P. Mattis, and S. Vandoren, "Multi-instanton calculus and the AdS / CFT correspondence in N=4 superconformal field theory," *Nucl. Phys. B* **552** (1999) 88–168, `arXiv:hep-th/9901128`.

[126] M. B. Green and P. Vanhove, "D instantons, strings and M theory," *Phys. Lett. B* **408** (1997) 122–134, `arXiv:hep-th/9704145`.

[127] M. B. Green, M. Gutperle, and P. Vanhove, "One loop in eleven-dimensions," *Phys. Lett. B* **409** (1997) 177–184, `arXiv:hep-th/9706175`.

[128] M. Hanada, Y. Matsuo, and T. Morita, "Instanton dynamics in finite temperature QCD via holography," *Nucl. Phys. B* **899** (2015) 631–650, `arXiv:1505.04498 [hep-th]`.

[129] F. Bigazzi, A. Caddeo, A. L. Cotrone, and A. Paredes, "Dark Holograms and Gravitational Waves," `arXiv:2011.08757 [hep-ph]`.

[130] D. Mateos, R. C. Myers, and R. M. Thomson, "Holographic phase transitions with fundamental matter," *Phys. Rev. Lett.* **97** (2006) 091601, `arXiv:hep-th/0605046`.

[131] J. Callan, Curtis G. and S. R. Coleman, "The Fate of the False Vacuum. 2. First Quantum Corrections," *Phys. Rev. D* **16** (1977) 1762–1768.

[132] S. R. Coleman and F. De Luccia, "Gravitational Effects on and of Vacuum Decay," *Phys. Rev. D* **21** (1980) 3305.

[133] L. Randall and G. Servant, "Gravitational waves from warped spacetime," *JHEP* **05** (2007) 054, `arXiv:hep-ph/0607158`.

[134] G. Nardini, M. Quiros, and A. Wulzer, "A Confining Strong First-Order Electroweak Phase Transition," *JHEP* **09** (2007) 077, `arXiv:0706.3388 [hep-ph]`.

[135] T. Konstandin, G. Nardini, and M. Quiros, "Gravitational Backreaction Effects on the Holographic Phase Transition," *Phys. Rev. D* **82** (2010) 083513, `arXiv:1007.1468 [hep-ph]`.

[136] D. Bunk, J. Hubisz, and B. Jain, "A Perturbative RS I Cosmological Phase Transition," *Eur. Phys. J. C* **78** no. 1, (2018) 78, `arXiv:1705.00001 [hep-ph]`.

[137] B. M. Dillon, B. K. El-Menoufi, S. J. Huber, and J. P. Manuel, "Rapid holographic phase transition with brane-localized curvature," *Phys. Rev. D* **98** no. 8, (2018) 086005, `arXiv:1708.02953 [hep-th]`.

[138] E. Megías, G. Nardini, and M. Quirós, "Cosmological Phase Transitions in Warped Space: Gravitational Waves and Collider Signatures," *JHEP* **09** (2018) 095, `arXiv:1806.04877 [hep-ph]`.

[139] P. Baratella, A. Pomarol, and F. Rompineve, "The Supercooled Universe," *JHEP* **03** (2019) 100, `arXiv:1812.06996 [hep-ph]`.

[140] K. Agashe, P. Du, M. Ekhterachian, S. Kumar, and R. Sundrum, "Cosmological Phase Transition of Spontaneous Confinement," *JHEP* **05** (2020) 086, `arXiv:1910.06238 [hep-ph]`.

[141] K. Fujikura, Y. Nakai, and M. Yamada, "A more attractive scheme for radion stabilization and supercooled phase transition," *JHEP* **02** (2020) 111, `arXiv:1910.07546 [hep-ph]`.

[142] L. Delle Rose, G. Panico, M. Redi, and A. Tesi, "Gravitational Waves from Supercool Axions," *JHEP* **04** (2020) 025, `arXiv:1912.06139 [hep-ph]`.

[143] B. Von Harling, A. Pomarol, O. Pujolàs, and F. Rompineve, "Peccei-Quinn Phase Transition at LIGO," *JHEP* **04** (2020) 195, `arXiv:1912.07587 [hep-ph]`.

[144] E. Megias, G. Nardini, and M. Quiros, "Gravitational Imprints from Heavy Kaluza-Klein Resonances," *Phys. Rev. D* **102** no. 5, (2020) 055004, `arXiv:2005.04127 [hep-ph]`.

[145] X. Li, Z.-Y. Nie, and Y. Tian, "Holographic boiling and generalized thermodynamic description beyond local equilibrium," *JHEP* **09** (2020) 063, `arXiv:2003.12987 [hep-th]`.

[146] G. T. Horowitz and M. M. Roberts, "Dynamics of First Order Transitions with Gravity Duals," *JHEP* **02** (2007) 076, `arXiv:hep-th/0701099`.

[147] O. Aharony, S. Minwalla, and T. Wiseman, "Plasma-balls in large N gauge theories and localized black holes," *Class. Quant. Grav.* **23** (2006) 2171–2210, `arXiv:hep-th/0507219`.

[148] D. V. Fursaev and S. N. Solodukhin, "On the description of the Riemannian geometry in the presence of conical defects," *Phys. Rev. D* **52** (1995) 2133–2143, `arXiv:hep-th/9501127`.

[149] W. D. Goldberger and M. B. Wise, "Phenomenology of a stabilized modulus," *Phys. Lett. B* **475** (2000) 275–279, `arXiv:hep-ph/9911457`.

[150] I. Kanitscheider, K. Skenderis, and M. Taylor, "Precision holography for non-conformal branes," *JHEP* **09** (2008) 094, `arXiv:0807.3324 [hep-th]`.

[151] A. Paredes, K. Peeters, and M. Zamaklar, "Mesons versus quasi-normal modes: Undercooling and overheating," *JHEP* **05** (2008) 027, `arXiv:0803.0759 [hep-th]`.

[152] M. R. Garousi and K. B. Fadafan, "Tachyon Tunnelling in D-brane-anti-D-brane," *JHEP* **04** (2006) 005, `arXiv:hep-th/0506055`.

[153] J. M. Cline, A. R. Frey, and G. D. Moore, "Composite magnetic dark matter and the 130 GeV line," *Phys. Rev. D* **86** (2012) 115013, `arXiv:1208.2685 [hep-ph]`.

[154] A. Ballon-Bayona, "Holographic deconfinement transition in the presence of a magnetic field," *JHEP* **11** (2013) 168, `arXiv:1307.6498 [hep-th]`.

[155] F. Bigazzi and A. L. Cotrone, "Holographic QCD with Dynamical Flavors," *JHEP* **01** (2015) 104, `arXiv:1410.2443 [hep-th]`.

[156] G. D. Moore and T. Prokopec, "How fast can the wall move? A Study of the electroweak phase transition dynamics," *Phys. Rev. D* **52** (1995) 7182–7204, `arXiv:hep-ph/9506475`.

[157] Y. Watanabe and E. Komatsu, "Improved Calculation of the Primordial Gravitational Wave Spectrum in the Standard Model," *Phys. Rev. D* **73** (2006) 123515, `arXiv:astro-ph/0604176`.

[158] Y. Bai and P. Schwaller, "Scale of dark QCD," *Phys. Rev. D* **89** no. 6, (2014) 063522, `arXiv:1306.4676 [hep-ph]`.

[159] P. Schwaller, "Gravitational Waves from a Dark Phase Transition," *Phys. Rev. Lett.* **115** no. 18, (2015) 181101, `arXiv:1504.07263 [hep-ph]`.

[160] K. Tsumura, M. Yamada, and Y. Yamaguchi, "Gravitational wave from dark sector with dark pion," *JCAP* **07** (2017) 044, `arXiv:1704.00219 [hep-ph]`.

[161] M. Aoki, H. Goto, and J. Kubo, "Gravitational Waves from Hidden QCD Phase Transition," *Phys. Rev. D* **96** no. 7, (2017) 075045, `arXiv:1709.07572 [hep-ph]`.

[162] Y. Bai, A. J. Long, and S. Lu, "Dark Quark Nuggets," *Phys. Rev. D* **99** no. 5, (2019) 055047, `arXiv:1810.04360 [hep-ph]`.

[163] A. J. Helmboldt, J. Kubo, and S. van der Woude, "Observational prospects for gravitational waves from hidden or dark chiral phase transitions," *Phys. Rev. D* **100** no. 5, (2019) 055025, `arXiv:1904.07891 [hep-ph]`.

[164] M. Aoki and J. Kubo, "Gravitational waves from chiral phase transition in a conformally extended standard model," *JCAP* **04** (2020) 001, `arXiv:1910.05025 [hep-ph]`.

[165] K. K. Boddy, J. L. Feng, M. Kaplinghat, and T. M. P. Tait, "Self-Interacting Dark Matter from a Non-Abelian Hidden Sector," *Phys. Rev. D* **89** no. 11, (2014) 115017, `arXiv:1402.3629 [hep-ph]`.

[166] M. Breitbach, J. Kopp, E. Madge, T. Opferkuch, and P. Schwaller, "Dark, Cold, and Noisy: Constraining Secluded Hidden Sectors with Gravitational Waves," *JCAP* **07** (2019) 007, `arXiv:1811.11175 [hep-ph]`.

[167] M. Fairbairn, E. Hardy, and A. Wickens, "Hearing without seeing: gravitational waves from hot and cold hidden sectors," *JHEP* **07** (2019) 044, `arXiv:1901.11038 [hep-ph]`.

[168] M. P. Lombardo and A. Trunin, "Topology and axions in QCD," *Int. J. Mod. Phys. A* **35** no. 20, (2020) 2030010, `arXiv:2005.06547 [hep-lat]`.

[169] D. Croon, R. Houtz, and V. Sanz, "Dynamical Axions and Gravitational Waves," *JHEP* **07** (2019) 146, `arXiv:1904.10967 [hep-ph]`.

[170] D. J. Weir, "Gravitational waves from a first order electroweak phase transition: a brief review," *Phil. Trans. Roy. Soc. Lond. A* **376** no. 2114, (2018) 20170126, `arXiv:1705.01783 [hep-ph]`.

[171] J. Ellis, M. Lewicki, and J. M. No, "On the Maximal Strength of a First-Order Electroweak Phase Transition and its Gravitational Wave Signal," *JCAP* **04** (2019) 003, `arXiv:1809.08242 [hep-ph]`.

[172] J. Ellis, M. Lewicki, J. M. No, and V. Vaskonen, "Gravitational wave energy budget in strongly supercooled phase transitions," *JCAP* **06** (2019) 024, `arXiv:1903.09642 [hep-ph]`.

[173] J. Ellis, M. Lewicki, and J. M. No, "Gravitational waves from first-order cosmological phase transitions: lifetime of the sound wave source," *JCAP* **07** (2020) 050, `arXiv:2003.07360 [hep-ph]`.

[174] H.-K. Guo, K. Sinha, D. Vagie, and G. White, "Phase Transitions in an Expanding Universe: Stochastic Gravitational Waves in Standard and Non-Standard Histories," `arXiv:2007.08537 [hep-ph]`.

[175] K. Schmitz, "New Sensitivity Curves for Gravitational-Wave Experiments," `arXiv:2002.04615 [hep-ph]`.

[176] Y. Nakai, M. Suzuki, F. Takahashi, and M. Yamada, "Gravitational Waves and Dark Radiation from Dark Phase Transition: Connecting NANOGrav Pulsar Timing Data and Hubble Tension," `arXiv:2009.09754 [astro-ph.CO]`.

[177] A. Addazi, Y.-F. Cai, Q. Gan, A. Marciano, and K. Zeng, "NANOGrav results and Dark First Order Phase Transitions," `arXiv:2009.10327 [hep-ph]`.

[178] W. Ratzinger and P. Schwaller, "Whispers from the dark side: Confronting light new physics with NANOGrav data," `arXiv:2009.11875 [astro-ph.CO]`.

[179] M. Kamionkowski, A. Kosowsky, and M. S. Turner, "Gravitational radiation from first order phase transitions," *Phys. Rev. D* **49** (1994) 2837–2851, `arXiv:astro-ph/9310044`.

[180] D. Bodeker and G. D. Moore, "Electroweak Bubble Wall Speed Limit," *JCAP* **05** (2017) 025, `arXiv:1703.08215 [hep-ph]`.

[181] D. Cutting, M. Hindmarsh, and D. J. Weir, "Vorticity, kinetic energy, and suppressed gravitational wave production in strong first order phase transitions," *Phys. Rev. Lett.* **125** no. 2, (2020) 021302, `arXiv:1906.00480 [hep-ph]`.

[182] M. Hindmarsh, S. J. Huber, K. Rummukainen, and D. J. Weir, "Shape of the acoustic gravitational wave power spectrum from a first order phase transition," *Phys. Rev. D* **96** no. 10, (2017) 103520, `arXiv:1704.05871 [astro-ph.CO]`. [Erratum: Phys.Rev.D 101, 089902 (2020)].

[183] B. S. Acharya, K. Bobkov, and P. Kumar, "An M Theory Solution to the Strong CP Problem and Constraints on the Axiverse," *JHEP* **11** (2010) 105, `arXiv:1004.5138 [hep-th]`.